DEVELOPMENT AND EVALUATION OF INTERFACIAL STRUCTURES FOR HYBRID MANUFACTURING

A Dissertation
Presented to
The Academic Faculty

by

Thomas Feldhausen

In Partial Fulfillment
of the Requirements for the Degree
Doctor of Philosophy in the
George W. Woodruff School of Mechanical Engineering

Georgia Institute of Technology
August 2020

DEVELOPMENT AND EVALUATION OF INTERFACIAL STRUCTURES FOR HYBRID MANUFACTURING

Approved by:

Dr. Thomas Kurfess, Advisor
George W. Woodruff School of
Mechanical Engineering
Georgia Institute of Technology

Dr. Shreyes Melkote
George W. Woodruff School of
Mechanical Engineering
Georgia Institute of Technology

Dr. Christopher Saldana
George W. Woodruff School of
Mechanical Engineering
Georgia Institute of Technology

Dr. Lonnie Love
Manufacturing Systems Research Group
Manufacturing Demonstration Facility
Oak Ridge National Laboratory

Dr. Katherine Fu
George W. Woodruff School of
Mechanical Engineering
Georgia Institute of Technology

Date Approved: July 7, 2020

To my wife Cheyanne and my son Elias James

ACKNOWLEDGEMENTS

It has been my experience that there are numerous people who aid in the education of an individual student. The people who have assisted me are numerous and each deserves recognition and acknowledgement. Their assistance, guidance, and advice have been something that I truly appreciate.

I owe special thanks to my advisor, Dr. Thomas Kurfess, for his ecouragement, support, and guidance on both personal and professional levels. Thanks are also due to Dr. Lonnie Love, who welcomed me to his research team with open arms and enabled this research to be conducted at a national laboratory. I would also like to acknowledge the support and suggestions of my reading committee, Dr. Katherine Fu, Dr. Shreyes Melkote, and Dr. Christopher Saldana. Thanks also goes to the entire Manufacturing Demonstration Facility team at Oak Ridge National Laboratory for assisting in this research and providing world-class equipment and facilities to conduct it at.

The group of people who deserves the most acknoledgement, however, is my family. No words can express the patience my wife, Cheyanne, has endured. Without her love and support, this work would be meaningless. In addition, I would like to thank my parents, Bruce and Joyce, who have always been supportive of my decisions and lovingly started me down the path of education despite my kicking and screaming. To all these people, and countless others who have helped in their own special way, thank you.

TABLE OF CONTENTS

LIST OF TABLES

LIST OF FIGURES

LIST OF SYMBOLS AND ABBREVIATIONS

CAM	Computer Aided Manufacturing
CMB	Combined Metal Build-Up
CTE	Coefficient of Thermal Expansion
DED	Direct Energy Deposition
DIC	Digital Image Correlation
EBSD	Electron Backscatter Diffraction
EDM	Electrical Discharge Machining
HP-DLD	High Powered Directed Laser Deposition
HWD	Hot-Wire Deposition
LAMP	Laser Aided Manufacturing Process
LBAM	Laser-Based Additive Manufacturing
LENS	Laser Engineered Net Shaping
L-PBF	Laser Powder Bed Fusion
MDF	Manufacturing Demonstration Facility
ORNL	Oak Ridge National Laboratory
SLC	Selective Laser Cladding
SLM	Selective Laser Melting
SNS	Spallation Neutron Source

SUMMARY

Hybrid manufacturing is a combination of additive (deposition) and subtractive (machining) manufacturing in a single machine tool. Such a system can be used for near net shape manufacturing and component repair using either similar or dissimilar materials. This dissertation investigates methodologies for laser wire-fed hybrid manufacturing processing for commercially available systems and demonstrates how process parameters can be optimized resulting in a deposition rate of 2.5 kg/hr of steel. Integrated into a single system, transition between additive and subtractive manufacturing can occur immediately and be leveraged to generate large components by alternating between the processes. This dissertation investigates how this capability can reduce overall cycle time by up to 68%, improve average elongation to failure by 22%, and reduce average porosity by 16%. With hybrid manufacturing systems, it is now feasible to control the interfacial conditions between the substrate and deposition. Other deposition processes require substrates to be planar, but hybrid manufacturing's subtractive capability allows for unlimited surface structures and conditions. This dissertation further investigates multiple surface structures for similar and dissimilar materials but concludes that these structures do not result in any improvement of mechanical properties. As a result, these investigations has not only set the foundation for laser wire-fed hybrid manufacturing process development, but has influenced the direction of future research in the field.

CHAPTER 1. INTRODUCTION

Hybrid manufacturing systems provide a platform for integrated additive and subtractive methods on a single machine setup. These systems can be used to refurbish or create new components with up to a 50% reduction in manufacturing costs [1, 2]. With commercially available hybrid manufacturing systems capable of 5-axis deposition and subtraction, it is now feasible to control the interfacial conditions between substrate and deposition. Unlike other deposition processes where substrates are required to be planar, hybrid manufacturing's subtractive capability enables unlimited surface structures and conditions. The goal of this research is to evaluate the use of various material and structure combinations to enhance the mechanical properties associated with hybrid manufactured components.

1.1 Introduction

The concept of hybrid manufacturing has existed for over two decades, yet its momentum in the commercial sector has taken off in only the last five years. Known applications of hybrid manufacturing include near net shape deposition, component repair, surface coatings, etching, cutting, localized heat treating, and embedded components [3]. This chapter introduces the concept of hybrid manufacturing and provides the current status of the technology.

1.2 Overview of Hybrid Manufacturing

Hybrid manufacturing systems provide a platform for integrated additive, subtractive, and inspection manufacturing methods. The traditional advantages of additive

manufacturing are efficient material utilization, geometric complexity and tool-less, low volume production. The main limitations are low precision surface finish and slow production rate. Increased production rate is possible but at the expense of surface finish. Conversely, conventional machining provides high precision, good surface finish and high productivity. The major disadvantages are material waste and geometric constraints. Hybrid manufacturing explores the development of new machine tools that integrate the best of both manufacturing technologies into a single system.

The additive process for the hybrid manufacturing systems studied in this dissertation is a laser-wire based directed energy deposition (DED) process. DED is an additive manufacturing process in which focused thermal energy is used to fuse materials by melting them as they are being deposited [4]. In a typical setup, the feedstock, either wire or powder, is fed into a melt pool generated on the surface of the component by a laser energy source. This melt pool adheres to underlying surfaces or layers, analogous to a form of automated build-up welding. Figure 1 depicts this process for a metal wire feedstock. This laser cladding process is combined with computer numerical control (CNC) machining inside of a commercially available machining center. These combined systems seek to reduce potential setup, fixturing, and transfer errors associated with disjointed manufacturing processes by integrating additive and subtractive operations into a single machine [5].

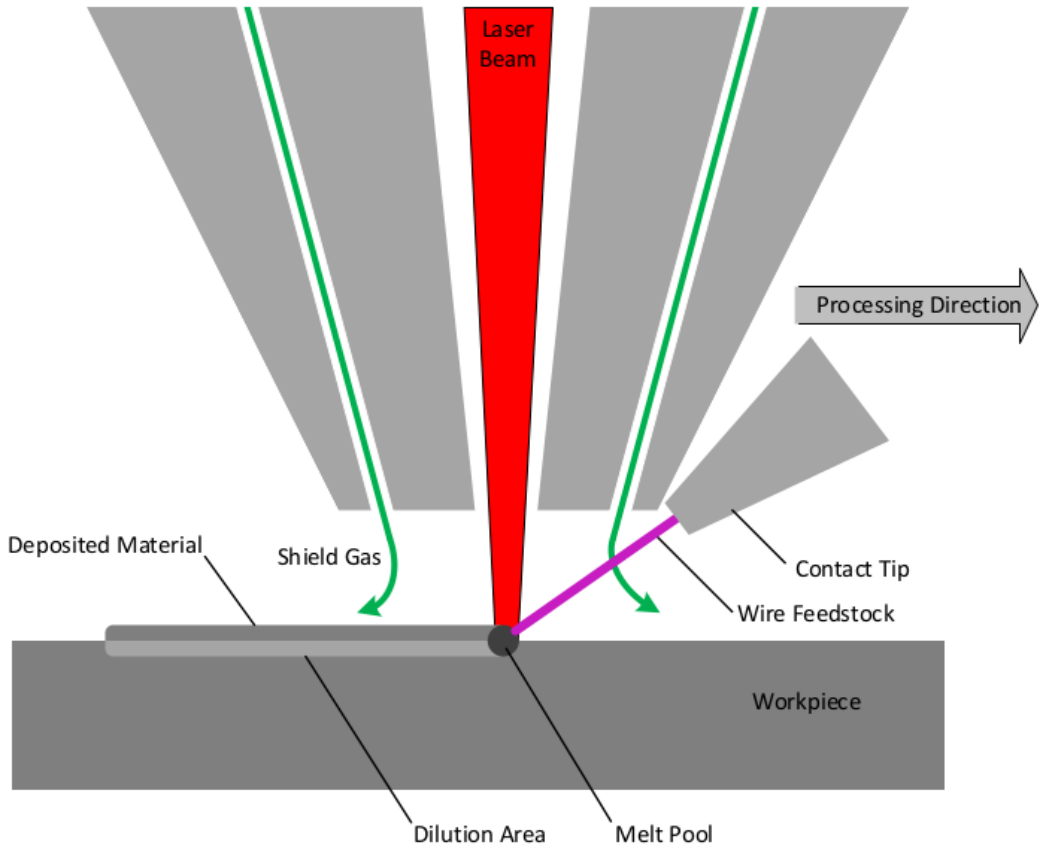

Figure 1: Wire-Feed Directed Energy Deposition Process

Deposition rates vary depending on the type of feedstock used. Material deposition efficiency for blown powder systems is reported to be 60%-80% but can be less than 50% for complex geometries [6-8]. Assuming 50% efficiency, blown powder systems such as the Mazak VC-500 AM are capable of depositing 0.25 kg/hr of Inconel 718 [9]. Such deposition rates make the feasibility of the complete buildup of a large component unreasonable for this feedstock. However, wire-fed systems such as the Mazak VC-500A/5X AM HWD can deposit 2.22 kg/hr with a material utilization rate of 98%, resulting in an economically viable solution for complete component buildup [10].

Many hybrid manufacturing systems are equipped with two rotary axes for 5-axis motion. Unlike traditional 3-axis polymer extrusion printers, a 5-axis system permits the workplane to be strategically oriented mitigating the need for support structures [11]. For example, as shown in Figure 2, the hybrid manufacturing workplane can be rotated such that the secondary deposition of the right-angled component can be completed without the need for support structure.

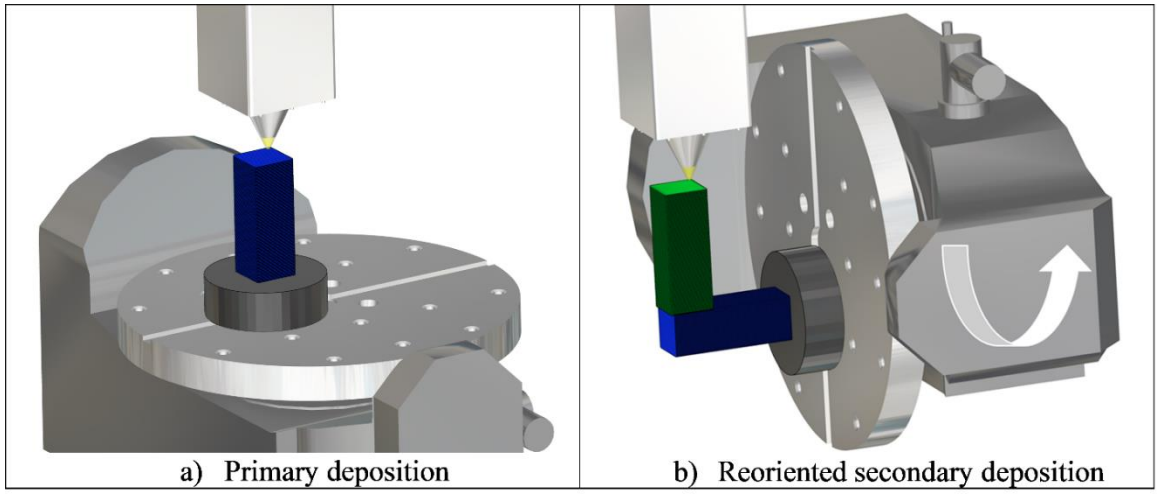

Figure 2: Mitigation of Support Structure

With a system capable of both additive and subtractive manufacturing, it is now possible to build large components in incremental steps. Components that require long and expensive subtractive tooling for reach and access problems can now be manufactured in multiple steps. Instead of printing an entire component before machining, it is now possible to print and machine small increments while the geometry can be easily accessed with standard subtractive tooling.

1.3 Technology Deficiencies

Before hybrid manufacturing can become a main-stream, push-button process, that is easily implementable for industry adoption, there are some technological deficiencies that need to be addressed [6, 12]. Similar to hybrid manufacturing systems, computer aided manufacturing (CAM) software for hybrid manufacturing is equally new to industry and has its own set of deficiencies. CAM software must be able to leverage the full capability of hybrid manufacturing if industry is to adopt hybrid manufacturing. The ensuing sections discuss a few of the technology deficiencies associated with hybrid manufacturing and the accompany CAM software that are addressed in this research.

1.3.1 Wire-Fed Hybrid Manufacturing Systems

Unlike powder-fed systems, wire-fed hybrid manufacturing systems have efficiencies near 98% [6, 10]. These systems are capable of depositing both reactive and un-reactive metals, but are currently unable to create functionally graded materials. The wire deposition process inherently has fewer process control parameters than the powder-fed process and is much more amenable to improved process control. Unfortunately, the deposition start/stop procedure for a wire-fed system is more awkward and prone to process variation issues than powder-fed systems. As seen in Figure 3, excess material deposited at both ends of the deposited bead results in non-uniform depositions. Furthermore, the front face is non-uniform and has many bulges. Although these defects can be mitigated by means of subtractive manufacturing, the addition of the subtractive manufacturing to remove defects results in a disjointed, inefficient process that is not be easily adopted by industry.

Figure 3: Un-Optimized Wire-Deposited Wall

Additionally, controlling the heat during the additive process is crucial for proper build-up, or gradual accumulation of material during the deposition process. The process temperature for laser welding of stainless steels is above the material's melting point of 1500°C, which poses challenges in regard to dimensional accuracy of the component, and to the health of the machine [13]. Furthermore, material properties and residual stresses are driven by cooling rates and temperature gradients, respectively [14]. Thus, poor thermal control can lead to poor mechanical properties.

As previously discussed, the idea of a hybrid process that transitions multiple times between the additive and subtractive processes is an attractive advantage of hybrid

manufacturing. However, the effect of alternating additive and machining operations has yet to be explored.

1.3.2 Computer Aided Manufacturing Software

Analogous to commercial hybrid manufacturing systems, CAM software for hybrid manufacturing has been on the market since 2016. Major contributors include OPEN MIND Technologies (*hyperMILL*), Autodesk (*PowerMill*), DP Technology (*ESPRIT*), and Siemens (*NX*). Each software package has its own specific advantages and disadvantages, but one major limitation that all packages have is their ability to seamlessly transition between the additive and subtractive processes.

Although hybrid manufacturing is a small sector for CAM software packages, there have been tremendous efforts made to improve them over the last few years. Most of these improvements work towards seamless transitions between additive and subtractive path planning as well as making hybrid manufacturing interfaces more user friendly. In the opinion of the researcher, based on extensive use, currently no software package for hybrid manufacturing is superior to the rest.

1.4 Conclusion

Research must be done on designing for hybrid manufacturing before it is adopted by industry. Understanding and leveraging the ability and flexibility of hybrid manufacturing is key for its adoption and successful implementation. Thus, the research presented in this work evaluates the effect of different structures being applied to the interface of similar and dissimilar materials. The research will result in the understanding

of, and the ability to, enhance the mechanical properties of hybrid manufactured components. The ensuing chapter outlines this research project and discusses relevant literature.

CHAPTER 2. PROJECT DESCRIPTION

This chapter outlines the research project on hybrid structures. This project is fundamentally different because it utilizes the subtractive ability of hybrid manufacturing to create varying interfacial geometry. Like carpentry, joints such as a dovetail or tongue and groove can be created at the interface of the added material to enhance material properties. It is hypothesized that these joints can be made stronger by adding these structures when compared to planar interfaces. This research project will result in the standardization of the hybrid manufacturing process development as well as an understanding of the mechanical properties of various interfacial joints created by hybrid manufacturing.

2.1 Introduction

This project is split into three phases. The first phase is the characterization of process parameters. This phase focuses on developing optimized process parameters for hybrid manufacturing. The second phase explores the effect that different hybrid processing variations have on the mechanical properties of produced components. Phase three investigates the concept of hybrid structures. During this phase, tensile test samples are generated with varying material and interfacial geometry. Each test case is evaluated for porosity and hardness, then destructively tested. This dissertation results in an understanding of the effect that the hybrid process and hybrid structures have on the mechanical properties of a manufactured component. This understanding supports hybrid manufacturing's advancement towards industry adoption.

2.2 Phase I – Characterize Process Parameters

The VC-500AM HWD system used in this research project is the first wire-fed hybrid manufacturing system produced by Mazak. Thus, an important part of this project is developing an understanding of the hybrid manufacturing process. The first phase of this project is to develop a working knowledge of the additive process. Table 1 shows the process parameters that are relevant to the wire-fed additive process. It has been identified from early experimentation that some of these parameters, such as the hot wire power, can be coarsely changed without much effect on the process. Other parameters, such as the focal distance and wire feed rate, need to be finely tuned to the process. Since there are nine variables to the process, previous research on DED that outlines process parameter development will be leveraged [15-21].

Table 1: Additive Process Parameters

Parameter	Description	Range [22]	Units
Surface Feed	Traverse speed	0-8000	mm/min
Standoff Distance	Distance between substrate and nozzle	0-N/A	mm
Laser Output	Laser energy output	0-4000	W
Nozzle Gas Flow	Coaxial gas flow through laser to reduce lens contamination	0-50	l/min
Shielding Gas Flow	Inert gas flow to reduce oxidation	0-50	l/min
Wire Feed Speed	Rate of wire extrusion	30-300	in/min
Hot Wire Power	Wire energy input by wire extruder	0-1000	W
Stepover	Distance between consecutively deposited beads	0-N/A	mm
Layer Height	Distance between consecutive layers	0-N/A	mm
Wire Position	Wire position adjustment relative to laser position	N/A	N/A

2.3 Phase II – Hybrid Manufacturing Characterization

The second phase explores the effect that different hybrid processing variations have on the mechanical properties of produced components. Hex walls will be manufactured using two distinct processes: the first being complete additive build-up before machining, while the second will demonstrate hybrid manufacturing's ability to machine a component at different intervals during the additive process.

Hybrid manufacturing allows for additive and subtractive processes to be conducted without breaking machine setup. Thus, the transition between additive and subtractive processes can occur in seconds. Subsequently, the component temperature and use of lubrication (coolant) during the subtractive process can vary during the experiments. An outline capturing the varying processing scenarios for these experiments is shown in Table 2. An example this application would be the manufacturing of a 3 ft tall nosecone. If deposited entirely, it would require an expensive, custom made, 3 ft long boring bar to machine. If deposited in 2-inch increments, it can be machined with a low-cost, off the self, boring bar.

Table 2: Phase 2 Experiments

Experiment	Machining Sequence	Coolant Status
Additive Hex Wall	Machine after cooling	N/A
Additive Hex Wall	Machine while hot	No coolant
Additive Hex Wall	Machine while hot	Coolant
Hybrid Hex Wall	Machine after cooling at intervals	Coolant
Hybrid Hex Wall	Machine after cooling at intervals	No Coolant
Hybrid Hex Wall	Machine while hot at intervals	No Coolant
Hybrid Hex Wall	Machine while hot at intervals	Coolant

2.4 Phase III - Hybrid Structures

The third phase is the development and demonstration of the hybrid structures in a plane wall configuration. Starting with a substrate block, a hybrid structure will be applied at the interface where deposition will occur. Examples of these structures are shown in Table 3 and further discussed in Chapter 5. These structures were selected because they exemplify the full capability of hybrid manufacturing. This deposition may be between similar or dissimilar materials. A graphical representation of this process is shown in Figure 4.

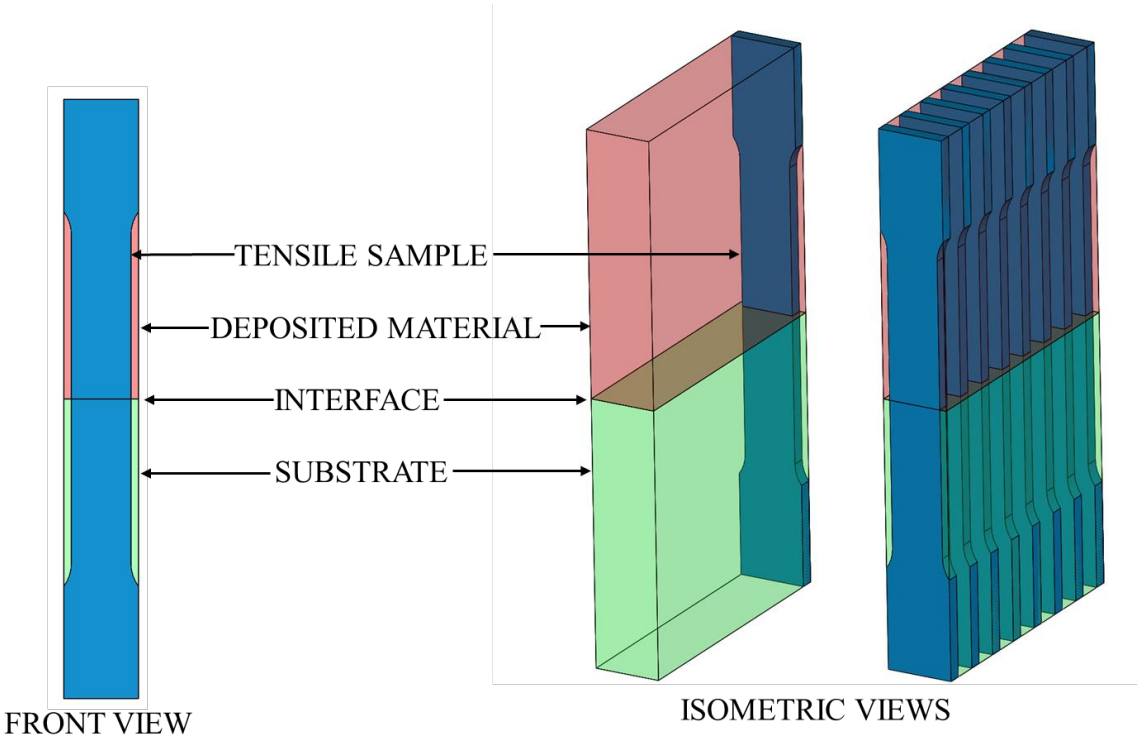

Figure 4: Sample Creation Process

Once deposition is complete, the tensile samples conforming to the ASTM E8/E8M-16a standard for tension testing of metallic materials [23] will be machined from the resulting

block for testing. It is noted that the importance of the mechanical testing results is not comparing them to those of wrought material, but to compare the structures to one another.

Table 3: Phase III Experimental Roadmap

Structure		Deposited Material	Substrate Material - 1	Substrate Material - 2
Planar	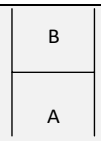	316L Stainless Steel	316L Stainless Steel	Gray Cast Iron
Angled	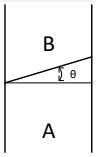	316L Stainless Steel	316L Stainless Steel	Gray Cast Iron
Scalloped	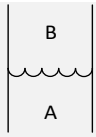	316L Stainless Steel	316L Stainless Steel	Gray Cast Iron
Tongue and Groove	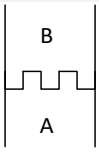	316L Stainless Steel	316L Stainless Steel	Gray Cast Iron
Dovetail	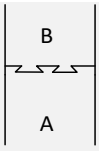	316L Stainless Steel	316L Stainless Steel	Gray Cast Iron

2.5 Conclusion

This project will develop and characterize hybrid manufactured structures of similar and dissimilar materials. Specifically, this project will look at how the subtractive capabilities of hybrid manufacturing can be leveraged to enhance the mechanical properties of the resulting component through the use of interlocking interfacial features. Traditional additive manufacturing is constrained by its inability to deposit material on non-planar geometry. Thus, the utilization of hybrid manufacturing's capabilities will allow research to be conducted on different geometrical structures that form the surface of the substrate.

It will be seen that this project is fundamentally different from other previous work as this project embraces hybrid manufacturing's ability to seamlessly alternate between subtracting and depositing material.

CHAPTER 3. HYBRID PROCESS DEVELOPMENT

Although additive and subtractive manufacturing are not new concepts, the combination of the processes for hybrid manufacturing is a relatively new research area. Specific to laser-wire deposition, only one commercial system platform exists. This chapter focuses on the process development using the commercially available laser-wire hybrid manufacturing, the Mazak VC-500A/5X AM HWD.

3.1 Introduction

Although it is unclear specifically when hybrid manufacturing was first developed, some of the earliest works were documented and published in the mid to late 1990s by Klocke and Wirtz [24]. The most popular research approach to hybrid manufacturing has been to integrate a blown powder laser DED head into a vertical or horizontal machining center [11, 24-29]. This chapter presents a literature survey regarding process development for hybrid manufacturing and provide methodology and a discussion on the laser-wire process for hybrid manufacturing was developed.

3.2 Literature Review

A review of hybrid manufacturing was written by Lorenz and Jones that includes a brief history of hybrid manufacturing from inception to the first release of a commercially available hybrid manufacturing system [6]. Their development timeline is shown in Table 4. This table the various research groups that have contributed to the field of hybrid manufacturing. The first known instance of hybrid manufacturing is unknown, but it is typically designated to the Laser Aided Manufacturing Process (LAMP) at the University

of Missouri. Furthermore, this table shows the machine tool type and processing head mounting position for the respective research system. All the outlined systems are blown powder directed energy deposition heads retrofitted to existing CNC platforms. This further accentuates how this research is fundamentally different than all other research in the field.

Table 4: Development of Hybrid Manufacturing [6]

Date	Process Name	Institute or Company	Machine tool type	Processing head mounting position	
1996	Combined Metal Build-Up (CMB)	Fraunhofer Institute of Production Technology & Fraunhofer Institute of Laser Technology	3-axis vertical	Fixed to side of spindle	[24]
1990's	Laser Aided Manufacturing Process (LAMP)	University of Missouri	5-axis vertical	Fixed to side of spindle	[5]
2000	Selective Laser Cladding (SLC) and milling	National Taiwan University of Science and Technology	3-axis vertical	Fixed optics (separate station)	[30]
2004	Hybrid Manufacturing	Joanneum Research Forschungsgesellschaft mbH, Austria	5-axis vertical	Fixed to side of spindle	[31]
2006	System and method for fabricating and repairing part	Southern Methodist University	Multi-axis	Attached to a robot	[32]
2008	Hybrid Manufacturing	De Montfort University & The Manufacturing Technology Centre	3-axis vertical	In spindle stored in tool magazine	[33]
2013	Hybrid Manufacturing	Hamuel & Hybrid Manufacturing Technologies	Retrofit	In spindle stored in tool magazine	[34]
2013	Hybrid Manufacturing	DMG Mori	5-axis vertical	In spindle stored in own compartment	[35]
2014	Hybrid Multi-Tasking	Mazak & Hybrid Manufacturing Technology	5-axis horizontal	In spindle stored in tool magazine	[36]

In the years following DMG Mori and Mazak both releasing their hybrid manufacturing systems in 2013 and 2014, respectively, other large machine tool companies such as Okuma, Hermle, and Matsuura now offer hybrid manufacturing machine tools [37].

Furthermore, there are companies such as Hybrid Manufacturing Technologies and 3D-Hybrid that specialize in retrofitting any machining center for hybrid manufacturing [37].

It is reported by Nau [15] that the implementation of any technology to create a hybrid system is divided into the following four activities: (1) process and parameter development; (2) integration into a commercial manufacturing environment; (3) evaluation and testing; (4) production. Previously, developments of hybrid manufacturing processes were mostly based on intuitively or randomly found solutions, such as simply putting an additive system on a machine tool [15]. From reviewing the literature, it is clear that a specific methodology for hybrid manufacturing process development does not yet exist [6, 15]. One reason for this gap in the literature can be attributed to many of these systems being retrofits or one-of-a-kind systems such as those developed at universities for research purposes [6]. This research uses a system that is commercially available, mitigating challenges associated with retrofitting a standard machine tool. Furthermore, unlike many additive manufacturing systems, machine tools have been developed for stiffness. Many additive systems are compliant and do not provide accurate motion. Thus, it makes sense to integrate additive manufacturing into a machine tool rather than integrating machining into an additive manufacturing system. This research can provide a standard for process development of these newly developed systems that will be common across the industry.

3.2.1 Hybrid Manufacturing Workflow

With the release of commercially available 5-axis hybrid manufacturing systems, a methodology for hybrid manufacturing workflow needs to be developed. Two aspects of this research are to embrace the ability to use subtractive manufacturing and non-planar

deposition. Traditional additive manufacturing is done with 2-axis movements at a certain stepover to create overhangs. With hybrid manufacturing, it was proven by Ruan [38] that it is possible to achieve curved structures by generating non-uniform layer slices. This was done by first depositing a uniform layer, then modifying it to be non-uniform by subtractive manufacturing. The resulting structure is shown in Figure 5.

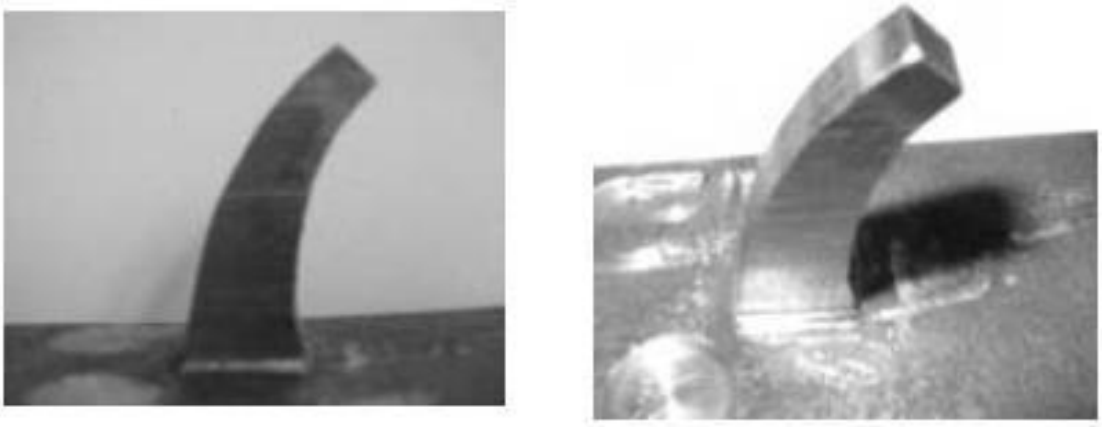

Figure 5: Hybrid Manufactured Structure [38]

Other researchers such as Paris [39] and Ma [40] evaluated how the decision making process of hybrid manufacturing can affect the overall part geometry. As shown in Figure 6, it is apparent that care must be taken when developing the deposition tool path. This figure shows that different programming strategies on an identical component have different outcomes. Although each strategy resulted in the proper overall shape, defects from the start/stop process can be seen. These defects and their effect on the component's performance need to be taken into consideration when designing the toolpath strategy. With the existence of CAM packages capable of driving hybrid manufacturing systems, consistency and standards similar to polymer additive manufacturing can developed and utilized [3].

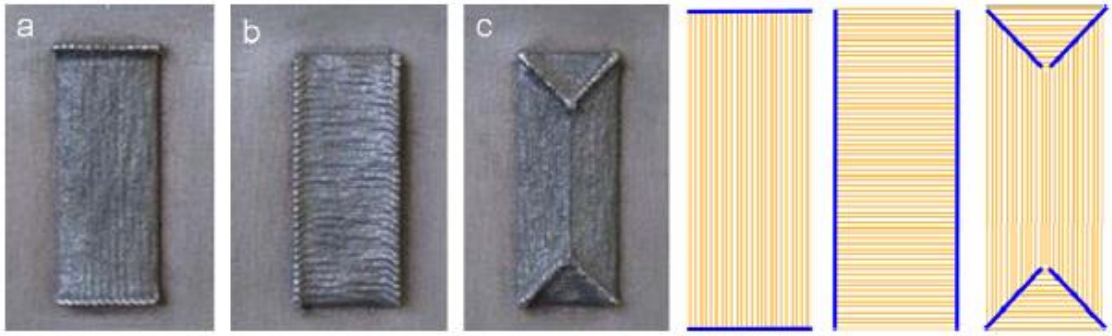

Figure 6: Different Laser Scanning Patterns [40]

3.2.2 Process Parameters for Additive Manufacturing

Understanding the relationship between the process parameters and the material properties is crucial to make additive manufacturing competitive with traditional manufacturing processes [16]. There has been significant work done in the area of understanding and controlling process parameters for additive manufacturing and their influences on resulting geometry and material characteristics. Much of the work is specific to only the additive process and focuses on metal powder as the feedstock. A substantial amount of this previous work is applicable to the laser hot-wire process investigated in this dissertation; yet, there has been little work performed on the baseline or optimal process parameters of this process [17]. Most of this work is on single bead deposits such as a study on laser hot-wire cladding by Liu et al. [18].

One method to develop process parameters was done by Hansel et al. where they determined optimal process parameters by using the Taguchi Method. This method utilizes orthogonal arrays to conduct experiments to optimize a process [19]. Though it only required nine experiments to optimize the system, this study relied on “process know-how” and only evaluated three different processing conditions for four parameters.

To achieve better quality assurance and control in additive manufacturing processes, correlations between the process parameters and the output parameters must be investigated [20, 21]. Since there are many process parameters in an additive manufacturing processes, it is difficult to build correlations between the inputs and outputs [20]. Much of the literature in DED processes mainly focus on temperature monitoring as the process parameter of choice [41, 42].

It has been shown that thermal gradients can also have detrimental effects on DED processes. Manufactured components with "dishing" or "humping" geometry is due to rapid hydrodynamic motions known as Marangoni Flow [43]. This is caused by thermal gradients and associated surface tension. One of the most fundamental surface quality phenomena researched is the "staircase effect," which is a result of the layer-wise approximation of part geometry [3]. These phenomena discussed are shown in Figure 7.

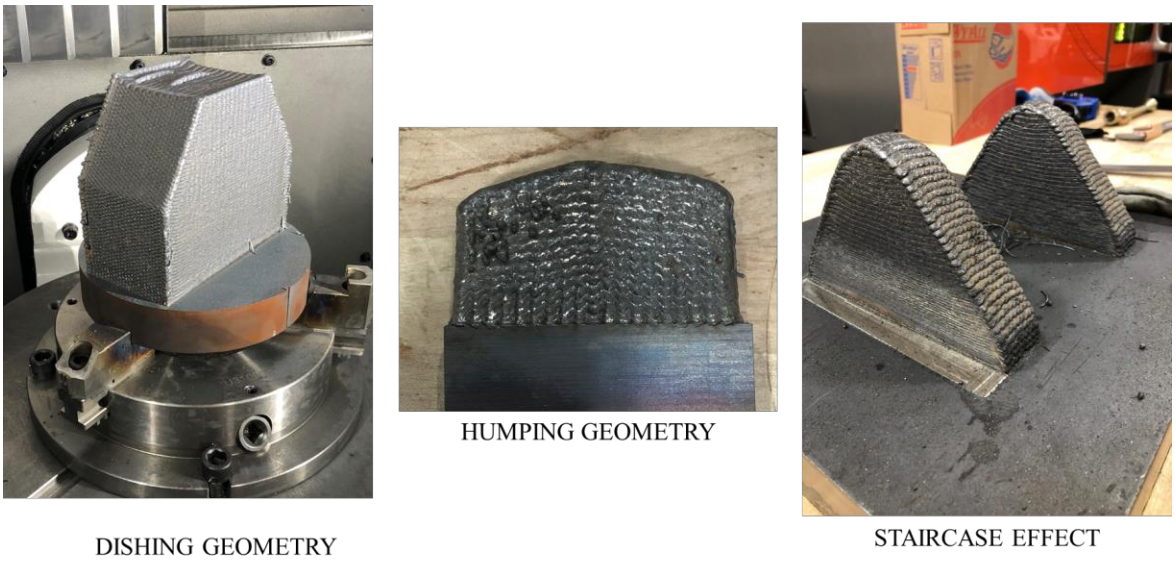

Figure 7: Effects of Thermal Gradients on DED Processes

With regards to the precision of the deposited geometry, the resolution is dictated by the melt-pool geometry, or geometrical shape of the liquid metal as it is being deposited [44-46]. This melt-pool geometry is affected by laser power, surface feed, material feedrate, stepover, layer thickness, and feedstock [3, 47-50]. As seen in powder bed fusion, the thermal history of the build can affect the melt-pool geometry since adjacent, previously heated material can be re-melted on adjacent toolpath tracks [42, 51-54]. This error compounds over the build and leads to a change in the standoff distance between the nozzle and substrate, which also has an effect on the melt-pool geometry [45].

3.2.3 Machining of Additive Components

Additive manufacturing allows for the rapid manufacturing of complex geometries that cannot otherwise be manufactured. However, there is still a significant need for subsequent machining operations of these components [55-57]. Subsequent machining is necessary dur to a number of reasons including providing features and datum surfaces that cannot be accurately generated via the additive process and improving the surface finish of the produced component. Understanding the machining process of additively produced components is a new area that has little relevant research [58].

A study on the machinability of 316L stainless steel by Guo et al. indicated that cutting forces are anisotropic when compared to the deposition orientation [59]. In this study, two orientations were evaluated: one variation where tensile samples were produced along the deposited layers (0°), and the other being across the deposited layers (90°). As shown in Figure 8, it can be seen that the cutting forces measured by a dynamometer were

significantly higher for the case where machining occurred along the layer, which is attributed to the increased hardness [59].

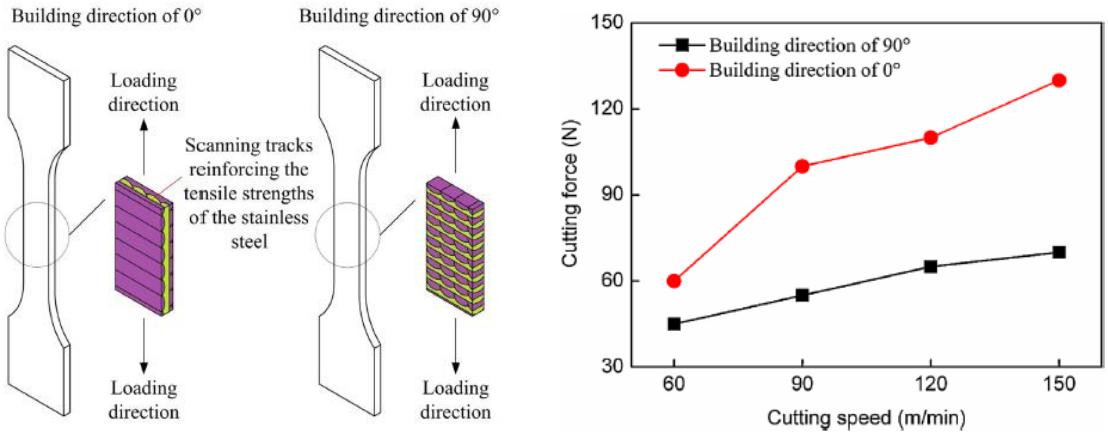

Figure 8: Cutting Speed/ Force Relationship on Deposited Stainless Steels [59]

Similar results were seen by Montevecchi et al. when evaluating cutting forces of additively manufactured H13 tool steel [57]. In this study, slotting cutting forces of additively manufactured components from both wire and powder feedstocks were compared to wrought material. It was seen that the tangential cutting coefficients were higher for the wire feedstock produced component, but the radial cutting coefficients were higher for the powder feedstock produced component. Again, these higher cutting forces are attributed to the increased harness measurements of the produced material [57].

3.3 Methodology

The methodology used to develop the process parameters for hybrid manufacturing consists of various experiments. Before any deposition experiments can occur, the system must be aligned, ensuring omnidirectional deposition, and precise machining of additive parts. Subsequent to alignment, three experiments consisting of single beads, stepover

beads, and cubes will be conducted to determine the additive settings, stepover, and layer height respectively. Furthermore, identified defects from incorrect process parameters are characterized and mitigation strategies are provided. Finally, slicing and machining strategies researched, and lessons learned, are outlined. All experimental setups in this work for process parameter development employed 1.143 mm (0.045”) diameter 316L stainless steel wire and was deposited on A108 steel stock.

3.4 Results

This section presents the setup and results from various experiments conducted to develop process parameters for hybrid manufacturing. The outcome of these experiments provides the foundation for common hybrid manufacturing process development.

3.4.1 Alignment Testing

Omnidirectionality is critical to a successful additive manufacturing process. Unlike other welding processes such as tungsten inert gas (TIG) welding or robotic welding where directionality is often kept constant, additive manufacturing often occurs in two directions and can sometimes occur in all directions. For example, the wire interfaces with the weld-pool from all directions from a Lagrangian perspective when depositing a cylinder.

As shown in Figure 9, the laser system is outfitted with a low power laser spot generated for alignment. This laser spot is generated from the same optics as the welding laser but has a different spot diameter. The contact tip is mounted to a linear stage that can be minimally adjusted for alignment purposes. This alignment should be done at the proper

standoff distance (25.4 mm per manufacturer's recommendation) from a qualified surface. When properly aligned, the wire enters the weld-pool at the center of the laser spot.

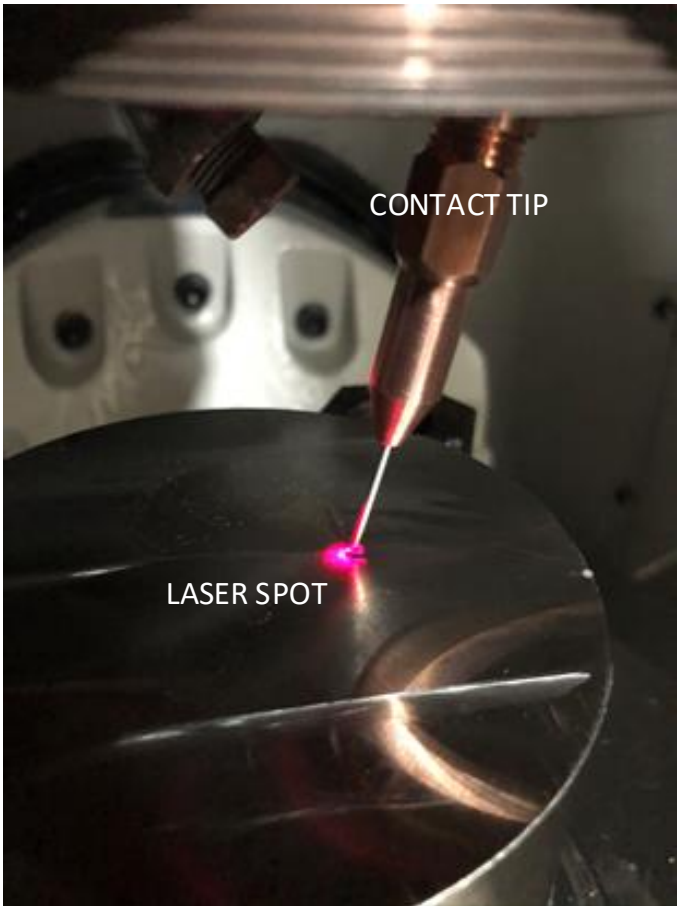

Figure 9: Laser / Wire Interaction

As shown in Figure 10, it is desired to have the wire centrally located to the weld-pool to mitigate any directionality issues. Since the temperature varies across the weld-pool, having the wire centrally located results in a consistent processing temperature regardless of direction.

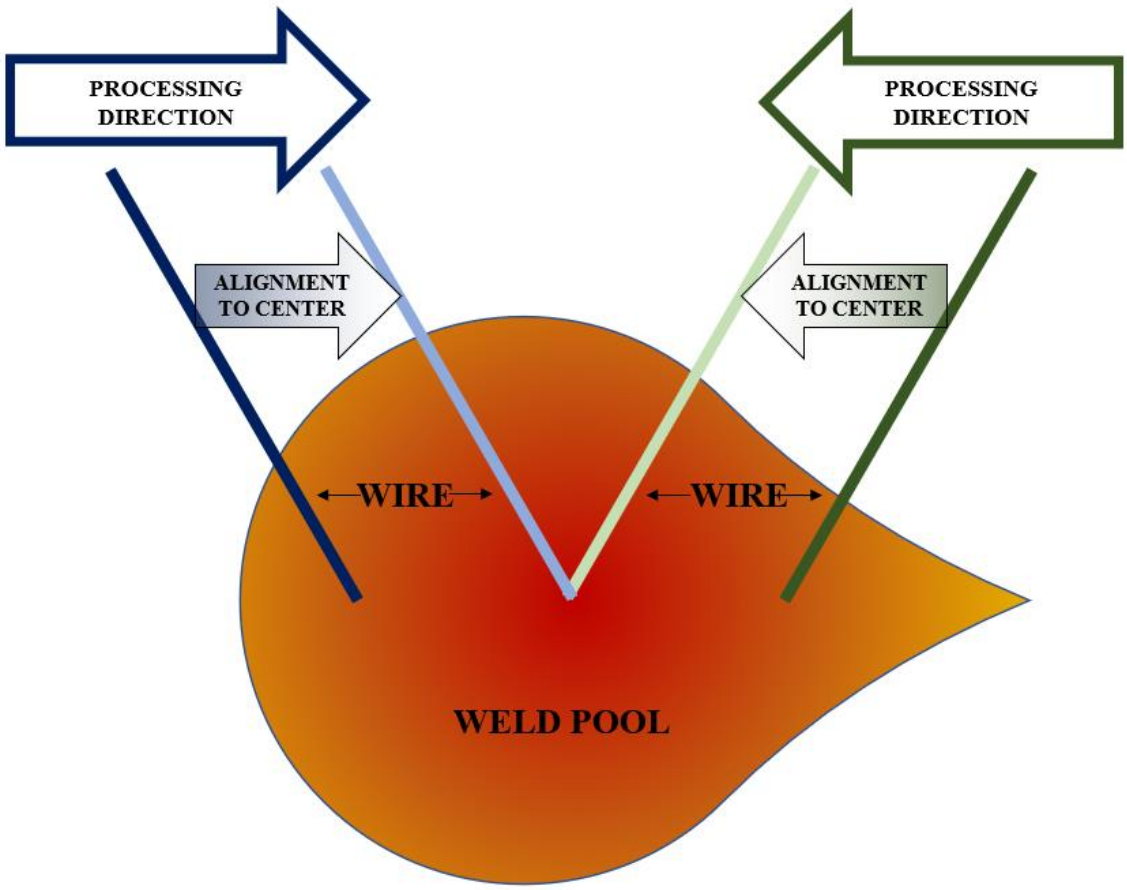

Figure 10: Weld-pool Wire Alignment

To test for proper alignment, a series of single beads should be deposited bi-directionally along both the X and Y axes. Furthermore, as shown in Figure 11, circles should be deposited in both clockwise, and counterclockwise strategies. These tests mimic the wire entering the weld pool from all directions and check the omnidirectionality of the wire alignment.

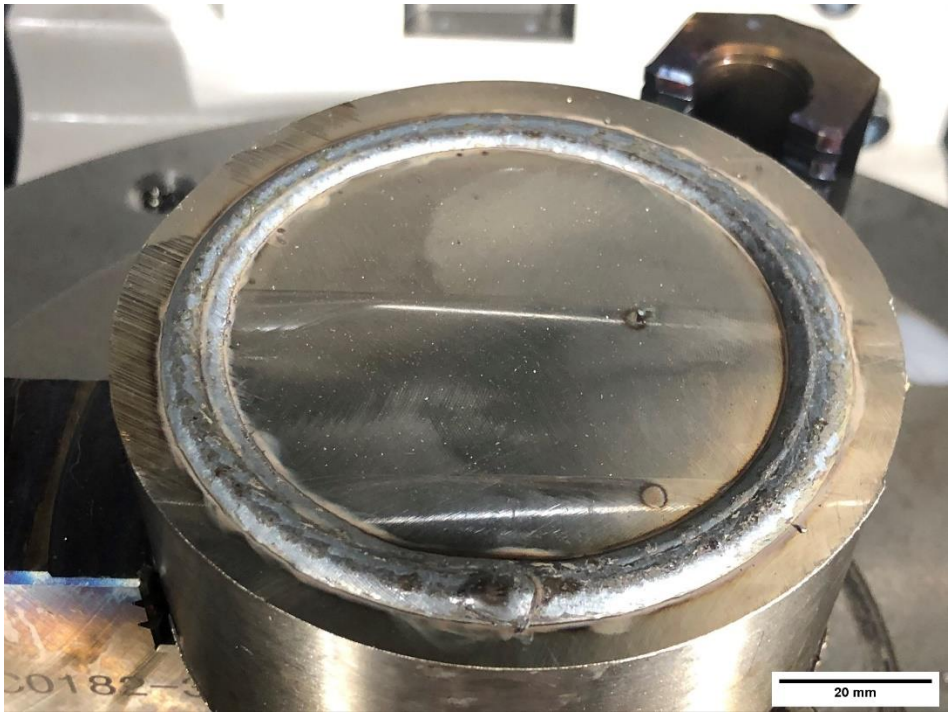

Figure 11: Circle Alignment Deposition

3.4.2 Single Bead Experiments

Before subtractive or complex additive strategies can be developed, additive parameters for singles beads must first be understood. If hybrid manufacturing is to be adopted by industry, it must be optimized to have high deposition rates while maintaining process stability. Thus, the first set of experiments executed in this research address the optimization of single beads for maximum deposition rates while maintaining a stable process.

Since there is a wide range of combinations that result in acceptable welds, a common variable called *Linear Energy of Deposition (LED) [J*s/mm^4]* is proposed to characterize each bead. This proposed metric allows the machine user to compare a wide range of parameter setting combinations by means of a single number. Excluding standoff

distance and gas flow parameters, this proposed variable determines the amount of energy inputted to the wire relative to the traverse speed. This relationship is shown in Equation (1) where E is laser power, HWP is the hot-wire power, A_w is the area of the deposited wire, WFS is the wire feed rate, and f is the traverse feed rate.

$$LED = \frac{\left(\frac{Power\ Input}{Volumetric\ flow\ of\ wire}\right)}{Machine\ Traverse\ Speed} = \frac{\frac{E + HWP}{A_w * WFS}}{f} \quad (1)$$

This relationship was developed so that different parameter configurations could be easily compared to one another through a common platform.

A demonstration of this is shown in Table 5, where wire feed rate and traverse feed rate were progressively modified to find the optimal linear energy of deposition for a set of parameters. These experiments were qualitatively analyzed for geometry uniformity and deposition stability.

Table 5 Linear Energy of Deposition Experiment Settings

	Wire Feed Rate [mm/min]	**Traverse Feed Rate [mm/min]**	**Hot-Wire Preheat [W]**	**Laser Power [W]**	**Linear Energy of Deposition [J*s/mm^4]**
1	5080	762	300	4000	3.90
2	4445	762	300	4000	4.45
3	4445	1500	300	4000	2.26
4	5080	1500	300	4000	1.98
5	5715	1500	300	4000	1.76
6	3810	1500	300	4000	2.64
7	3175	1500	300	4000	3.17

Figure 12 shows the resulting deposited beads generated during these experiments. It can be seen in the figure that many of these beads have discontinuities from the wire

being pushed out of the melt-pool due to excessive wire feeding. This was also visually apparent to the operator during the experiment and could be seen in the weld-pool video recordings. During these experiments, these beads were visually examined for width uniformity from start to finish. From this examination, it was observed that beginning and end of each bead is wider when compared to the center. Such a result is undesirable in additive manufacturing as a uniform weld-bead is necessary to mitigate porosity and produce geometrically accurate components.

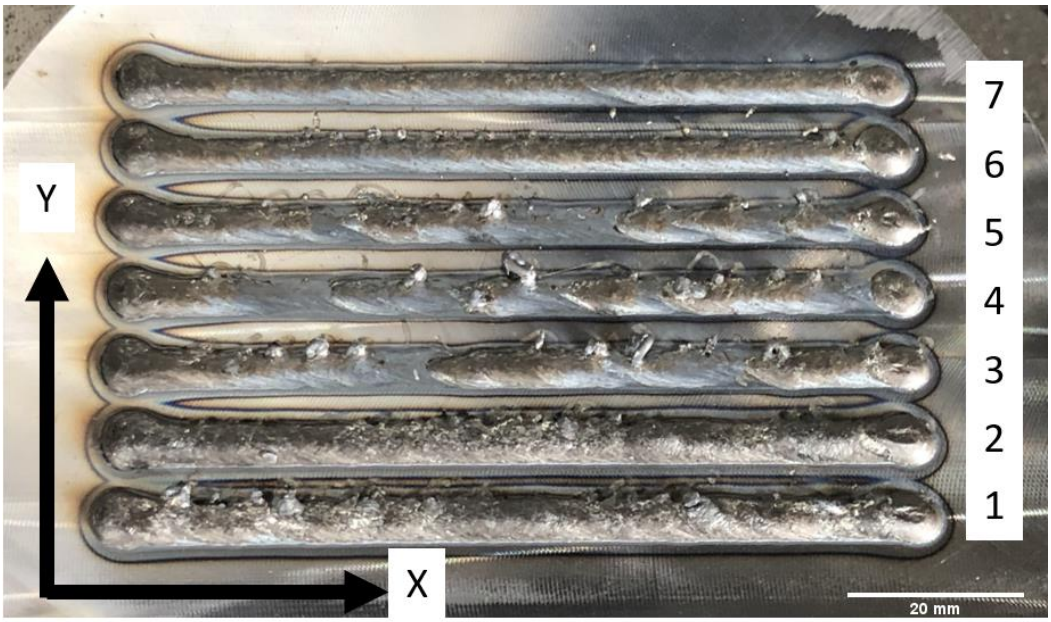

Figure 12: Single Bead Experiments

Subsequent experiments were conducted to find the maximum deposition rate while keeping the process stable. As shown in Figure 13, some of the resulting weld beads in the experiments appear identical. To augment the data collected, a weld camera (Baselor acA800-200gc) was mounted to the spindle to monitor the weld-pool during deposition. This close-up view of the process provides the ability to monitor the stability of the process.

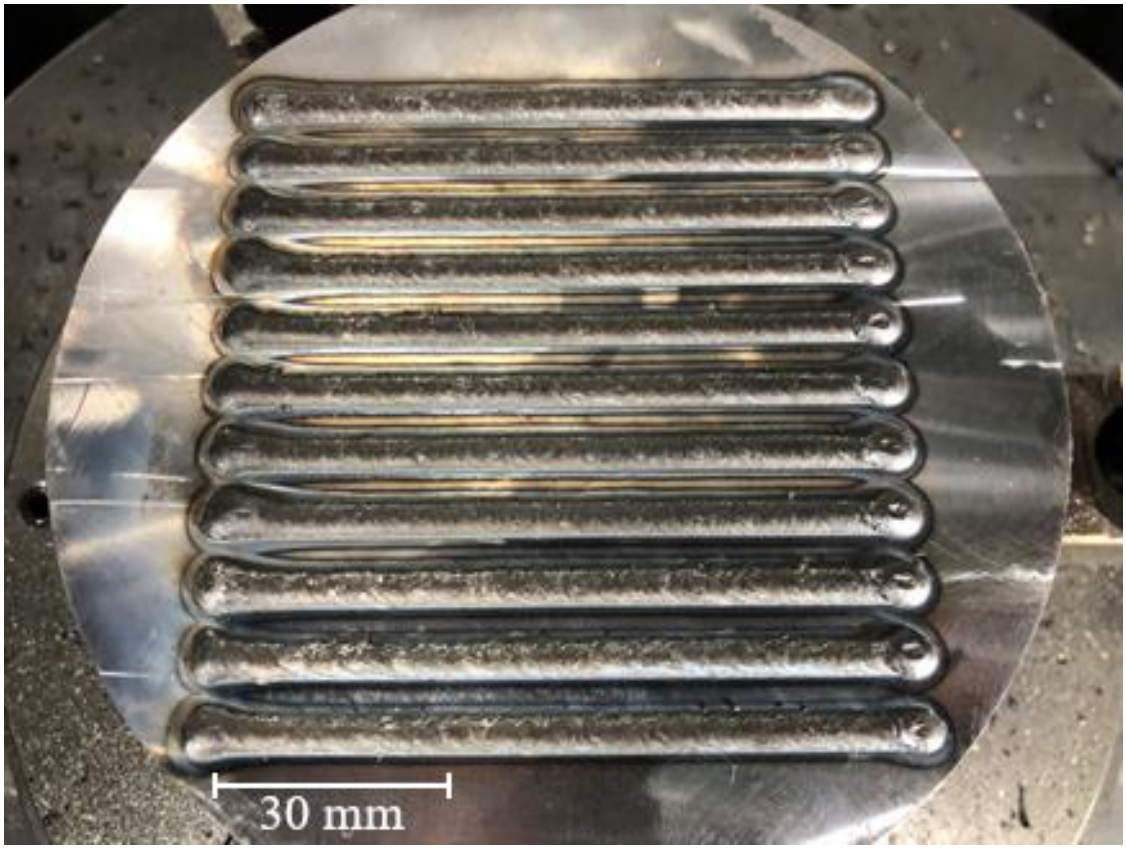

Figure 13: Single Bead Weld Camera Experiments

As shown in Figure 14, the dynamics of the weld-pool during deposition can be characterized via data gathered from the video. The left image shows a discontinuity in the wire due to either wire underfeeding or overheating the wire before it reaches the weld-pool. This defect can cause porosity in components due to skips in the weld. The center image shows the wire being displaced to one side during the deposition. This often results in a swirling motion that is due to wire overfeeding or underheating. The right image shows a stable process. The optimal set of parameters from these experiments that give the maximum deposition rate with a stable process is given in Table 6.

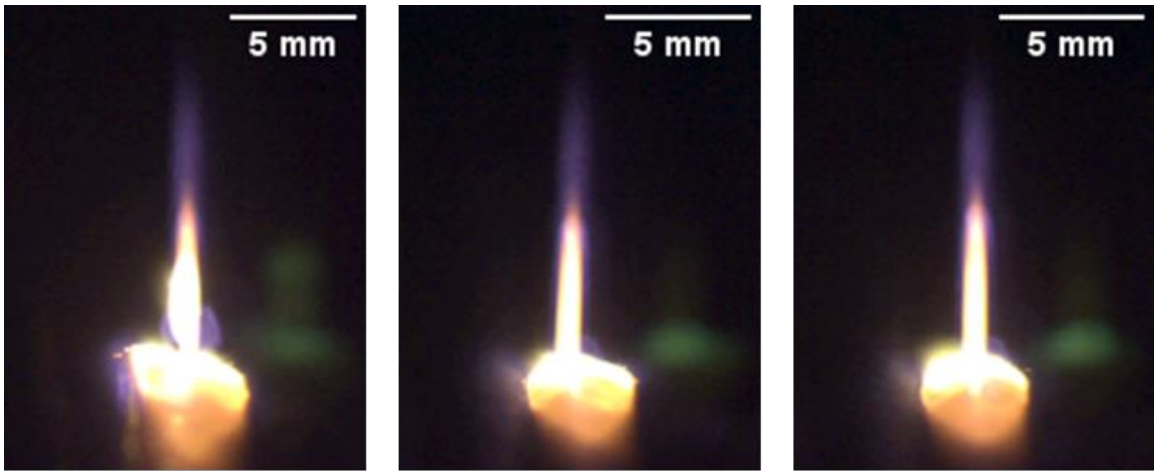

Figure 14: Weld-Pool Wire Placement

The single beads produced with optimal parameters were evaluated by X-ray computed tomography for internal porosity using a ZEISS METROTOM 800. Figure 15 shows a cross-sectional image generated via tomography near the center of a bead. It was determined that no porosity is present in any of the single beads that were characterized.

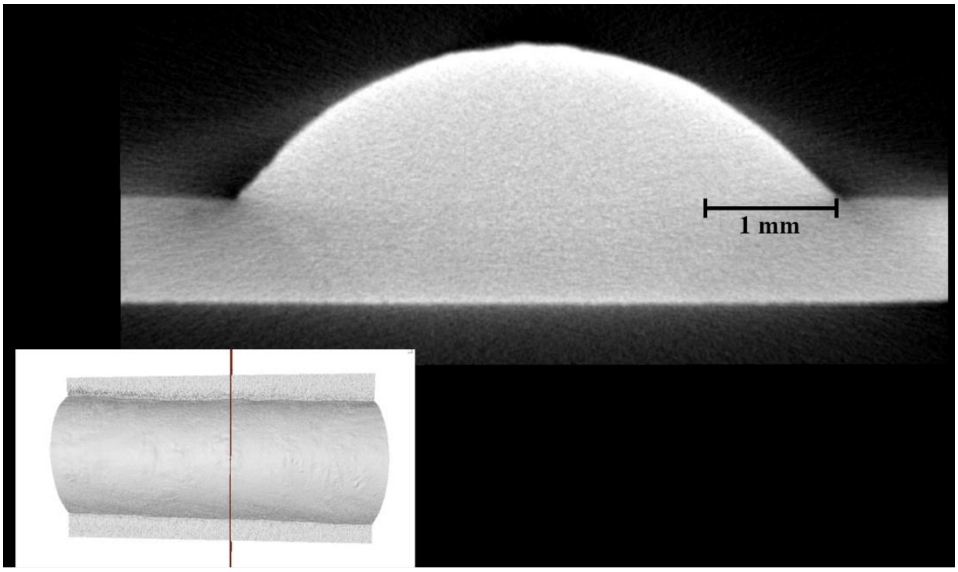

Figure 15: X-Ray Computed Tomography of Optimized Single Bead

3.4.3 Stepover Characterization

Once the parameters for single beads were determined, experiments were conducted to characterize stepover distance. Stepover is the distance between the centerlines of two adjacent beads. This technique is needed when generating a raster pattern, the programmed motion path to sequentially sweep a two-dimensional area and fill it with material. This setting affects porosity, layer height, and deposition time. A general rule-of-thumb for this value is 60%-80% of the bead width [60]. The results of an experiment conducted to characterize this is shown in Figure 16. Four beads in a flat pad configuration were deposited at varying stepover values to qualitatively characterize the flatness of the layers. Since the optimum stepover is a factor of the weld geometry, the experiment should be completed each time process parameters that affect the resulting geometry are varied. The selected stepover of 70%, which yielded the most consistent deposition with regards to flatness, is given in Table 6.

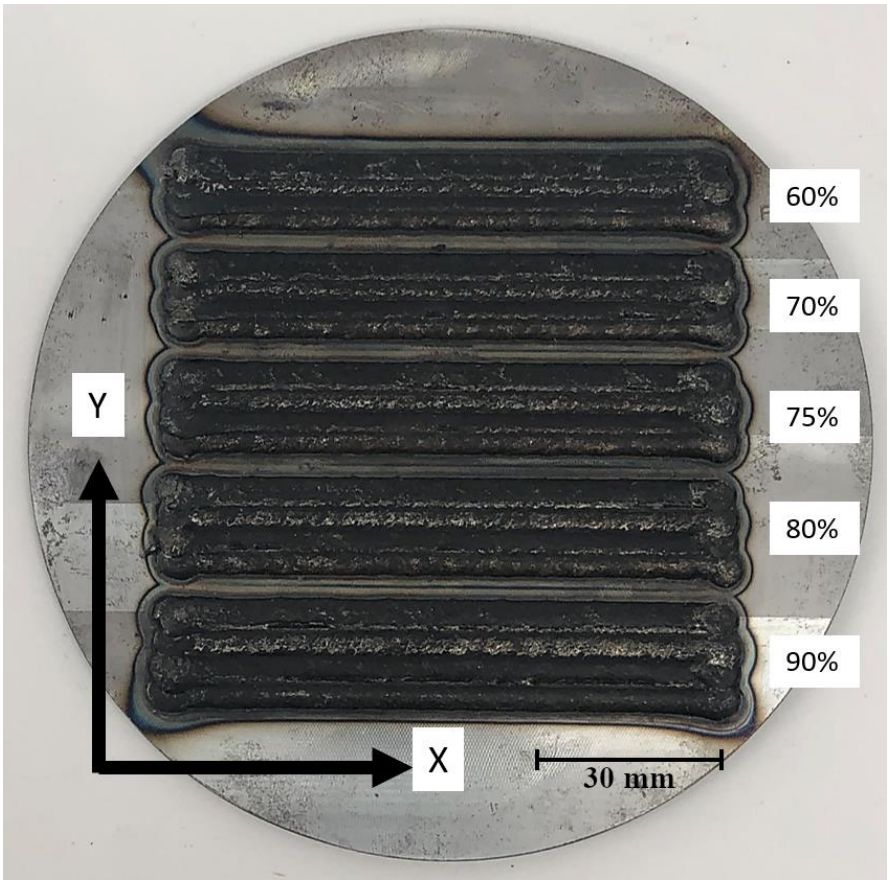

Figure 16: Stepover Characterization

3.4.4 Layer Height Characterization

Once the optimum stepover was identified, cubes with a varying number of layers were produced to characterize layer buildup. It is important to have proper layer heights throughout a build. As previously discussed, wire alignment occurs at a specified standoff distance from a qualified surface. During an additive build, the programmed layer height is used to determine the standoff distance. As shown in Figure 17, the standoff distance is also important in keeping the wire alignment constant.

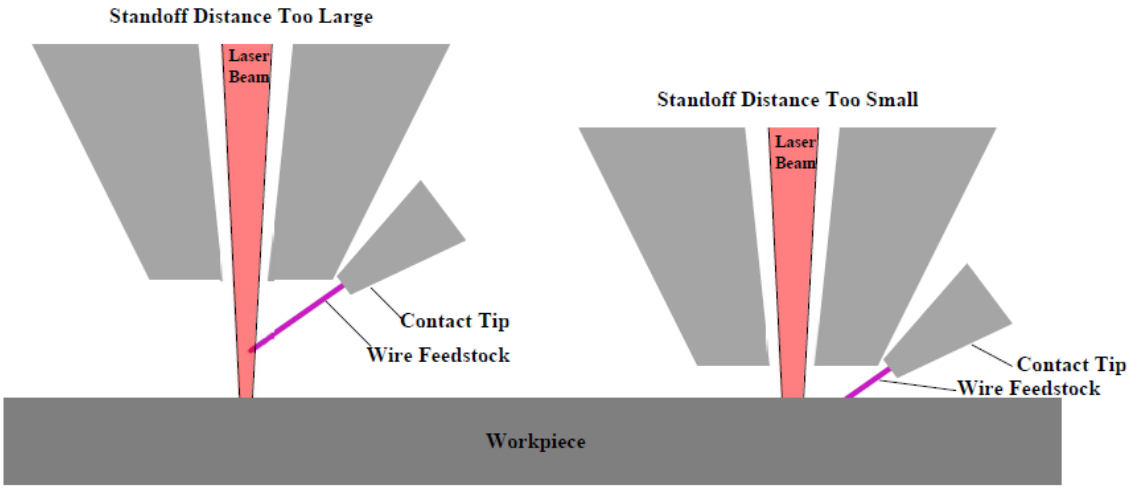

Figure 17: Standoff Distance Adjustment

For this experiment, as shown in Figure 18, nine cubes were deposited varying from two to eighteen layers with an initial layer height of 1.5mm. This initial layer height was measured from the previous stepover experiment. The toolpath was rotated 180º between layers, and a raster pattern with no profile pass was used. All nine cubes were printed simultaneously, which permitted requisite cooling between subsequent layers.

Figure 18: Layer Height Experiment

The geometries of the cubes were inspected using a Zeiss Duramax coordinate measuring machine (CMM). The results of this experiment, shown in Figure 19, provide insight into the required distance between each deposited layer of a structure. The slope of the best-fit line provides the average layer height for each cube. As seen in Figure 19, the measured layer height was 1.43 mm.

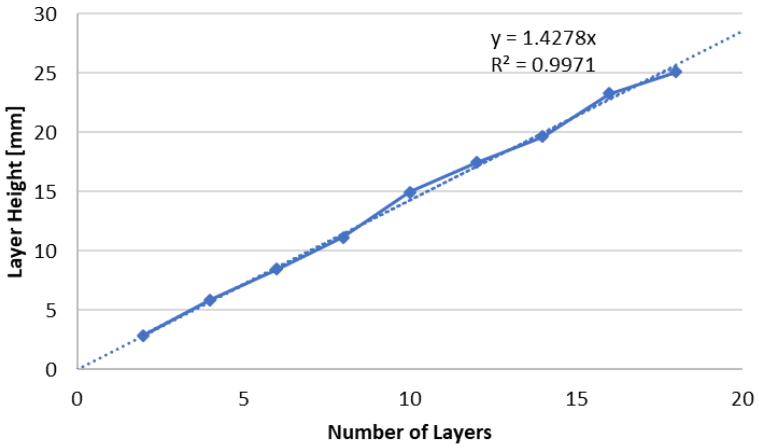

Figure 19: Layer Height Characterization

From these three process development techniques, the recommended process parameters were determined. These parameters listed in Table 6 are specific to the chosen material feedstock composition, but also serve as a viable baseline for other materials. Furthermore, ongoing research demonstrates that these process parameters are geometry-specific, so printing different geometries may cause unpredictable effects when evaluating process parameters. For example, solid components have a higher thermal mass and require less laser power when compared to thin walled geometries. Thus, this highlights that it is advantageous to research adaptive processing abilities rather than process parameters for simple geometry. This is further evaluated in the Discussion section of this chapter.

Table 6: Process Parameters

Parameter	Setting
Traverse Feed Rate	1067 mm/min
Wire Feed Rate	4445 mm/min
Hot-Wire Preheat	420 W
Laser Power	2750 W
Nozzle Gas	20 L/min
Shielding Gas	20 L/min
Linear Energy of Deposition	2.35 J*s/mm^4
Stepover	70% (3.29mm)
Layer Height	1.43 mm

3.4.5 Slicing Strategies

In addition to having effective process parameters, it is important to have an effective toolpath strategy. G-Code, which is produced by a computer aided manufacturing (CAM) software, is used to generate the coordinated axis trajectories of the machine tool.

Like hybrid manufacturing equipment, CAM software for hybrid manufacturing is also new to the commercial sector.

For buildup of large parts, it is important to have uniform layer thicknesses. Furthermore, build-up during the additive process is directionally dependent. Figure 20 demonstrates that bi-directional deposition of the weld material is critical in achieving uniform layer thickness. The figure shows results of two separate experiments where a plane wall is generated that is three beads wide and 152.4 mm (6”) tall. The wall shown in Figure 20a is generated by laying down material while traversing in a single direction. This is an inefficient deposition strategy because significant cycle time is wasted when the additive head repositions to the repeated starting location between each deposited bead. Thus, it causes the height of the resulting geometry to be non-uniform. However, if the deposition is bi-directional and the traverse feed is reversed for each layer, the resulting geometry is uniform as shown Figure 20b. For the two experiments shown, the bi-directional deposition reduced the cycle time by 57% since most of the cycle time is spent depositing.

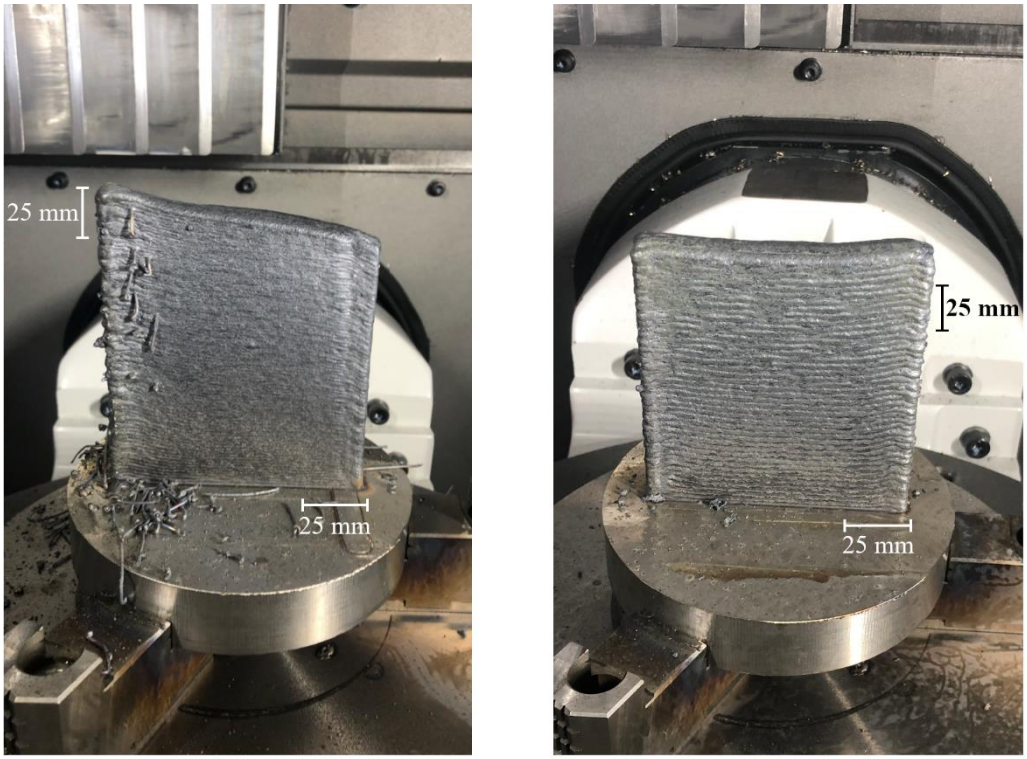

a) Unidiretional Deposition b) Bidirectional Deposition

Figure 20: Plane Wall Deposition Strategies

It is noted that non-uniform buildup can be mitigated with hybrid manufacturing's ability to machine away unwanted buildup to generate a flat surface. This process, called requalification, increases the overall cycle time, reduces material utilization efficiency, and yields a discontinuity in the thermal properties. Determining the effects of requalification on the mechanical properties of the produced component is discussed in the ensuing chapter.

A useful toolpath generation strategy is the variation of deposition start points. This is a common strategy in the additive manufacturing industry to improve geometric accuracy of manufactured components [61]. A defect due to buildup is introduced each time there is a discontinuity (start/stop) in the deposition path. Thus, it is important to vary

the location of these discontinuities for each layer. This defect is due to the dwell associated with the communication between the additive and motion systems. The defects resulting from path discontinuities and the associated mitigation strategy are shown in Figure 21.

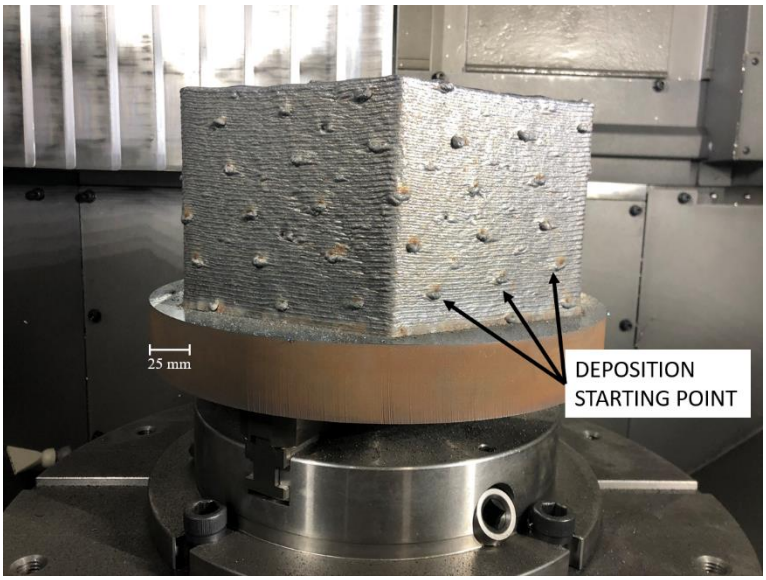

Figure 21: Importance of Layer Rotation

It is noted that these defects can be removed via machining after the deposition process for a layer is completed. This is a benefit of hybrid systems, but the resulting varying depth-of-cut during the subtractive process can result in tool chatter (poor surface finish) and increased cycle time due to the need for subsequent roughing passes.

Traditional slicing strategies break components up by z-level, but for thin-walled negative curvature geometry, the concept of chord slicing has been shown to be beneficial. As shown in Figure 22, a vase with a large flare was produced using this strategy. The overall component is 175 mm tall and is 200 mm in diameter.

Figure 22: Chord Sliced Component

A representation of chord slicing is shown in Figure 23. The red lines correspond to traditional z-level slicing while the blue lines correspond to chord slicing, where the layers are evenly spaced along a length instead of a height.

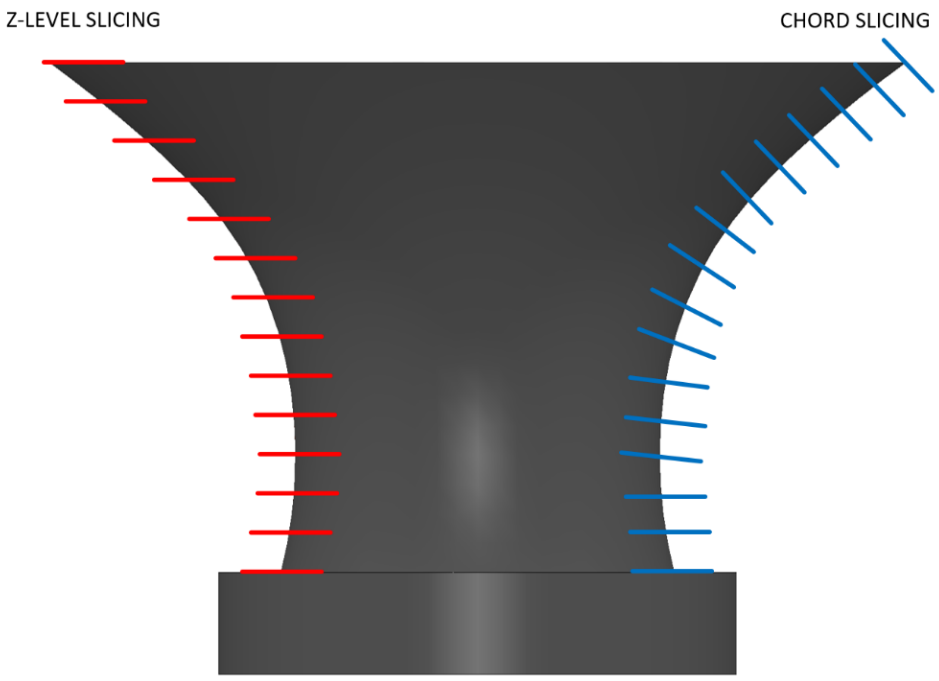

Figure 23: Chord Slicing

For a complex geometry such as a propeller blade shown in Figure 24, the concept of non-uniform layer heights was evaluated. The curved geometry requires the component to be built in sections. Furthermore, the varying cross-section, overall size, and complexity of the geometry does not lend itself to chord slicing strategies.

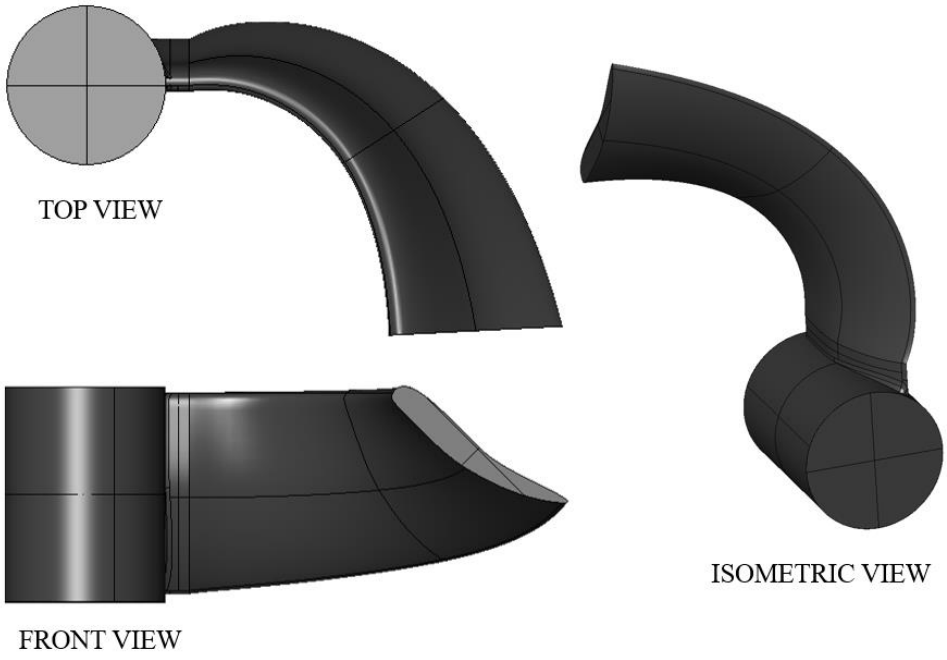

Figure 24: Propeller CAD Model

To address this issue, non-uniform layer slices were generated by breaking the component into multiple sections. In other words, the geometry was treated as multiple parts instead of one large one. The toolpath trajectory for the entire part can be seen in Figure 25. The various colors correspond to individual toolpath trajectories that can be combined to produce the entire part.

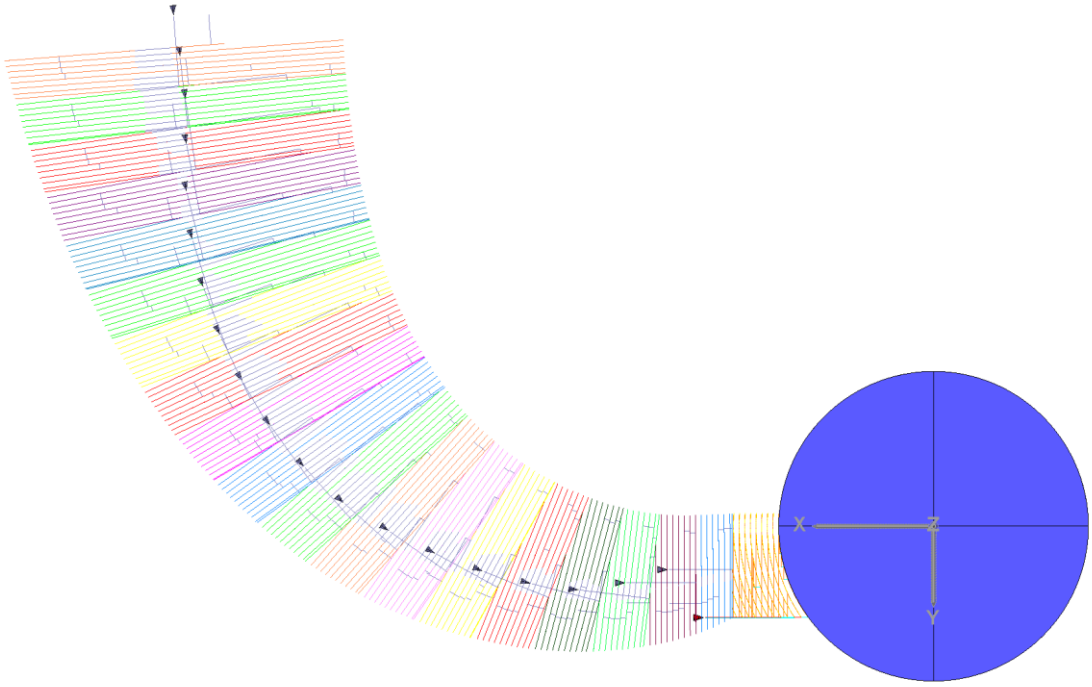

Figure 25: Propeller Slicing Strategy

A close-up view of an individual toolpath, as shown in Figure 26**,** shows how planar toolpath strategies can be enhanced to produce non-uniform layer slices. Future work includes machining this geometry in-situ to reduce issues with reach and access. Currently, this geometry requires expensive, specialized tooling to finish machining operations. The proposed hybrid machining strategies do not require such specialized tools yielding one of the main advantages of hybrid manufacturing. This topic is further investigated in the ensuing chapter.

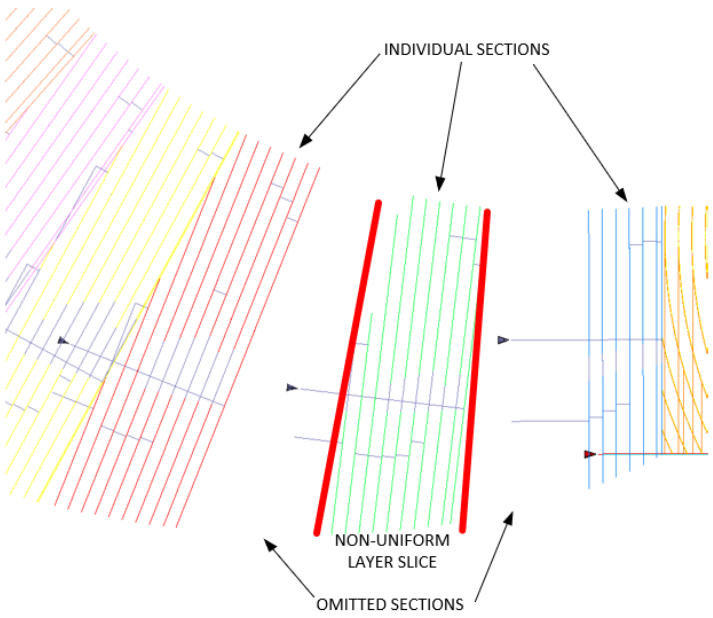

Figure 26: Non-Uniform Layer Slice

3.4.6 Machining Strategies

CAM programming for subtractive manufacturing has been employed for decades and is well understood. Though it is not discussed in detail, a few strategies specific to wire-fed hybrid manufacturing are presented in the section.

Excess wire, termed wire shoots, is often left on the component after deposition and is difficult to eliminate from the additive process; this can be seen in Figure 27. To reduce tool wear or destruction of subtractive tooling due to the excess wire being caught in the flutes, a conventional milling contour (where the tool rotates against the feed direction) with allowance around the geometry is often executed. This strategy removes the excess wire that can damage the flutes on tooling during climb milling contours (where the tool rotates with the feed direction).

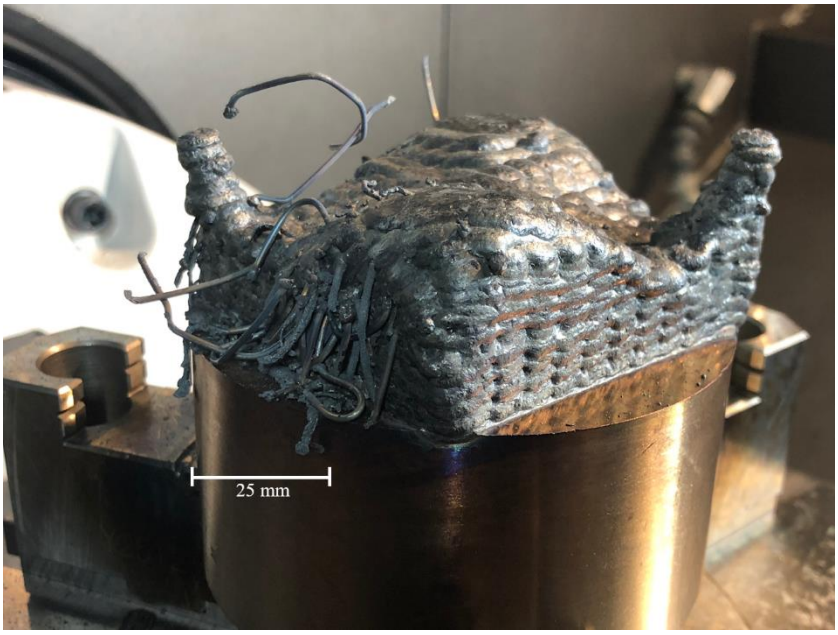

Figure 27: Excess Wire Shoots Shown After Deposition

Machining geometry produced from wire-feed additive manufacturing processes is not the same as machining of standard stock material. The exact dimensions of the build being made are typically unknown and cannot be easily determined without breaking setup for inspection. Thus, it is good practice to start with a roughing pass, with an allowance of half a bead width larger than the anticipated geometry (2mm), to remove grossly overbuilt geometry and excess wire (if applicable). If wire shoots are present, the first roughing pass should use a conventional milling strategy. This increases overall cycle time of the operation but will remove any grossly overbuilt geometry and excess wire that may damage tooling. This approach is similar in nature to considering casting tolerances when machining a cast part. In many instances, the machine tool is programmed to make its initial roughing pass just beyond the maximum material condition of the casting, which is the worst-case scenario for the casting. In the hybrid scenario, the worst case is one half the bead width.

Finally, it is recommended to oversize the model that is being deposited by half a bead width (2 mm) to compensate for distortion and any areas that are underbuilt due to wire loss. Depositing just enough material to meet the final geometry results in a surface finish with underbuilt edges as depicted in Figure 28. Thus, it is better to have the deposited model oversized by a small amount, and machine it to the final dimensions. Though more material is wasted by oversizing the deposited model, it mitigates any underbuilt features.

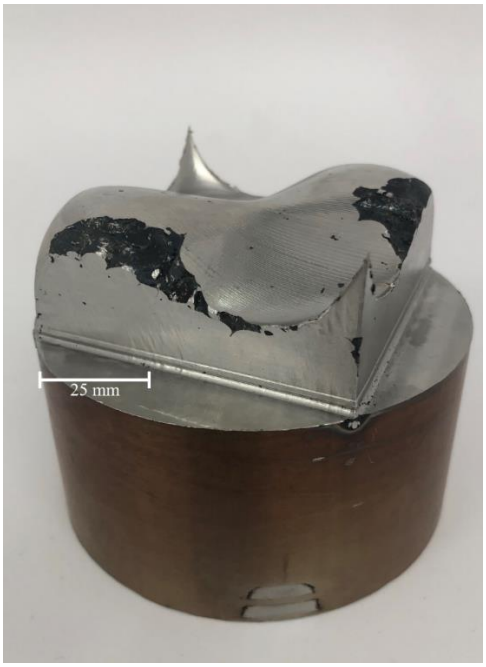

Figure 28: Geometry with Rough Surface Finish

3.5 Discussion and Limitations

This chapter outlines experiments and lessons learned during the development of a new hybrid laser hot-wire process. The investigated development provides a foundation for industrial adoption, yet there were limitations identified that require more investigation. This section identifies and discusses these issues.

The additive experimental setup developed in this dissertation does not consider the temperature of the substrate (or previous layer). As a result, it is hypothesized that this residual heat has an effect on the processing window and can be used to increase deposition rates. If it is not considered, this heat will compound when building large parts resulting in large amounts of distortion and non-uniform buildup [62]. Thus, it is determined to be critical that in-situ sensing and control be integrated into this equipment to mitigate issues that arise due to varying processing needs. With in-situ monitoring and control, the machine can adapt for varying temperature, geometry, and deposited material [63]. Furthermore, it also mitigates issues associated with process parameters being applicable to all processing scenarios. These in-situ sensors are being developed and the resulting adaptive processing strategies are a topic of future work.

The outlined experiments are straightforward and provide the foundation for process development, but their implementation is not always linear. It was found that the wire/laser alignment can depend on process parameters and vise-versa. Thus, these experiments are an iterative process that are repeated until satisfactory parameters are found. As seen in the ensuing chapters, the optimal parameters selected are not optimal for all processing scenarios. Furthermore, the experiments developed in this research optimize for geometrical accuracy, not material properties. Thus, this echoes the critical need for adaptive processing.

3.6 Conclusion

This chapter outlines experiments and lessons learned during the development of a new hybrid laser hot-wire process. Specifically, it discusses how to develop process

parameters through three experimental techniques, characterize certain deposition defects, and program for additive and subtractive processes. These techniques result in high deposition rates (2.5 kg/hr of 316L stainless steel) that lend itself to hybrid manufacturing being adopted by industry. Key outcomes from this research are:

- Introduction of per unit time variable (Linear Energy of Deposition) to relate and evaluate deposition parameters.
- Development of standard experimental techniques to be used for hybrid process development for any material feedstock.
- Key slicing (Chord Slicing / Non-uniform Layers) and machining strategies for complex curved components that are better produced in non-planar slices.

This work also highlights the need for various sensing solutions for in-situ process monitoring. The foundation built from this research will help advance these commercial hybrid manufacturing systems to industrial applications. Now that process parameters have been determined, the ensuing chapter evaluates the effect that the hybrid workflow has on the mechanical properties of the resulting components.

CHAPTER 4. HYBRID HEXAGONAL STRUCTURE PROCESS DEVELOPMENT

Hybrid manufacturing allows for additive and subtractive processes to be conducted in the same machine setup, enabling the transition between additive and subtractive processes to rapidly occur. Subsequently, the component temperature and use of coolant during the subtractive process can vary during the experiments. This chapter investigates the effect that the hybrid manufacturing process has on the mechanical properties of the resulting components.

4.1 Introduction

This chapter investigates the development and demonstration of hybrid manufactured hexagonal structures via various processing means. This hexagonal structure is be manufactured using two distinct processes: the first being complete additive build-up before machining, while the second demonstrates hybrid manufacturing's ability to machine a component at different intervals during the additive process. Furthermore, the components are machined under different conditions by varying whether coolant is used, and the temperature at which machining occurs. The temperature at which machining occurs can affect machining characteristics. Typically, coolant is used to reduce the temperature at the cutting interface. This is done to improve tool life as well as to prevent thermal damage to the part being machined (e.g., burning the part). However, using coolant on a hot part (e.g., one that has just been printed) can rapidly cool a part, resulting in potential material characteristic changes (e.g., quenching). The goal of this chapter is to determine if machining temperature and use of coolant in the hybrid manufacturing process influences the material properties of the resulting components.

4.2 Literature Review

To build upon previous research, a review of relevant literature is conducted below. Literature related to mechanical properties of DED produced components and the resulting geometrical distortion are presented in the ensuing section.

4.2.1 Mechanical Properties of Additive Components

It is believed that a component produced by hybrid manufacturing presents higher fatigue strength than one produced solely by additive manufacturing because of the difference in surface quality [64, 65]. It was shown by Spierings et al. [66] that the finishing of additively produced parts had a limited effect on the fatigue strength at 10^6 cycles, but significant effect at 10^7 cycles. Microcracks are generated on the surface of a rough additively manufactured surface, which can be stress concentration points promoting crack initiation. Thus, subsequent machining is important towards improving the fatigue resistance and ductility of the part as surface microcracks are removed from the part [64]. The differences in surface finish can be easily seen in Figure 29.

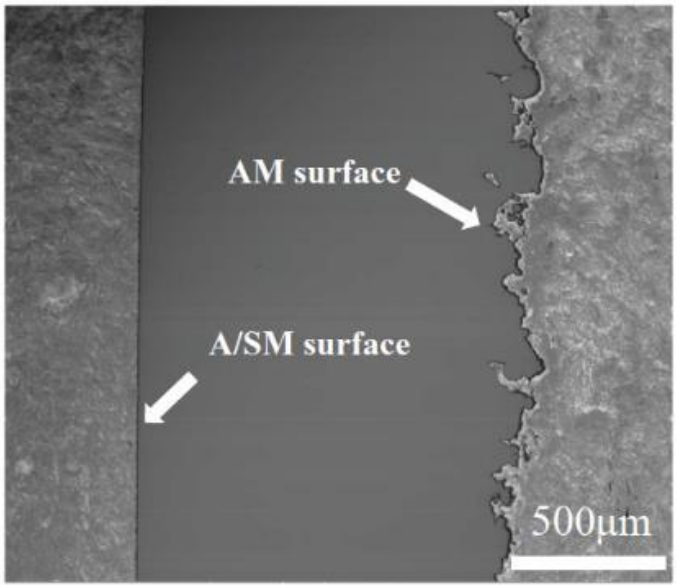

Figure 29: Cross-Section of Additive and Machined Surfaces [65]

It has been shown through tensile tests on various parts that laser-cladding strategies have a significant influence on the resulting product's mechanical properties [2, 67]. Tabernero et al. showed that IN718 samples created with a longitudinal raster pattern across a produced tensile sample had 55%-60% lower ultimate tensile strength when compared to a transverse raster pattern [67]. Through studying the orientation effects on tensile samples of 304L stainless steel parts, Smith et al. saw a 25% increase in yield strength by changing the build orientation [68]. It was further observed that the ultimate tensile strength was increased by 9%, but maximum elongation was reduced by 27% [68]. The disparity in the mechanical properties is attributed to a difference in manufacturing defect populations. Shrestha et al. showed similar results for 316L stainless steel components produced by L-PBF [69]. They showed that, despite the presence of defects between layers, the specimens exhibited higher yield strength, ultimate tensile strength, and elongation to failure when compared to wrought material. Olakanmi et al. has

highlighted the detrimental effects that porosity has on elongation to failure [70]. Table 7 shows reported mechanical properties of austenitic stainless steels produced by additive manufacturing. It is seen that orientation effects the yield strength, ultimate tensile strength, and elongation. However, due to the variation in the data, one orientation does not always result in improved mechanical properties.

Table 7: Mechanical Properties of Austenitic Stainless Steels

Material	Process	Orientation	Yield [MPa]	σ^{UTS} [MPa]	Elongation [%]	
316L SS	SLM	Horizontal - YX	397	668	37	[71]
		Horizontal - XZ	423	695	41	
		Vertical	387	564	35	
304L SS	DED	Vertical	440	670	70	[68]
		Horizontal	552	730	51	
316L SS	LENS	Vertical	448/455	545/638	4/25	[72]
		Horizontal	538/552	690/703	35/38	
AISI 316L	HP DLD	Vertical	580	900	6.5	[59]
		Horizontal	415	770	4	
316 SS	LBAM	Vertical	558	639	21	[73]
		Horizontal	352	536	46	
316L SS	L-PBF	Horizontal - Machined	545	689	29	[69]
		Horizontal -As-built	N/A	N/A	N/A	
		Vertical - Machined	495	587	59	
		Vertical - As-built	485	594	58	
		Diagonal - Machined	573	722	48	
		Diagonal - As-built	535	697	50	

Work by Hansel et al. compared tensile strength, yield, and elongation of powder DED components to cast and wrought material [19]. It was reported, as shown in Table 8, that the tensile strength for the deposited samples were between cast and wrought values, while the yield strength was increased compared to the cast and wrought samples [19]. It was further discussed that yield strength is normally more important in an industrial setting.

Table 8: Stainless Steel Mechanical Property Comparison [19]

316L Stainless Steel	Cast	Deposited	Wrought
Tensile (MPa)	517	520	580
Yield (MPa)	172	297	290
Elongation (%)	39	27	50

From reviewing the literature, there appears to be little consensus on what causes anisotropic mechanical properties, though it is likely due to numerous factors. While DED-produced austenitic stainless steels have been studied extensively in the literature, there is little work performed to understand the effect of build orientation on mechanical properties.

Due to the nature of the process, the microstructure of a DED component can be different between layers and even within layers [74]. For DED, the typically small weld-pool and fast traverse speed produce high cooling rates and large thermal gradients. Depending on the deposited alloy, these gradients can result in unique solidification grain structures which are not possible using traditional manufacturing means [74]. At lower cooling rates, which is more common for wire DED than powder DED, the grain features grow and look similar to those of cast structures [74]. Microstructure can also be predicted by using a 3D Rosenthal solution for a moving heat source on an infinite plate. This simplified model, developed in the early 20^{th} century, ignores deposited material, but can be used to determine the temperature, cooling rates, and thermal gradient at any given location and time [74, 75].

Residual stresses are also a concern in metal additive manufacturing [42, 76, 77]. Localized heating and phase transformations induce stresses within the part. These stresses can be large enough to cause distortion or even fracture [3]. The resulting geometrical errors are difficult to estimate for subsequent machining operations [78, 79]. Salonitis [80] reported that the residual stresses could be significant enough that the part could deform during the post-process machining operation to the point where the tool no longer engages with the material.

4.3 Distortion Modelling of Additive Components

To manufacture geometrically correct components, the residual stresses and distortions that occur due to the laser welding process must be understood. This section builds the foundation for understanding and quantifying residual stresses and distortions that occur during the welding process.

Highly localized transient heat input results in considerable residual stresses and deformations during and after the welding process [14, 81]. In contrast to load stresses, where internal and external forces are in equilibrium, residual stresses occur in the presence of internal forces without external forces. Residual stresses may cause brittle fractures in the finished structures [3]. Subsequent machining of components relaxes residual stresses which may result in dimensional changes [78-80, 82]. Though steps are traditionally taken to mitigate residual stresses, the hybrid structures investigated in this project leverage the residual stresses to create stronger joints.

Research dating back to 1930 has been conducted on residual stresses and distortion through predictive methodology, experiments, or empirical formulations [14, 79, 82].

Attempts have also been made to predict residual stresses through computer simulations of the welding process [14]. One significant conclusion of these studies is that the weld residual stresses are not heavily influenced by the weld heating cycle, but rather as a result of shrinking in the deposited material and its adjacent base metal during cooling [82]. Therefore, analysis of the shrinkage phenomena of welds alone may be sufficiently accurate to predict residual stresses and deformations [14, 82]. This modeling scheme is often referred to as the "inherent shrinkage model" [82].

During the welding process, the localized area is quickly heated relative to the surrounding area resulting in volumetric expansion. The expanding material is restrained by the surrounding colder area, which gives rise to thermal stresses. The resulting thermal stresses slightly exceed the yield limit, which is lowered at elevated temperatures. Consequently, the weld area is plastically compressed and, after cooling, is geometrically too small relative to the surrounding area. Thus, the weld displays tensile residual stresses while the surrounding area displays compressive residual stresses. Microstructural transformation during cooling involves an increase in volume. If this occurs at a temperature at which the yield limit is sufficiently high, it results in compressive residual stresses in the weld area, and tensile residual stresses in the surrounding area. The residual stress distributions and the amount of weld distortion depend on the final state of the plastic strain distributions and their compatibility in the joint [82].

The induced incompatible inelastic strains in the weldment during the heating and cooling cycles include transient thermal strains, cumulative plastic strains, and final inherent shrinkage strains. At any instant during welding, mechanical strains are generated by the non-linear temperature distributions from the incompatible thermal strains. This

leads to incremental plastic strains if yielding occurs. The cumulative plastic strains build up with each welding cycle. This final state of compressive, inelastic strains is referred to as the "inherent shrinkage strains" first introduced by Ueda [83, 84]. Induced incompatible plastic strains (assuming 2-dimensional plane-strain condition) at each heating or cooling time increment may be described mathematically as follows:

$$\nabla^2(\sigma_x + \sigma_y) = -\frac{E}{1-\nu}\nabla^2(\alpha\theta) - [g(x,y) + \Delta g(x,y)] \tag{2}$$

where the $\nabla^2$is the Laplacian operator, σ_x and σ_y are thermal stress components in the x and y directions, E is Young's modulus, ν is Poisson's ratio, α is the thermal expansion coefficient, θ is a temperature function, $g(x,y)$ is a cumulative plastic strain function and $\Delta g(x,y)$ is the plastic strain increment function over each thermal cycle. The plastic strain functions may be written as follows:

$$g(x,y) = \frac{E}{1-\nu^2}\left(\frac{\partial^2\varepsilon_x^p}{\partial y^2} + \frac{\partial^2\varepsilon_y^p}{\partial x^2} - 2\frac{\partial^2\varepsilon_{xy}^p}{\partial x\partial y}\right) - \frac{\nu E}{1-\nu^2}\nabla^2\left(\varepsilon_x^p + \varepsilon_y^p\right) \tag{3}$$

$$\Delta g(x,y) = \frac{E}{1-\nu^2}\left(\frac{\partial^2(\Delta\varepsilon_x^p)}{\partial y^2} + \frac{\partial^2(\Delta\varepsilon_y^p)}{\partial x^2} - 2\frac{\partial^2(\Delta\varepsilon_{xy}^p)}{\partial x\partial y}\right) - \frac{\nu E}{1-\nu^2}\nabla^2\left(\Delta\varepsilon_x^p + \Delta\varepsilon_y^p\right) \tag{4}$$

The Laplacian thermal strains shown are governed by the rate of enthalpy change in the welded component. Once the thermal cycling is complete, the cumulative plastic strains in the weldment are usually compressive and become the inherent shrinking strains $g^I(x,y)$. These shrinking strains interact with the structural rigidity resulting in residual

stresses σ_x^R and σ_y^R and distortion strains ε_x^D and ε_y^D. Residual stresses may be written with a possible reverse yielding $g^R(x,y)$ as follows:

$$\nabla^2\left(\sigma_x^R + \sigma_y^R\right) + g^R(x,y) = -g^I(x,y) \tag{5}$$

The distortion strains may be written in the form of final total strains as follows:

$$\varepsilon_x^D - \varepsilon_x^I = \frac{1}{E}\left[\sigma_x^R - \nu\left(\sigma_y^R + \sigma_z^R\right)\right] + \varepsilon_x^{PR} \tag{6}$$

$$\varepsilon_y^D - \varepsilon_y^I = \frac{1}{E}\left[\sigma_y^R - \nu(\sigma_z^R + \sigma_x^R)\right] + \varepsilon_y^{PR} \tag{7}$$

$$\varepsilon_z^D - \left(\varepsilon_x^I + \varepsilon_y^I\right) = \frac{1}{E}\left[\sigma_z^R - \nu\left(\sigma_x^R + \sigma_y^R\right)\right] - \varepsilon_x^{PR} - \varepsilon_y^{PR} = constants \times \tan t \tag{8}$$

$$\gamma_{xy}^D - \gamma_{xy}^I = \frac{2(1+\nu)}{E}\tau_{xy}^R + \gamma_{xy}^{PR} \tag{9}$$

Here, D represents distortion strains, I represents the inherent (cumulative) shrinkage strains, R represents residual stresses, and PR represents plastic strains due to reverse yielding.

The inherent shrinkage plastic strains can be determined from the known distortion strains. Thus, the distortion shape of a component can be determined by integrating these strains with respect to spatial coordinate variables. For example, when welding along a longitudinal plate, the total strain ε_{cg}^D at the center of gravity of any cross-sections and its curvature C may be written as follows:

$$\varepsilon_{cg}^D = \frac{\iint_{A_I} \varepsilon_x^I \, dy \, dz}{A_{section}} \tag{10}$$

$$C = \frac{\delta_{cg}^{section} - \delta_{cg}^{I}}{I} \iint_{A_I} \varepsilon_x^I \, dy \, dz \tag{11}$$

where $A_{section}$ is the geometrical cross-sectional area and A_I is the shrinkage strain area containing the inherent shrinkage plastic strains. $\delta_{cg}^{section}$ and δ_{cg}^{I} are the distances from weld to the centers of gravity of these two areas respectively. The amount of longitudinal shrinkage can be shown from the average shrinking strain ε_{cg}^{D} at the section centroid. The curvature C is the curvature of the cross-section at a given location along the weld axis.

Equations 2-11 demonstrate that cumulative plastic strains govern the final state of residual stresses and distortion in a welded component [83, 84]. Therefore, an engineering approach to estimating residual stresses or distortion is to establish the relationships between these plastic strains and variables associated with the process. Though these equations provide a good estimation, some phenomena that occur during the welding process can only be analyzed by numerical solutions.

4.3.1 Temperature Distribution in Welding

Equation 2 uses a temperature function to describe the temperature of a component as a function of position. Rosenthal was first to investigate the temperature distribution by using a travelling point heat source model [75]. In this simplified model that is widely used, material deposition is ignored and only heat conduction is considered from within the melt-pool and substrate due to a heat source moving at velocity V [85]. It is assumed that the beam only moves in the x direction. The amount of energy absorbed is αQ, which is the simplified version of the complex temperature dependent absorption of laser beam. Here, Q represents the total amount of energy input to the process, and α represents the ratio of

the absorbed energy to the total energy. It is assumed that the energy source moves in the x direction at a constant velocity, and the relative coordinates of the beam (x_0, y_0, z_0) can be related to the fixed coordinates (x, y, z) at any given time t as $(x_0, y_0, z_0) = (x - Vt, y, z)$. With the given conditions, the Rosenthal solution for temperature T at time t for any location in an infinite half-space can be expressed in dimensionless form as [74, 75]:

$$\overline{T} = \frac{\exp\left(-(\overline{x}_0 + \sqrt{\overline{x}_0^2 + \overline{y}_0^2 + \overline{z}_0^2}\right)}{2\sqrt{\overline{x}_0^2 + \overline{y}_0^2 + \overline{z}_0^2}} \tag{12}$$

where

$$\overline{T} = \frac{T - T_0}{\left(\frac{\alpha Q}{\pi k}\right)\left(\frac{\rho c V}{2k}\right)}, \overline{x}_0 = \frac{x_0}{\left(\frac{2k}{\rho c V}\right)}, \overline{y}_0 = \frac{y_0}{\left(\frac{2k}{\rho c V}\right)} \text{ and } \quad \overline{z}_0 = \frac{z_0}{\left(\frac{2k}{\rho c V}\right)} \tag{13}$$

In these equations, T_0 is the initial temperature, $\rho, c,$ and k are density, specific heat, and thermal conductivity of the substrate, respectively. As shown by Gibson et al., this equation can also be modified by differentiating with respect to time and the dimensionless spatial coordinates to result in a formulation for cooling rates, and thermal gradients for any location (*x, y, z*) and time, (*t*) [74].

Building upon Rosenthal's model, Goldak was able to develop an accurate model for a heat source that is useful for laser welding [86, 87]. Specifically, Goldak's double-ellipsoidal heat source model is widely used in computational welding modeling [88]. Its geometric parameters are shown in Figure 30.

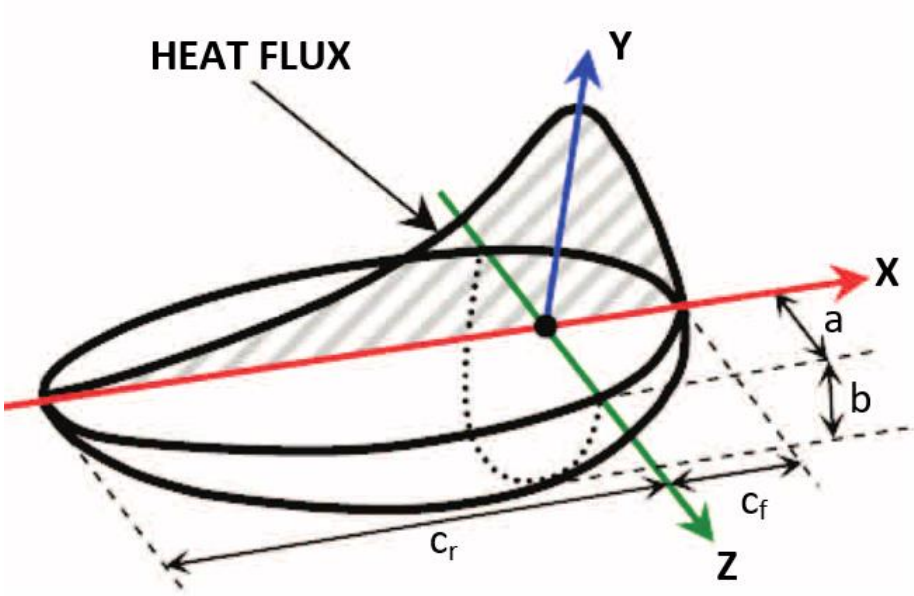

Figure 30: Goldak Geometric Parameters [89]

This model is based on a Gaussian distribution of power density [86]. The double ellipsoidal geometry is used such that the size and shape of the heat source can be used to model both shallow penetration of arc welding as well as deeper penetration processes such as laser and electron beam welding. The derived power density equation for the inside of the front quadrant is [86]:

$$q(x,y,z,t) = \frac{6\sqrt{3}f_f Q}{abc\pi\sqrt{\pi}} \exp\left(-\frac{3z^2}{a^2} - \frac{3y^2}{b^2} - \frac{3[x+v(\tau-t)]^2}{c_f^2}\right) \qquad (14)$$

Similarly, the power density for inside of the rear quadrant is [86]:

$$q(x,y,z,t) = \frac{6\sqrt{3}f_r Q}{abc\pi\sqrt{\pi}} \exp\left(-\frac{3z^2}{a^2} - \frac{3y^2}{b^2} - \frac{3[x+v(\tau-t)]^2}{c_r^2}\right) \qquad (15)$$

where Q is the power input, v is the welding speed, and τ is the lag factor necessary to define the position of the heat source at $t = 0$. The variables a, b, and c are the semi-axis of the heat source model, respectively. The fractions of the heat, f_f and f_r, represent the heat flux in the front and rear quadrants, respectively, where $f_f + f_r = 2$.

These base equations, from the literature, provide the foundation for common computational welding computations. Though manual calculations are not explicitly discussed in this work, they are used to enhance the creation and understanding of the distortion modeling conducted in this chapter.

4.4 Methodology

The methodology of this research is to manufacture hexagonal structures with varying processing means. The experimental setup will be held consistent by using 1.14 mm (0.045") diameter 316L stainless steel wire deposited on either gray cast iron or A36 steel substrate. The difference in substrate does not affect the results of this research as the area of interest is away from the substrate interface. The hexagonal structure, as shown in Figure 31, is dimensioned such that it can be used to produce tensile samples conforming to the ASTM E8/E8M-16a standard for tension testing of metallic materials [23]. Tensile specimens are produced in both horizontal and vertical orientations to characterize mechanical properties between and along the additively manufactured layers.

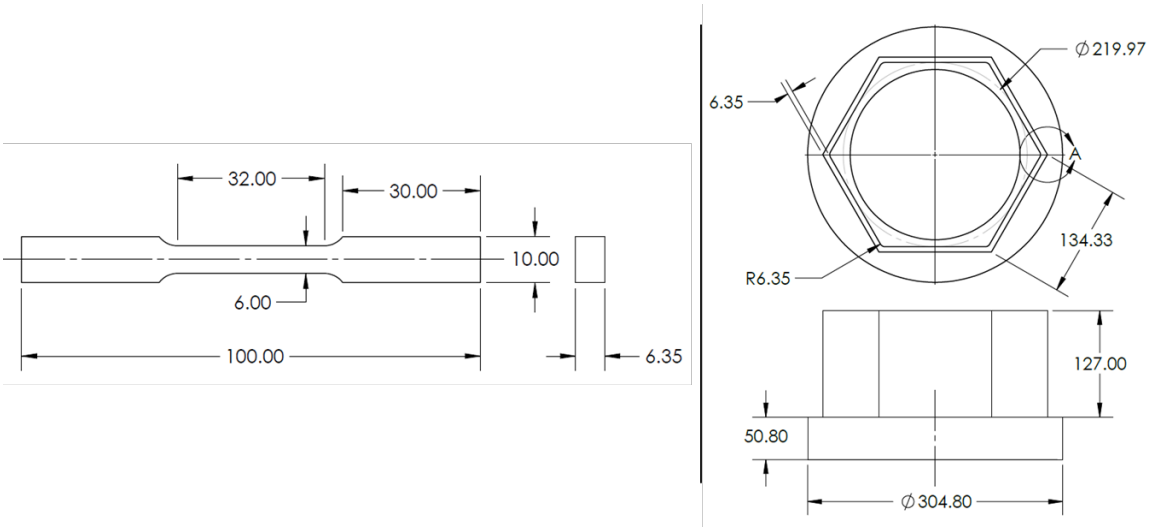

Figure 31: Left-Tensile Sample, Right-Hexagonal Structure

Along with being destructively tested for mechanical properties, each sample is evaluated for porosity using X-ray computed tomography by the Zeiss team at ORNL. Optical microscopy and hardness evaluation will also be conducted. Table 9 provides the experimental methodology for the varying processing means. Two machining sequences have been selected; one sequence where the component will be machined directly after deposition while it is still hot, the other sequence will allow the component to be naturally cooled before machining. Furthermore, experiments were added depending if coolant will be used or not. Using coolant improves tool life, but also results in the hexagonal structure to be quenched during the machining sequence.

Table 9: Hexagonal Structure Experimental Methodology

Experiment	Machining Sequence	Coolant Status
Additive Hexagonal Structure	Machine cool	N/A
Additive Hexagonal Structure	Machine hot	No Coolant
Additive Hexagonal Structure	Machine hot	Coolant
Hybrid Hexagonal Structure	Machine cool at intervals	Coolant
Hybrid Hexagonal Structure	Machine cool at intervals	No Coolant
Hybrid Hexagonal Structure	Machine hot at intervals	No Coolant
Hybrid Hexagonal Structure	Machine hot at intervals	Coolant

The toolpath trajectory for the deposition was programmed using Autodesk's PowerMILL. This program takes the nominal CAD geometry and creates g-code for the developed toolpath trajectories. Initial toolpath trajectories used 3-axis motion for the deposition, but it was seen during collision simulation that the toolpath exceeded the machine axis limits. Figure 32 depicts this issue for a standard vertical 5-axis hybrid manufacturing machine. Since the additive and subtractive heads share the same motion drives, there is a discrepancy between the size of parts that can be deposited compared to what can be machined. For example, if the offset between the spindle and additive head is 150 mm, the effective machine volume is reduced by 300mm.

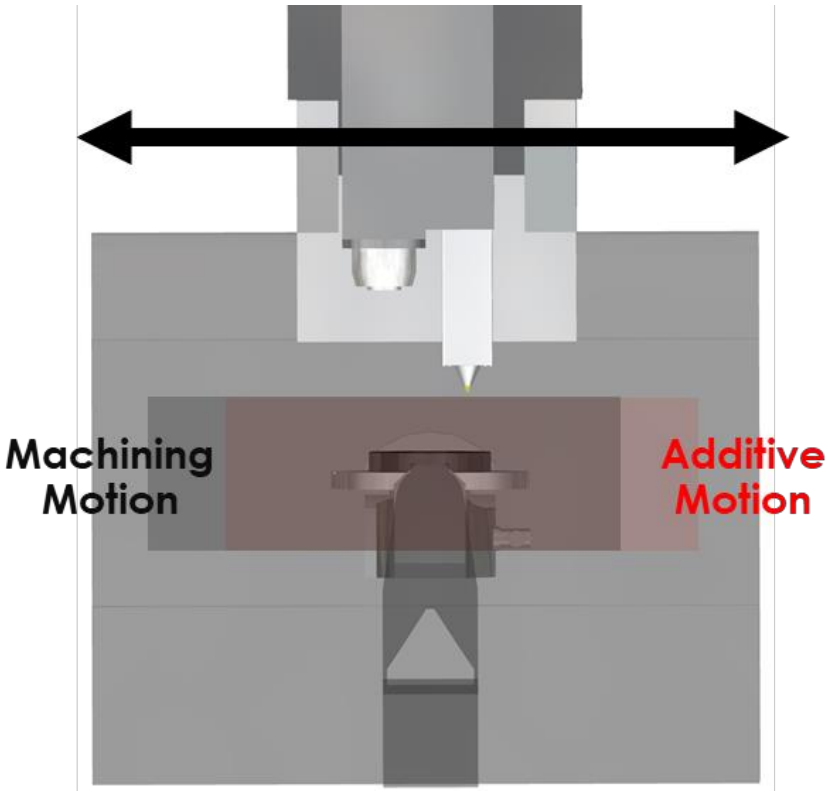

Figure 32: Hybrid Machine Stroke Issues

To compensate for this issue, the toolpath was modified such that it utilized the rotary motion. During deposition, the additive head will stay in a constant Y-axis position while moving the workpiece around the C-axis. Figure 33 shows the developed toolpath for the hexagonal structure.

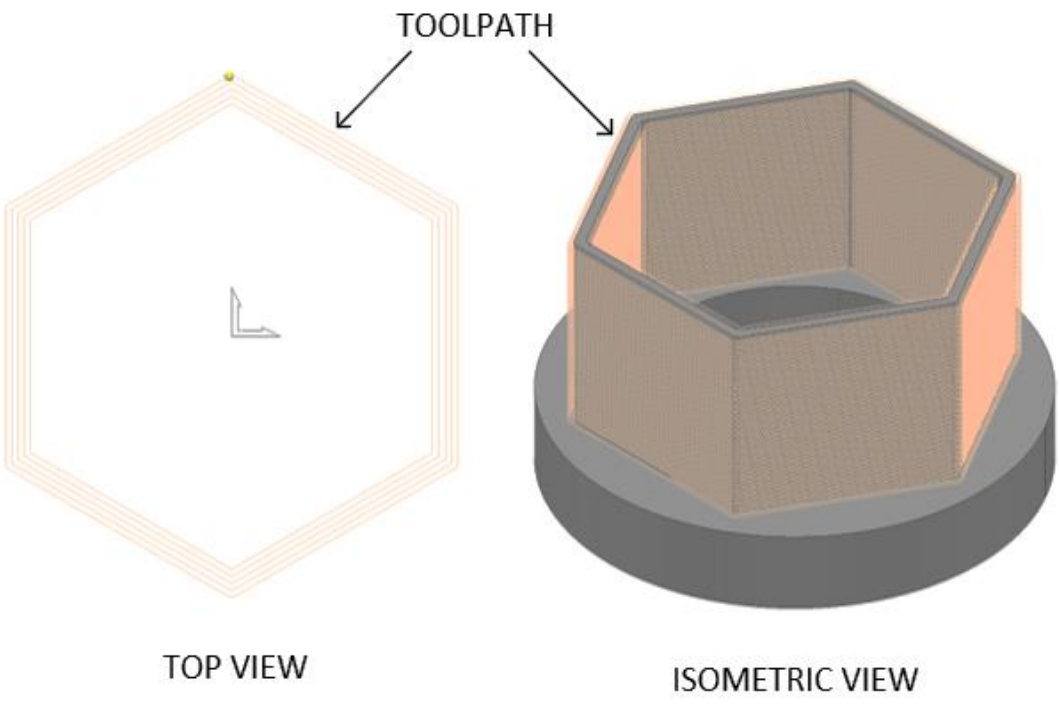

Figure 33: Hexagonal Structure Toolpath

4.4.1 Additive Hexagonal Structure

The process variation where the entire component was deposited before machining is known as the additive hexagonal structure. As shown in Figure 33, four beads were deposited in a hexagonal pattern centered to the CAD model. A wall thickness of four beads for the hexagonal structure was selected as early experimentation with three beads resulted in underbuilding in the corners due to thermal distortion. The resulting cycle time of the deposition process was 4.5 hours. Table 10 shows the process parameters used during the deposition process.

Table 10: Hexagonal Structure Additive Parameters

Parameter	Value
Surface Feed	1067 mm/min
Laser power	2750 W
Wire Feed Speed	4445 mm/min
Hot-Wire Power	420 W
Nozzle Gas Flow	20 CFH
Shielding Gas Flow	20 CFH

From early experimentation, it was determined that the gray cast iron substrate used for the hexagonal structures needed to be prepared such that the hexagonal structure are metallurgically compatible. This process is commonly known as “buttering” in the welding industry. Without this buttering, the hexagonal structures delaminate from the surface as shown in Figure 34 and Figure 35. For this instance, a single layer of 316L stainless steel was deposited across the entire cast iron surface. Subsequent machining occurred to result in a qualified surface.

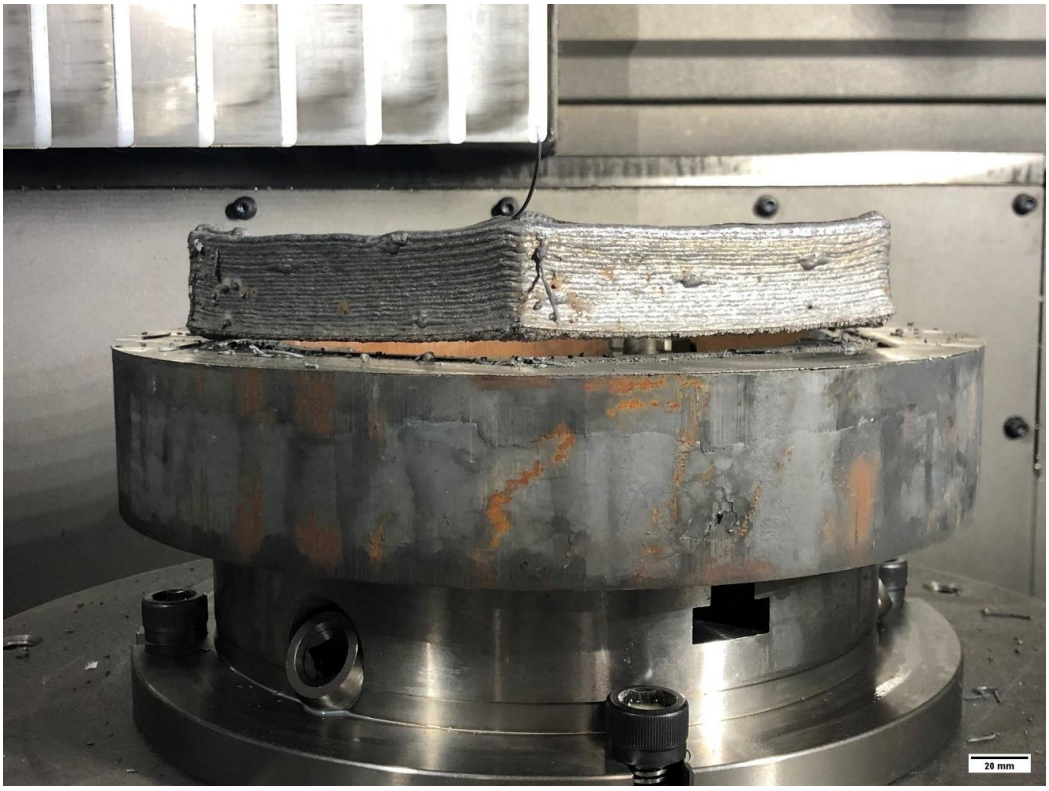

Figure 34: Cast Iron Delamination

Figure 35: Cast Iron Delamination Close-up

The machining portion of the additive hexagonal structure was created in Open Mind's HyperMILL. Analogous to the additive toolpath planning, some modifications to the initial toolpath had to be made to accommodate the limited machine motion. The toolpath is comprised of five operations as shown in Figure 36**.**

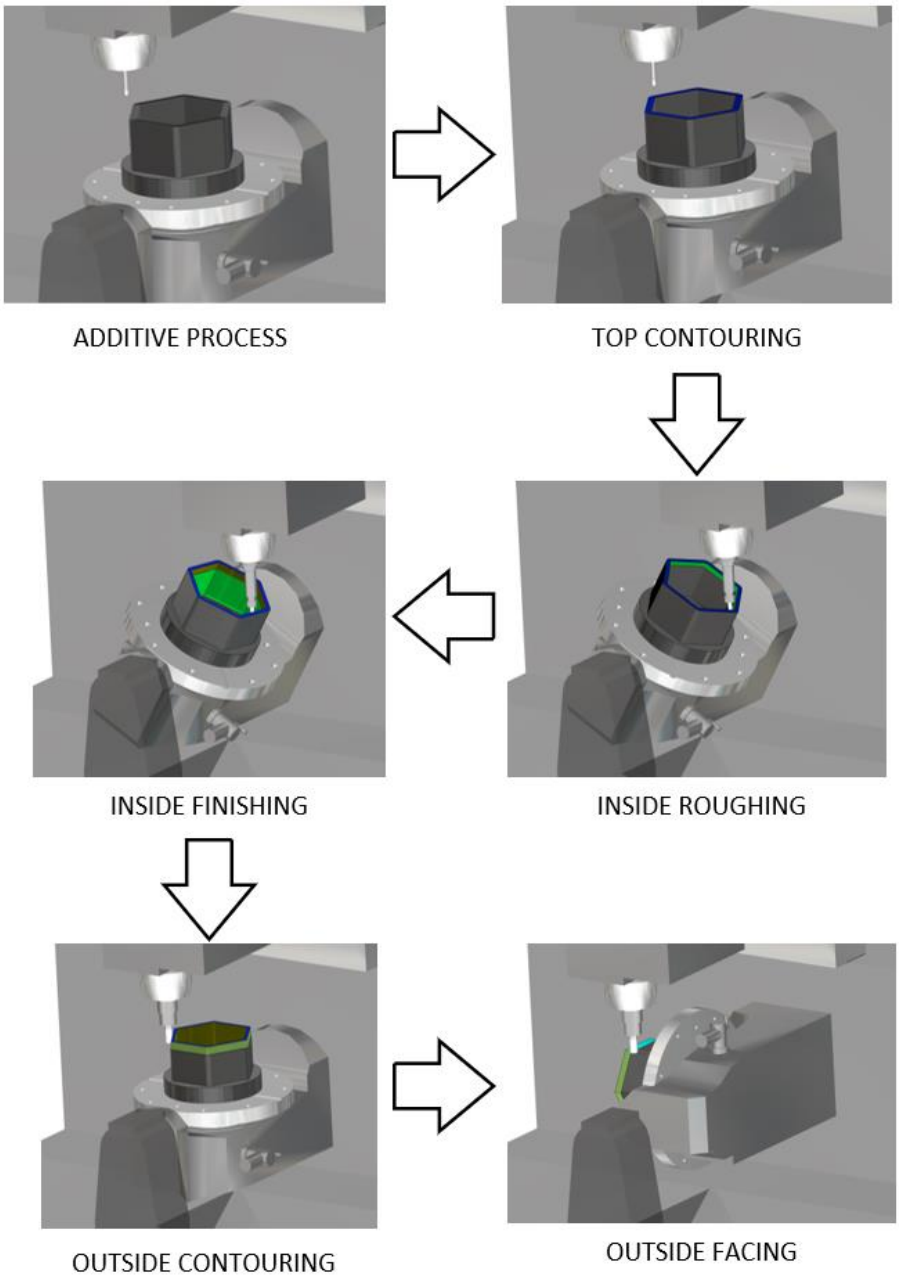

Figure 36: Additive Hexagonal Structure Machining Workflow

The tooling used and respective process parameters for the machining operations are shown in Table 11. The process parameters were selected based on the manufacturer's recommendations and were held constant through each experiment.

Table 11: Additive Hexagonal Structure Machining Parameters

Tool Description	Process Parameters**	Process Where Used
9.525 mm Diameter 4-Flute End Mill	Surface Feed: 70 m/min Feed-Rate: 0.03 mm/tooth	Top Contouring
12.7 mm Diameter 4-Flute End Mill	Surface Feed: 90 m/min Feed-Rate: 0.05 mm/tooth	Inside Roughing Inside Finishing
25.4 mm 5-Flute Diameter End Mill	Surface Feed: 70 m/min Feed-Rate: 0.06 mm/tooth	Outside Contouring Outside Facing

****All Process Parameters Per Manufacturers Recommendation**

The cycle time for the machining operation was 16 hours. This long cycle is attributed to the spiral toolpath on the inside contour due to reach and access problems. As discussed in the ensuing section, being able to mitigate reach and access issues is one of the benefits of hybrid manufacturing.

4.4.2 Hybrid Hexagonal Structure

The process variation where the hexagonal structure is built in consecutive sections is known as the hybrid hexagonal structure. For simplicity, the 127 mm tall component is comprised of 5 equal sections of 25.4 mm. Each section is deposited and fully machined before continuing to the next section. Since the previous section is fully machined, the additive toolpath is modified to a 3-bead configuration, as the 4-bead configuration creates an overhang that is too large for deposition as shown in Figure 37. It is noted that 5-axis deposition strategies are possible, but it was determined that completing the entire deposition using 3-axis motion was more beneficial to the research goals of the project as

it is applicable to both 3 and 5-axis systems. The same deposition settings as shown in Table 10 were used for this set of experiments.

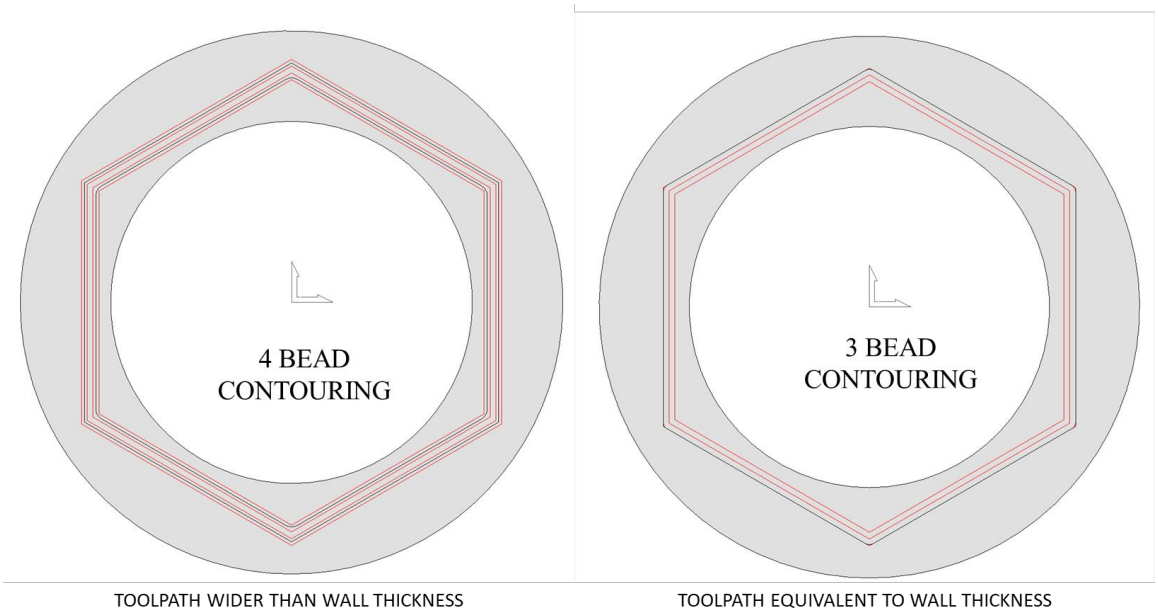

Figure 37: Hybrid Contouring Toolpath Development

For the machining strategy, the top contouring and outside contouring were re-used, and an analogous inside contouring using the 12.7 mm diameter 4-flute end mill was developed. This inside contouring reduced the total machining time by 85% to 2.5 hours. The same machining process parameters for the respective tools as shown in Table 11 were used. Variations of the inside and outside contours that machine 5 mm lower were generated to use with the subsequent sections. These variations are used to generate a seamless blend between the sections.

Once completed, the samples were prepared for evaluation by using wire electrical discharge machining (EDM) and standard subtractive machining. They were tensile tested by following the ASTM E8/E8M standard test methods for tension testing of metallic

materials [23]. Optical microscopy and hardness evaluations were also completed by the materials team at ORNL, and X-Ray computed tomography was conducted by the Zeiss team at ORNL.

4.5 Results

Hexagonal structures were produced using various processing means to understand the influence that the hybrid manufacturing process has on the mechanical properties of a produced component. This section outlines the results from the various experiments and discusses lessons-learned from the study. Table 12 shows the labeling strategy for the experimental cases.

Table 12: Hexagon Experiment Labeling

Hexagonal Structure Label	Deposition Strategy	Machining Status	Coolant Status
Hexagon 1	3 Beads – Full Additive	Cold	Coolant
Hexagon 2	4 Beads – Full Additive	Cold	Coolant
Hexagon 3	4 Beads – Full Additive	Hot	Coolant
Hexagon 4	4 Beads – Full Additive	Hot	No Coolant
Hexagon 5	4 Beads – Hybrid	Hot	No Coolant
Hexagon 6	4 Beads – Hybrid	Cold	Coolant
Hexagon 7	4 Beads – Hybrid	Cold	No Coolant
Hexagon 8	4 Beads – Hybrid	Hot	Coolant

4.5.1 Additive Hexagonal Structures

Hexagonal structures that were completely deposited before machining have been termed additive hexagonal structures. For this set of experiments, three scenarios were evaluated. The first case was produced from machining after the component had completely cooled to room temperature after deposition. The other two were machined directly after printing. One case was machined dry without coolant, while the other was quenched with coolant.

It was identified from early experiments that a four-bead geometry needed to be used to compensate for distortions. Hexagon 1 was generated using a three-bead strategy before the moving to the four-bead strategy. This test case generated a component good enough for creating samples but had underbuilt geometry in the corners. The data set was kept for analysis to determine if the change in deposition strategy had any effect on the material properties.

Machining of the additive hexagonal structures occurred as expected without any issues as seen in Figure 38 and Figure 39. Upon finishing, surface porosity was observed. This is attributed to instability in the deposition process. This results from the wire exiting the weld-pool and leaving a void in the deposited bead as seen in Figure 40. This defect is common in thin-walled components.

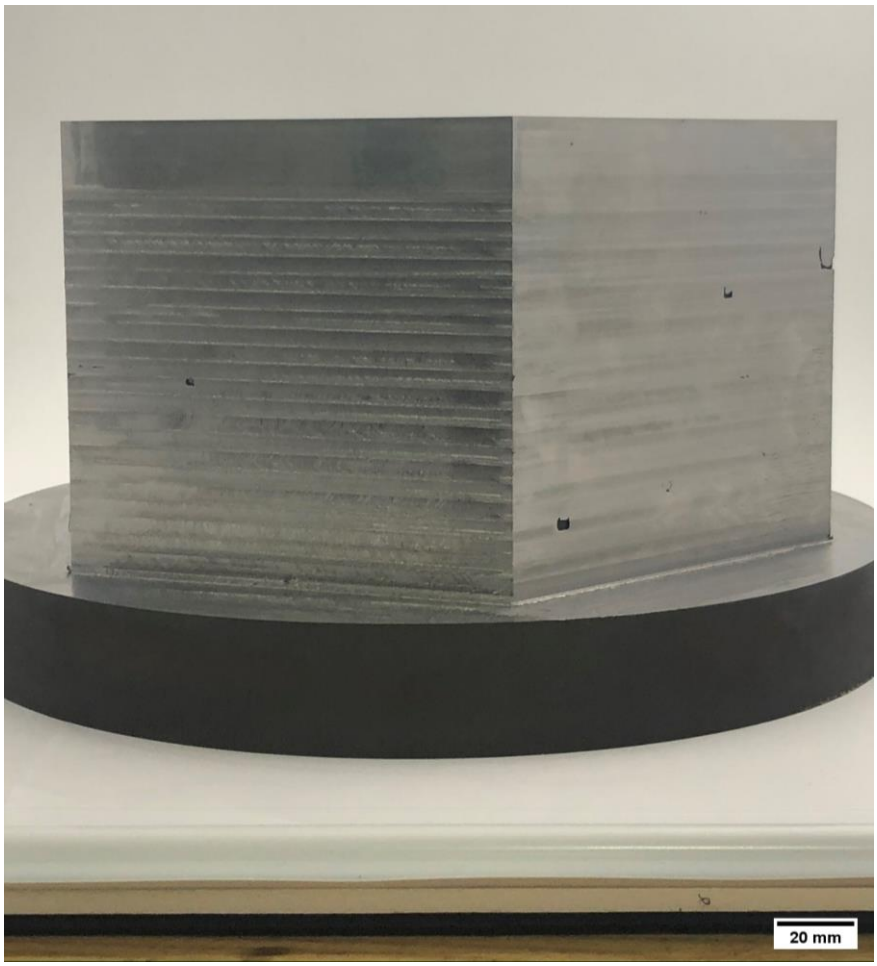

Figure 38: Front View of Machined Hexagonal Structure

Figure 39: Isometric View of Machined Hexagonal Structure

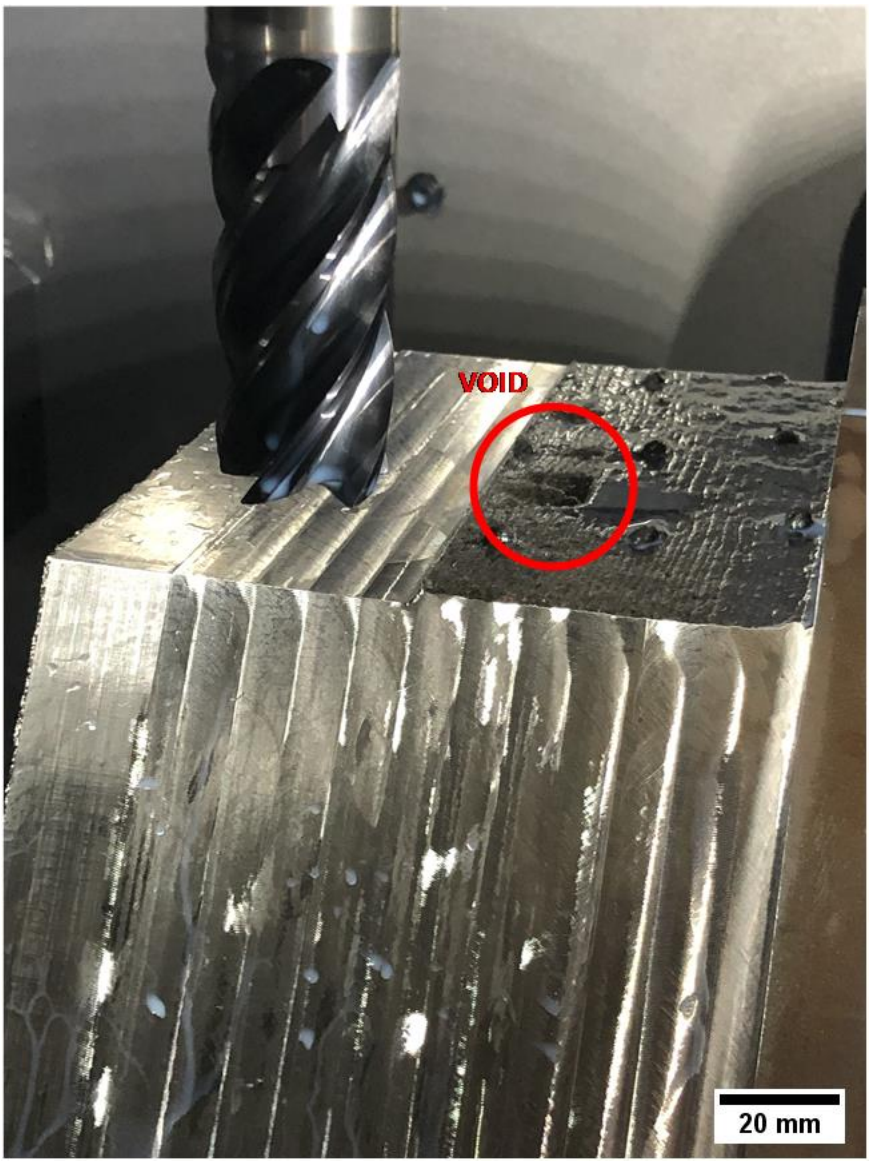

Figure 40: Deposited Void

4.5.2 Hybrid Hexagonal Structures

The hexagonal structures generated in consecutive sections are termed hybrid hexagonal structures. For these hexagonal structures, five equal sections measuring 25.4 mm tall were generated by alternating additive and subtractive manufacturing. For this set of experiments, four scenarios were evaluated. Two cases were machined after the

component had cooled, one variation with coolant while the other without. The other two cases were machined directly after deposition, with analogous coolant variations.

Initial attempts resulted in slight modifications to the toolpath trajectory. As shown in Figure 41, a constant surface feed resulted in a non-uniform build-up on consecutive layers. This is attributed to the first layer having an overhang and not wetting against the substrate.

Figure 41: Non-uniform Buildup of Hybrid Hex

To mitigate this phenomenon, the surface feed for the first layer was reduced by 50% to 500 mm/min. The resulting uniform geometry is shown in Figure 42. It is noted that this component was produced by machining the geometry directly after deposition.

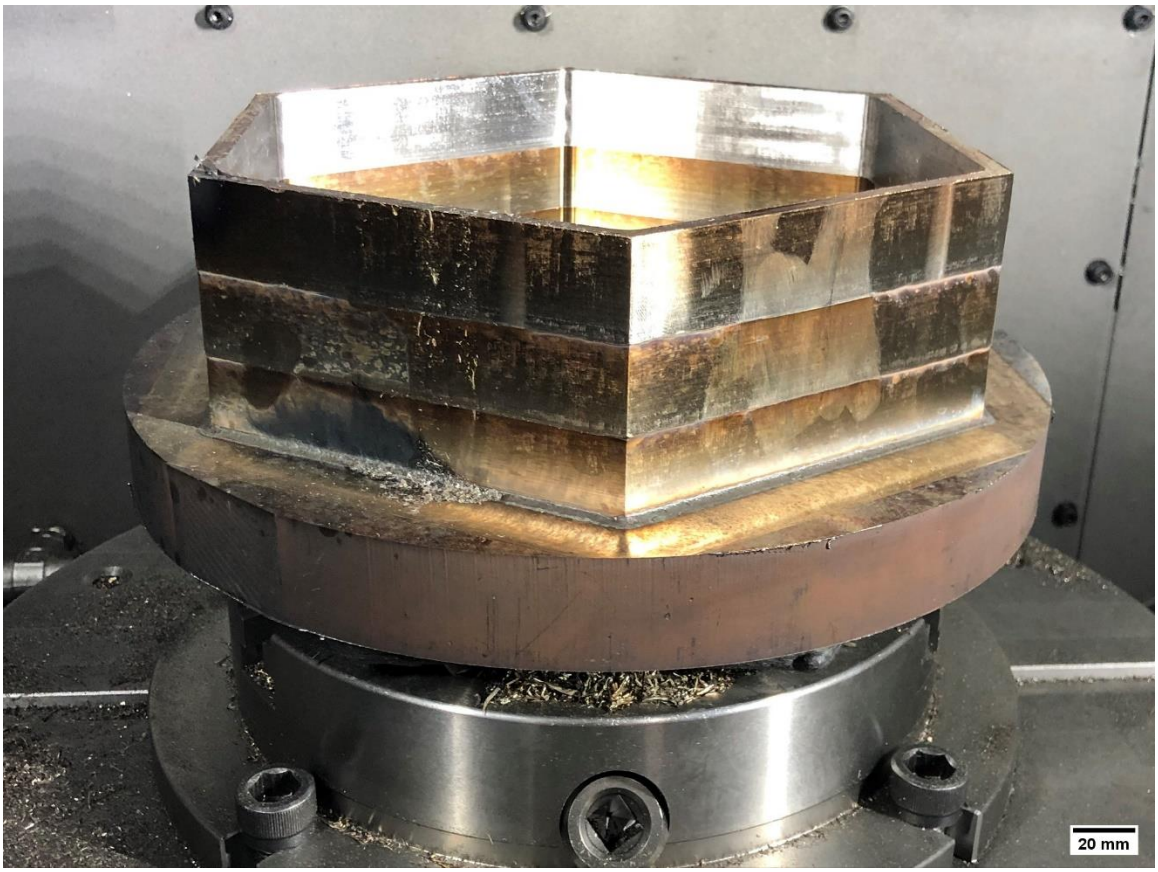

Figure 42: Uniform Buildup of Hybrid Hexagonal Structure

The experiments in which the hexagonal structure was completed cooled before machining resulted in large amounts of distortion. The distortion was large enough that the final geometry was not attainable from the deposited geometry. It is hypothesized that there was distortion with the additive hexagonal structures, but the 4-bead variation generated a wall thickness large enough to keep the part contained. As shown in Figure 43, the first section of hexagon 6 resulted in the top of the part being distorted inward enough such that the machining operation did not sufficiently remove material.

Figure 43: Distorted Section

To better understand this distortion, simulation of the DED process was conducted to provide a quantitative result of the distortion. The ensuing section discusses the simulation study and evaluates its results.

4.5.3 Distortion Simulation Study

A distortion simulation was conducted to enhance the understanding of how the hexagonal structure was distorted. The software package selected was Autodesk's Netfabb. This package is beneficial to this study as it leverages the generated toolpath trajectory from Autodesk's PowerMill for the simulation. Conducting directed energy deposition

simulations with Netfabb is a newer feature that is not fully released. Thus, the simulations were conducted in collaboration with Autodesk.

The Netfabb simulation solver utilizes the Goldak [86] heat source model to conduct a thermal simulation that is then leveraged to conduct a mechanical simulation. The workflow of the Netfabb distortion simulation is shown in Figure 44.

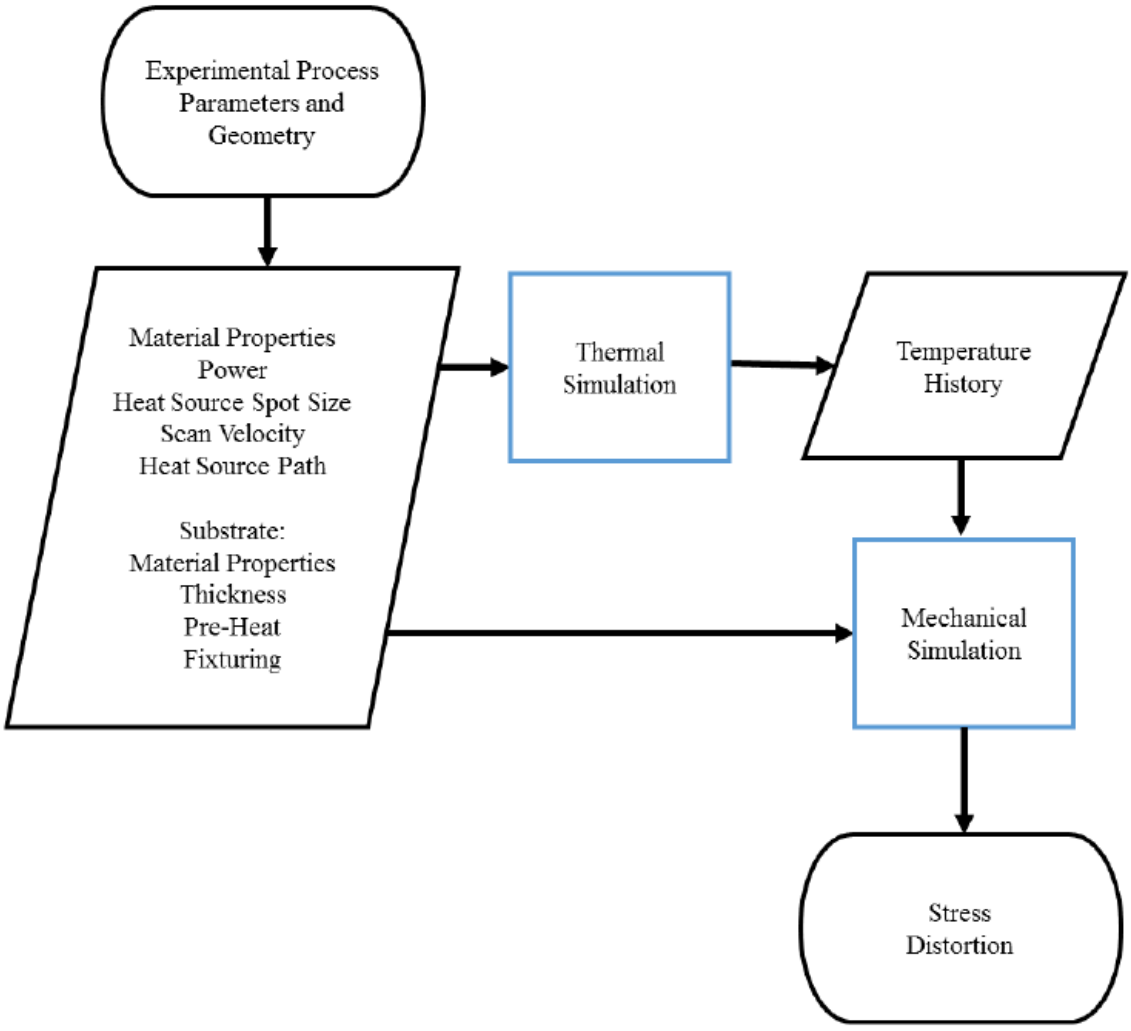

Figure 44: Netfabb Distortion Simulation Workflow [90]

Figure 45 shows the results from the distortion simulation. The simulation model utilizes well-known 316L stainless steel material properties used in power-bed fusion simulations for both the deposited material and substrate. Furthermore, the ability to modify the substrate geometry does not currently exist. However, it is seen in the figure that the resulting maximum distortion after cooling to 25 °C is 0.793 mm. This maximum distortion occurs 94 minutes after deposition is complete on the top surface of a corner vertex. Despite the numerous assumptions needed for this simulation, the results are comparable to the actual values. The distortion of the component shown in Figure 43 was measured to be 1 mm with calipers. This was done by taking measurements directly after deposition, and again after being allowed to cool to room temperature.

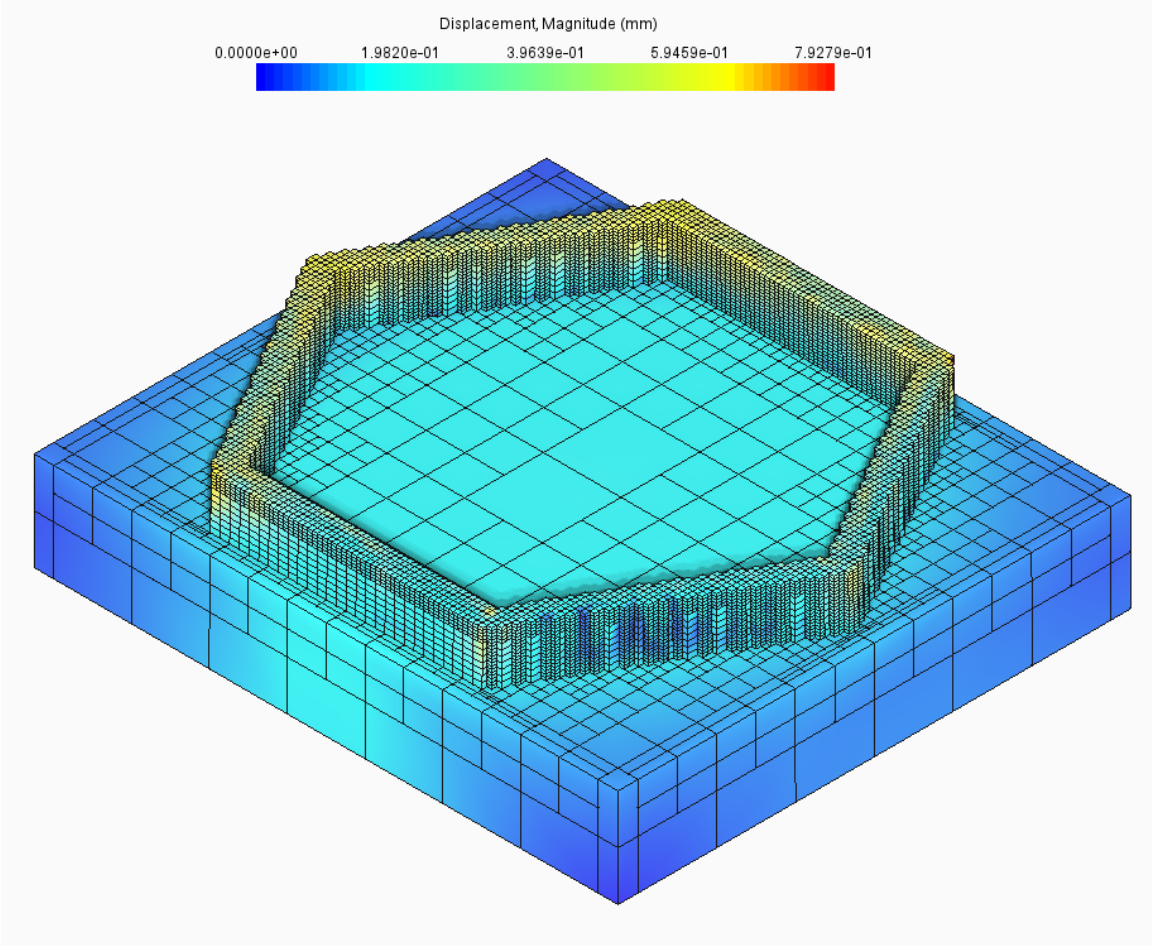

Figure 45: Distortion Simulation

From the thermal distortion analysis, it was determined to modify the additive toolpath trajectory to include a 3° outward taper to the wall. The hypothesis is that once cooled, the geometry distorts inwards and bring the part back into the preform. As shown in Figure 46, the first section was successfully manufactured as it can be observed that the entire surface was machined. Unfortunately, the compensation was not sufficient for the subsequent sections as shown in Figure 46. It is hypothesized that the issue observed with the second section is due to the component being distorted inwards during the cooling cycle. A depiction of this hypothesis is shown in Figure 47.

Figure 46: Distortion Compensation

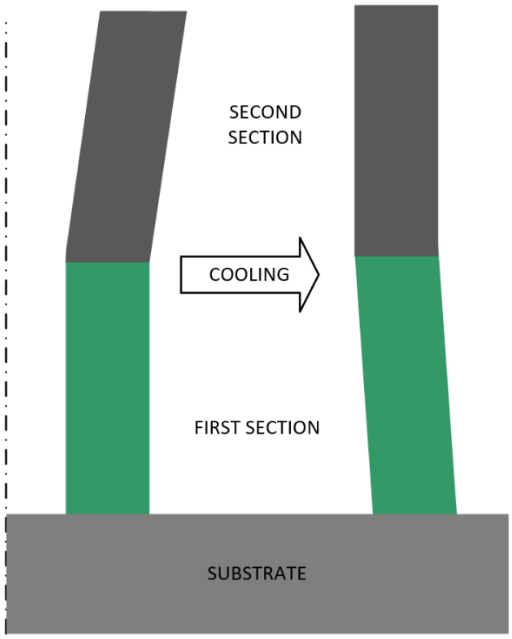

Figure 47: Cooling Distortion

To mitigate the distortion, a pre-heat cycle was developed. This pre-heat cycle utilizes the laser as a heat source to heat the substrate before deposition occurs. To create this cycle, the first layer of the deposition toolpath was used. By applying a shift to the work coordinates, the laser can be de-focused to evenly heat the entire surface without melting the machined base surface. For the pre-heat, 2000 W laser power at a surface feed of 2000 mm/min was used. The timed cycle ran for 10 minutes and the top surface after pre-heat was measured with a surface pyrometer to be 400ºC. Infrared images of the component before and after are shown in Figure 48. The pre-heat cycle was used on hexagons where the part was allowed to cool between sections (hexagons 6, 7, and 8). Results of the implementation on hexagon 8 are shown in Figure 49.

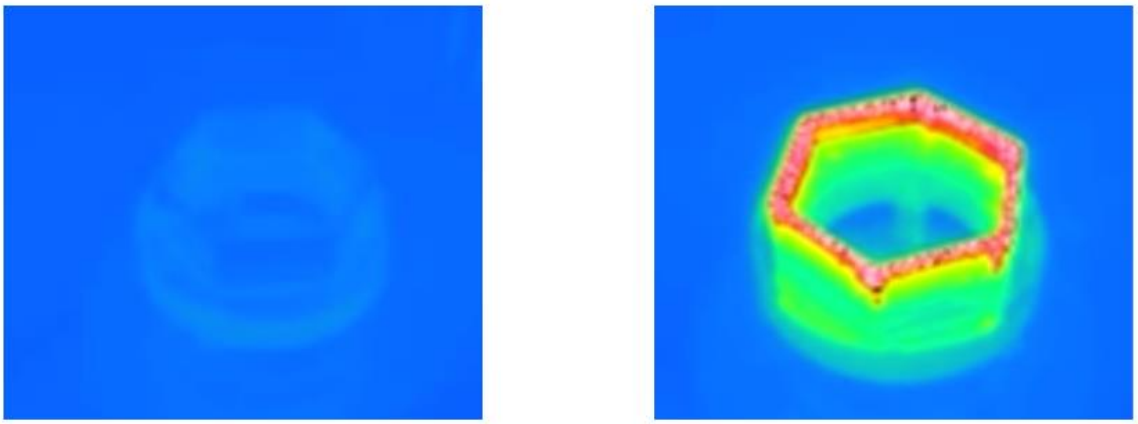

A) Before Preheat

B) After Preheat

Figure 48: Pre-Heat Cycle

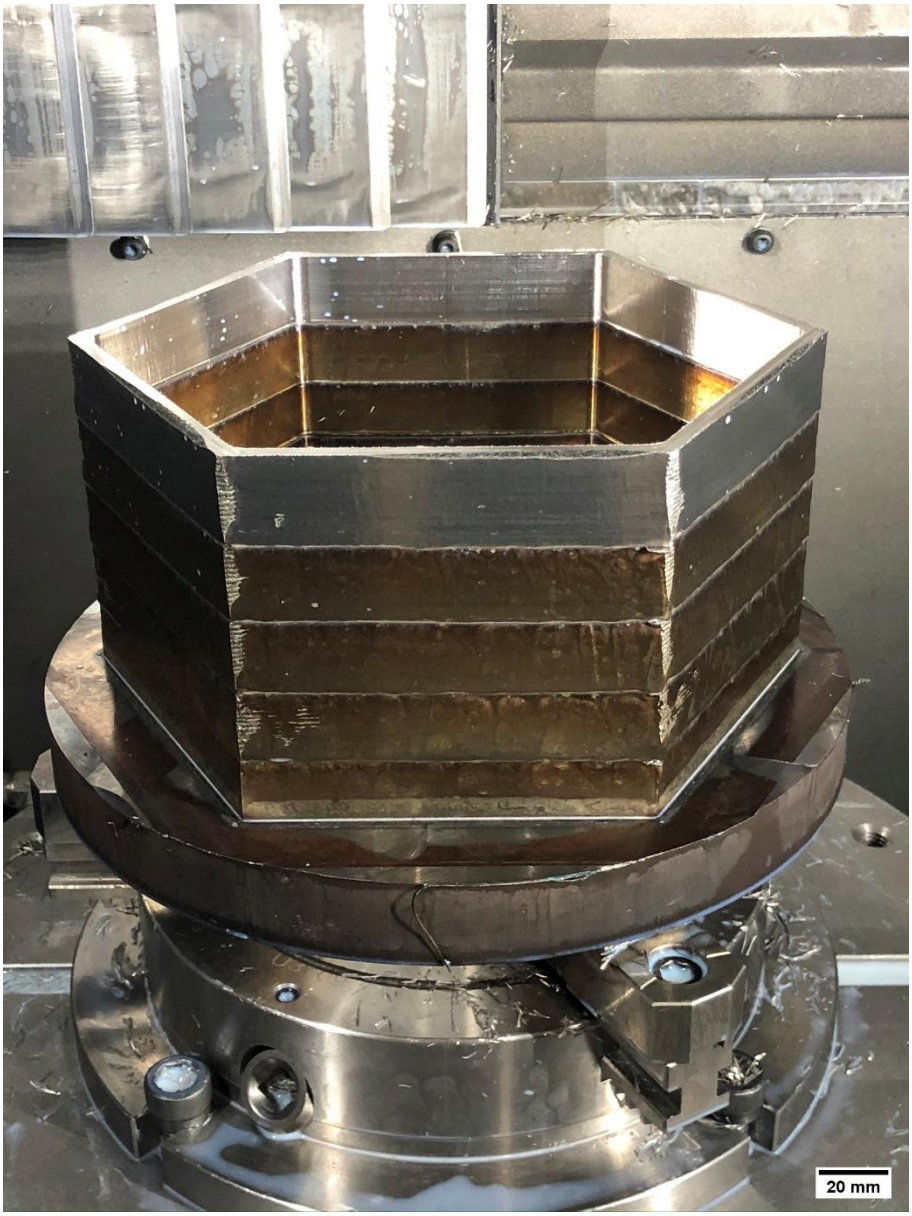

Figure 49: Hexagon 8

4.5.4 Distortion Results

After manufacturing of the hybrid hexagonal structures, each was scanned using a GOM structured light scanner. These results were evaluated using a metrology and visualization software called Volume Graphics.

The imported scans were compared to the nominal CAD geometry as shown in Figure 50. The figure shows the resulting saw-tooth effect due to the cyclical heating and cooling of the component. Distortion figures from each processing scenario is provided in Appendix A.

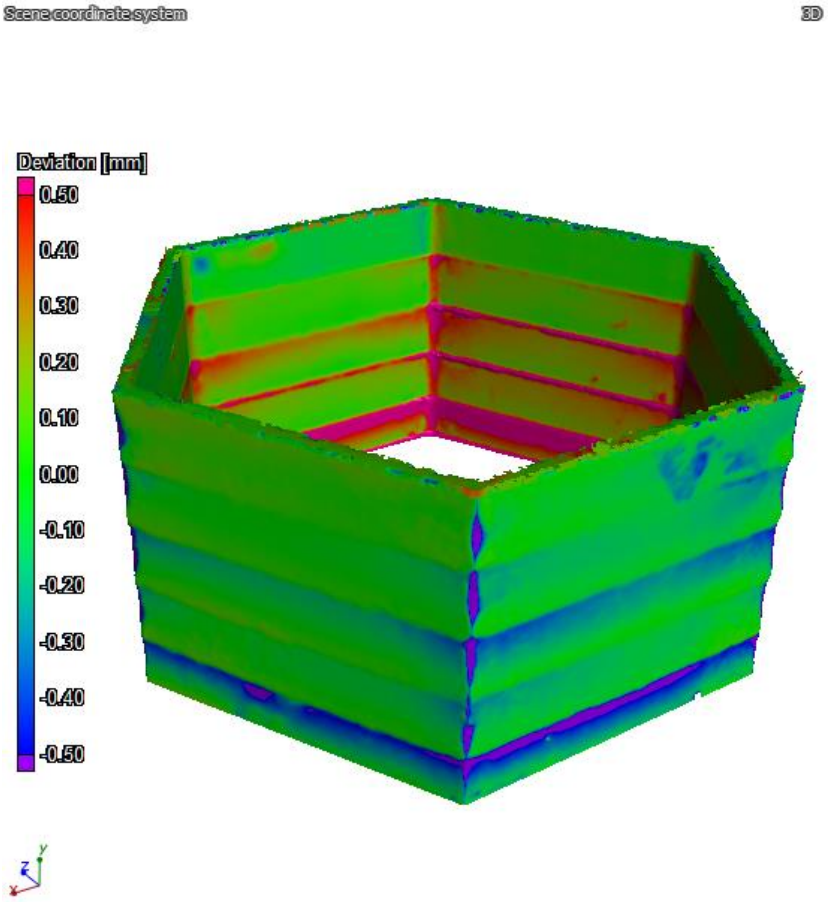

Figure 50: Distortion Comparison for Hexagon 7

To better understand the accuracy of these produced components, the percentage of the surface relative to the absolute distortion of 0.45 mm was determined. For example, only 51% of the geometry for hexagon 5 is within 0.45 mm of the nominal surface.

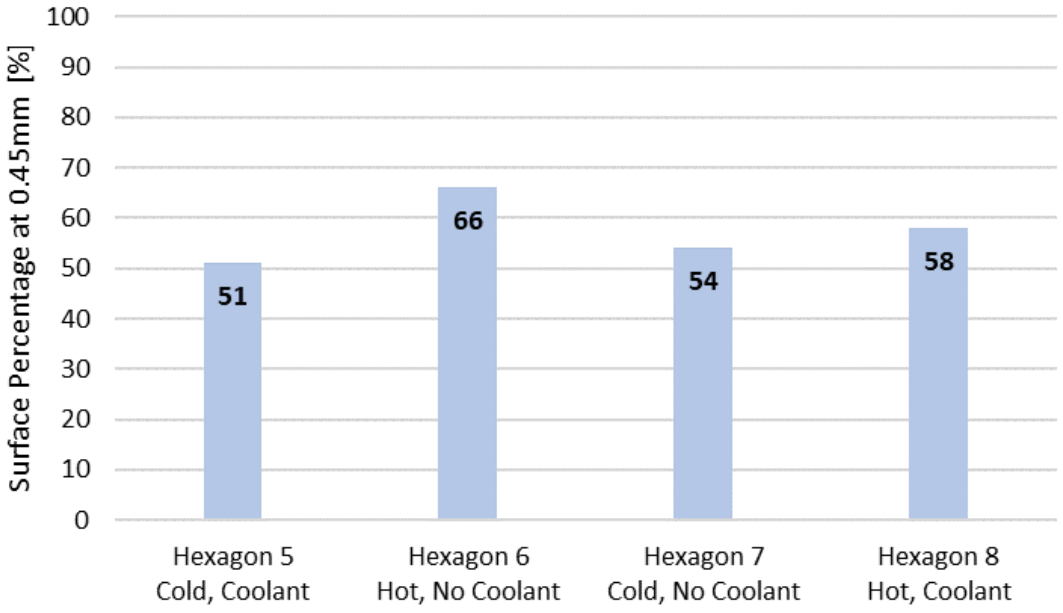

Figure 51: Geometrical Accuracy of Hybrid Hexagonal Structures

Figure 51 shows that the overall accuracy of the final components is poor as all of them are below 70%, but it is seen that Hexagon 6 is the most accurate at 66%. This agrees with the hypothesis that allowing components to completely cool and machining with coolant (reducing cutting forces) yields improved accuracy. This can also be seen in the surface distribution chart shown in Figure 52. Hexagons 6 and 7 both have an increased normal distribution compared to hexagons 5 and 8. It is noted that these data are generated by aligning the scanned model to the nominal CAD model in Volume Graphics. This is done automatically using a least squares technique with little input from the user. Thus, the generated distortion data is not exact but provides a good representation of the resulting distortions.

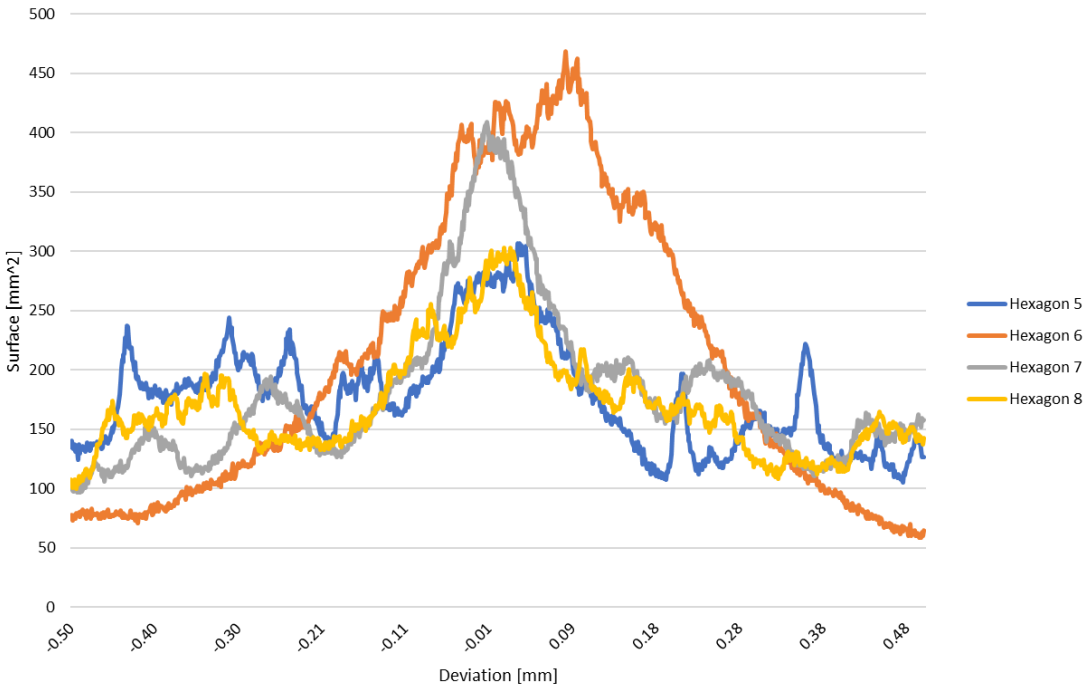

Figure 52: Surface Distribution

From these analyses, it can be concluded that distortion is an important factor for hybrid manufacturing and must be considered. Ongoing research is evaluating the concept of updating toolpath trajectories in-situ to the process to compensate for distortion.

4.5.5 Mechanical Data

As discussed in the methodology section, twelve samples from each hexagonal structure were destructively tested for mechanical properties. The results are discussed below, and the stress-strain curves are shown in Appendix B.

Figure 53 shows the average yield strength and the associated standard deviation for each hexagonal structure. For each case, the yield strength is higher for samples created horizontally along layers when compared to the vertical samples along the build direction. For the hybrid hexagons (5-8) this decrease was greater than the additive hexagons (1-4).

Furthermore, the hybrid hexagons (5-8) have slightly lower yield strengths when compared to the additive hexagons (1-4). Compared to values from literature in Table 8, the yield strength from this study is significantly higher than the wrought 316L stainless steel value of 290 MPa [19].

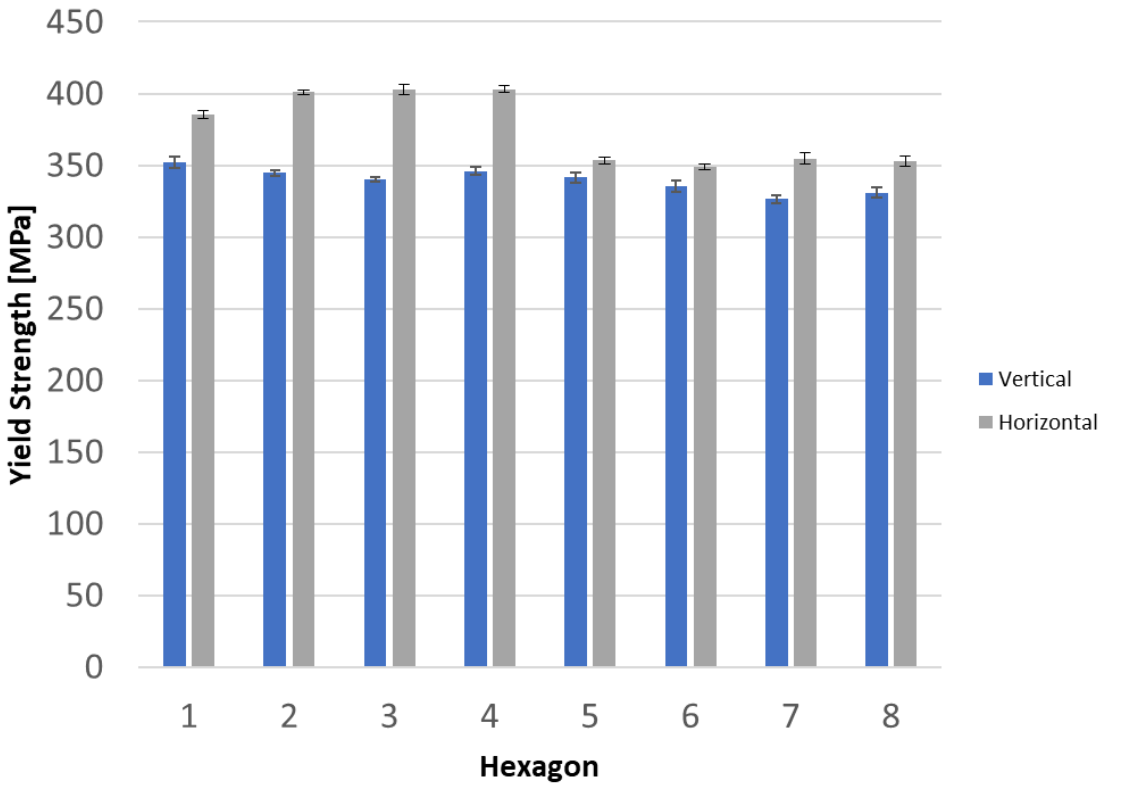

Figure 53: Hexagonal Structure Yield Strength

To help understand if machining influences the mechanical properties of the produced component, yield strength was plotted with respect to elongation. These figures are shown in Appendix B. It is well known that an increased yield strength is coupled with increased elongation [91]. This is the basis and desired outcome for most cold working operations. Yet, the results from this study show that the increase in yield strength results in lower elongation values. The exact underlying mechanism is yet to be determined;

however, it is hypothesized that this can be attributed to cellular microstructure or residual stresses. Furthermore, as discussed in the ensuing section, the significant porosity in the samples can scatter the results enough to mask the expected behavior.

Figure 54 shows the average ultimate tensile strength and the associated standard deviation for each hexagonal structure. For each case, the ultimate tensile strength is higher for the samples created horizontally along layers when compared to the vertical samples along the build direction. For the additive hexagons (1-4), a larger drop in ultimate tensile strength between the orientations is observed when compared to the hybrid hexagons (5-8). Overall, all cases have similar nominal values, with no significant changes between the hybrid (5-8) and the additive (1-4) hexagons. Compared to the wrought 316L stainless steel ultimate tensile strength of 580 MPa, as shown in Table 8, the ultimate tensile strength is similar for the samples produced in this study [19].

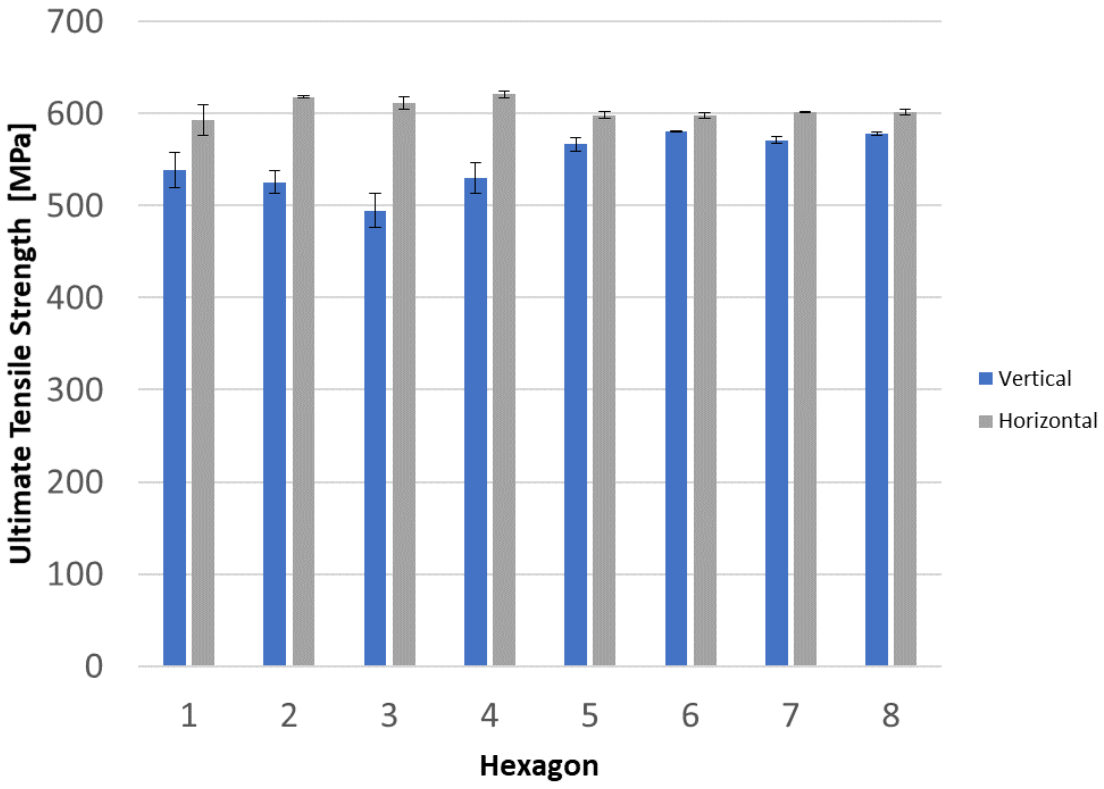

Figure 54: Hexagonal Structure Ultimate Tensile Strength

Figure 55 shows the average elongation and the associated standard deviation for each hexagonal structure. For each case, the elongation is higher for the samples created horizontally along layers when compared to the vertical samples along the build direction. A significant decrease in elongation is seen in the additive hexagons (1-4) when compared to the hybrid hexagons (5-8). Yet, the deviations for these additive hexagons (1-4) are large with respect to their magnitude, indicating a large amount of variation in the data. Compared to the wrought 316L stainless steel elongation of 50%, as shown in Table 8, the hybrid hexagons (5-8) display similar values [19]. The literature also shows deposited samples having lower elongation values of 27%, which is in agreement with the data collected for the additive hexagons (1-4) [19].

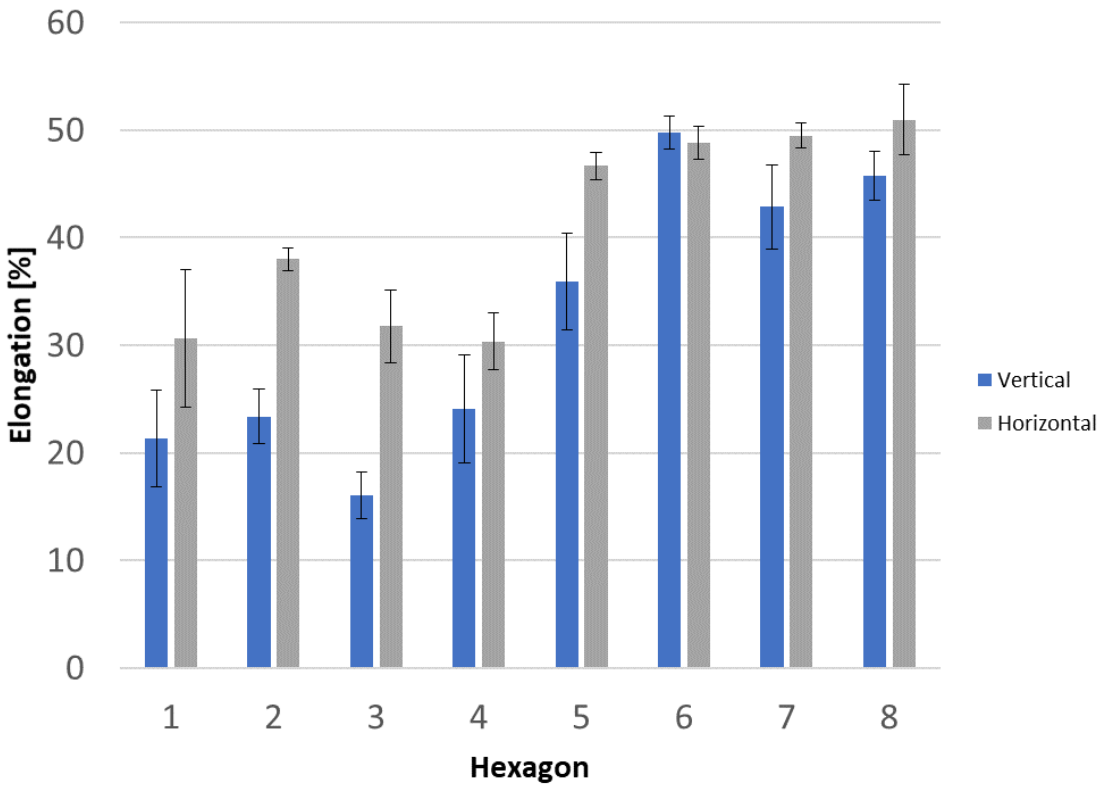

Figure 55: Hexagonal Structure Elongation

4.5.6 Optical Microscopy

Four samples were cut from each hexagonal structure for optical and hardness testing. The samples taken were equally spaced in the vertical direction. This allows for materials characterization to occur along the entire length of the build. These optical images are shown in Appendix B. From the images, it is seen that there is a significant reduction in porosity for the hybrid hexagons (5-8) when compared to the additive hexagons (1-4). Furthermore, many of the larger pores are aligned vertically. Thus, image processing was conducted to determine the distance between pores. As shown in Figure 56, the two pores analyzed are 3.526 mm apart, compared to a 3.29 mm stepover distance. Likewise, the vertical displacement is 2.584 mm, compared to a 1.4 mm layer height (2.8

mm for two layers). It is concluded from the spacing between them that this porosity is between overlapping beads, rather than internal to the deposited bead. Work evaluating the resulting microstructure using electron backscatter diffraction (EBSD) is ongoing and will be published later.

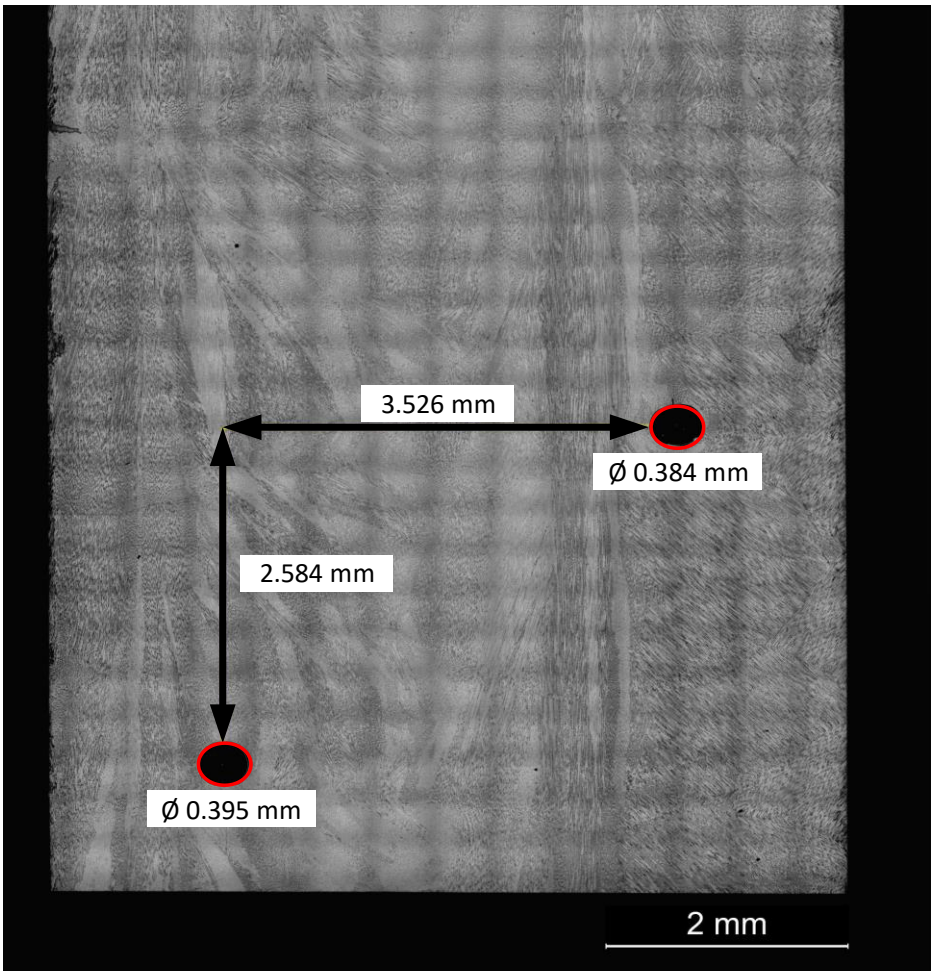

Figure 56: Hexagon 4 Optical Analysis

4.5.7 Hardness

The samples used for optical microscopy were also evaluated for hardness. As shown in Figure 57, 20 data points were taken from each sample. The test method used

was Vickers hardness. This test is independent of the indenter size and can be used for all metals. The load used for these tests was 100 grams.

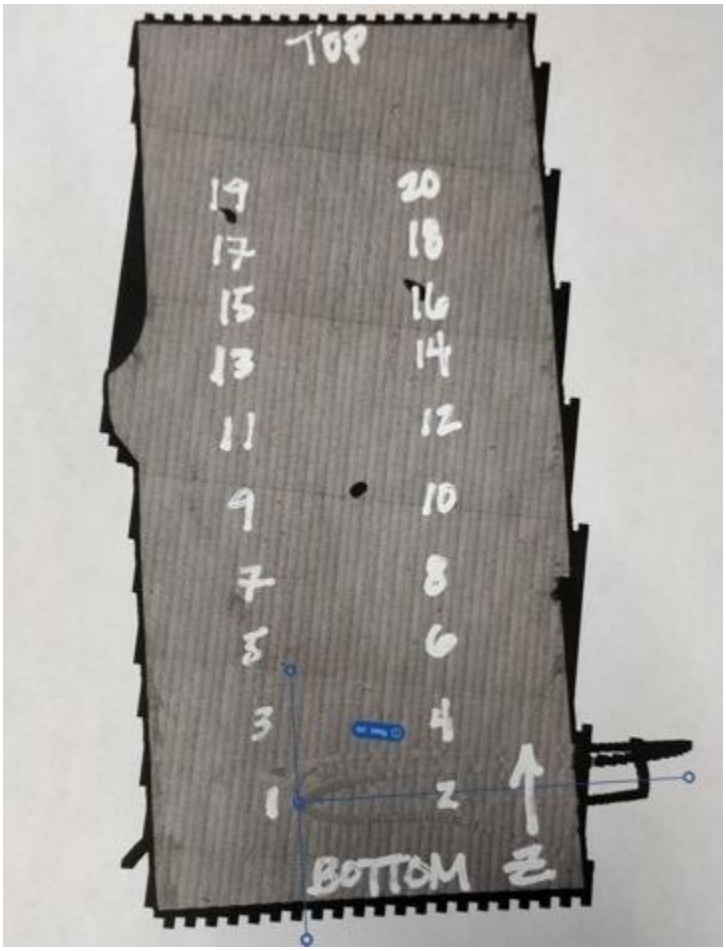

Figure 57: Hardness Testing Locations

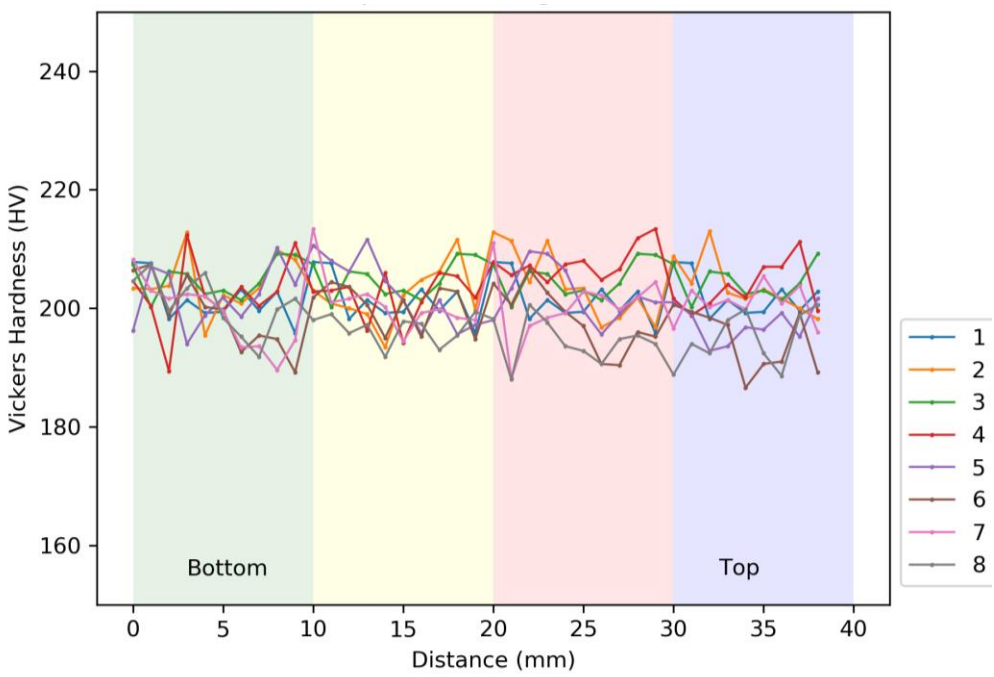

Figure 58: Vickers Hardness Data

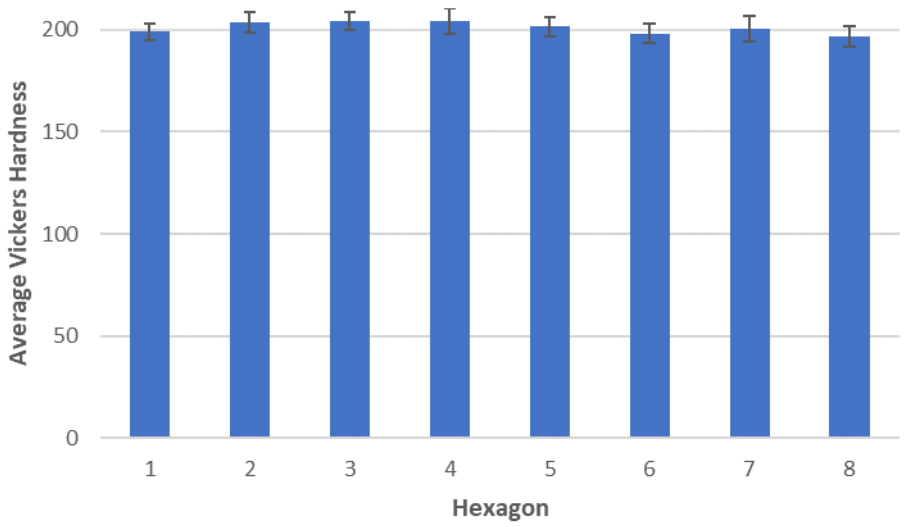

Figure 59: Average Vickers Hardness

As shown in Figure 58 and Figure 59, the hardness for each hexagonal structure is similar and does not contain much variation. The measured values of approximately 200

HV is well above that of 316L stainless steel annealed bar values of 155 HV [92]. From the wire-feed additive manufacturing literature, these values are in agreement with other hardness values [59].

4.5.8 X-Ray Computed Tomography

X-Ray Computed Tomography was conducted on each of the builds to further investigate the porosity identified in the optical microscopy images. This evaluation was conducted on a ZEISS METROTOM 800. This system has a tube voltage of 225 kV, tube power of 500 W, and a resolution of 6 μm. The data were evaluated using Volume Graphics, and images are shown in Appendix B.

It can be seen in Figure 60, that the additive hexagons (1-4) are significantly more porous than the hybrid hexagons (5-8). It is also seen that hexagon 1 is an outlier as it contains 3 times as many pores as the next highest hexagonal structure. It is hypothesized that this is due to the combination of an inconsistent standoff distance (due to incorrect programmed layer height) and a lower heat input. The lower heat input is from this hexagonal structure being deposited using a 3-bead wall-thickness strategy, while the others used a 4-bead strategy. This lower heat input coupled with an incorrect standoff distance caused a significant increase of lack-of-fusion defects, where there is no fusion between successive layers of beads of weld material.

It's hypothesized that the porosity can be directly related back to the elongation to failure for each hexagon. When comparing the two data sets, the hybrid hexagons are less porous while having improved elongation to failure values when compared to the additive

hexagons. This correlation is documented in the literature and has been seen in both additive and casting applications [70, 93].

Figure 61 displays the average pore diameter for each hexagonal structure. It is seen that most of the pores are between 0.5 mm and 1.5 mm in diameter. There is no significant difference between the additive (1-4) and the hybrid (5-8) hexagons. Though an increase is seen with hexagon 3, this rise is attributed to the sample evaluated being an unused tensile sample as no wall sections were available.

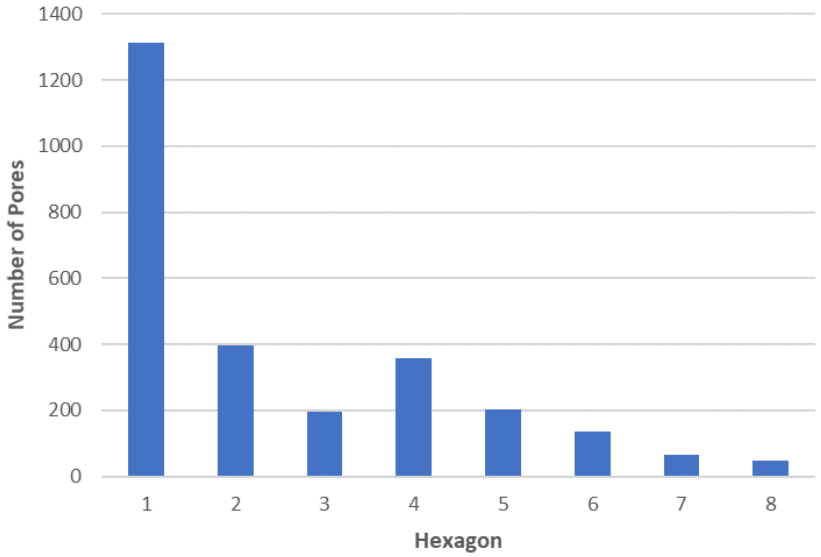

Figure 60: Number of Pores

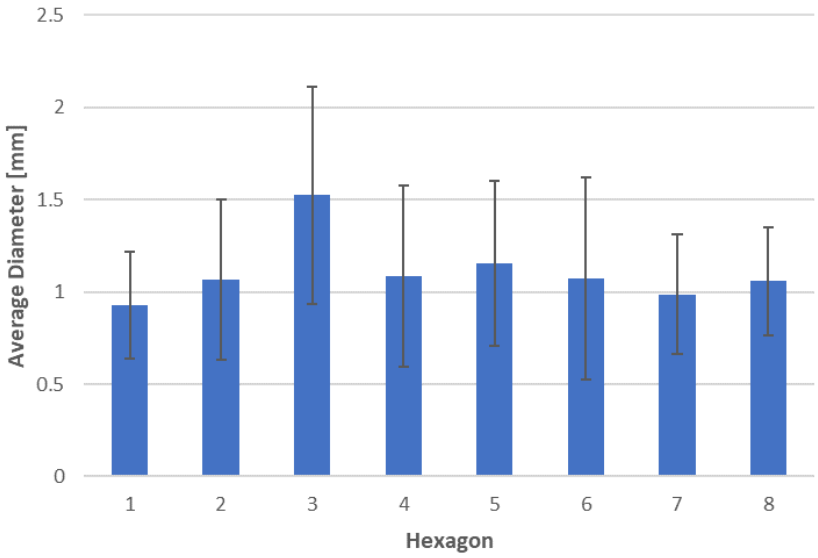

Figure 61: Average Pore Diameter

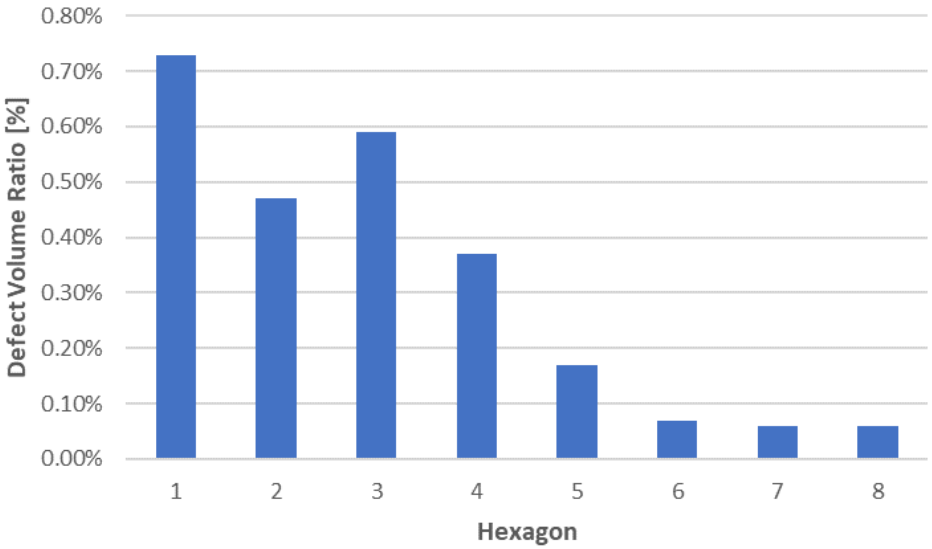

Figure 62: Defect Volume Ratio

Figure 62 shows the defect volume ratio for each of the hexagonal structures. It is seen that all the hexagonal structures are less than 1% porous, but a significant decrease is

seen for the hybrid hexagons (5-8). It is noted that the software package used to evaluate the CT data is unable to identify surface pores as they are not entirely closed. Thus, the reported defect volume ratio often underrepresents the true value.

It is seen from the figures shown in Appendix B that the porosity in the additive hexagons (1-4) is evenly distributed throughout the entire build structure while the hybrid hexagons (5-8) are non-uniform in distribution. It is seen that the first few layers deposited after machining are porous, then subsequently become non-porous. It is hypothesized that this porosity is due to the thermal discontinuity between the deposited layer and the material below it. After the first few layers, the process reaches a thermal equilibrium and the lack-of-fusion defects are mitigated. This reduction of porosity highlights one of the benefits of hybrid manufacturing and reinforces the need for adaptive processing abilities. Hybrid manufacturing's ability to requalify the surface in increments allows for issues associated incorrect processing parameters to be mitigated. For example, if the programmed layer height is incorrect, the standoff distance will be incrementally changed with each deposited layer. It's hypothesized that this can attribute to porosity in the resulting component. However, hybrid manufacturing allows the standoff distance to be corrected as machining creates a known datum for the additive manufacturing process.

4.6 Discussion and Limitations

This chapter investigates the influence that hybrid manufacturing has on the mechanical properties of produced components. Specifically, tensile, hardness, and porosity were evaluated under varying processing scenarios. During the investigation, it was observed that controlling distortion is critical to the hybrid manufacturing process.

Other outcomes that were identified but outside of the scope of this study are outlined and briefly discussed in this section.

For this research investigation, the interleave interval between additive and subtractive manufacturing was selected to decrease overall cycle time. The flute length of the subtractive tooling used was 25.4 mm. Thus, that was selected as the distance to the be deposited before machining occurs. This is a new concept to the field of hybrid manufacturing with little previous work conducted. Chen et. al. developed an algorithm to minimize the number of printed sections by evaluating accessibility of the subtractive tooling [94]. Furthermore, Frank et. al. researched techniques for properly selecting the interleaving distance to mitigate concerns of machining thin walls or large overhangs [95]. The field of researching tool accessibility regions has been prosperous in the past, but little of this work has been applied to additive, or hybrid manufacturing [96]. Thus, this is an area of interest that is highlighted with this research study and should be further investigated.

This research did not investigate the tool-wear due to various machining conditions. Though it was outside of the scope of work, it was evaluated, and tools were replaced as needed. Large amounts of flank-wear, or the wear taking place on the flank face of a single point cutting tool, was observed on the tooling used. There has been significant previous research conducted on linking flank wear to cutting temperature [97, 98]. With elevated cutting temperature, and conditions without cutting fluid investigated during this study, it is not surprising to see higher wear on tooling. The evaluation of cutting forces and tool wear due to hot machining is an ongoing research topic that will be published later.

The produced hexagonal structures are considered thin-walled structures. Thus, they are prone to chatter, a type of vibration between the cutting tool and workpiece, during the machining operation. Chatter only occurred during the hybrid hexagonal structure builds and often occurred only in the last 2 sections. This phenomenon does not affect the mechanical properties of the produced component but reduces the surface finish. It is hypothesized that chatter can be mitigated by using relief tooling for undercut machining. This is an ongoing research topic that will be published later.

Analogous to compensating for distortion within the additive manufacturing toolpath, compensation can also occur during the machining operation. For the scenario where dry machining directly after deposition occurred (hexagons 4 and 5), it is hypothesized that the component was distorting during the machining operation. Though it was not investigated during this study, such compensation is a new area of research in the field of hybrid manufacturing that did not previously exist.

4.7 Conclusion

Hybrid manufacturing allows for additive and subtractive processes to be conducted without breaking machine setup. This chapter investigated the effect that hybrid manufacturing has on the mechanical properties of the resulting components. Hexagonal structures were produced by varying processing means such as the machining temperature and use of coolant. Key outcomes from this research were:

- Manufacturing hexagonal structures using a hybrid manufacturing strategy reduces the overall cycle time by 68%.

- Hexagonal structures produced by hybrid manufacturing have improved elongation to failure by 22% and reduced porosity by 16% when compared to the additive hexagonal structures.
- All experimental cases perform comparable to expected values from literature with respect to yield strength, ultimate tensile strength, and hardness.

This study identified the need for thermal distortion modeling in hybrid manufacturing. As shown in this chapter, components such as the hexagonal structure were unable to be manufactured without compensation of the toolpath trajectories. As a result, this work builds the foundation needed for technology maturation toward the industrial adoption of hybrid manufacturing. Now that an understanding of how hybrid manufacturing influences the mechanical properties of components has been established, the ensuing chapter investigates the use of hybrid manufacturing to improve the mechanical locking between added material and substrate.

CHAPTER 5. HYBRID STRUCTURES

Hybrid manufacturing systems provide a platform for integrated additive and subtractive capabilities. Unlike other deposition processes where substrates are required to be planar, hybrid manufacturing's subtractive capability allows for unlimited surface structures and conditions. This chapter investigates the use of various material and structure combinations to enhance the mechanical properties associated with hybrid manufactured components.

5.1 Introduction

Hybrid manufacturing now provides the ability for mechanical interfaces to be developed between cladded and substrate materials. These interfaces, termed hybrid structures, are generated using common subtractive tooling such as endmills and dovetail cutters. Analogous to joints in woodworking, it is hypothesized that the mechanical locking between the deposited material and substrate can be influenced by varying the geometrical interfaces. This study evaluates various hybrid structures for multiple material substrates. The ensuing section provides an overview of relevant literature that is the basis for this work.

5.2 Literature Review

Traditionally, welding is known as a joining process [99]. When welding is selected as the joining process, a filler material and a welding joint must be selected. The type of joint used is influenced, and often defined by, the intended application [81]. Joints are widely used as they enable the distribution of loads across a larger area and do not require

holes or increased weight for fasteners [100]. Welded joints can be classified into five basic categories: butt, fillet, corner, lap, and edge [101]. These joints are commonly used to join two components together, often in out-of-plane orientations.

While many researchers have studied purely additively produced components, the purpose of this research is to understand the effects of varying the interface geometry on the mechanical properties on the resulting component. Thus, it is important to investigate the interfacial bonding. Weak interfacial adhesion can result in premature failure along the interface region. Most of the interest in hybrid components has been limited to investigation of hard-facing applications. However, multi-layer deposition is unavoidable in large components. In practical applications, the interfacial bonding strength and the mechanical properties of the multi-material component should be equivalent to or exceed that of the parent material [102].

Few studies have focused on manufactured specimens in this manner. The available literature is limited to nickel-based deposits [5, 103, 104]. A study by Kim et al. found that tensile samples produced from a combination of DED deposited AISI 4140 and wrought AISI 4140 did not fail in the interfacial region [104]. From this study, it was concluded that as-deposited material has less inter-layer bond strength in the additive region than in the interface region. As compared to the wrought material, their as-built samples show 50% lower ultimate tensile strength with a 47% standard deviation, 64% reduction in yield strength with 32% standard deviation and almost half the maximum elongation with 65% standard deviation [104]. The high variance was attributed to metallurgical defects, which can result in largely brittle factures [105].

While there has been little to no research conducted on interface joints for additive manufacturing, such joints have been studied for other processes. Unlike welding, woodworking has been around for thousands of years; thus, there has been significant research done with respect to woodworking joint design. A study by Rao, et. al. showed that the angle and length of a finger joint, as shown in Figure 63, had an effect on the ultimate tensile strength of the joined component [106]. This research concluded that short (L) , low-sloped joints (α) resulted in the highest ultimate tensile strength of the joints tested [106]. It is seen that adding these finger joints can increase the tensile strength by 10 times when compared to a simple butt joint [107].

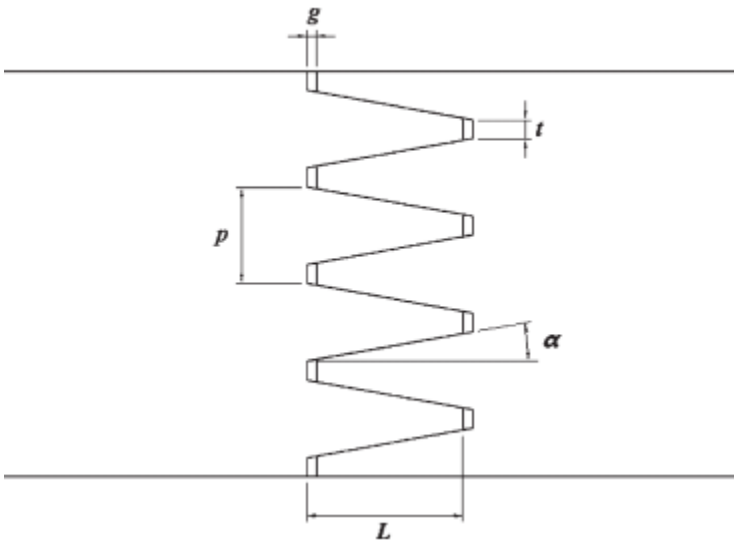

Figure 63: Finger Joint [106]

Joints between dissimilar metals, such as austenitic stainless steel and carbon steel are required in many applications in industry [108]. Two major concerns in these types of joints are martensite formation in the weld bead and a low-alloy heat affected zone which promotes cold cracking or hot cracking in fully austenitic weld material. The former is

controlled by normal precautions such as preheat, while the latter is mitigated by carefully controlling the material composition. Cyclical thermal profiles, which are seen in additive manufacturing, also result in high thermal stresses and carbon migration which result in component failure. The carbon diffuses into the austenite during welding, forming martensite and carbides at the weld interface. These give rise to poor elongation properties and high hardness values [109].

Physical properties that influence laser welding of dissimilar materials are thermal conductivity, absorptivity, density, specific heat capacity, CTE, and melting temperature [108]. Large differences in thermal expansion between cladded materials result in the formation of large residual stresses, with implications for joint strength and fatigue issues [108, 109]. To mitigate these issues, typically a filler metal with intermediate coefficient of thermal expansion (CTE) value is used to mitigate the thermal mismatch of dissimilar materials [108, 109]. For example, a joint between ductile cast iron and steel results in a single component that is easily cast yet has the toughness of steel. Welding cast iron typically requires preheating, but a nickel filler wire can be used to obtain austenitic weld metal without the need for preheating [110].

Using the literature as the foundation for this research, it is seen that there is a need to research the effect of mechanical interfaces between added and substrate material. Similar to tribal knowledge in woodworking, it is hypothesized that adding a joint to the interface will improve the strength of the resulting component.

5.3 Methodology

The methodology of this research is to manufacture components with varying interfaces, termed hybrid structures, and varying substrates to better understand the influence that the interface geometry has on the mechanical properties of the produced component. The experimental setup is held consistent by using 1.14 mm (0.045”) diameter 316L stainless steel wire deposited on a rectangular substrate, as depicted in Figure 64. The additive parameters used are identical to the hexagonal structure experiments and are shown in Table 10.

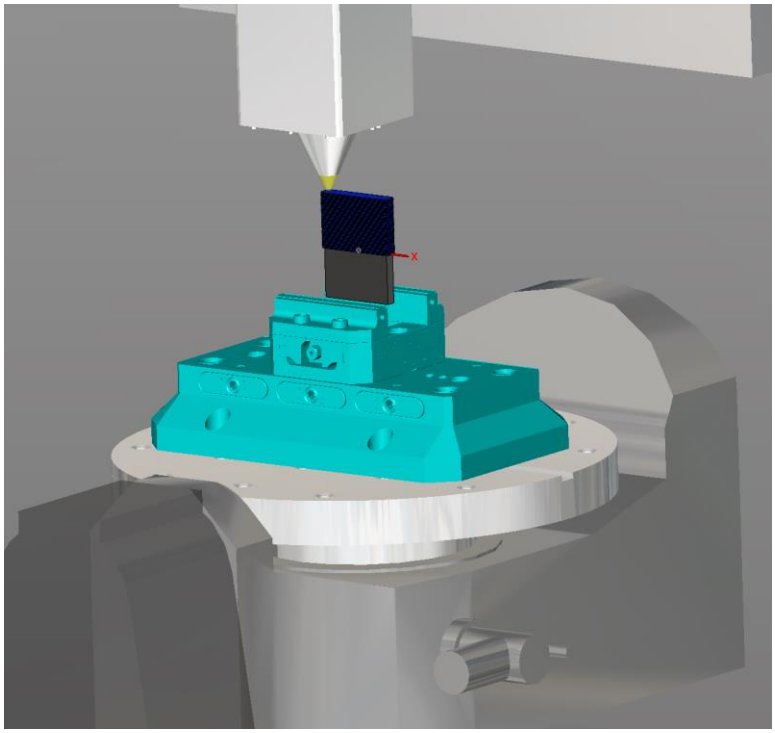

Figure 64: Hybrid Structure Deposition

Two substrate materials were selected for the investigation: one being 316L stainless steel to understand the influence of hybrid structures on similar material, and the other will be gray cast iron to understand the influence on dissimilar materials. This

material was selected as it has a lower CTE than the deposited material. The deposited material and substrate are sized such that they can be used to produce ASTM E8/E8M-16a tensile samples as shown in Figure 31 [23]. For consistency, the original interface between substrate and deposited material will be in the center of the tensile sample.

5.3.1 Flat Structure

For the null scenario, a flat structure will be analyzed. Most additive manufacturing is conducted on a planar surface. Thus, this test case, as shown in Figure 65, is the baseline for the investigation.

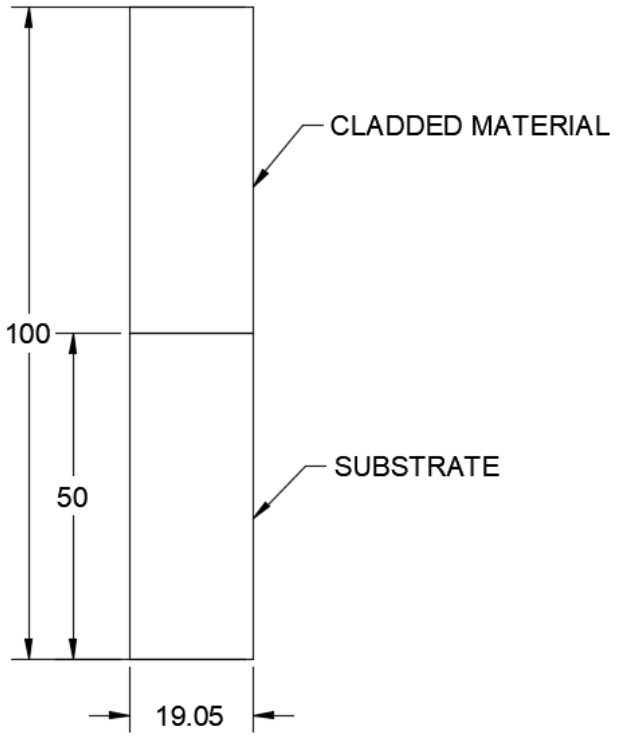

Figure 65: Flat Structure (Units in mm)

5.3.2 Angled Structure

One of the fracture modes in tension is shear fracture. It is also widely known from the Maximum Shear Stress (Tresca) Theory that maximum shear stress occurs at 45° to the direction of loading [99]. Thus, one hybrid structure evaluated should be a 45° angled structure, as shown in Figure 66. Research being conducted in parallel at Georgia Tech is also evaluating the influence that various angles have on mechanical properties of hybrid manufactured components.

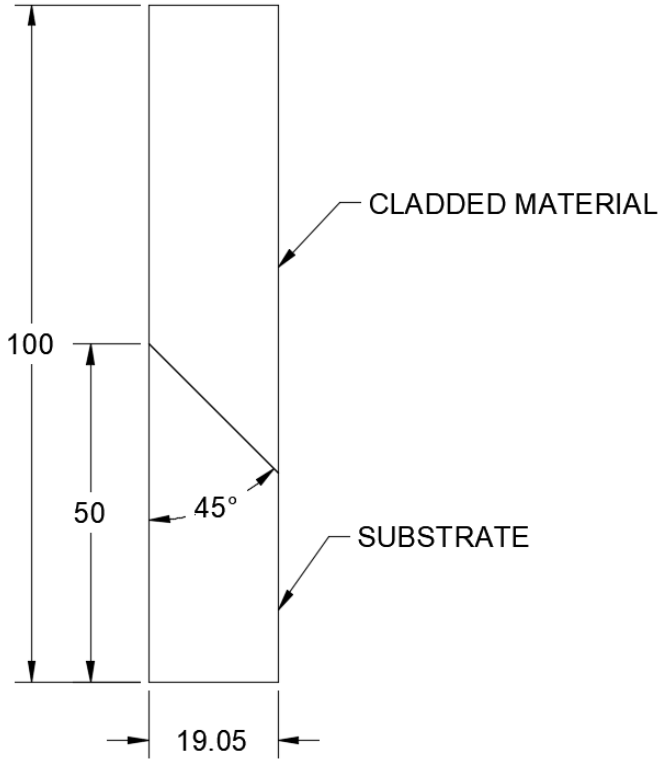

Figure 66: Angled Structure (Units in mm)

5.3.3 Scalloped Structure

When evaluating structures that could be easily produced and widely accepted by industry, it was determined that creating a hybrid structure that required specialized tooling

would not be advantageous. Thus, common tooling such as ball mills were evaluated. A 3.175 mm (1/8”) ball mill was selected as it would produce the smallest scalloped groove that is still larger than the laser diameter for the additive manufacturing process. It is also desirable for the structure feature size to be smaller than the cross-sectional area of the tensile sample. The depth is selected such that four layers are deposited in the groove. Figure 67 shows the dimensional sizing of the experimental setup.

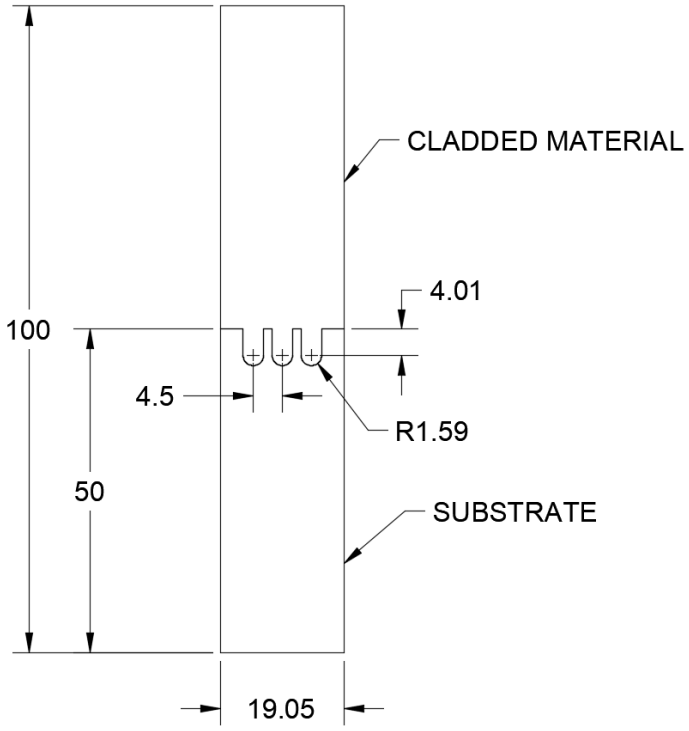

Figure 67: Scalloped Structure (Units in mm)

5.3.4 Tongue and Groove Structure

Another commonly used tool in machine shops are square end mills. This end mill would create a tongue and groove structure. Like the scalloped structure, a 3.175 mm (1/8”) mill was selected as it would produce the smallest square groove that was still larger than

the laser diameter for the additive manufacturing process. For this structure, the depth is selected such that the volume removed from the substrate remained constant when compared to the scalloped structure. During the additive process, four layers were deposited in the grooves. Figure 68 shows the dimensional sizing of the experimental setup.

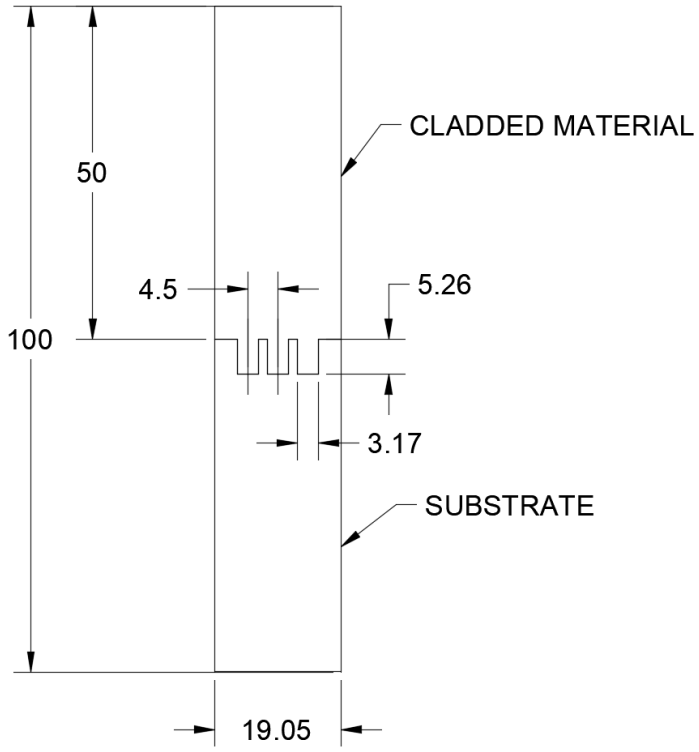

Figure 68: Tongue and Groove Structure (Units in mm)

5.3.5 Dovetail Structure

Another common tool used in CNC machining is a dovetail cutter. This cutter is commonly used to create grooves for better clamping of components in workholding. Dovetails also provide a hybrid structure with undercuts. It is hypothesized that this is the superior hybrid structure due to the mechanical locking that it would provide. Specifically, the shrinkage of the substrate material due to the thermal expansion during the deposition

process would mechanically lock the added material. The throat of the dovetail was kept consistent with the other structures, and the undercuts were sized such that they would be filled during the additive process. Analogous to the other structures, the depth is selected such that the volume of material removed from the substrate matched the other grooves. Due to this structure's small size, as shown in Figure 69, wire EDM is used to create the structure. To ensure that the groove filled, the feedrate for the first layer was reduced by 50% to 500 mm/min.

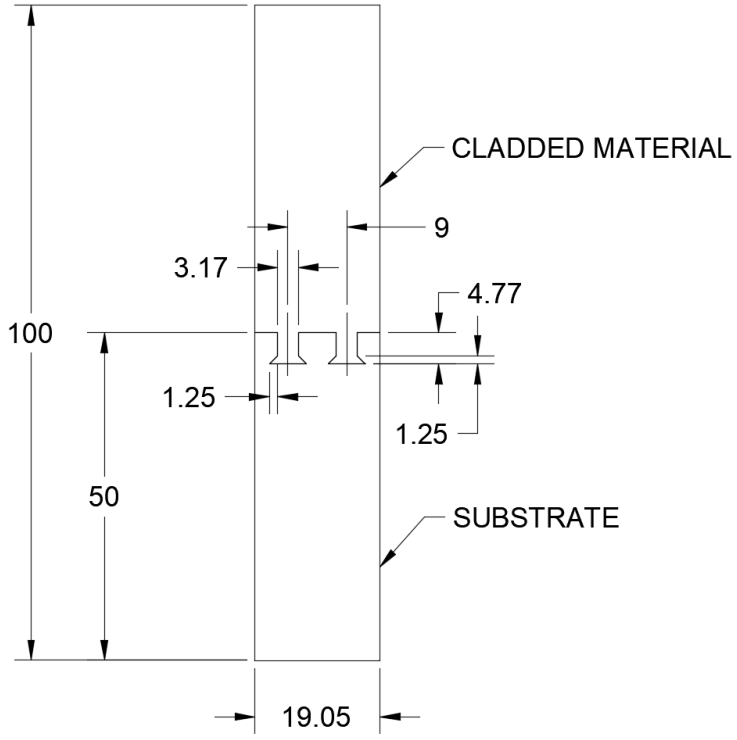

Figure 69: Dovetail Structure (Units in mm)

Tooling and associated machining parameters, per the manufacturer's recommendations, are used to generate the samples are shown in Table 13. Due to the sizing of the dovetail structure, it was manufactured using wire EDM.

Table 13: Hybrid Structure Machining Parameters

Tool	Application	Parameter	Stainless Steel	Cast Iron
25.4 mm 4-flute end mill	All	Surface Feed	70 m/min	135 m/min
		Feed-rate	0.0644 mm/tooth	0.0859 mm/tooth
3.175 mm (1/8”) 4-flute ball mill	Scalloped	Surface Feed	70 m/min	139 m/min
		Feed-rate	0.0151 mm/tooth	0.0201 mm/tooth
3.175 mm (1/8”) 4-flute end mill	Tongue and Groove	Surface Feed	70 m/min	135 m/min
		Feed-rate	0.0140 mm/tooth	0.0182 mm/tooth

For all experiments, the surface of the substrate is cleaned of contaminants with alcohol before the deposition process occurs. This removes any residual oil that may be left from the coolant used during structure preparation process. Once the samples have been made, they will be prepared by means of wire EDM and tensile tested per ASTM E8/E8M standard test methods for tension testing of metallic materials [23].

5.4 Results

Using the methodology above, the samples were successfully produced in a short period of time. After preparing the tensile samples, it was decided to not tensile test the dovetail structure. Although it was hypothesized that they were sized properly, the dovetail groove as shown in Figure 70 was not sufficiently filled to provide accurate data. Thus, it was omitted from all testing procedures.

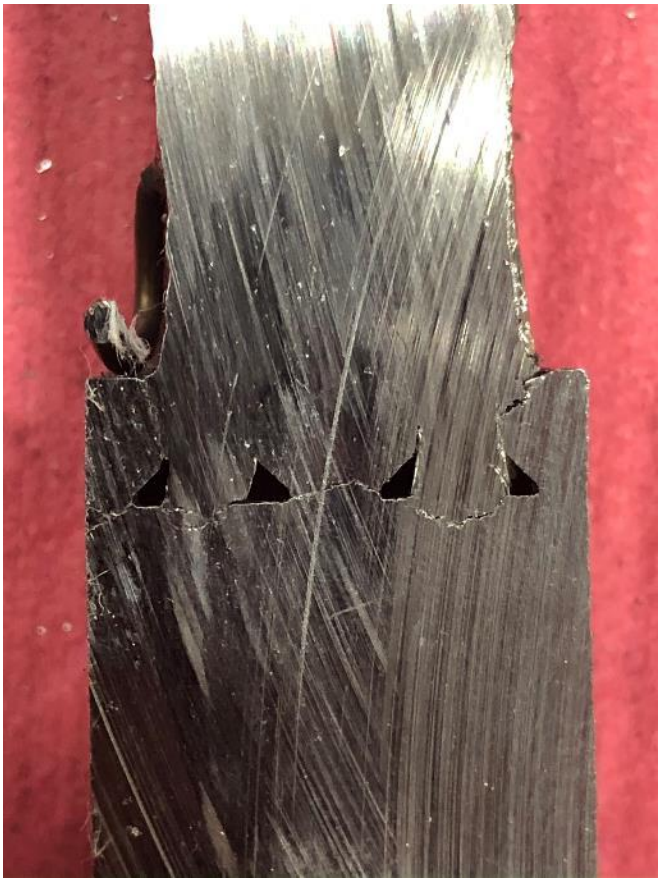

Figure 70: Un-Filled Dovetail Structure

The ensuing sections discuss the results of the tensile testing, optical, and X-ray computed tomography testing.

5.5 Stainless Steel Structures

The first variation of the hybrid structure study is to evaluate the influence that hybrid structures have on similar materials. Thus, 316L stainless steel was deposited on 316L stainless steel substrate for four different hybrid structures. Images of the manufactured components are shown in Appendix C.

5.5.1 Mechanical Data

From the manufactured hybrid structures, six samples were generated for mechanical testing. Results from the mechanical tests are shown in the ensuing figures. It is seen in Figure 71 that the elongation for the flat structure performed significantly better than all the other structures. Furthermore, it performed similarly to the hybrid hexagonal structures as discussed in the previous chapter.

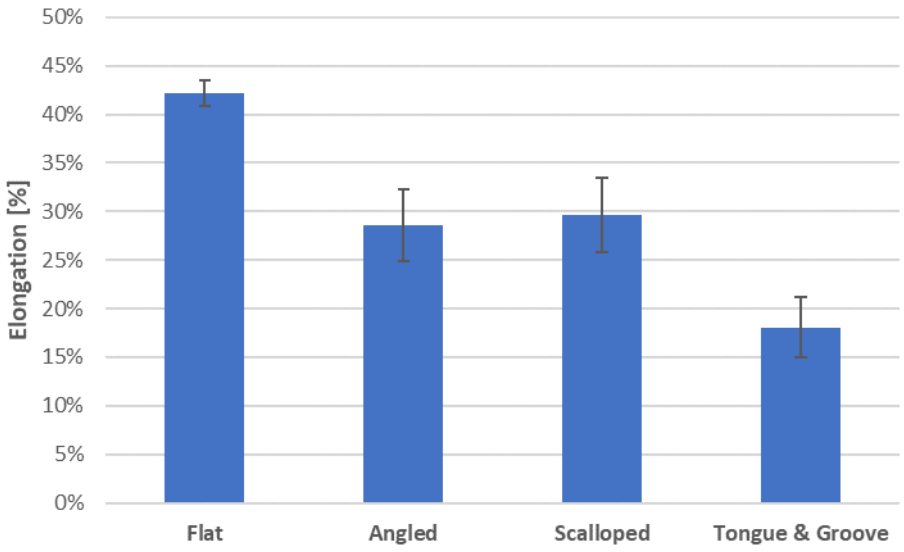

Figure 71: Elongation at Failure for Stainless Steel Structures

Similarly, Figure 72 shows the reported ultimate tensile strength from each of the tested structures. Once again, the flat structure performed the best. The reported values are slightly less, but comparable to what was reported from the hexagonal structure mechanical testing. It is hypothesized that the discrepancy is due to half of the tensile sample being comprised of substrate (316L Stainless Steel Annealed Bar).

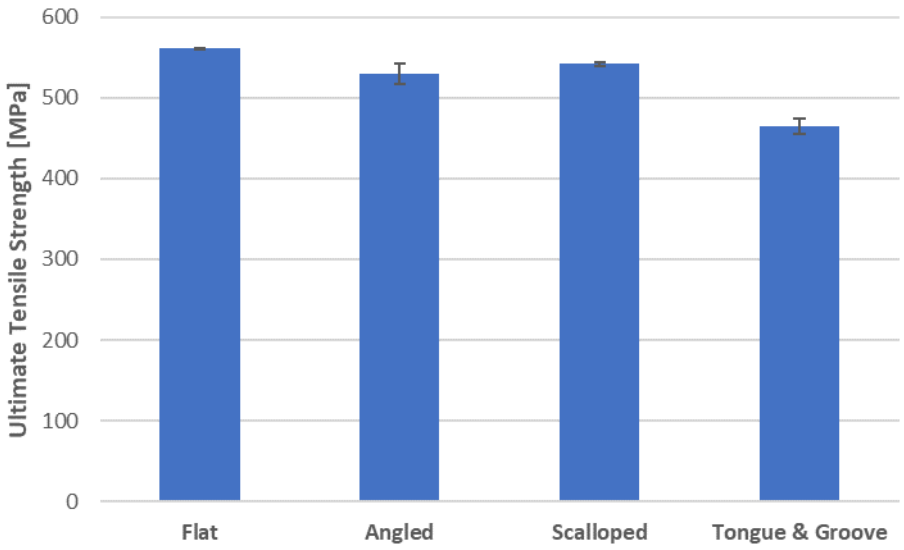

Figure 72: Ultimate Tensile Strength for Stainless Steel Structures

Figure 73 shows the reported yield strength of each stainless steel structure. In this instance, the flat and angled structures performed similarly, with the angled structure providing slightly better results to the angled structure. When compared to the reported values from the hexagonal structure tests, these values are much lower, but are similar to that of the wrought material with reported values of 290 MPa [19].

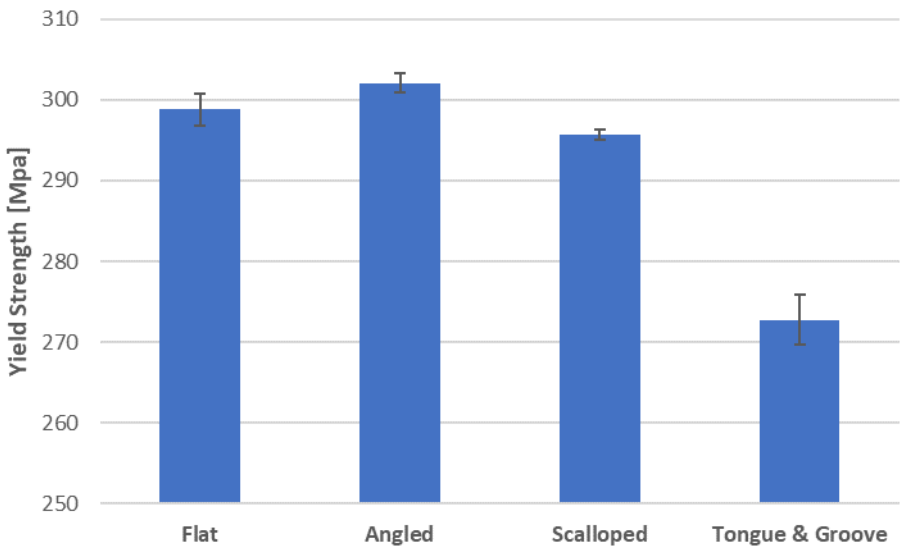

Figure 73: Yield Strength for Stainless Steel Structures

5.5.2 Optical Microscopy Data

Samples were taken from the unused material from each generated stainless steel structure. These samples were evaluated using optical microscopy to further understand the porosity at the interface. Few conclusions can be drawn from these images regarding microstructure without electron backscatter diffraction (EBSD) testing. However, porosity can be seen at the interface of all samples with the exception of the flat structure.

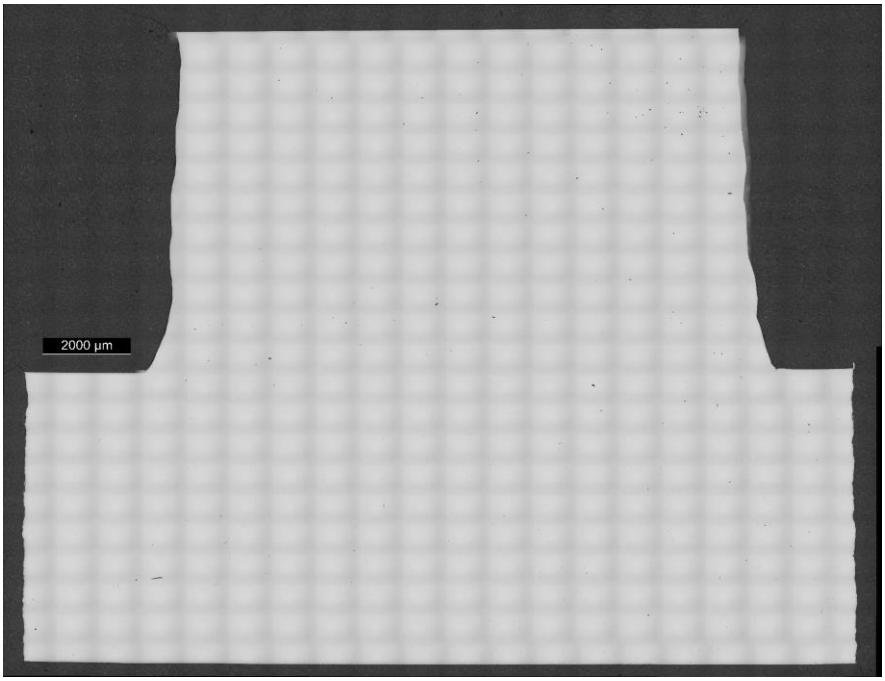

Figure 74: Stainless Steel Flat Structure

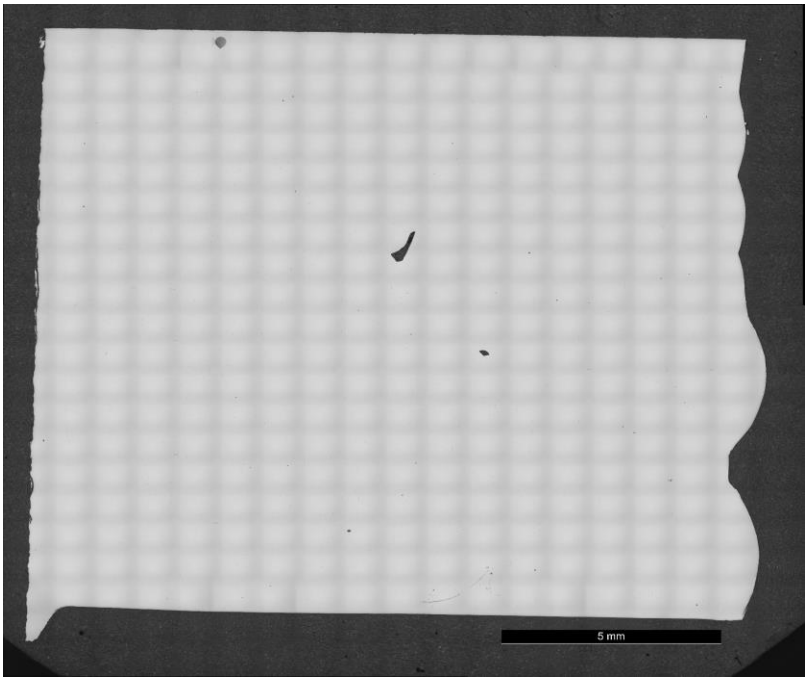

Figure 75: Stainless Steel Angled Structure

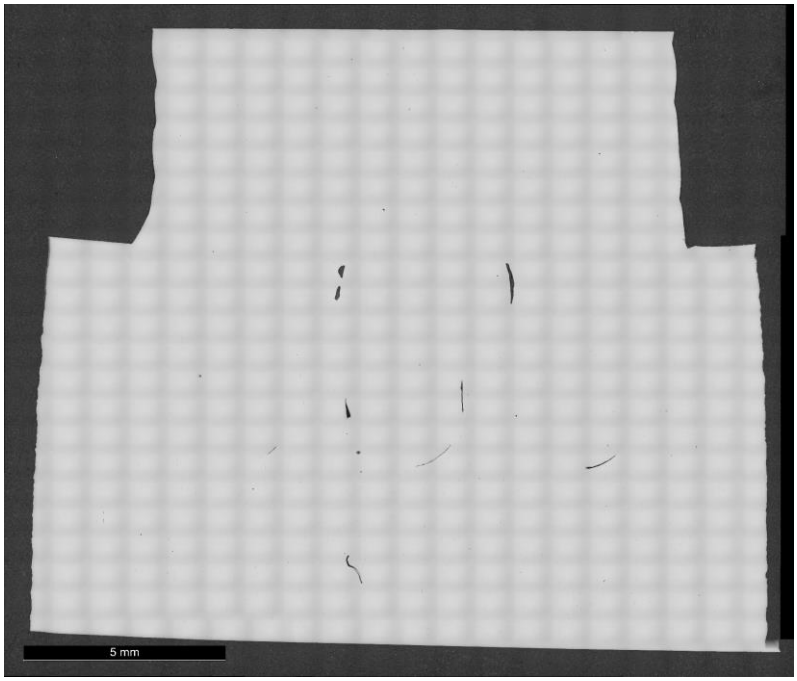

Figure 76: Stainless Steel Scalloped Structure

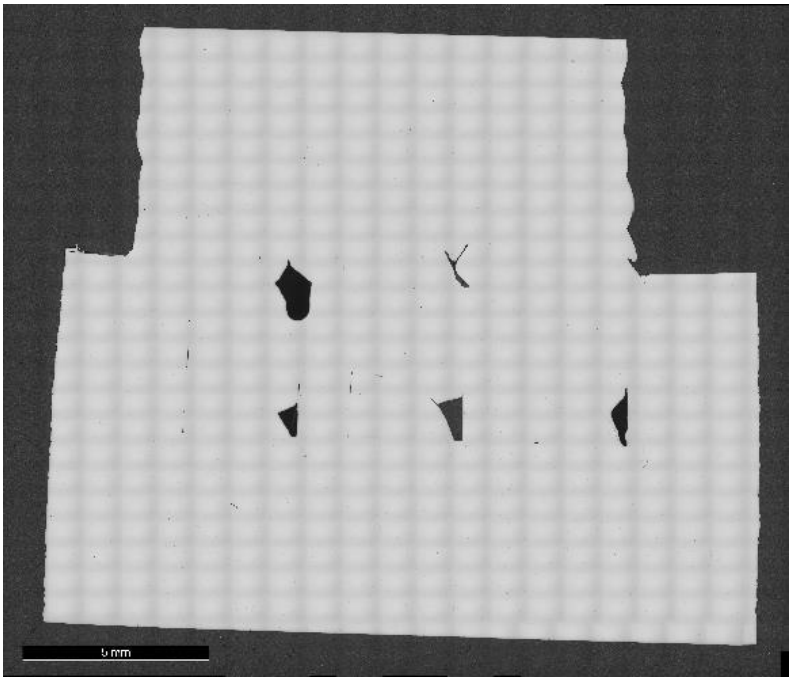

Figure 77: Stainless Steel Tongue and Groove Structure

5.5.3 X-Ray Computed Tomography Data

To further understand the full extent of the porosity in the generated samples, X-ray computed tomography was done on an extra tensile sample. Due to the excessive porosity in some of the samples, quantitative values were unable to be determined. In instances where there were voids throughout the entire length of the build, the software package used, Volume Graphics, is unable to distinguish these as voids. Thus, the reported values are vastly underrepresented. The generated X-ray computed tomography figures are shown in Appendix C.

5.6 Cast Iron Structures

The second variation of the hybrid structure study is to evaluate the influence that hybrid structures have on dissimilar materials. Thus, 316L stainless steel was deposited on gray cast iron substrate for four different hybrid structures. Images of the manufactured components are shown in Appendix C.

5.6.1 Mechanical Data

From the manufactured hybrid structures, six samples were generated for mechanical testing. As previously discussed, it is important to use the results to compare the structures to one another, and not to compare them against wrought cast iron or stainless steel. Results from the mechanical tests are shown in the ensuing figures. As seen from the results, the flat structure performed the best, similar to the outcome from the first variation using stainless steel.

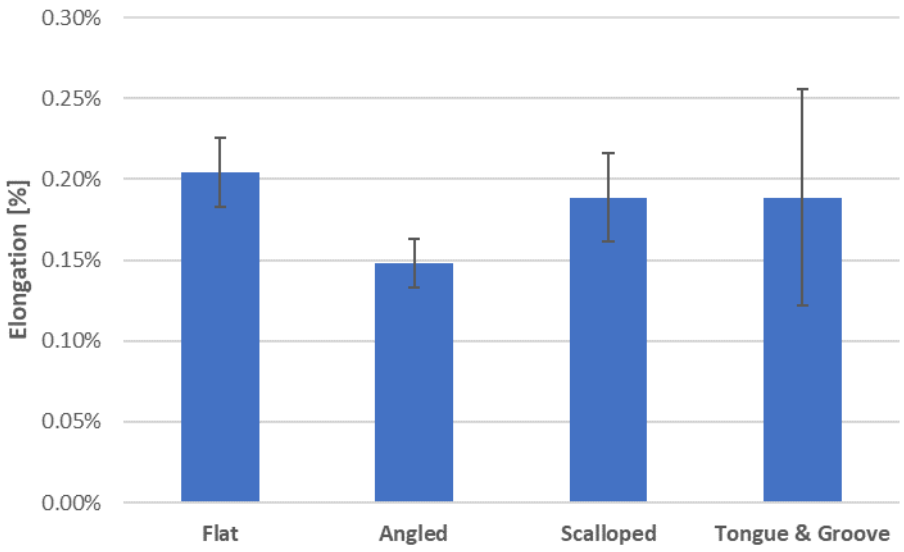

Figure 78: Elongation at Failure for Cast Iron Structures

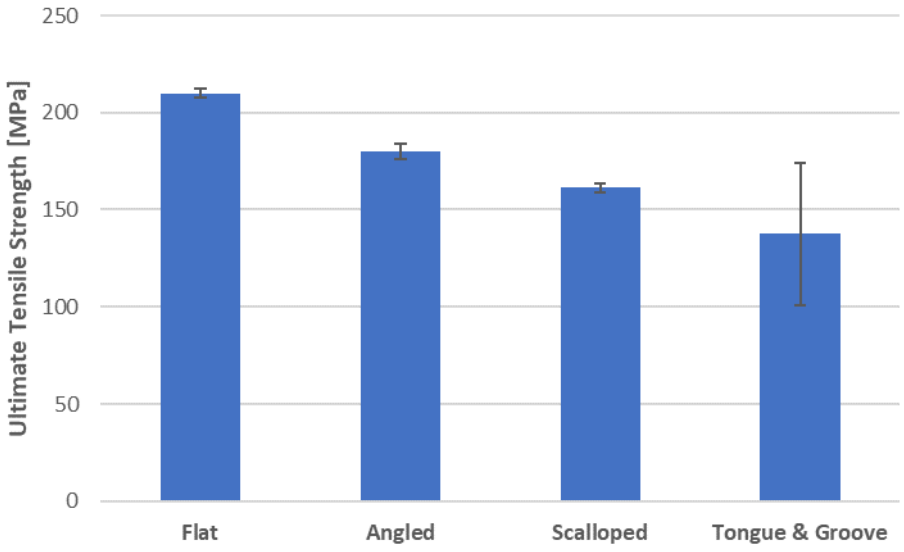

Figure 79: Ultimate Tensile Strength for Cast Iron Structures

5.6.2 Optical Microscopy Data

Samples were taken from the unused material from each generated cast iron structure. These samples were evaluated using optical microscopy to further understand

the porosity at the interface. Few conclusions can be drawn from these images regarding microstructure without electron backscatter diffraction (EBSD) testing. However, significant porosity and cracking can be seen at the interface of all samples.

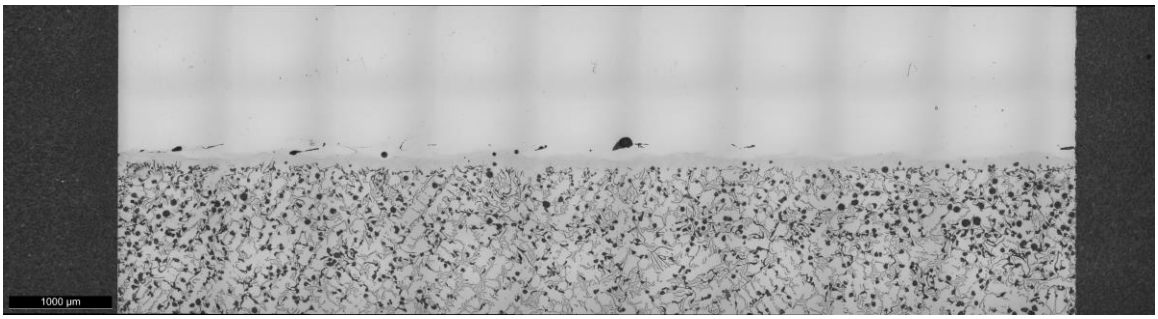

Figure 80: Cast Iron Flat Structure

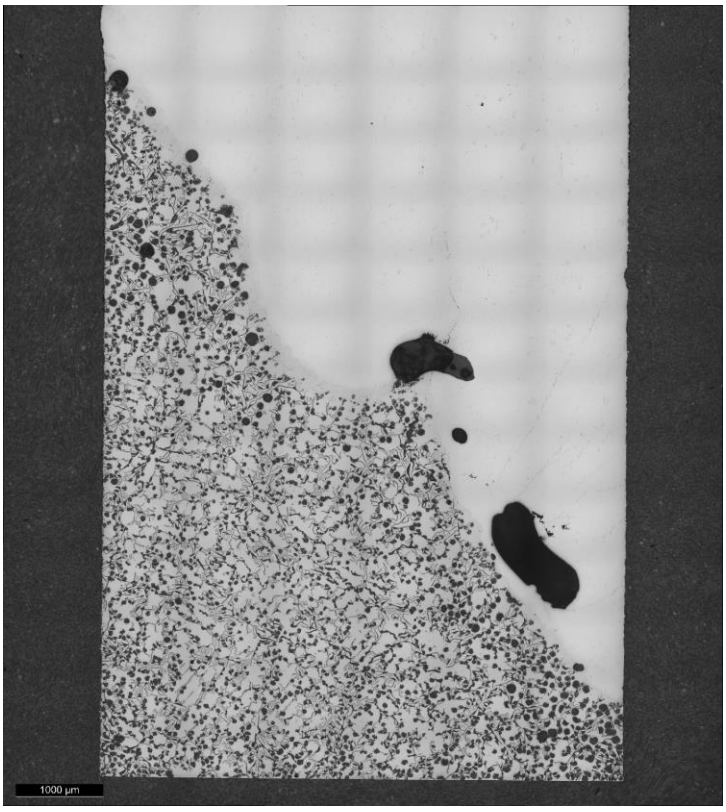

Figure 81: Cast Iron Angled Structure

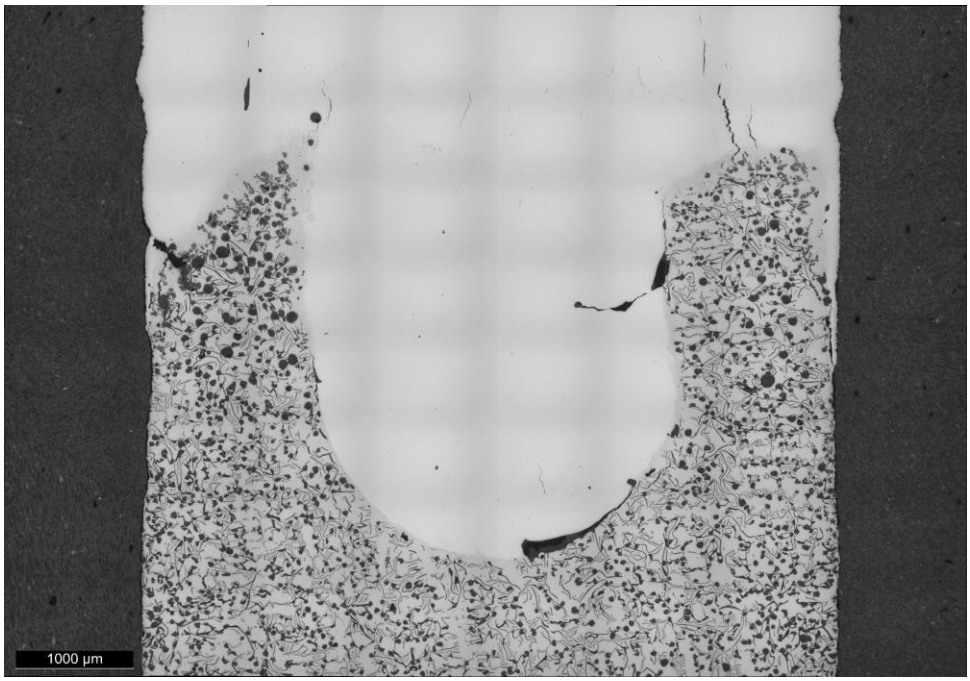

Figure 82: Cast Iron Scalloped Structure

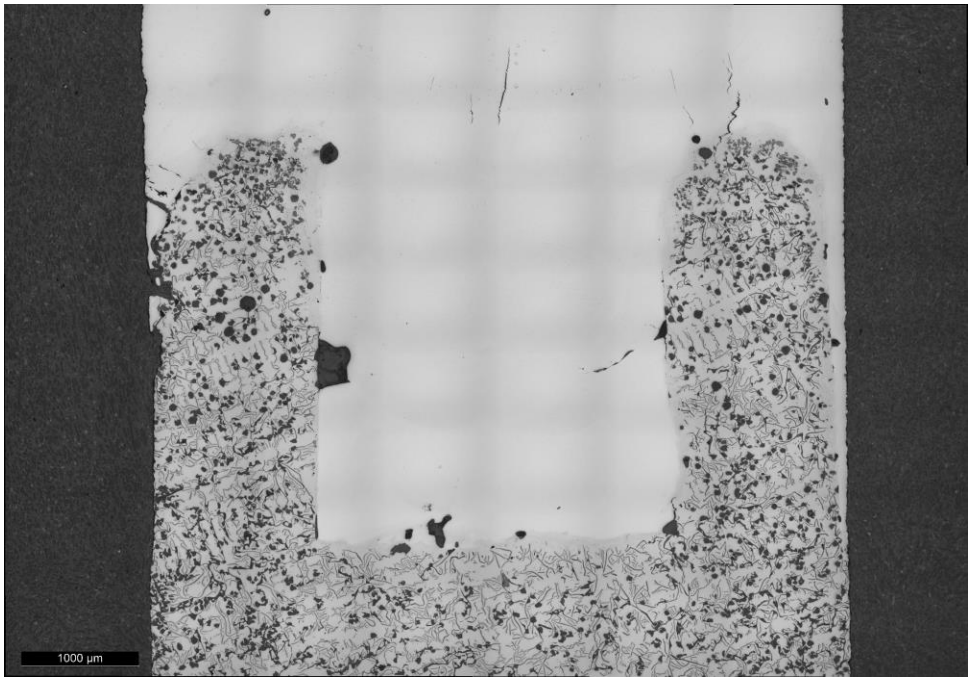

Figure 83: Cast Iron Tongue and Groove Structure

5.6.3 X-Ray Computed Tomography Data

To further understand the full extent of the porosity in the generated samples, X-ray computed tomography was done on an extra tensile sample. Due to the excessive porosity in some of the samples, quantitative values were unable to be determined. In instances where there were voids throughout the entire length of the build, the software package used, Volume Graphics, is unable to distinguish these as voids. Thus, the reported values are vastly underrepresented. The generated X-ray computed tomography figures are shown in Appendix C.

5.7 Discussion and Limitations

This chapter investigates the influence that various interface structures would have on the mechanical properties of components produced by hybrid manufacturing. Materials, geometry, and process parameters were selected such that they would mimic how the structures would be applied in industry. However, some issues and limitations were identified that provide insight and require more investigation. This section identifies and discusses these issues.

Many of the produced hybrid structures contained large amount of porosity, especially within the geometrical structures. This issue results from the limitation of not being able to make in-situ corrections to the processing parameters. It's hypothesized that many of the lack of fusion defects were due to insufficient heating caused by the material being deposited in a thin groove. Once further research is conducted on processing parameters resulting in non-porous components, it would be beneficial to re-evaluate the concept of hybrid structures.

It can be seen in the structure figures that cracking occurred in the samples deposited on the gray cast-iron substrate. This is a well-known problem due to cast-iron's high carbon content [111]. Though this is a common failure and could have been mitigated by selecting a different substrate material, it was determined that the cracking could be mitigated as the entire sample was not needed for testing. It also provided insight into whether one structure for performed better than others.

During the manufacturing of the hybrid structures, another hypothesis was developed: does the orientation of the grooves relative to the deposited material influence the mechanical properties due to DED being an anisotropic process? An example of this is shown in Figure 84.

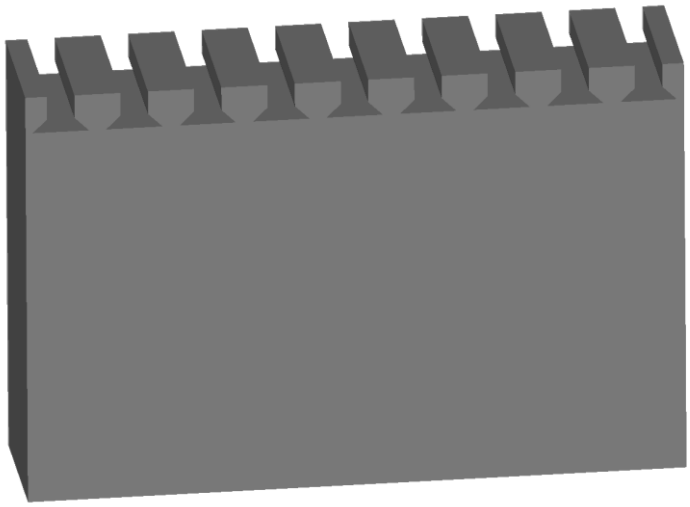

Figure 84: Transverse Hybrid Structure

Scalloped, tongue and groove, and dovetail structures utilizing these transverse grooves have been manufactured and are being tested, with results to be published later. It is hypothesized that transverse grooves would not influence the tensile properties of the

sample, but rather the resulting residual stress. Thus, the samples are being evaluated for residual stress by using the spallation neutron source (SNS) at ORNL.

The structure samples were designed such that their features would be captured in the tensile sample. If the dovetail structure was much larger than the cross-section of the tensile sample, it would act as though it was a flat structure when tested. Consequently, the dovetail structures evaluated in this study do not represent geometry that could be produced using commercially available tooling. Industrial dovetail cutters are much larger in diameter, which could have adverse impacts on the implementation.

For this investigation, only two material combinations were evaluated. For the dissimilar metal scenario, gray cast-iron was selected because it has a lower CTE when compared to stainless steel. It is hypothesized that using a substrate with a higher CTE would provide better mechanical locking.

Table 14: CTE for Various Materials [92]

Material	**CTE from room temperature to 100ºC [10^{-6}/ºC]**
Gray Cast Iron	9.5-12
Stainless Steel	9.8-25
6xxx Series Aluminum	16-24

Unfortunately, materials with significantly higher CTE values such as aluminum, copper, and bronze alloys are traditionally difficult to laser weld due their high reflectivity. Thus, this study was constrained to two material combinations. However, ongoing work is developing procedures to better process these highly reflective materials.

5.8 Conclusion

Hybrid manufacturing provides an integrated additive and subtractive solution for unlimited surface structures and conditions. This chapter shows that hybrid structures have an influence on the mechanical properties of components produced by hybrid manufacturing on similar and dissimilar material combinations. Although only 4 types of structures are evaluated, this provides a foundation for analogous research on other interfacial geometry to be conducted. Key outcomes of this investigation are:

- Adding mechanical interfaces does not improve the mechanical properties of the resulting component.
- Depositing crack-free, dissimilar metal needs further process parameter investigation.
- Further work is needed to improve deposition strategies of hybrid structure components.

As shown in this chapter, initial results show that the use of hybrid structures does not enhance the mechanical properties of the resulting components. Now that an understanding of how hybrid structures influence the mechanical properties of components has been developed, future work evaluating different deposition strategies, materials, and geometrical structures can build upon this study.

CHAPTER 6. FUTURE WORK

This dissertation investigates various aspects of laser hot-wire hybrid manufacturing. As a result of these investigations, a few areas for future work have been highlighted. This chapter introduces areas of future work that are applicable to the entire field of hybrid manufacturing, regardless of feedstock type or machine manufacturer.

6.1 Closed-Loop Process Control

Chapter 3 investigates the process parameters needed for laser hot-wire hybrid manufacturing. Though it has been shown that process parameters can be developed to produce a component, it is labor intensive and is geometry specific. Furthermore, it has been shown that this is feedstock agnostic, as similar issues are seen in the blown metal powder hybrid manufacturing machines. Currently, most DED manufacturing is conducted in a laboratory setting and equipment is operated by skilled individuals with a longstanding background in the field. If hybrid manufacturing is to become relevant to industry, there must be work done to take the skill and knowledge from these skilled operators and place it into the machine control systems. Thus, it is proposed that these hybrid systems evaluate closed-loop process control.

Closed-loop control systems use the concept of an open-loop system as its forward path, but has feedback loops between its output and input. These control systems are designed to automatically achieve and maintain desired output conditions by comparing them to the actual conditions. This is done by generating an error signal, which is the difference between the output and reference input signal. For example, consider constantly

monitoring the temperature of the weld-pool during deposition, and feeding a signal relating the temperature back to the controller as shown in Figure 85.

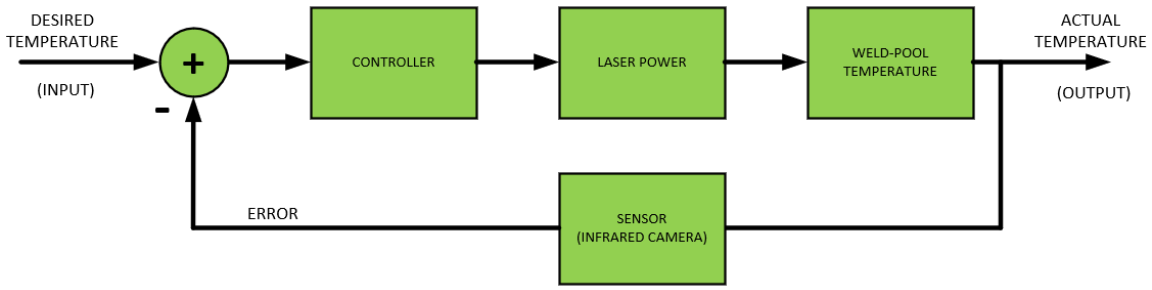

Figure 85: Closed-Loop Control

With closed-loop control, the processing parameters will no longer be geometry specific. Good starting parameters, as developed in this dissertation, can be used and constantly adapted throughout the process to mitigate effects from varying geometry and rising processing temperature. As a result, this reduces the need for expertise when programming the toolpath trajectory and allows the technology to be easily transferred to industrial applications.

6.2 Deformation Compensation

The concept of deformation compensation was investigated and applied in Chapter 4. It was required to produce the hexagonal structures due to the thermal cycling of the produced components. To do this, simulations were conducted to predict the amplitude of the deformations and then compensate for them in the additive toolpath trajectories. Though this is a viable process, it requires significant computation time as well as a variety of software suites. In addition, this process is geometry and process parameter specific, reducing its generalizability and usefulness in an industrial setting.

By using digital image correlation (DIC), it is possible to evaluate geometry distortions in-situ to the deposition and machining processes. Thus, it is proposed that research investigate the use of this technology to generate toolpath trajectories during the process. Instead of creating the entire toolpath program a priori, paths can be generated layer by layer. This may not eliminate the need for distortion simulations, but it may help streamline the process such that it is better suited for industrial applications.

6.3 Hybrid Manufacturing Machine Design

This research was conducted on an inaugural laser hot-wire hybrid manufacturing system. Furthermore, there are not many commercial hybrid manufacturing systems in industrial applications around the world. Unlike traditional subtractive systems, where there are many machine configurations, there are only a few configurations available for hybrid manufacturing systems. Most commercial hybrid systems are either vertical 5-axis or mill-turn configurations. As previously discussed, these systems are designed such that they utilize existing castings and linear drives. By doing this, these machines have travel limitations due to the offset between additive and subtractive systems. Other options include putting the additive head in the spindle, but this also significantly reduces height of components that are manufacturable in the system. As a result, there are industrial applications that are unable to leverage this technology because there is not a hybrid manufacturing machine configuration that fits their needs.

To mitigate these issues, it is proposed that future work be done regarding machine design for hybrid manufacturing. To increase the market share of hybrid manufacturing, machine manufacturers need to re-evaluate how these machines are designed. Instead of

treating hybrid manufacturing as a new machine platform, it may be more effective to have it as an add-on that is applicable to all existing configurations. This concept is actively being researched at ORNL and will be published later.

6.4 Conclusion

As a result of the investigations of the hypotheses presented in this dissertation, areas of future work in the field of hybrid manufacturing have been identified. Advanced process control, distortion compensation, and new machine designs are all critical to the development of hybrid manufacturing. The areas outlined here will enhance the entire field of hybrid manufacturing, regardless of feedstock type or machine manufacturer. As a result, these investigations have the potential to increase the industrial acceptance and implementation of hybrid manufacturing.

CHAPTER 7. CONCLUSIONS

Hybrid manufacturing is a combination of additive (deposition) and subtractive (machining) manufacturing in a single machine. This laser metal deposition process can be used for near net shape manufacturing and component repair using either similar or dissimilar materials. With commercially available hybrid manufacturing systems capable of 5-axis deposition and subtraction, it is now feasible to control the interfacial conditions between substrate and deposition. Other deposition processes require substrates to be planar, but hybrid manufacturing's subtractive capability allows for unlimited surface structures and conditions. Industry implementation has already occurred in the mold and die repair industry, but it will quickly expand to other applications. This dissertation investigates three areas of hybrid manufacturing. Specifically, it has developed a process for laser hot-wire hybrid manufacturing, evaluated the influence of the hybrid manufacturing process on mechanical properties of the produced component, and investigated the effect that the geometry of the interface between added and substrate materials has on the mechanical properties of the produced component. This chapter provides conclusions and major outcomes for each of these researched areas.

7.1 Hybrid Process Development

Laser hot-wire hybrid manufacturing is a new research area. Thus, there is little to no previous research on process development to build upon. The original research question was focused on selecting singular process parameters based on the material being deposited. Understanding the effect of process parameters on the DED process is not a new concept, but this research has shown that laser hot-wire hybrid manufacturing is not exempt

from the concept. However, it has also proven that it can produce medium sized geometry up to 150mm in height by depositing steel at a rate of 2.5 kg/hr with simple control systems and a single set of process parameters.

This research on process development has highlighted the need for an improved understanding and control of the process parameters. Specifically, it has shown that different toolpath planning trajectories can have a large influence on the deposition process. Furthermore, it has highlighted that complex geometries with varying wall thicknesses and overhangs require adaptive processing parameters. Thus, this research has not only set the foundation for laser hot-wire hybrid manufacturing process development but has influenced the direction of future research in the field.

7.2 Hybrid Hexagonal Structure Process Development

There has been significant research conducted on mechanical properties of additively produced components. However, there has been little work conducted on hybrid manufactured components. Most of the work done in the field has been on components that are fully produced additively before the subtractive process begins. Thus, the purpose of this research is to investigate the influence that the hybrid process has on the mechanical properties of the produced component. It was observed that, by using hybrid manufacturing, overall cycle times can be reduced by up to 68%, elongation to failure can be improved by 22%, and overall porosity is reduced by 16%.

This research has resulted in a better understanding of the distortion of hybrid manufactured components. Although it was not originally included in the initial investigation, it was seen that components such as the hexagonal structure cannot be

manufactured without compensating for the geometrical distortion due to the cyclical thermal process. As a result, it has been shown that geometrical distortion can be modeled and mitigated by compensated toolpath trajectories in the additive process. Hybrid manufacturing is the only manufacturing process where produced components can be machined directly after the additive process while they are still hot. Therefore, a new research area in thermal compensation for hybrid has been found and should be further investigated.

7.3 Hybrid Structures

Additive manufacturing has traditionally occurred on planar interfaces. Though it is not limited to them, it requires multiple set-ups and equipment to work with non-planar surfaces. With hybrid manufacturing, it is now possible to control geometry of the interface between deposited and substrate material without breaking setup. Thus, this research investigates the influence that the interface geometry, termed hybrid structure, has on the mechanical properties of the produced component. It was seen that these hybrid structures did not improve the mechanical properties of the produced component when compared to the common, planar interface.

This research has resulted in a better understanding of how hybrid structures influence the mechanical properties of produced geometry. The geometry produced with gray cast-iron substrate had significant cracking on the ends of the produced component. To mitigate this effect, it has been hypothesized that the orientation of the hybrid structure may also influence the resulting mechanical properties. As a result, research is being

conducted on how the orientation of the hybrid structure influences the mechanical properties of the produced component.

7.4 Conclusion

This dissertation investigates three areas of hybrid manufacturing, or the combination of additive and subtractive manufacturing in a single machine. Specifically, it has developed a process for laser hot-wire hybrid manufacturing, evaluated the influence of the hybrid manufacturing process on mechanical properties of the produced component, and investigated the effect that the geometry of the interface between added and substrate materials has on the mechanical properties of the produced component. As a result, this research has not only set the foundation for laser wire-fed hybrid manufacturing process development but has influenced the direction of future research in the field. Finally, the contributions of this research are:

- Methodology for developing the laser hot-wire hybrid manufacturing process.
- Improved understanding of developing toolpath trajectories for various geometrically complex components.
- Methodology for alternating additive and subtractive manufacturing to produce geometrically accurate components.
- Enhanced understanding of the effect that hybrid manufacturing has on the mechanical properties of the resulting component.
- Improved understanding of how various geometrical interfaces between substrate and deposited material effect the mechanical properties of a component.

APPENDIX A. HYBRID HEXAGONAL STRUCTURE DISTORTION ANALYSIS

This appendix provides additional information on the distortion analysis completed on the hybrid hexagonal structures. As discussed in Chapter 4, hexagonal structures were produced using a hybrid manufacturing workflow. Distortions were seen in the final geometry after manufacturing was finished. These distortions were captured by a structured light scanner and evaluated in Volume Graphics. The ensuing sections show the results and briefly discuss the findings.

For each hybrid hexagonal structure, three figures are provided. The first figure shows an analysis of the scan compared to the nominal geometry. In these figures, a deviation is positive with respect to the surface normal. For example, a positive deviation on the outside of the hexagonal structure means the actual part is larger than the nominal geometry, while a positive deviation on the inner surface means the actual part (internal diameter) is smaller than the nominal geometry. The second figure shows the deviation distribution of each component. Here, a normal distribution is desirable, but it was observed that many of the distributions are uniform. It's seen from the figures that hexagon 6 provides the most favorable distribution. The last figure shows cumulated deviation distribution for each hexagonal structure. These figures plot the percentage of a surface with respect to an absolute distribution. For example, it can be seen in Figure 87 that only 51% of the geometry is within 0.45 mm of the nominal surface.

A.1 Hexagon 5 – Machined Hot, No Coolant

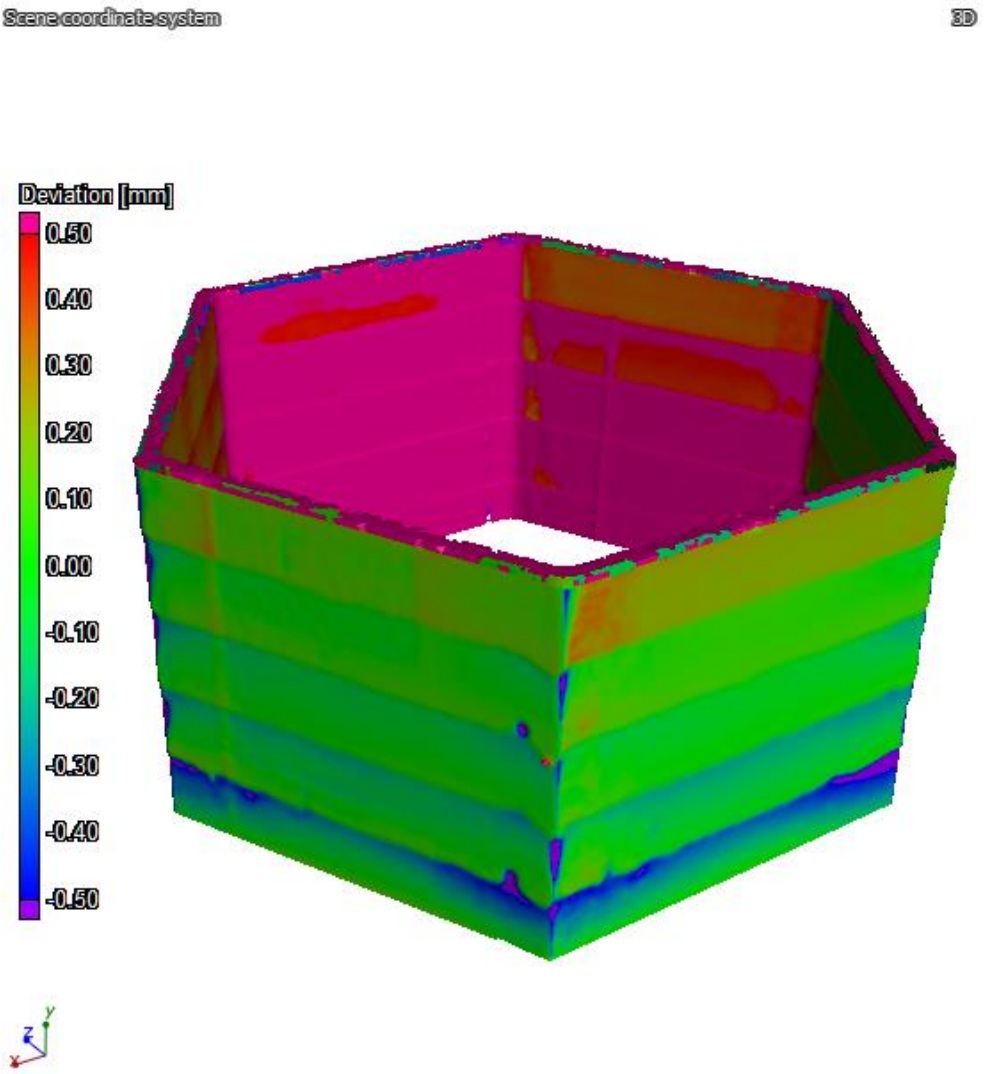

Figure 86: Hexagon 5 Distortion

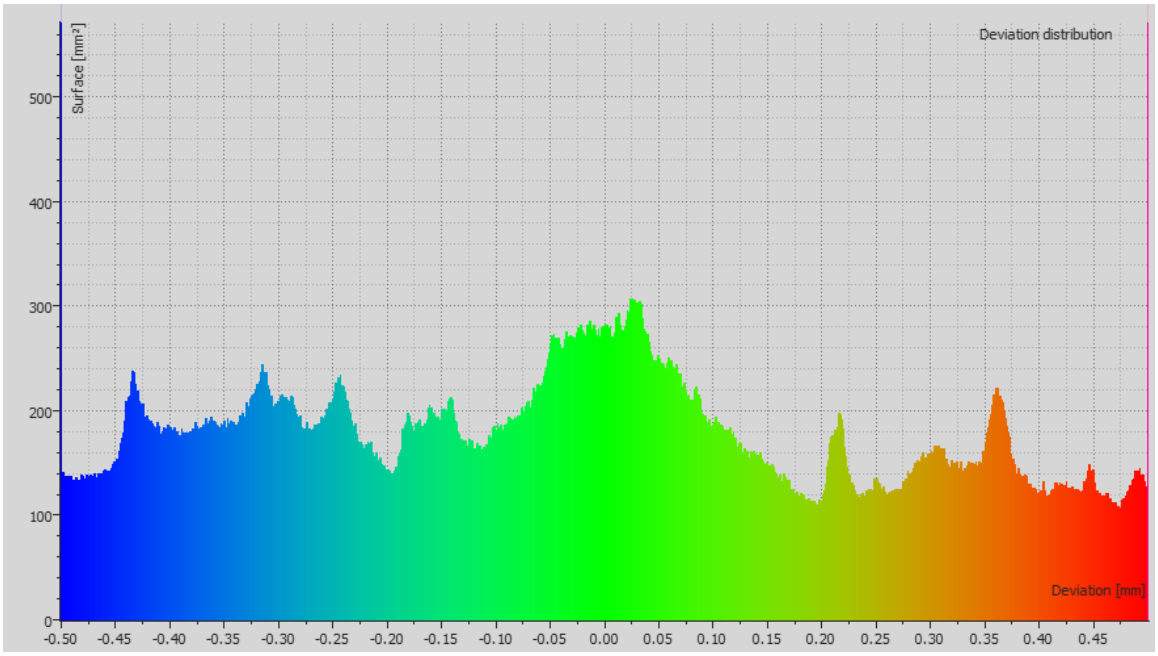

Figure 87: Hexagon 5 Deviation Distribution

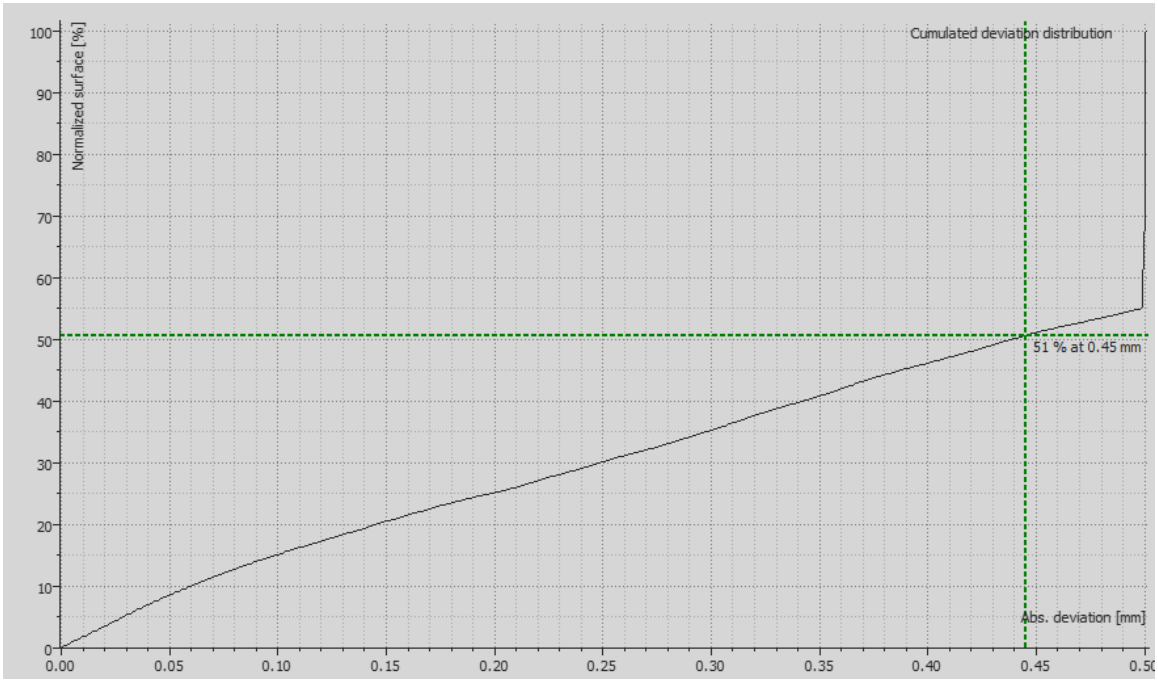

Figure 88: Hexagon 5 Cumulated Deviation Distribution

A.2 Hexagon 6 – Cold, With Coolant

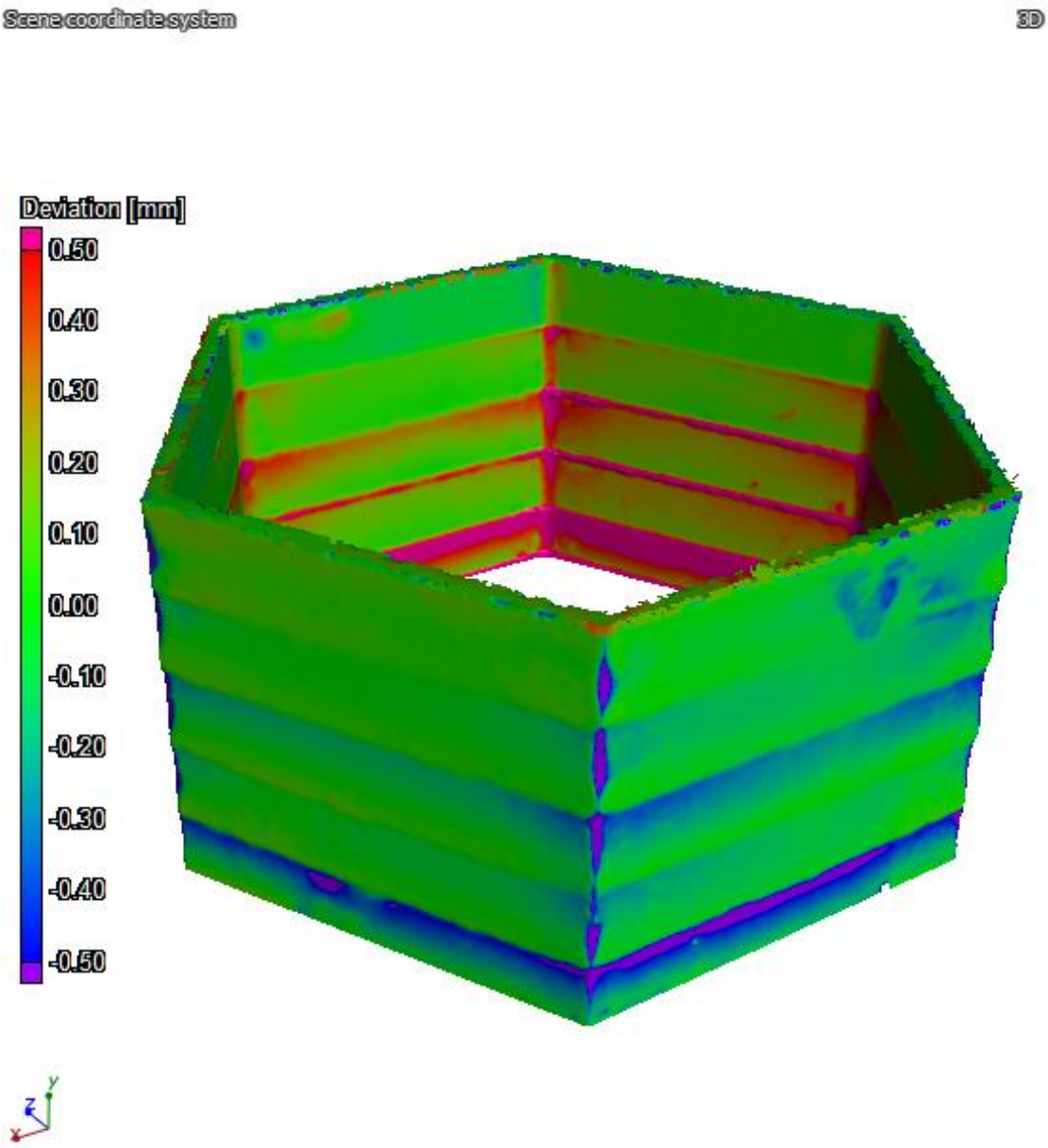

Figure 89: Hexagon 6 Distortion

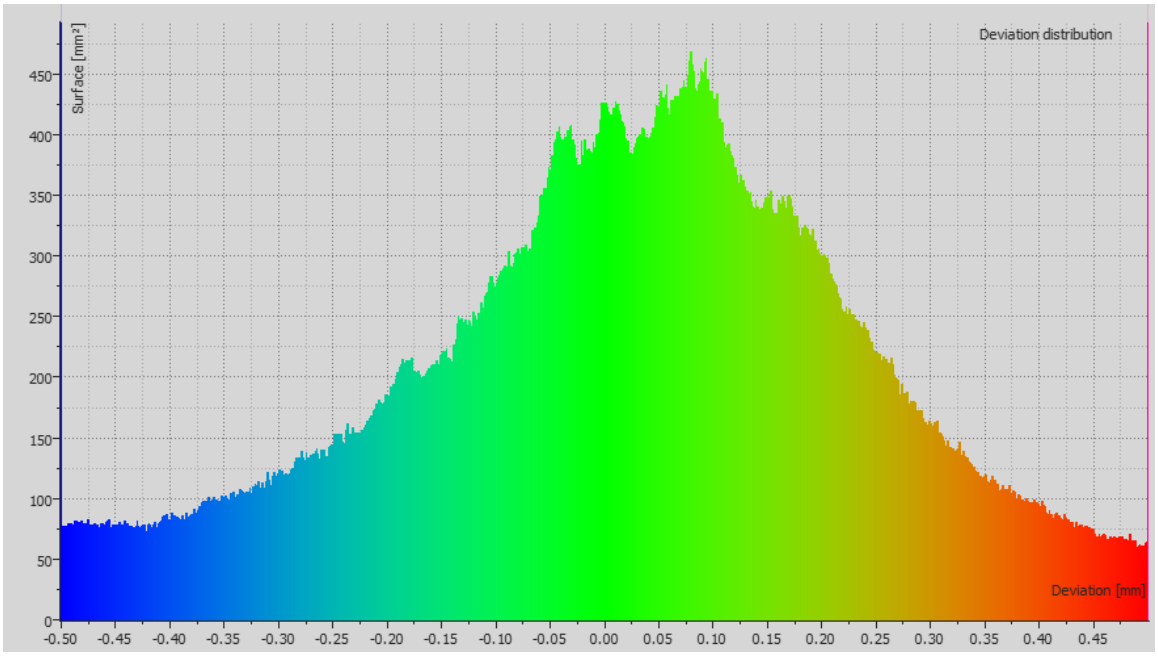

Figure 90: Hexagon 6 Deviation Distribution

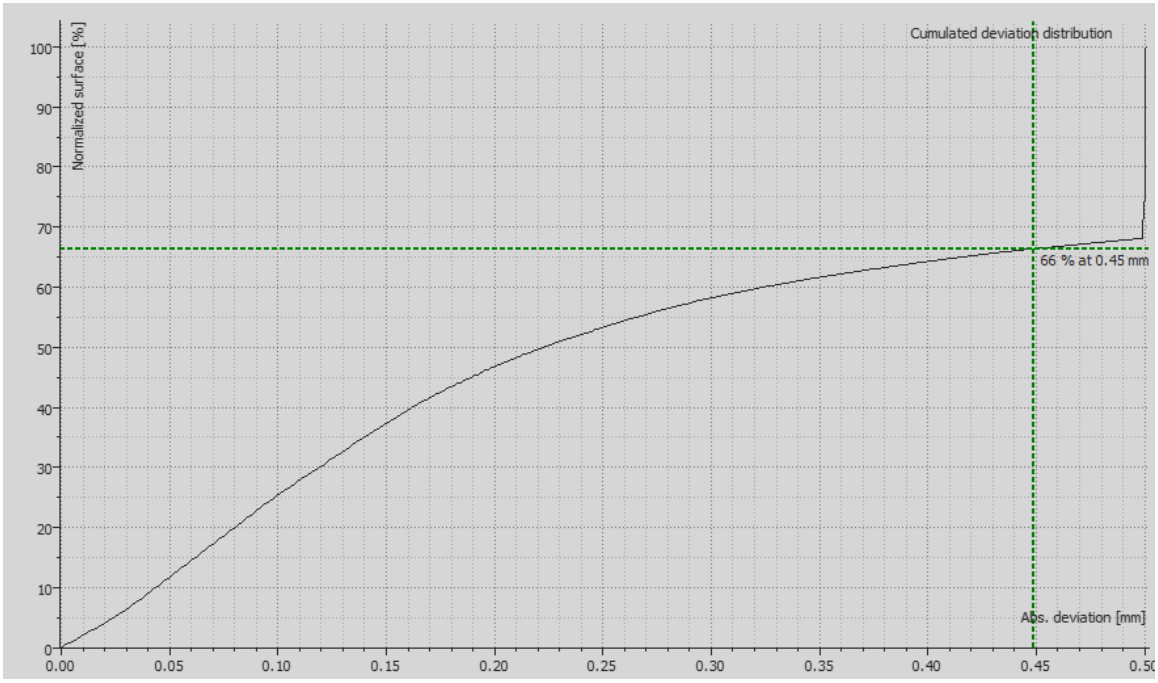

Figure 91: Hexagon 6 Cumulated Deviation Distribution

A.3 Hexagon 7 – Cold, With Coolant

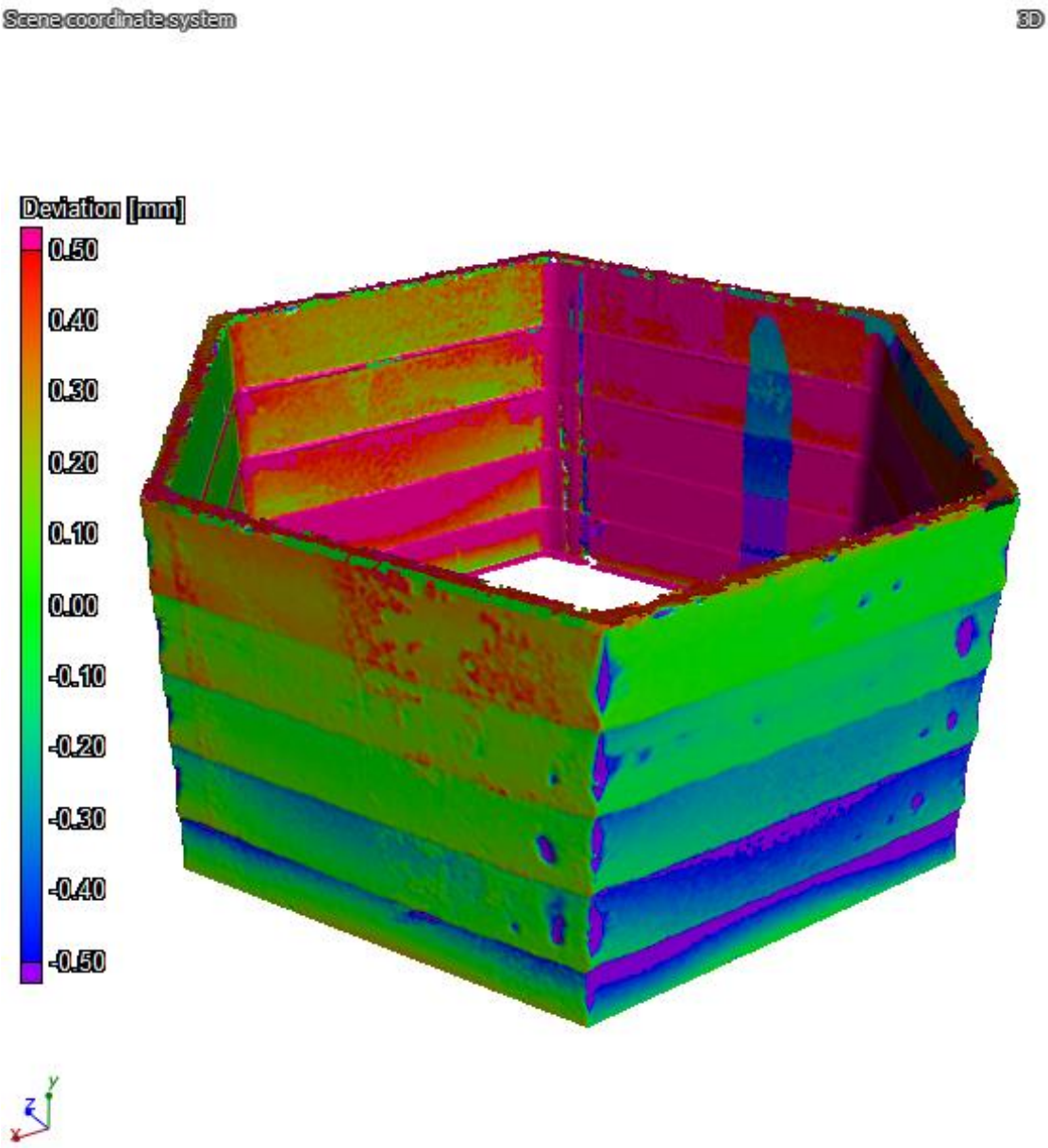

Figure 92: Hexagon 7 Distortion

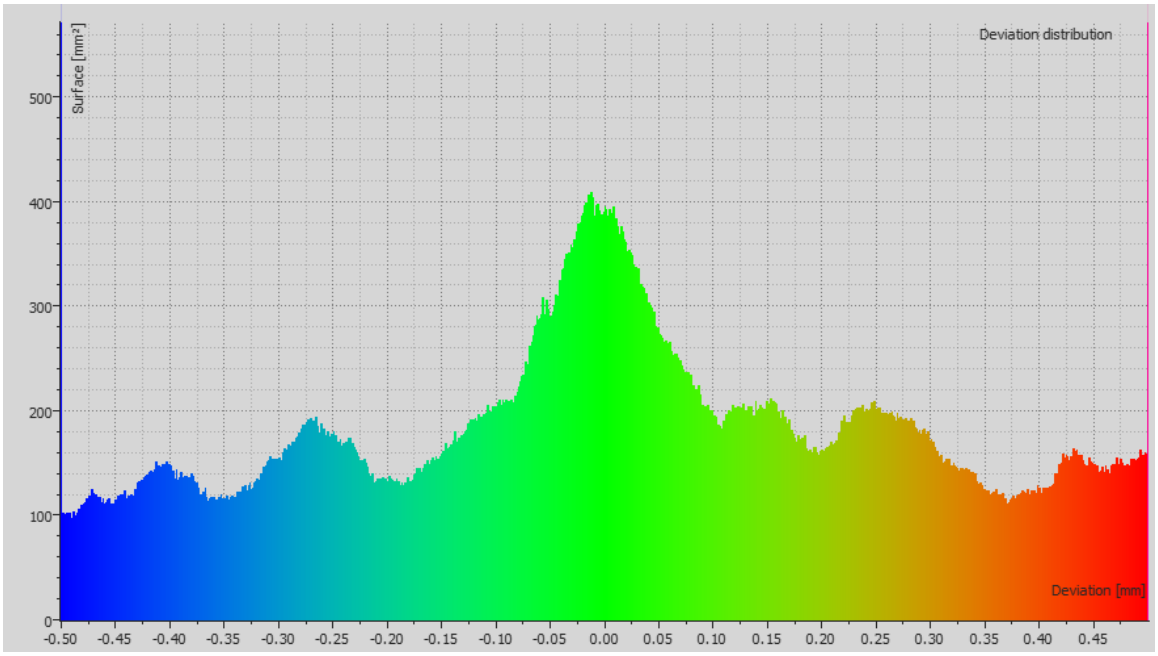

Figure 93: Hexagon 7 Deviation Distribution

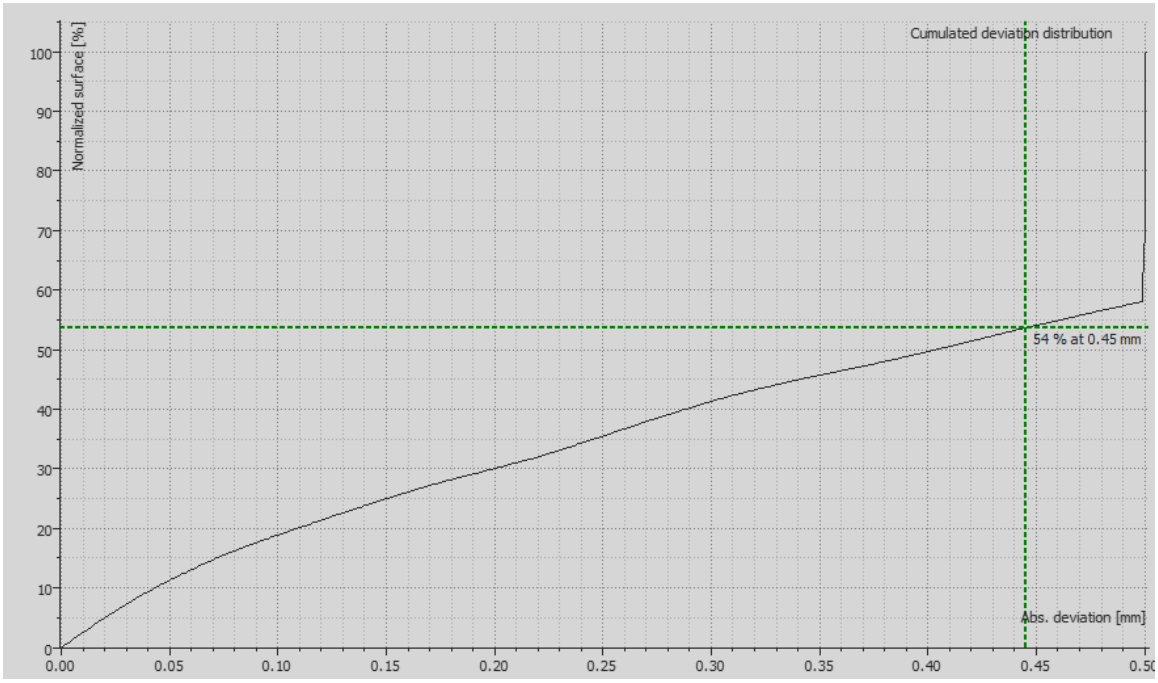

Figure 94: Hexagon 7 Cumulated Deviation Distribution

A.4 Hexagon 8 – Hot, With Coolant

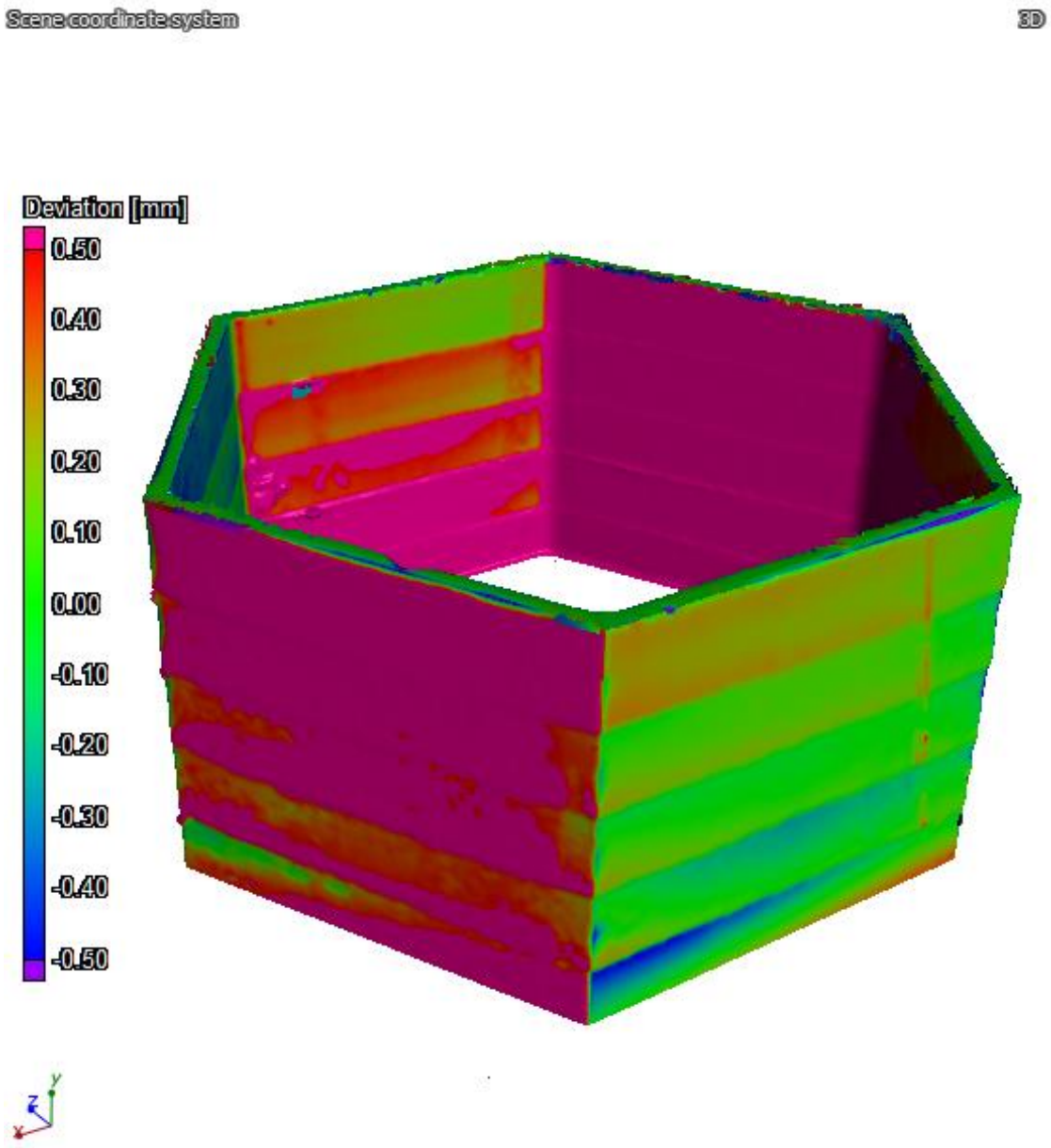

Figure 95: Hexagon 8 Distortion

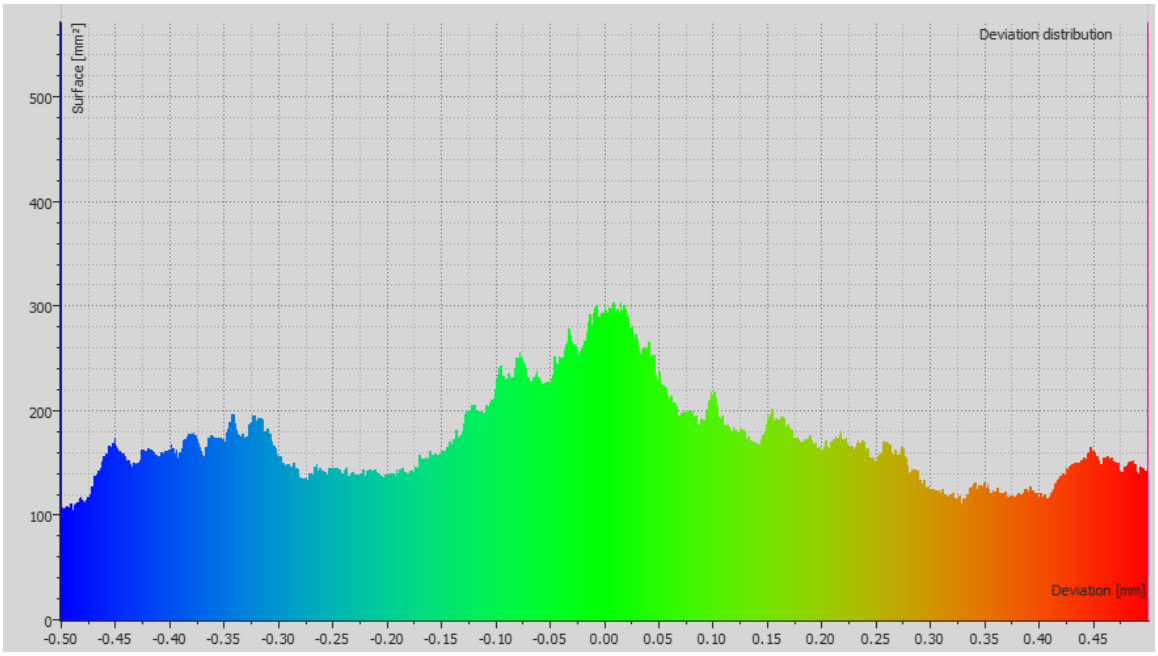

Figure 96: Hexagon 8 Deviation Distribution

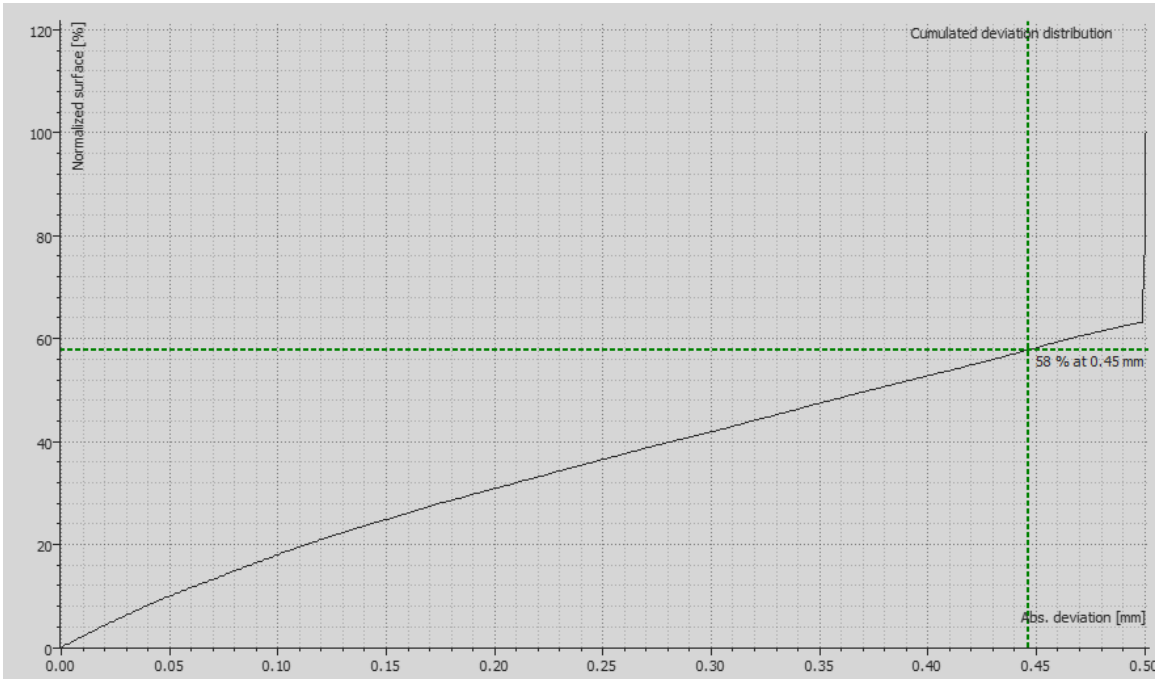

Figure 97: Hexagon 8 Cumulated Deviation Distribution

APPENDIX B. HEXAGONAL STRUCTURE MATERIAL AND MECHANICAL DATA

This appendix contains the mechanical and material data used in the discussion in Chapter 4. Stress-strain curves, comparison of yield strength to elongation, optimal images, and X-ray computed tomography images are provided for each hexagonal structure. Discussion and conclusions drawn from the results are provided in Chapter 4.

B.1 Hexagonal Structure Tensile Data

Table 15: Hexagonal Structure Yield Strength

Hexagonal Structure	Yield Strength [MPa] - Vertical	Standard Deviation	Yield Strength [MPa] - Horizontal	Standard Deviation
Hexagon 1	352.0	5.6	385.2	7.2
Hexagon 2	344.5	3.0	400.9	3.5
Hexagon 3	340.2	7.4	402.9	3.2
Hexagon 4	345.9	4.9	403.1	5.6
Hexagon 5	341.3	4.6	353.4	6.7
Hexagon 6	335.4	3.8	348.7	7.8
Hexagon 7	326.5	7.7	354.5	5.5
Hexagon 8	330.8	7.1	352.7	7.3

Table 16: Hexagonal Structure Ultimate Tensile Strength

Hexagonal Structure	Ultimate Tensile Strength [MPa] - Vertical	Standard Deviation	Ultimate Tensile Strength [MPa] - Horizontal	Standard Deviation
Hexagon 1	538.8	38.1	593.5	33.3
Hexagon 2	525.6	25.8	618.1	2.9
Hexagon 3	494.7	37.2	611.4	12.9
Hexagon 4	529.8	33.6	620.7	8.0
Hexagon 5	566.4	13.9	598.2	8.0
Hexagon 6	580.5	2.2	597.9	6.4
Hexagon 7	571.0	7.9	601.8	1.4
Hexagon 8	578.0	3.0	601.3	6.5

Table 17: Hexagonal Structure Elongation at Failure

Hexagonal Structure	Elongation at Failure [%] - Vertical	Standard Deviation	Elongation at Failure [%] - Horizontal	Standard Deviation
Hexagon 1	21.3	9.0	30.6	12.8
Hexagon 2	23.4	5.1	38.0	2.1
Hexagon 3	16.0	4.4	31.8	6.7
Hexagon 4	24.1	10.0	30.4	5.3
Hexagon 5	35.9	8.9	46.7	2.5
Hexagon 6	49.8	3.1	48.8	3.1
Hexagon 7	42.9	7.8	49.5	2.3
Hexagon 8	45.8	4.5	51.0	6.5

Table 18: Hexagonal Structure Average Hardness

Hexagonal Structure	Average Vickers Hardness [HV]	Standard Deviation
Hexagon 1	198.9	8.5
Hexagon 2	203.5	10.4
Hexagon 3	204.2	9.0
Hexagon 4	203.9	12.5
Hexagon 5	201.4	8.9
Hexagon 6	198.1	9.3
Hexagon 7	200.2	12.4
Hexagon 8	196.8	9.8

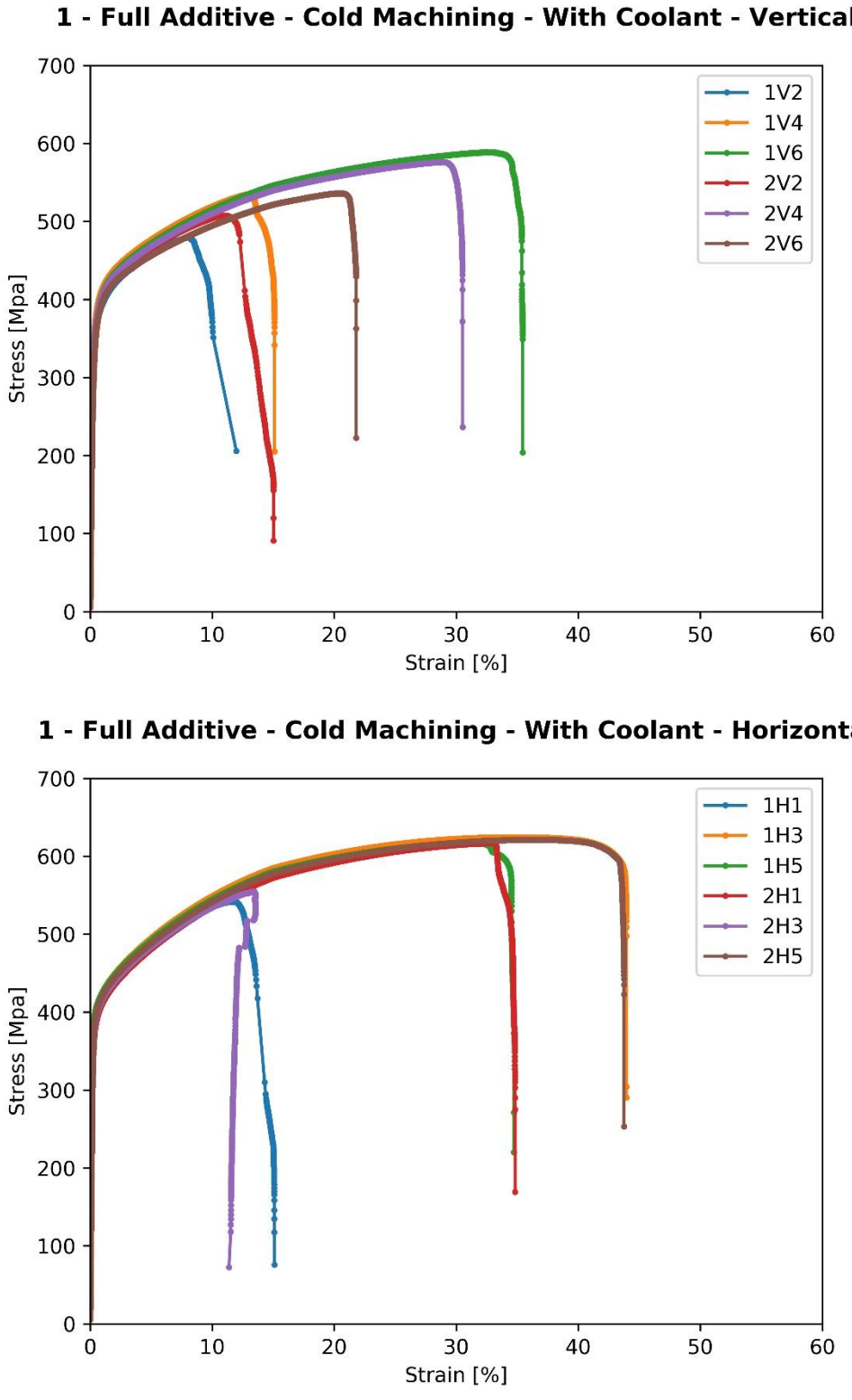

Figure 98: Hexagon 1 Tensile Data

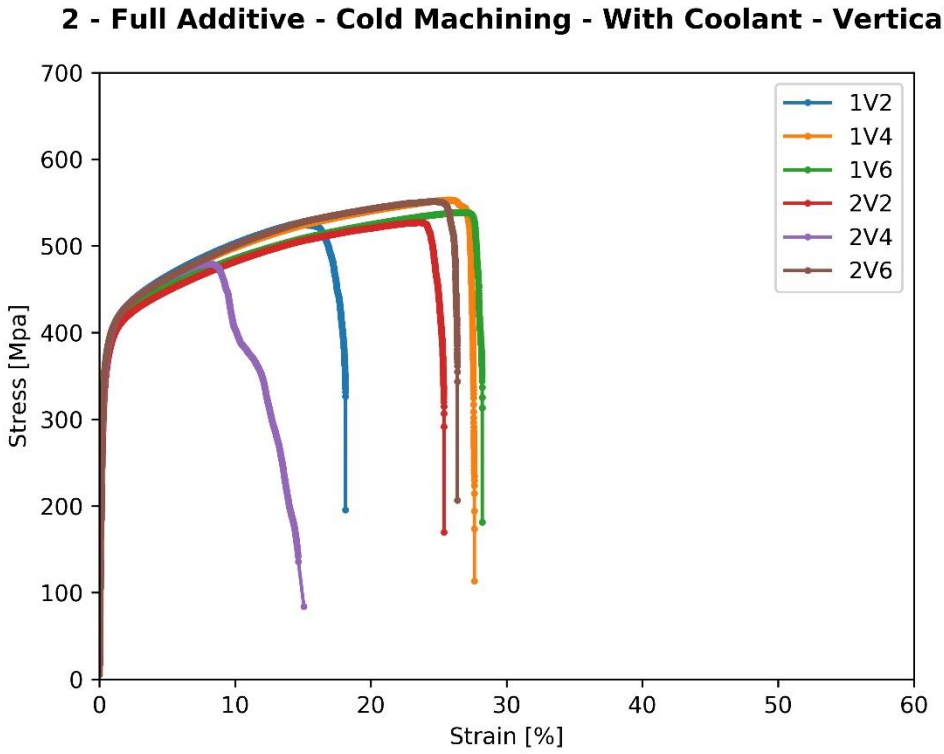

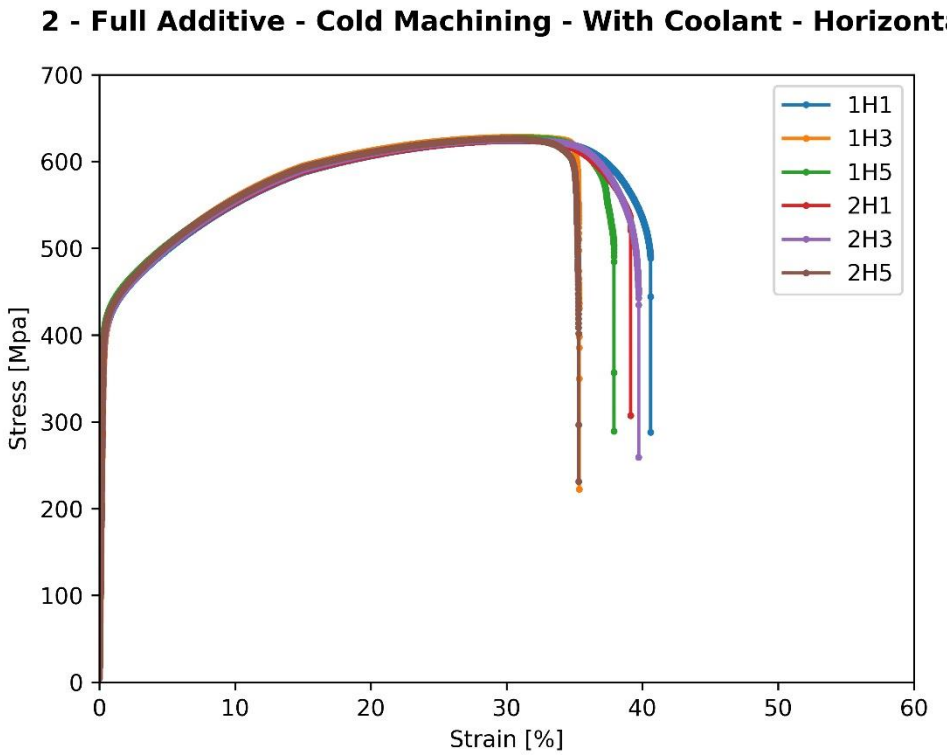

Figure 99: Hexagon 2 Tensile Data

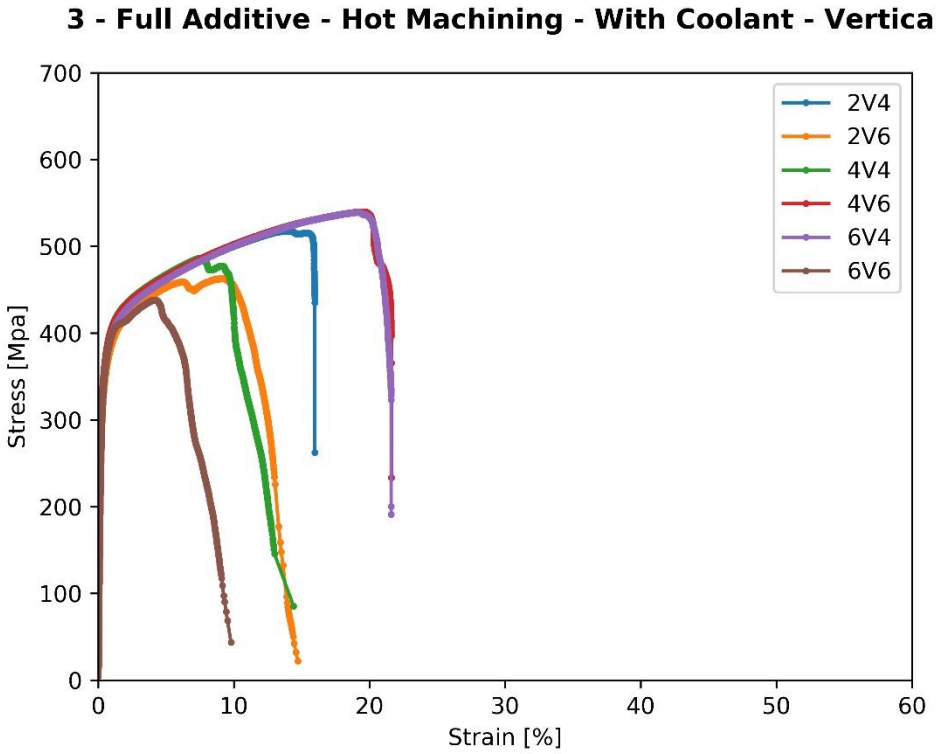

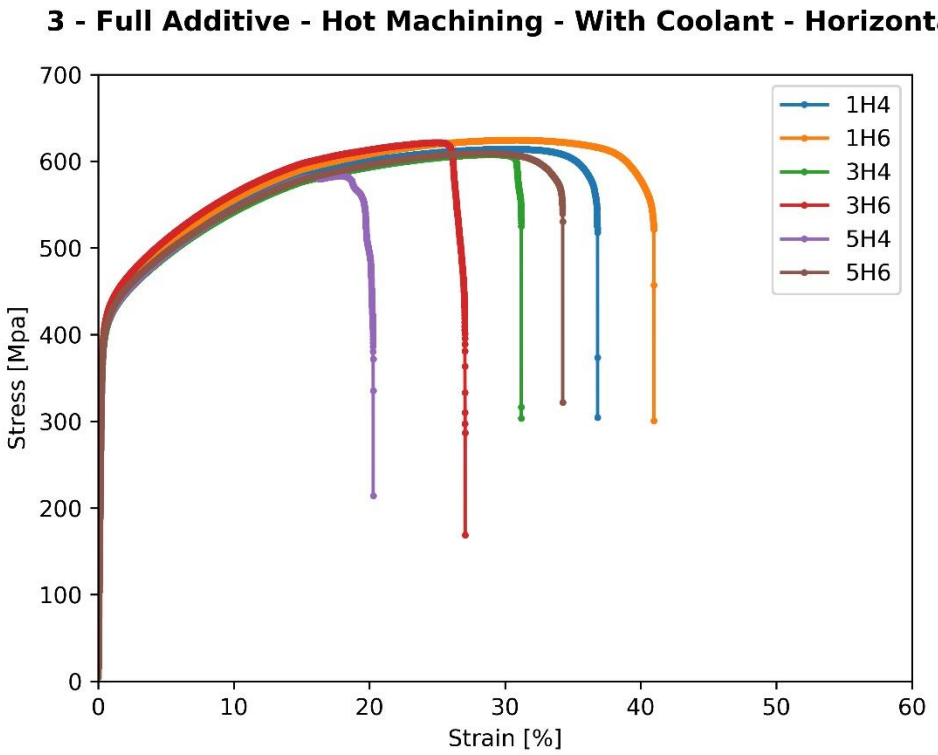

Figure 100: Hexagon 3 Tensile Data

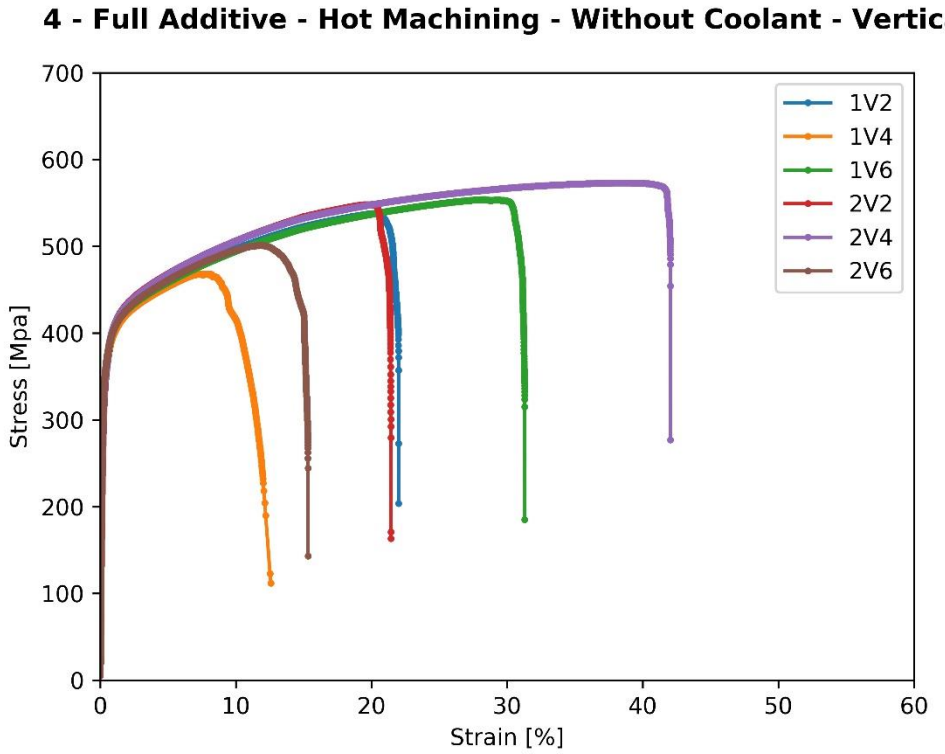

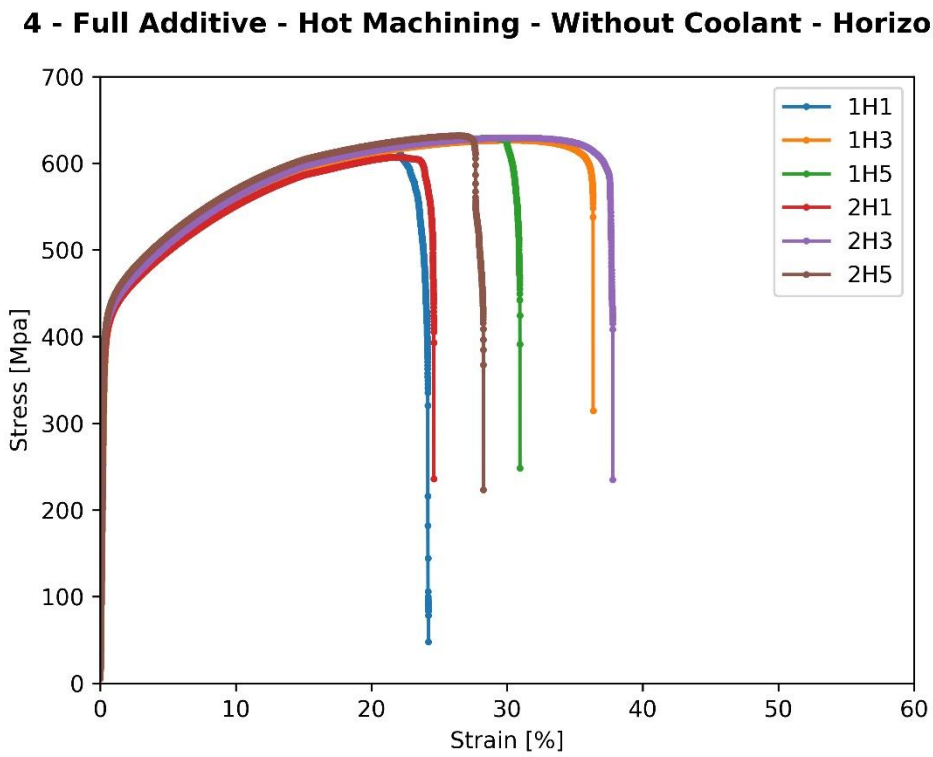

Figure 101: Hexagon 4 Tensile Data

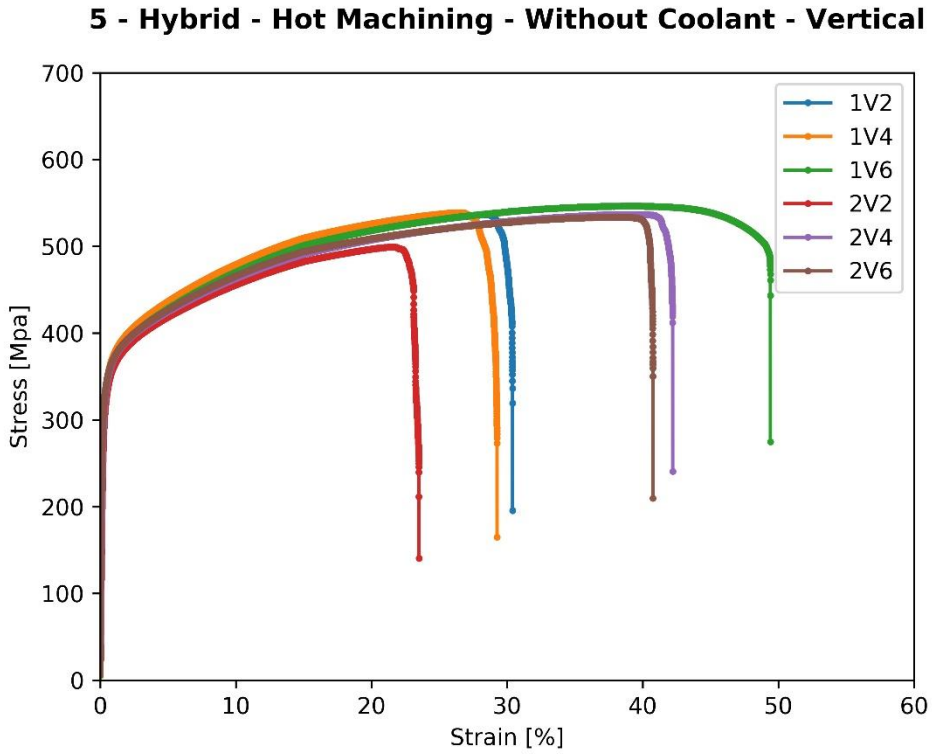

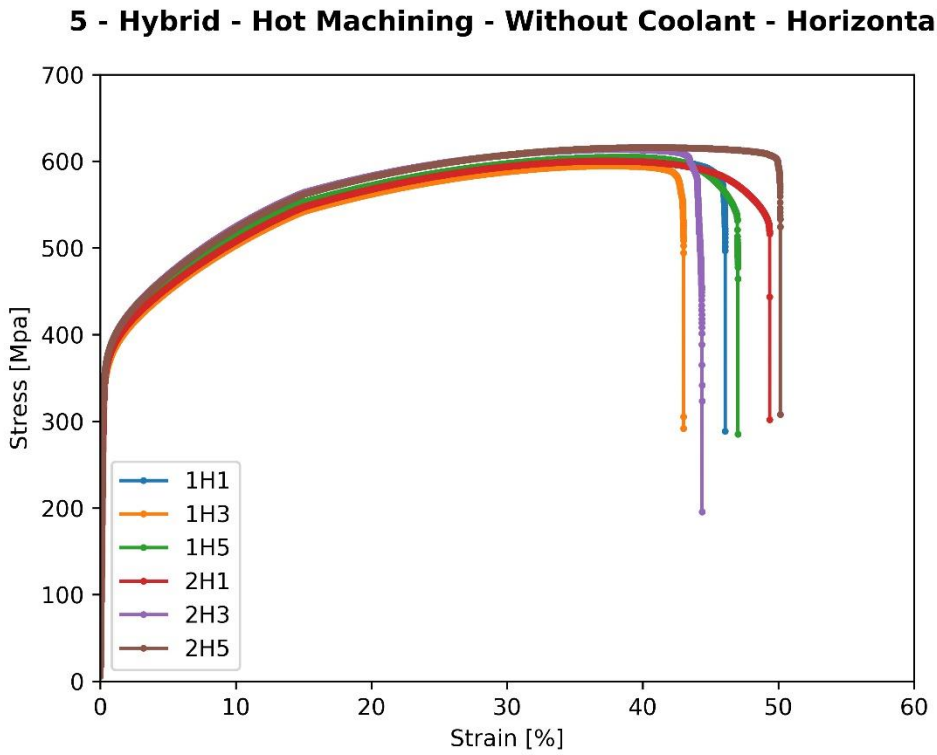

Figure 102: Hexagon 5 Tensile Data

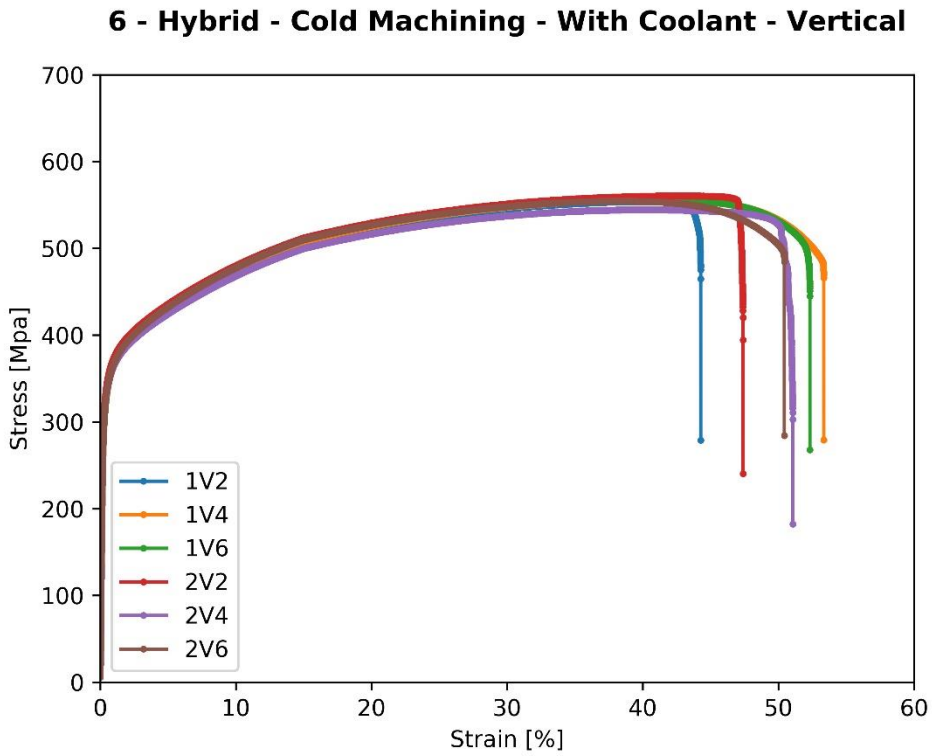

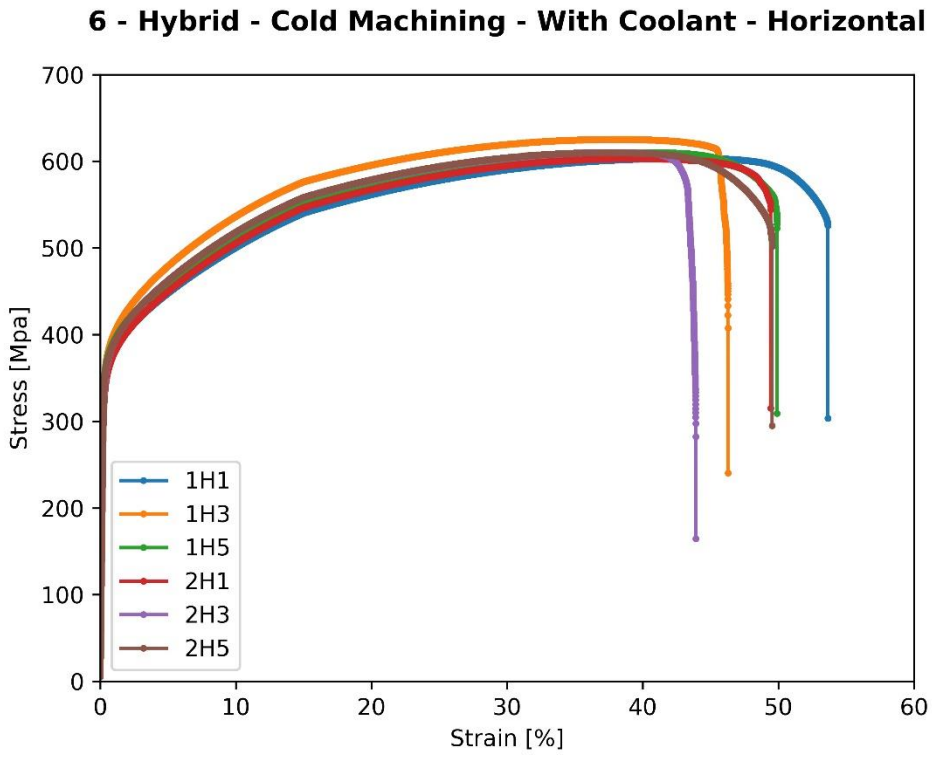

Figure 103: Hexagon 6 Tensile Data

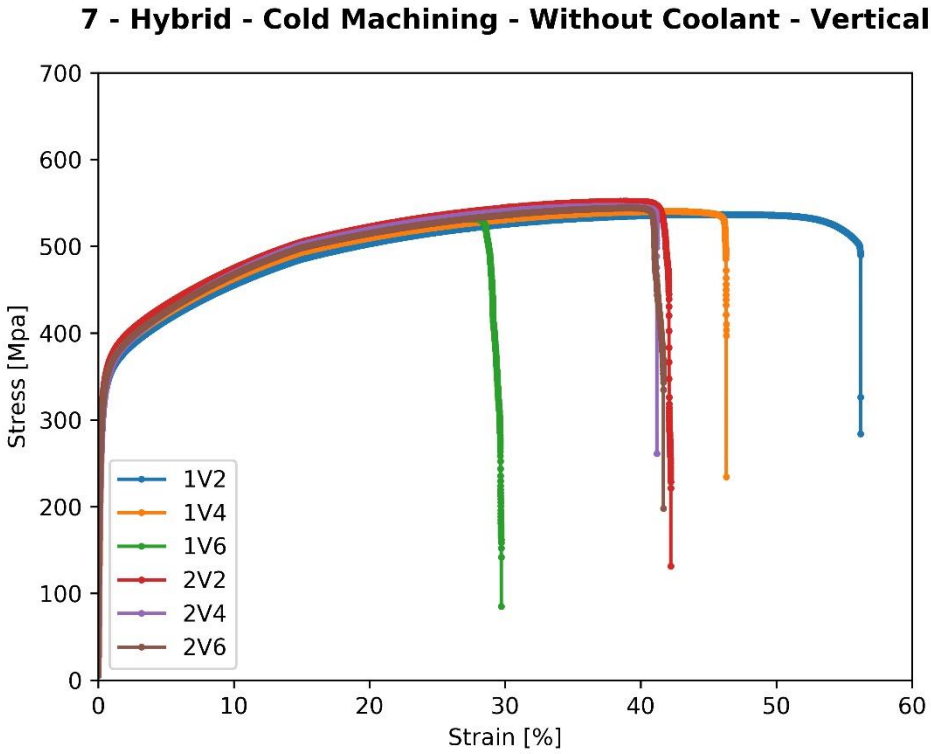

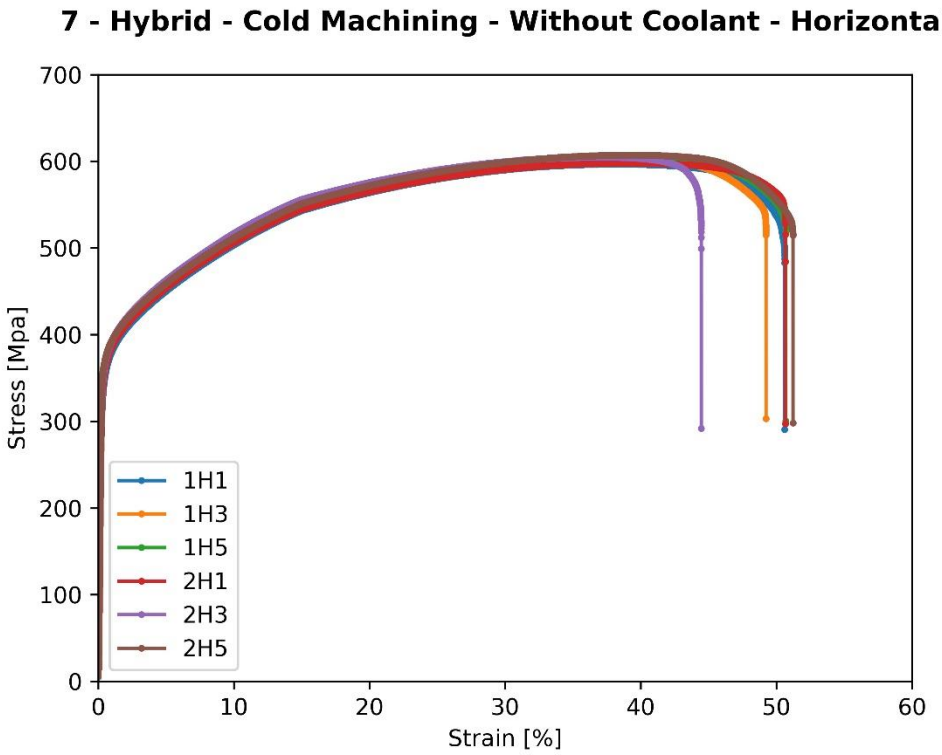

Figure 104: Hexagon 7 Tensile Data

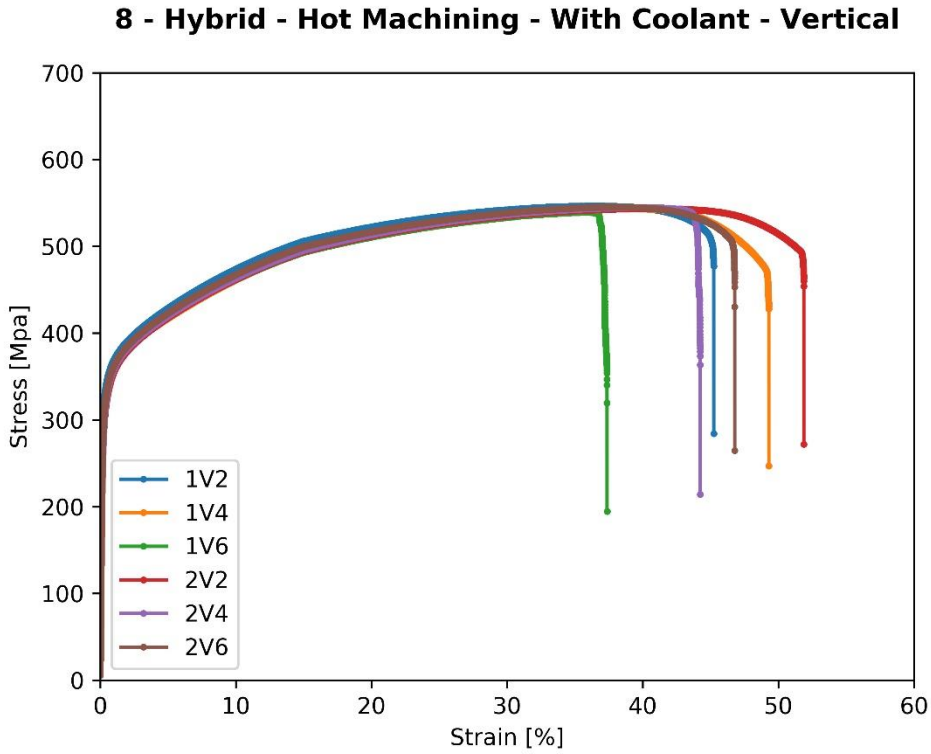

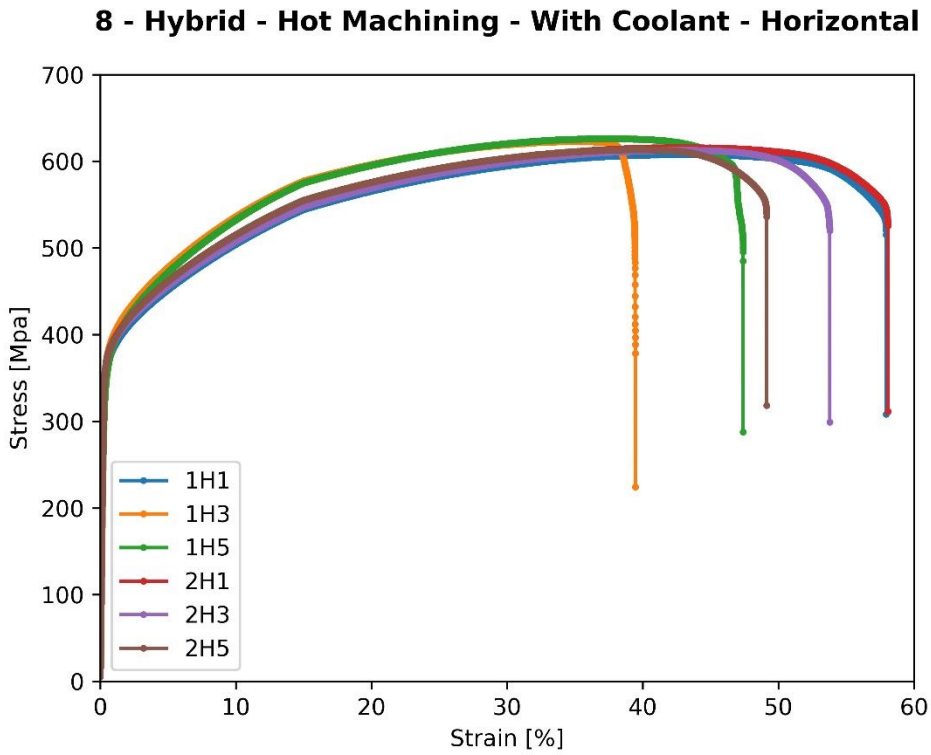

Figure 105: Hexagon 8 Tensile Data

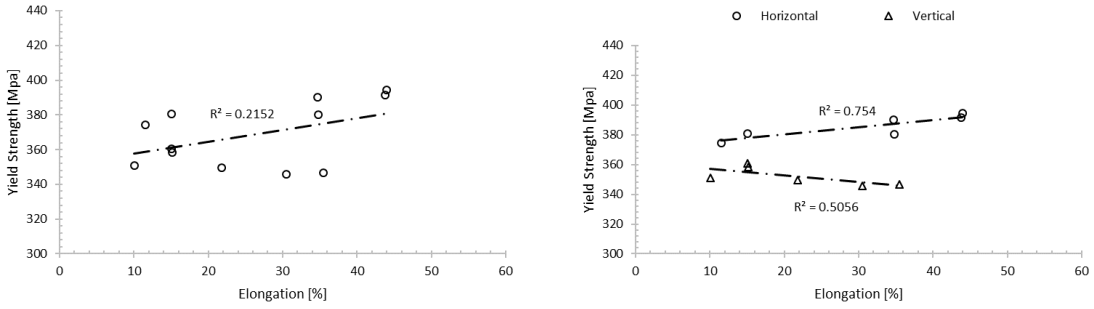

Figure 106: Yield Strength Versus Elongation for Hexagon 1

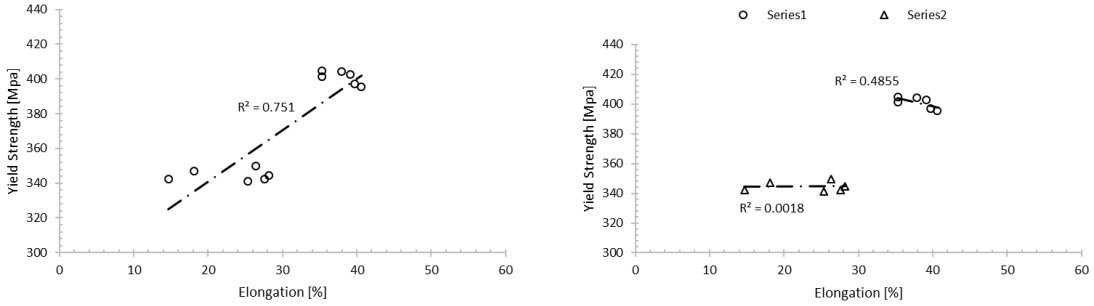

Figure 107: Yield Strength Versus Elongation for Hexagon 2

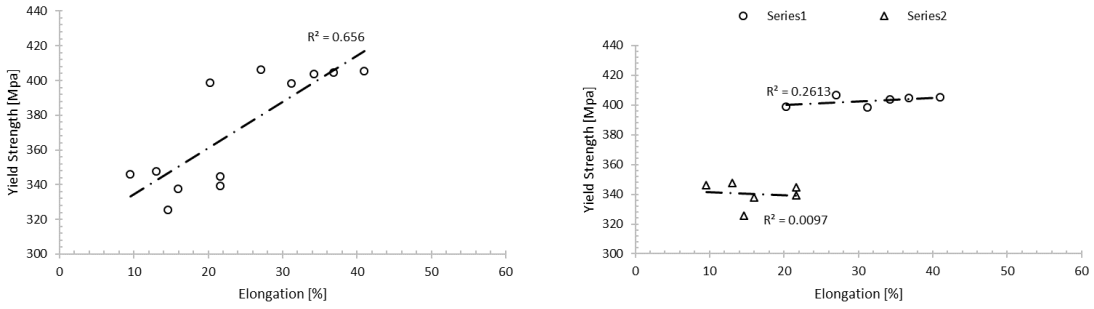

Figure 108: Yield Strength Versus Elongation for Hexagon 3

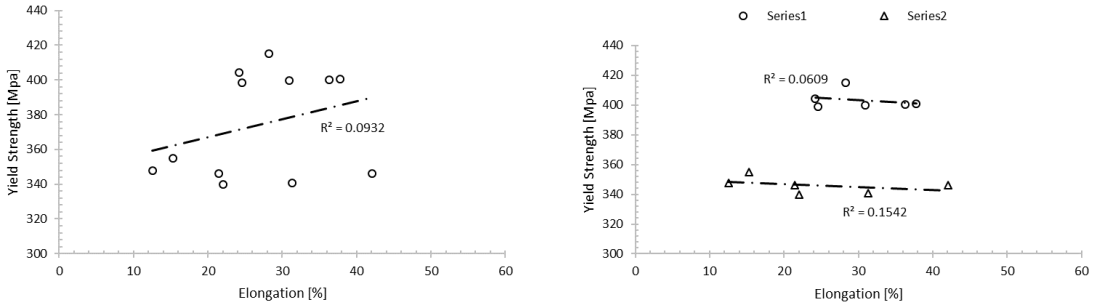

Figure 109: Yield Strength Versus Elongation for Hexagon 4

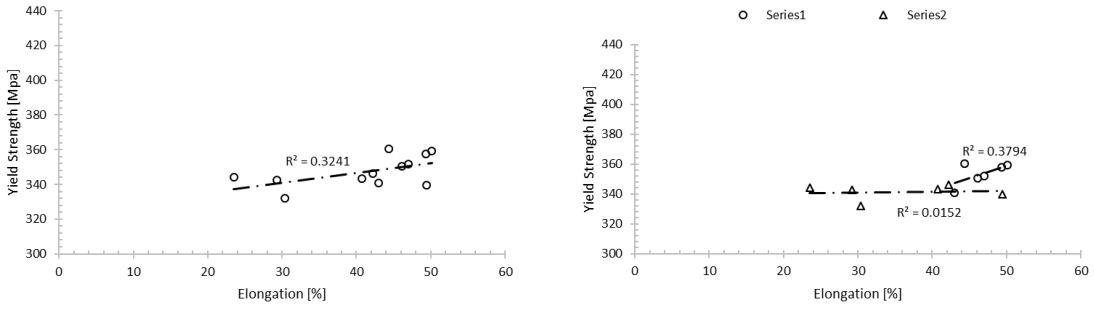

Figure 110: Yield Strength Versus Elongation for Hexagon 5

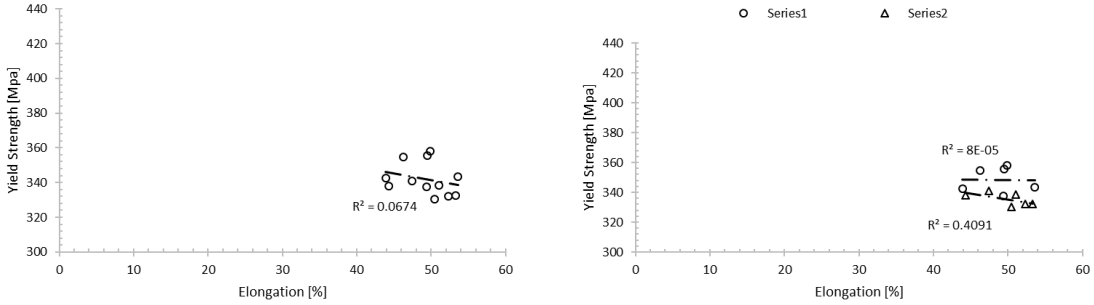

Figure 111: Yield Strength Versus Elongation for Hexagon 6

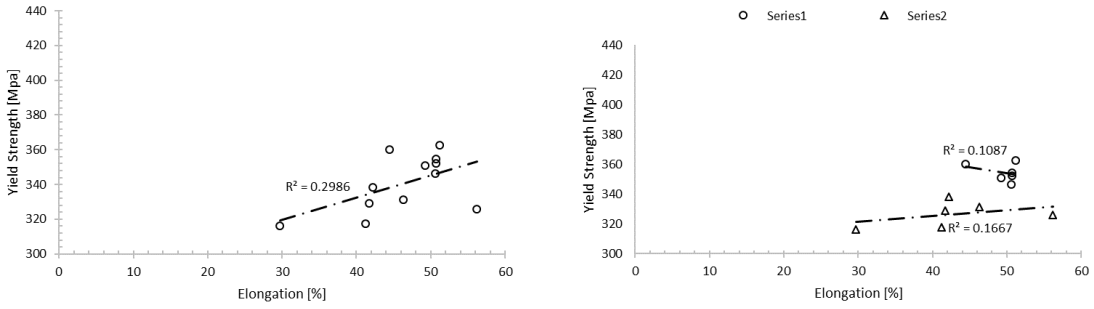

Figure 112: Yield Strength Versus Elongation for Hexagon 7

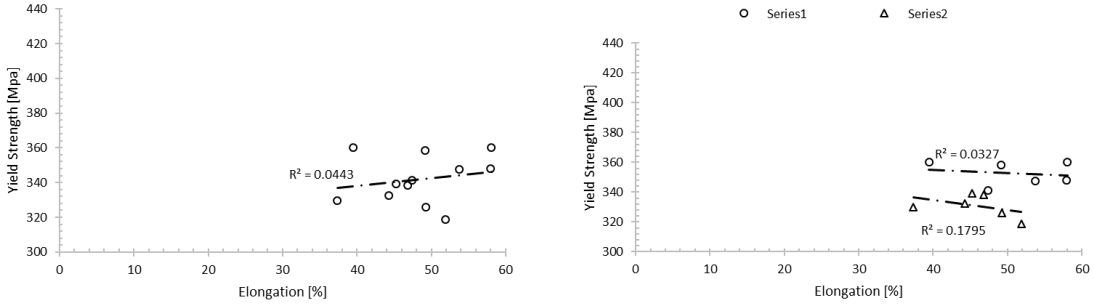

Figure 113: Yield Strength Versus Elongation for Hexagon 8

B.2 Hexagonal Structure Optical Data

This section provides optical images for each hexagonal structure. Four samples evenly spaced along the build height were taken from each hexagonal structure for evaluation.

Table 19: Hexagon 1 Optical Data

Top – Quadrant 4

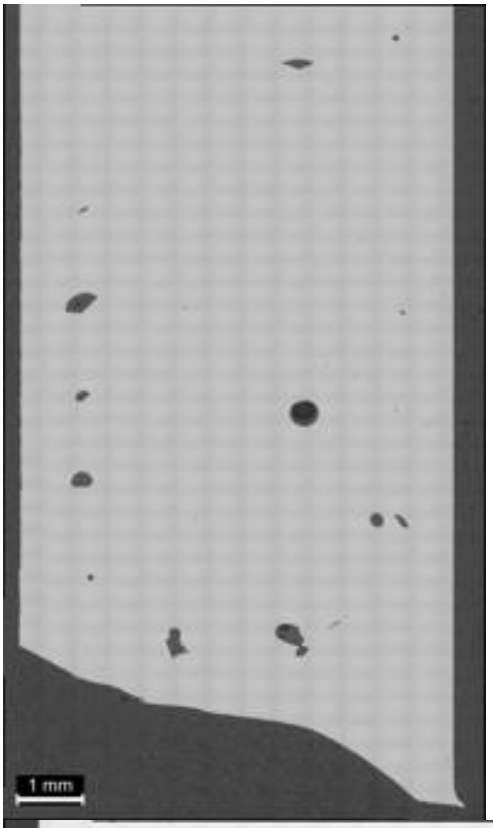

Quadrant 3

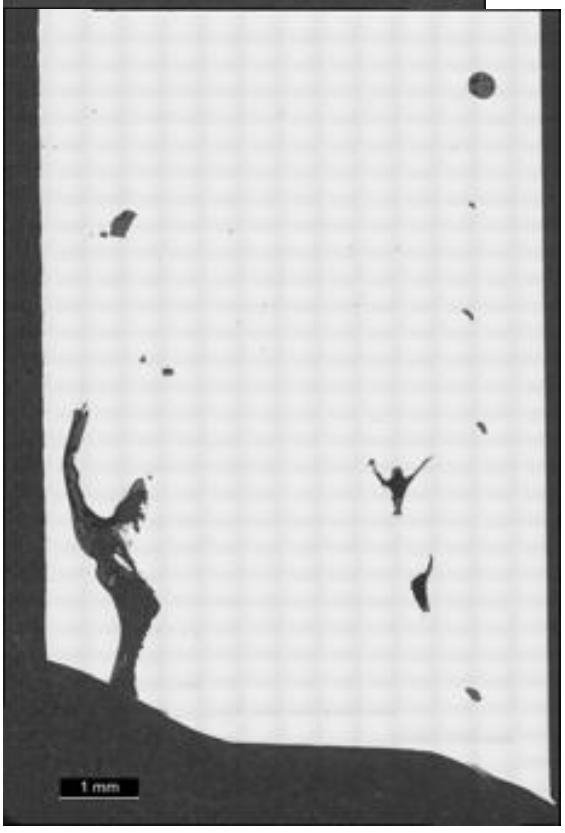

Quadrant 2

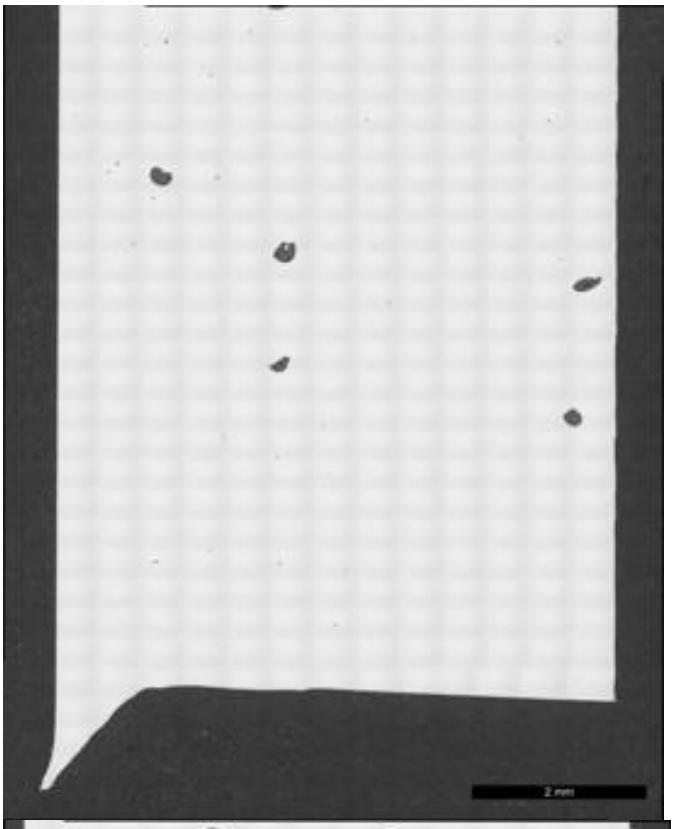

Bottom –
Quadrant 1

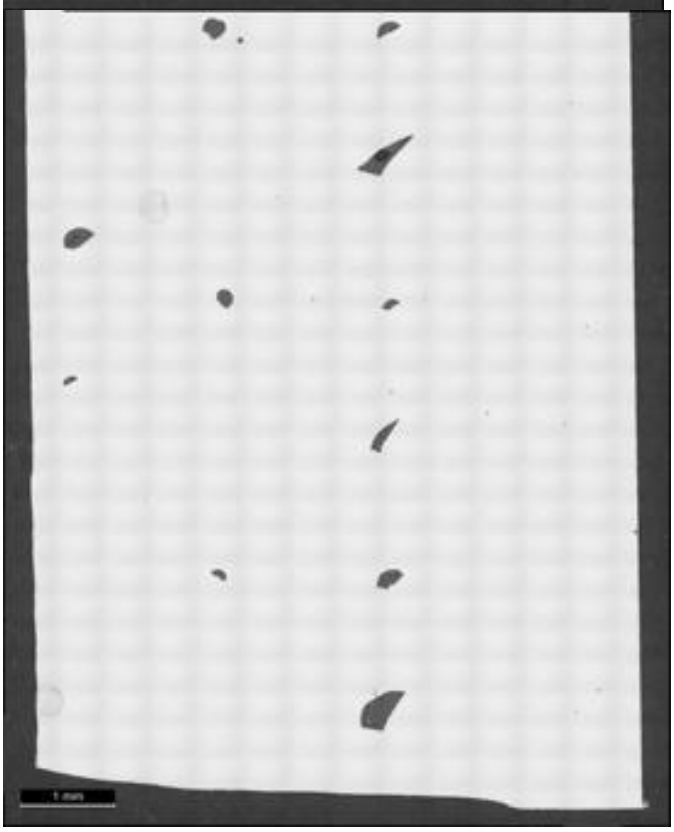

Table 20: Hexagon 2 Optical Data

Top – Quadrant 4

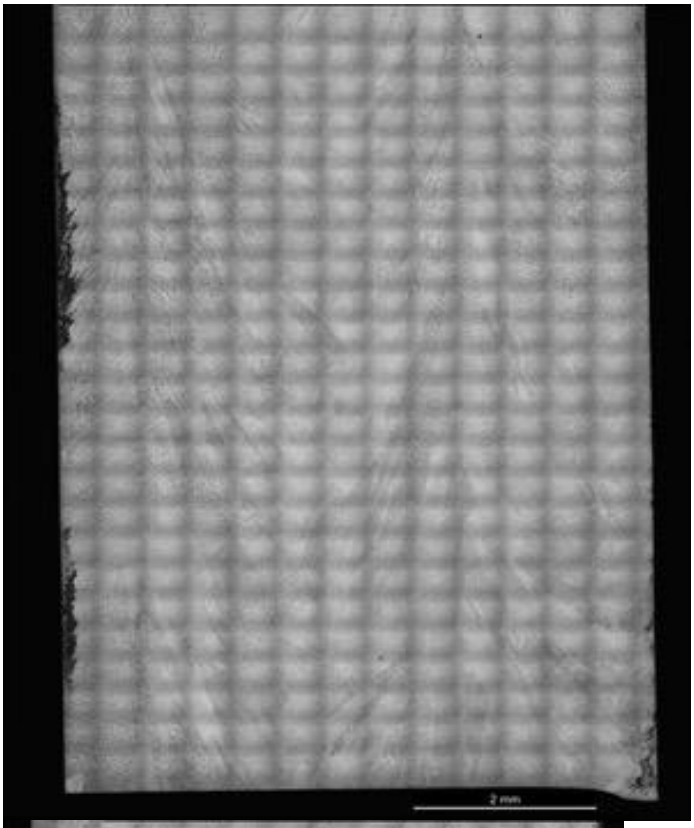

Quadrant 3

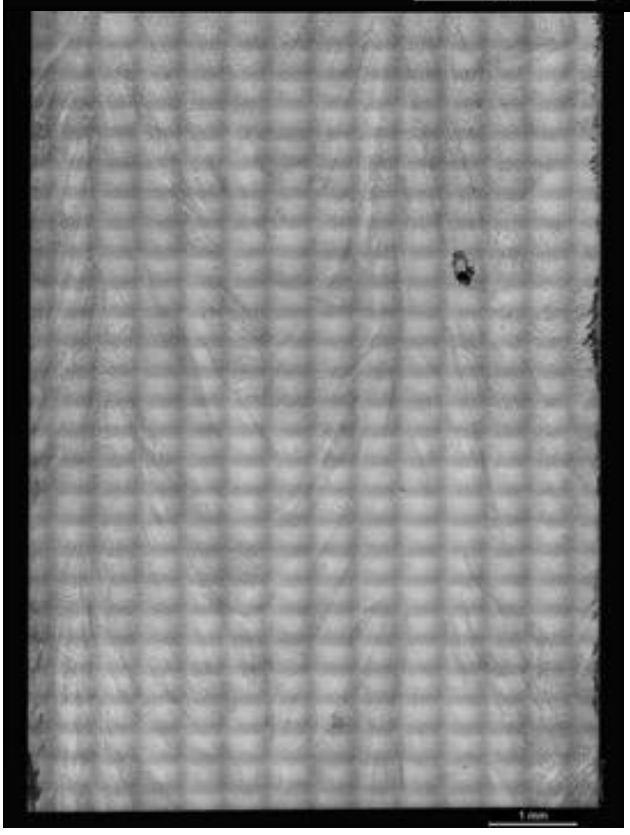

Quadrant 2

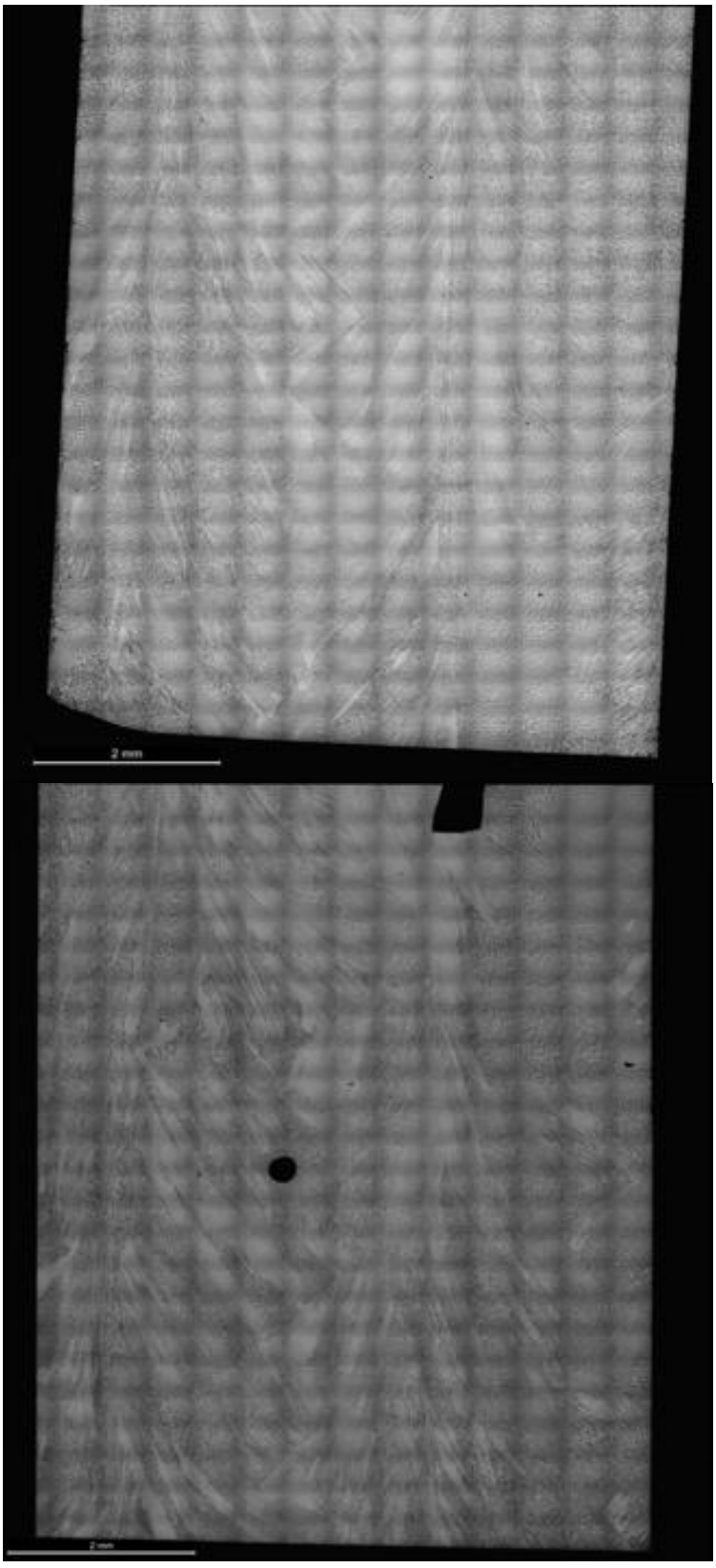

Bottom –
Quadrant 1

Table 21: Hexagon 3 Optical Data

Top – Quadrant 4

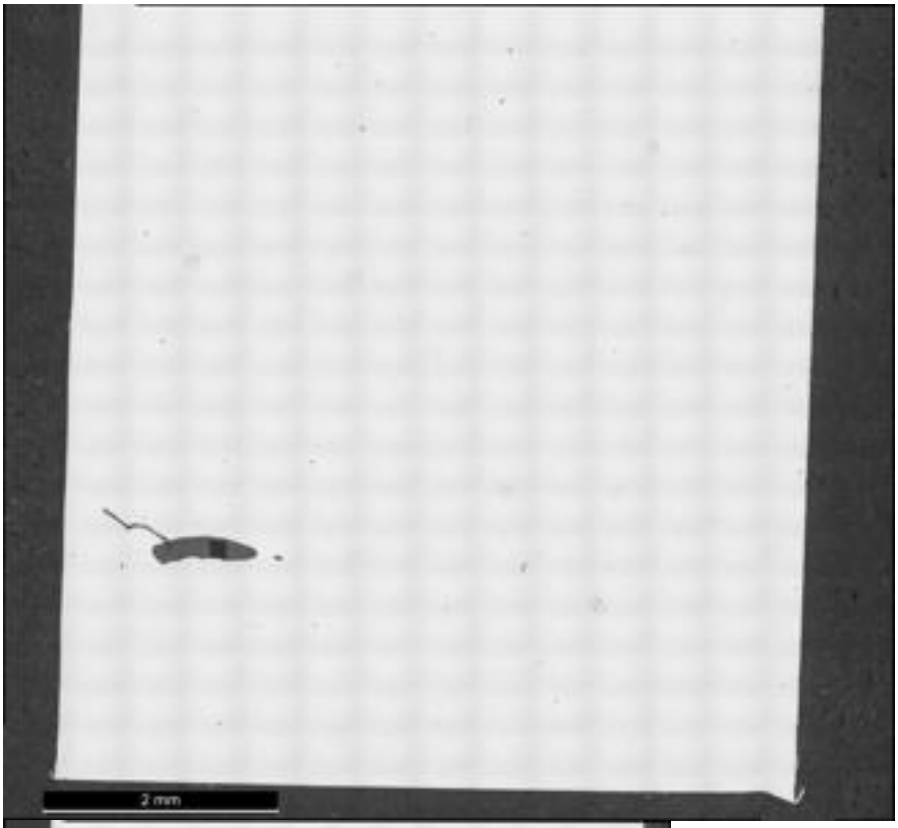

Quadrant 3

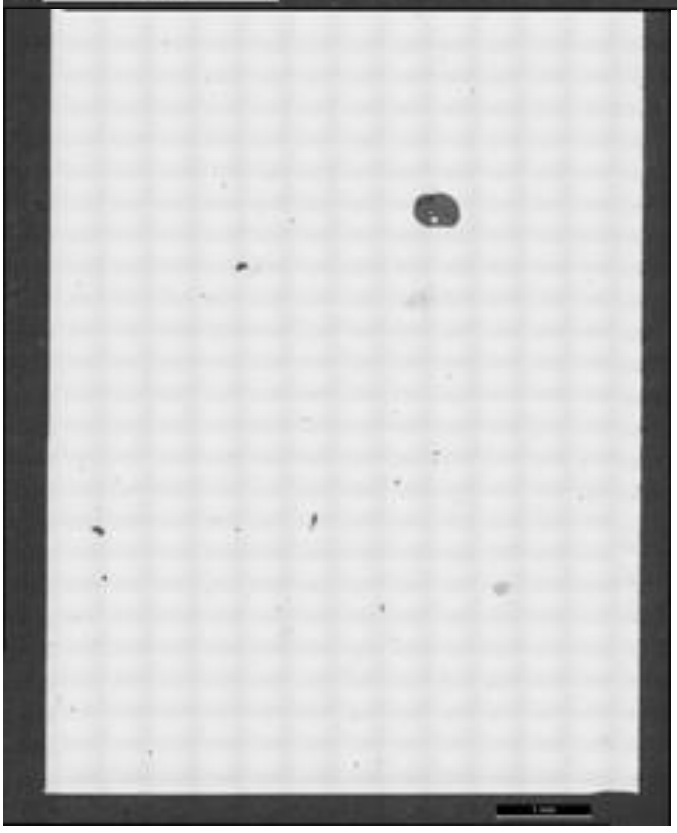

Quadrant 2

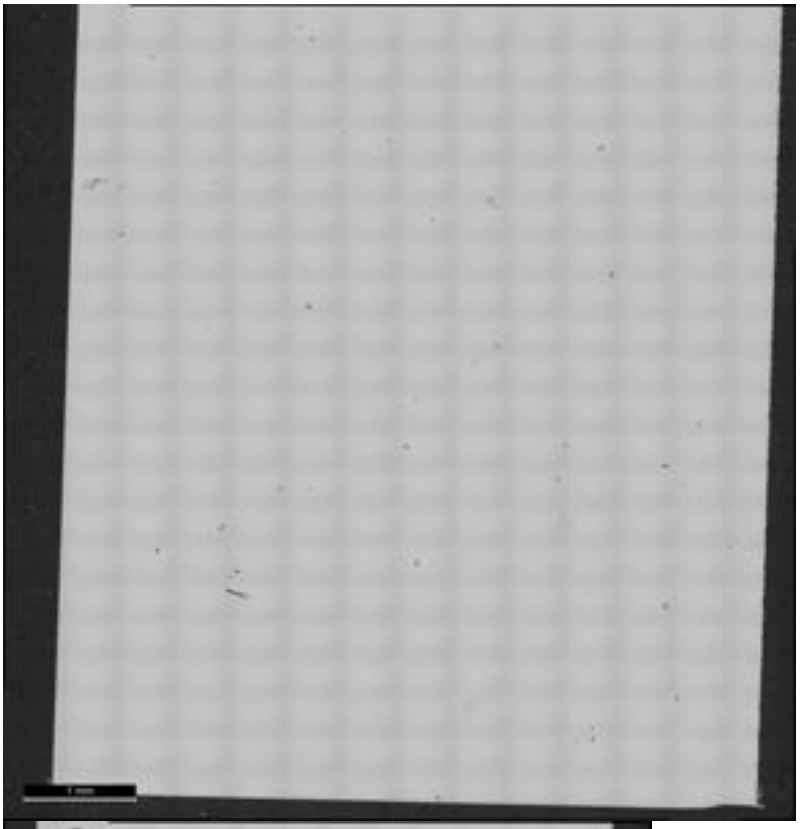

Bottom –
Quadrant 1

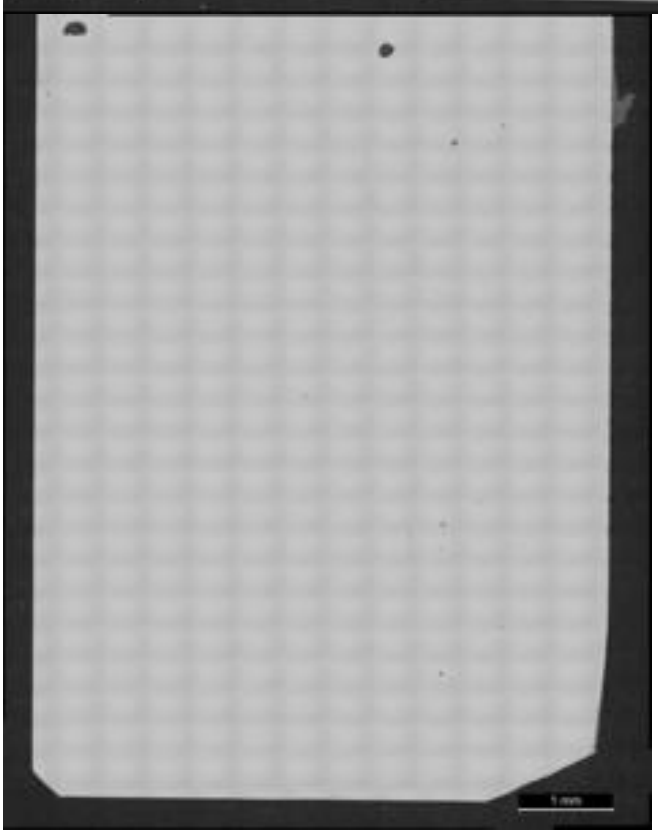

Table 22: Hexagon 4 Optical Data

Top – Quadrant 4

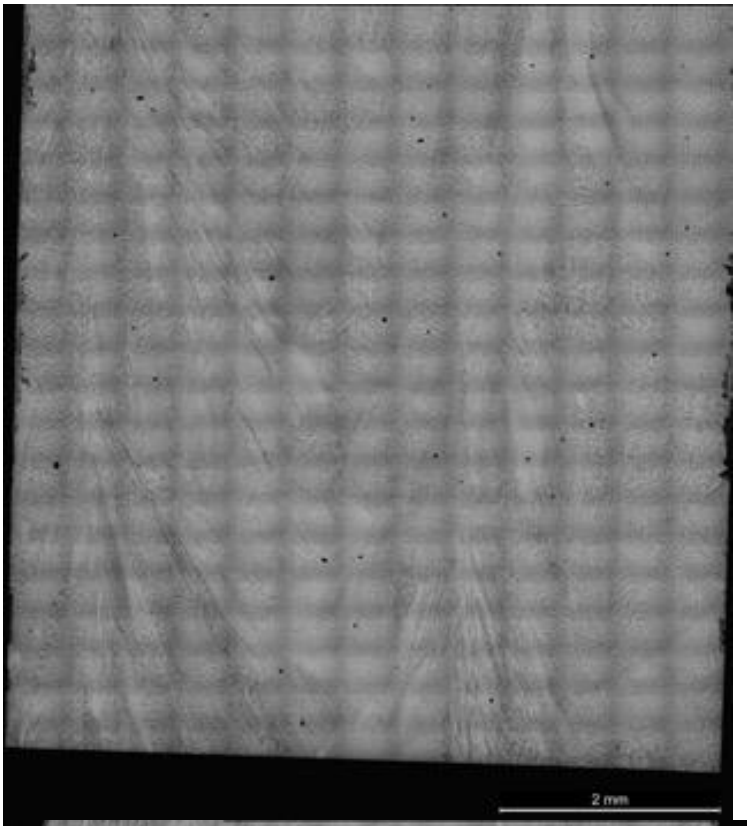

Quadrant 3

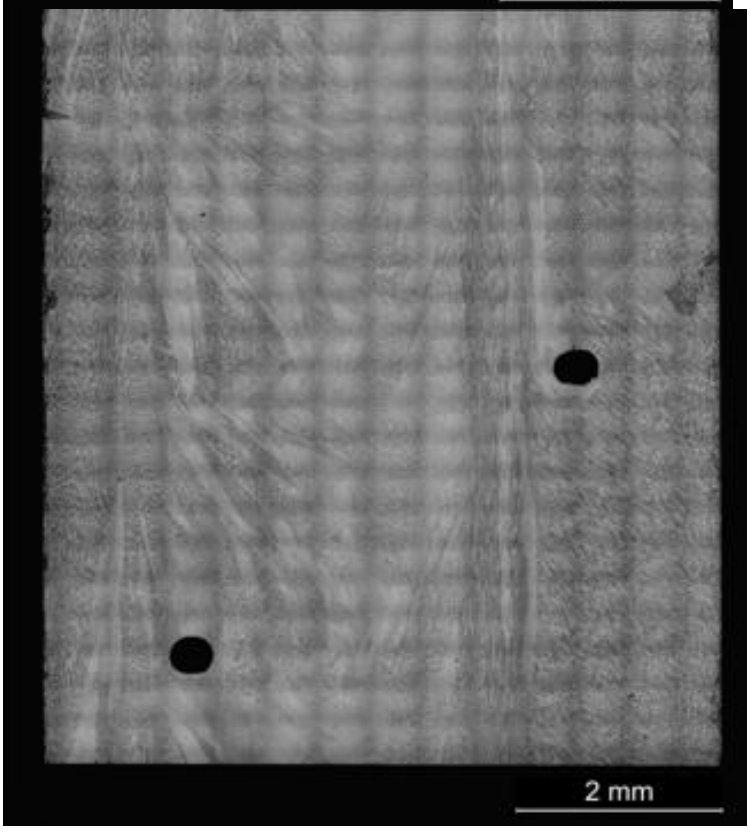

Quadrant 2

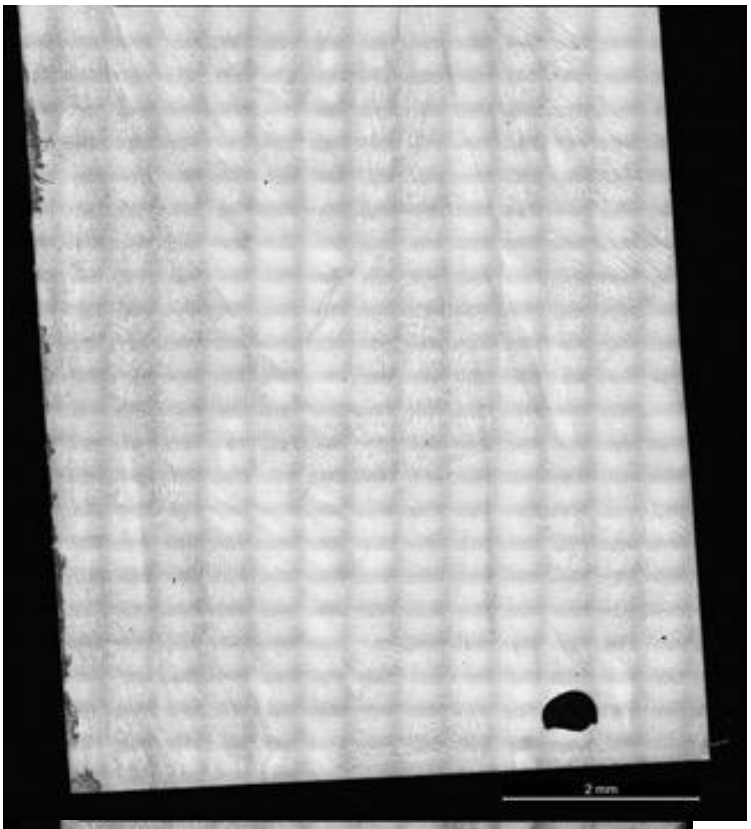

Bottom –
Quadrant 1

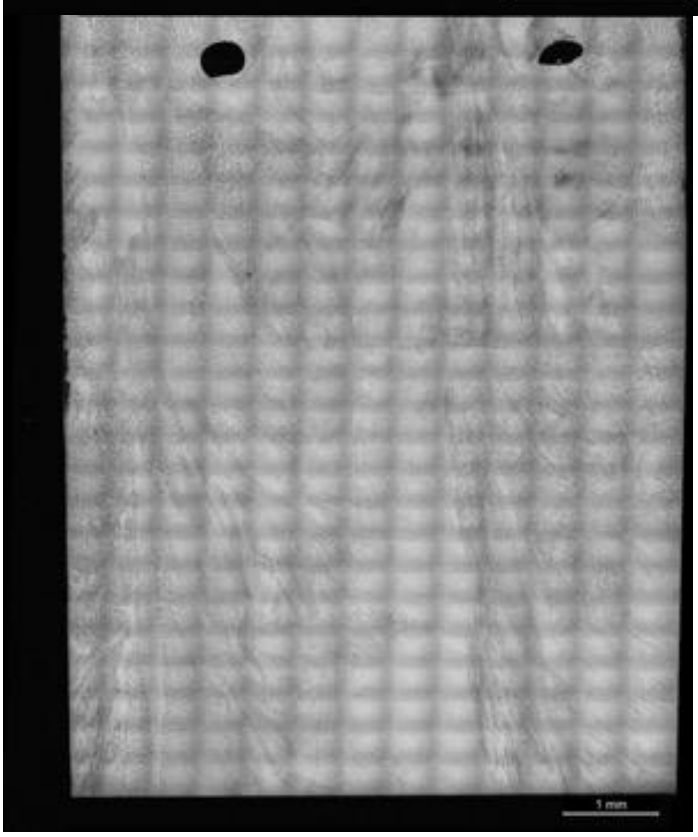

Table 23: Hexagon 5 Optical Data

Top – Quadrant 4

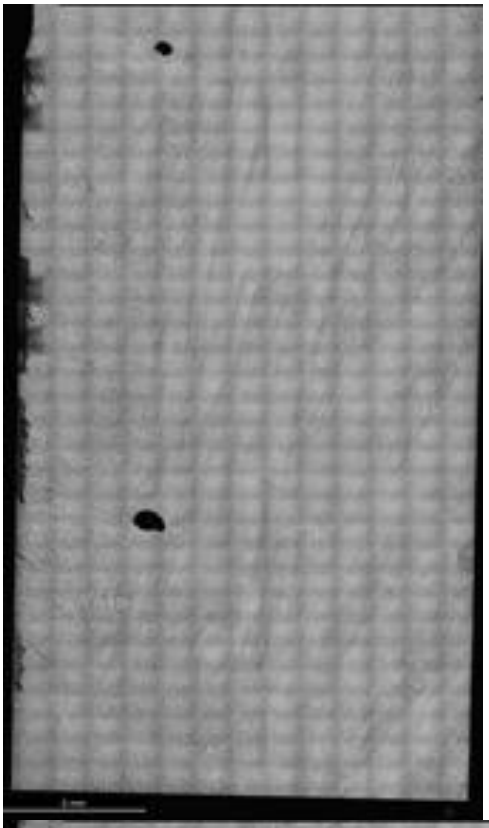

Quadrant 3

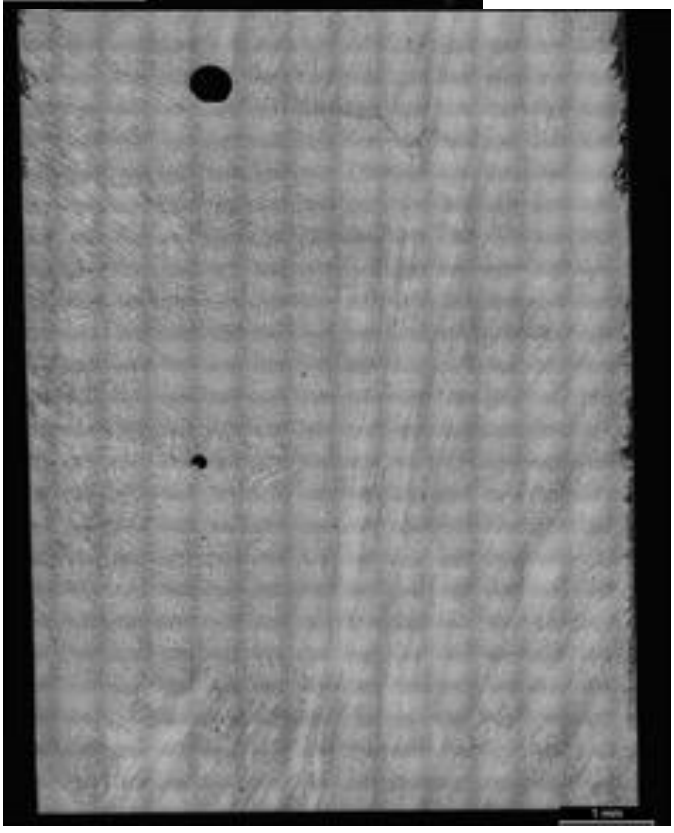

Quadrant 2

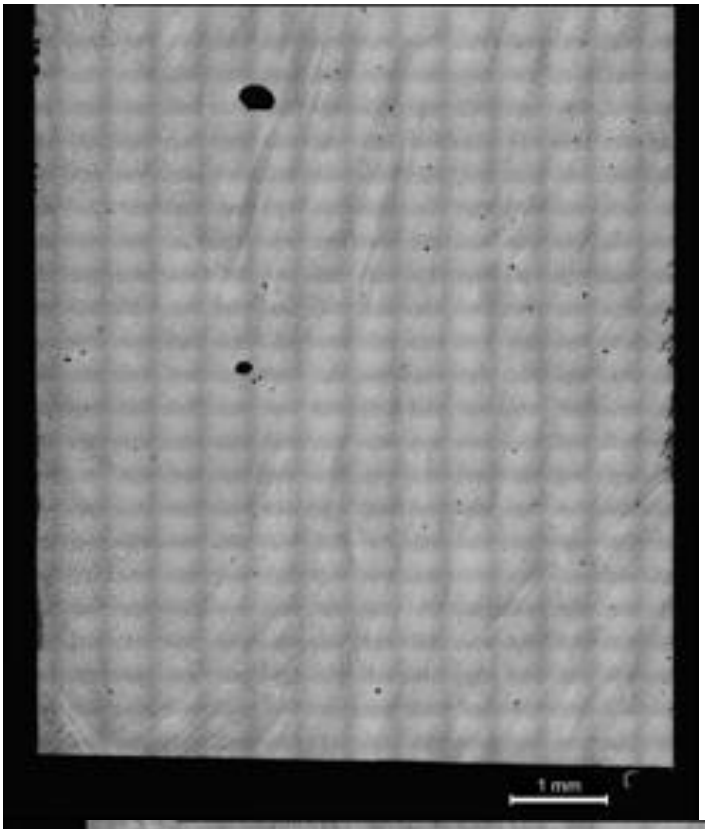

Bottom –
Quadrant 1

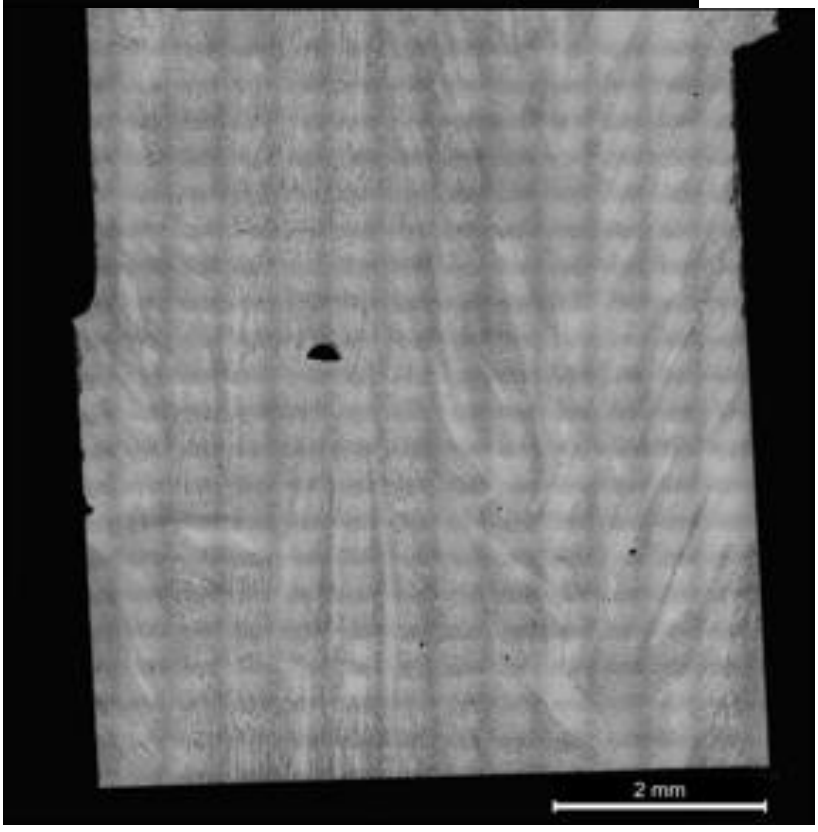

Table 24: Hexagon 6 Optical Data

Top – Quadrant 4

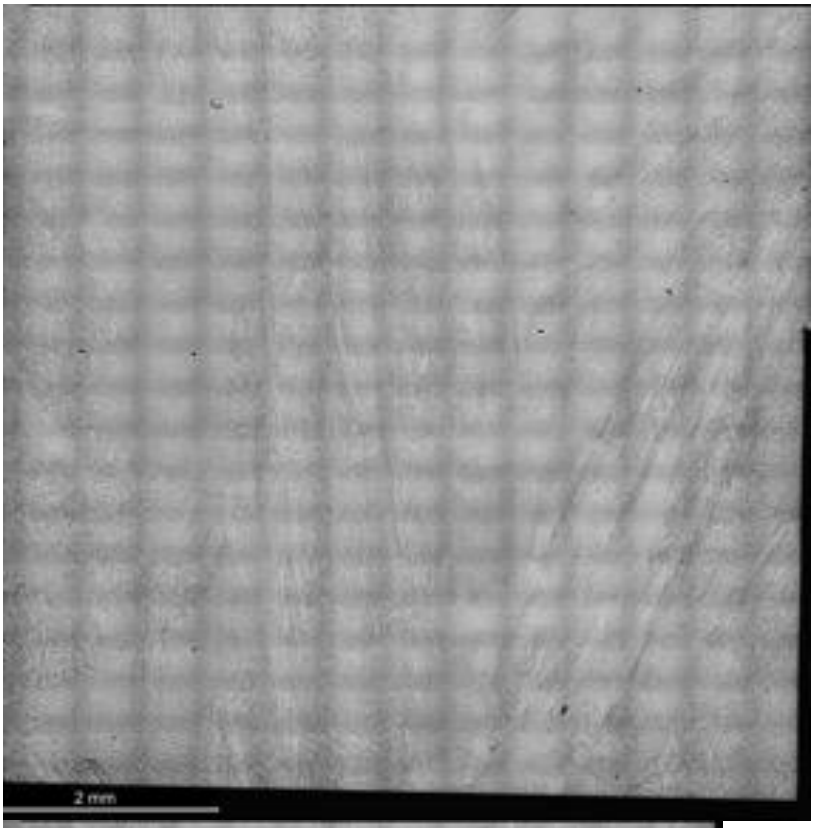

Quadrant 3

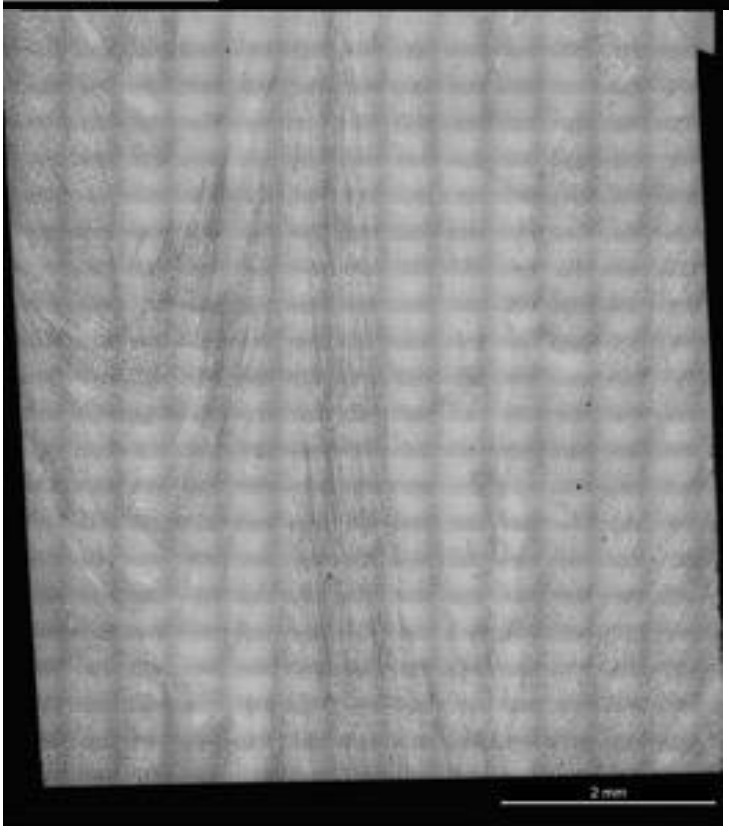

Quadrant 2

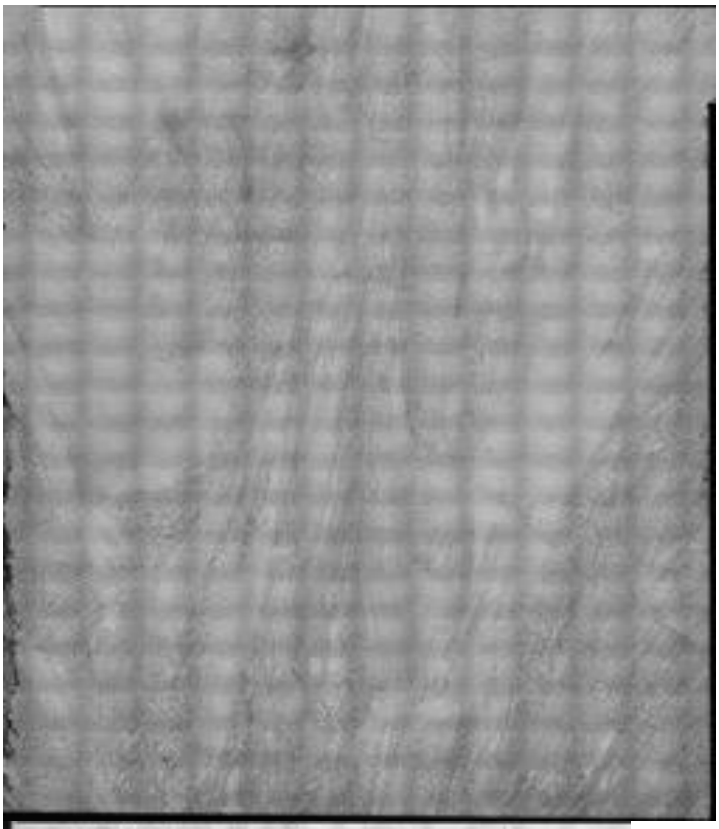

Bottom –
Quadrant 1

Table 25: Hexagon 7 Optical Data

Top – Quadrant 4

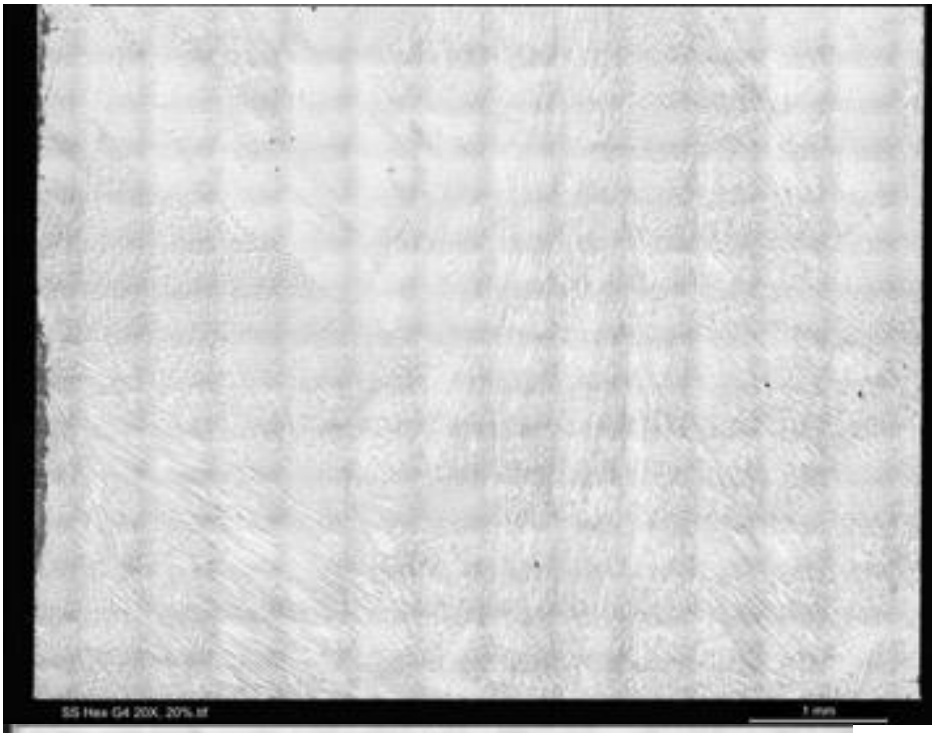

Quadrant 3

Quadrant 2

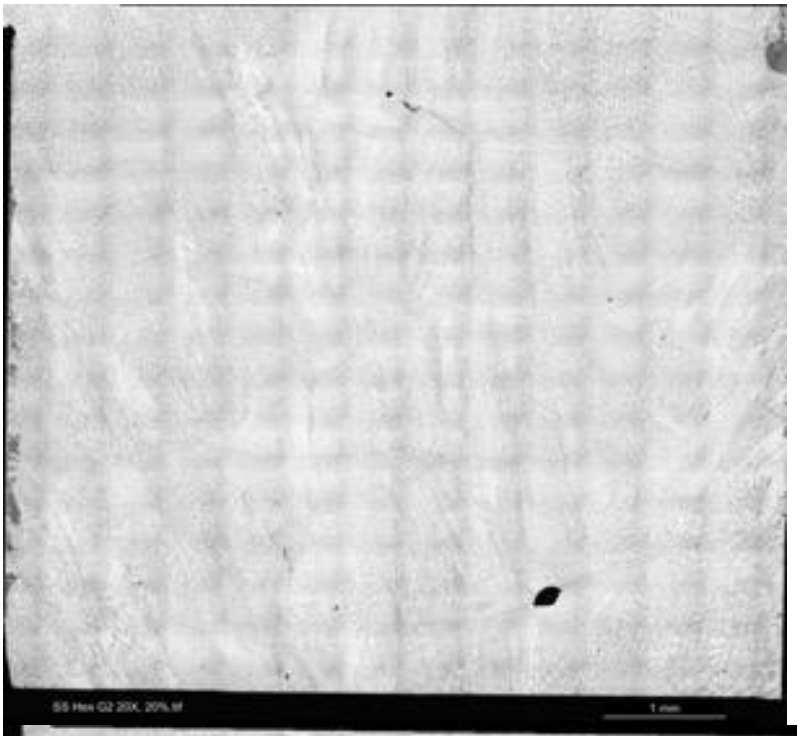

Bottom –
Quadrant 1

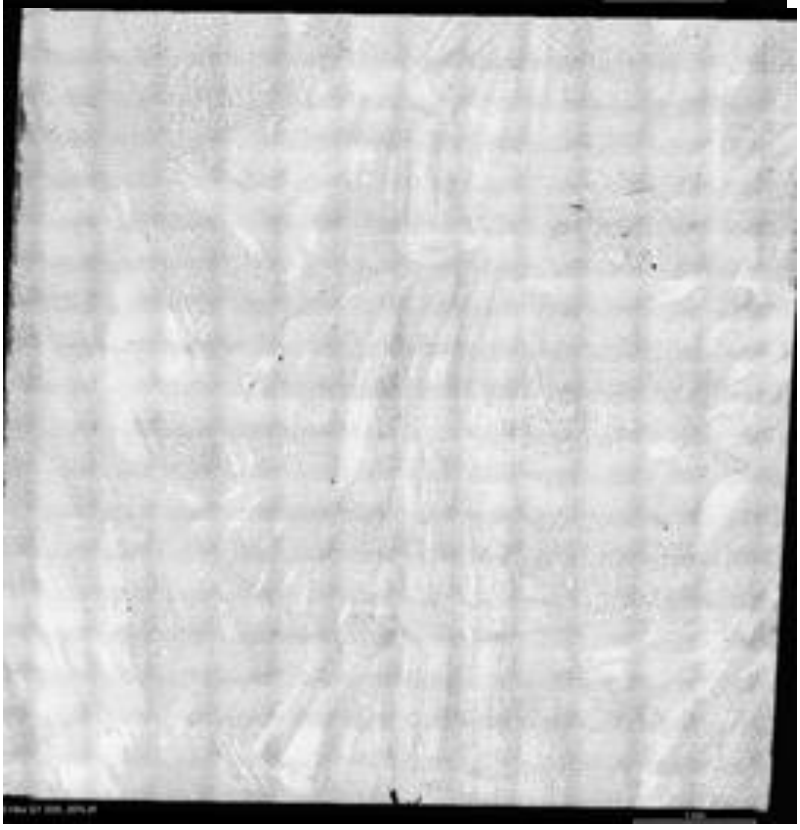

Table 26: Hexagon 8 Optical Data

Top – Quadrant 4

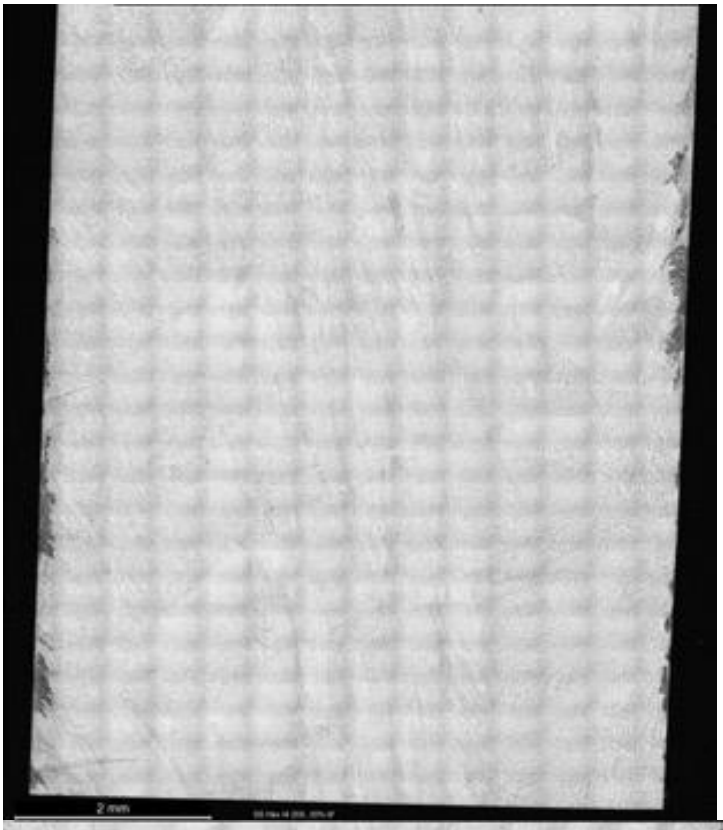

Quadrant 3

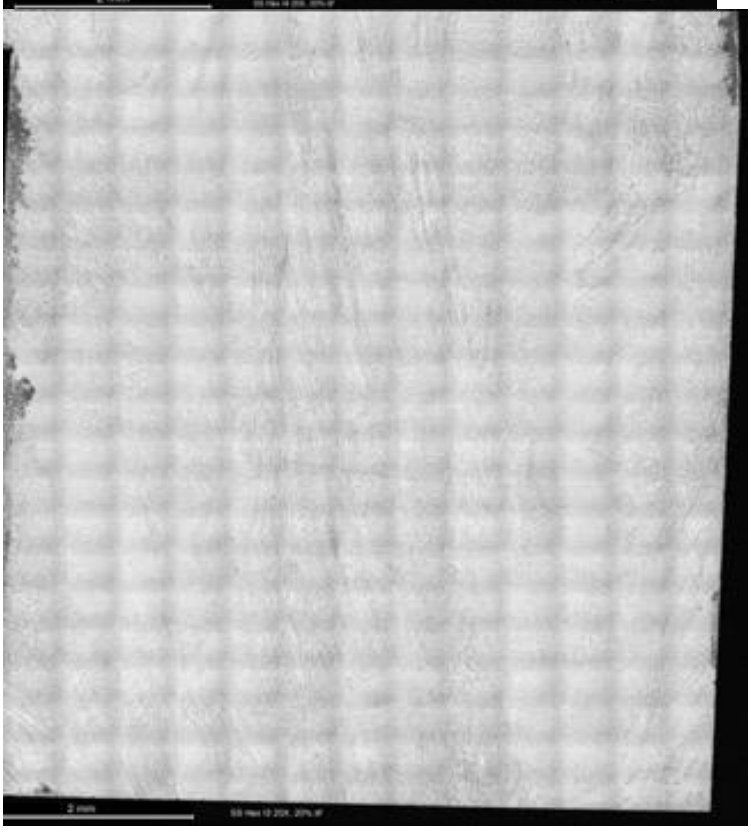

Quadrant 2

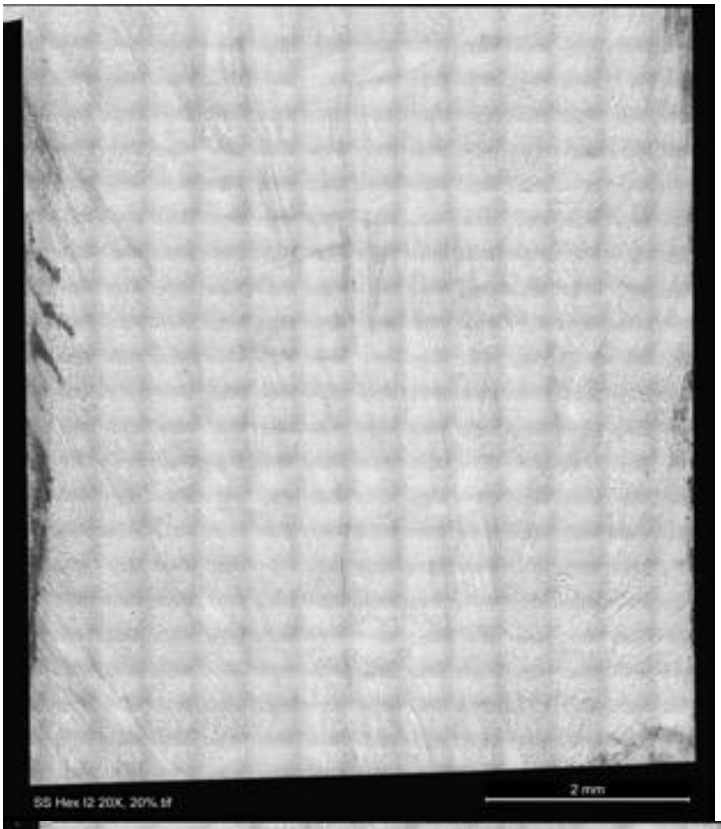

Bottom –
Quadrant 1

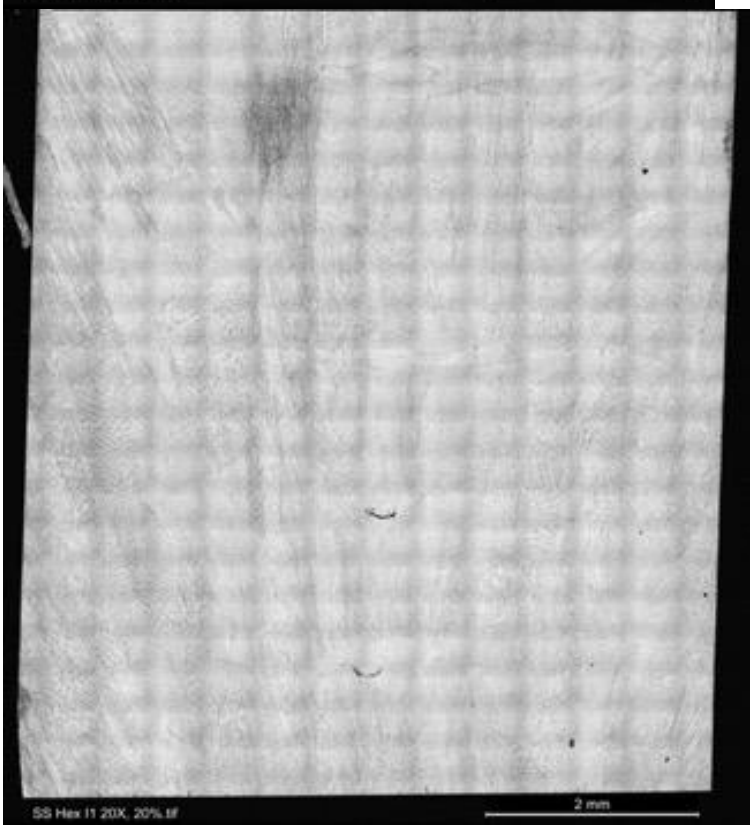

B.3 Hexagonal Structure X-ray Computed Tomography Data

This section shows figures generated from X-ray computed tomography data using Volume Graphics. The sections shown are oriented horizontally, with the build direction going from left to right.

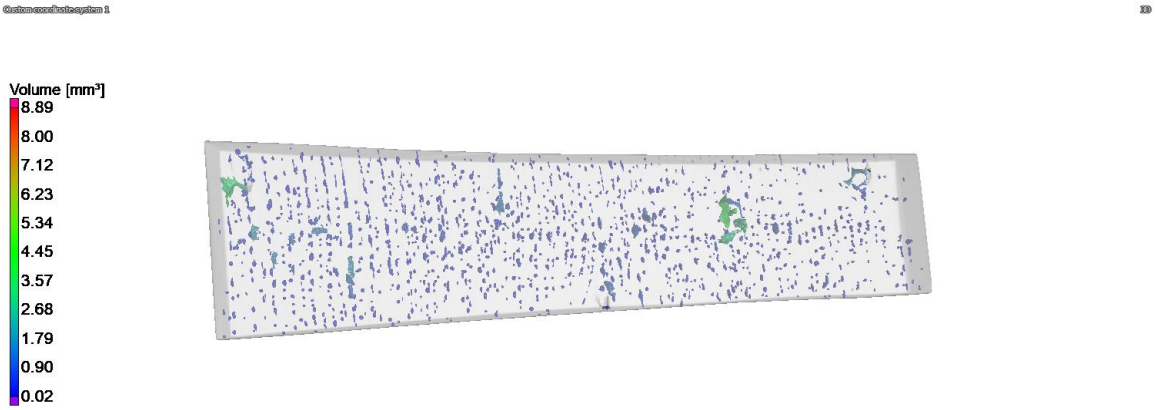

Figure 114: Hexagon 1 X-Ray Computed Tomography

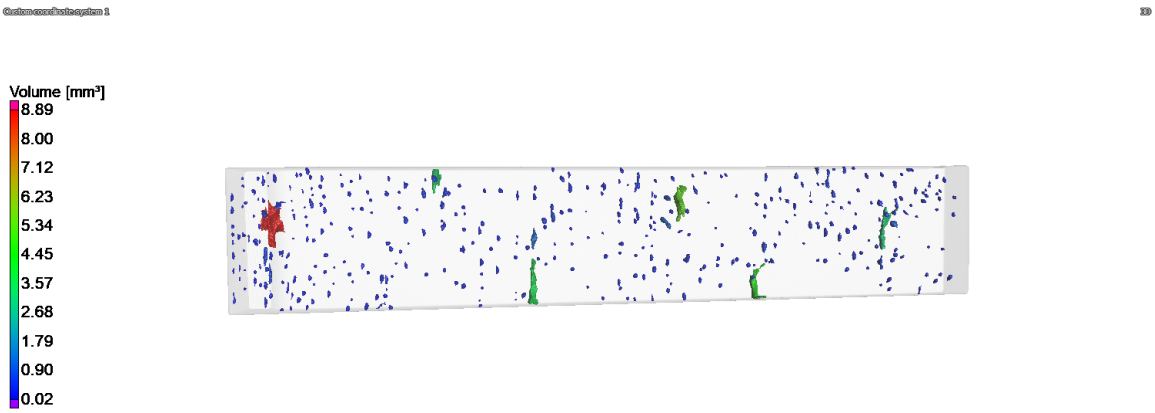

Figure 115: Hexagon 2 X-Ray Computed Tomography

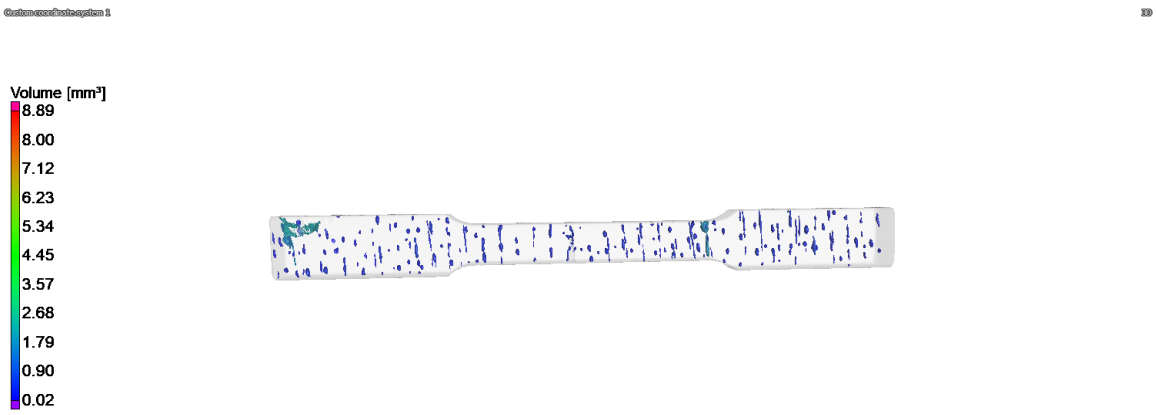

Figure 116: Hexagon 3 X-Ray Computed Tomography

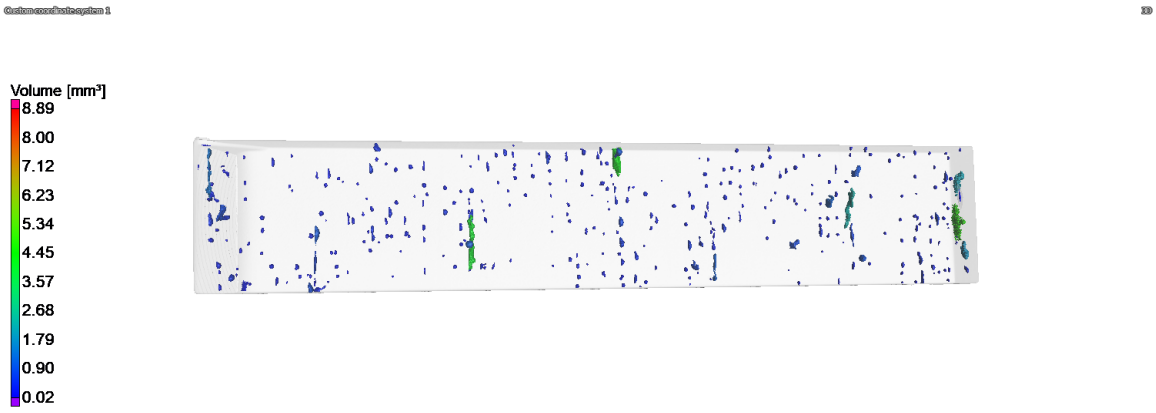

Figure 117: Hexagon 4 X-Ray Computed Tomography

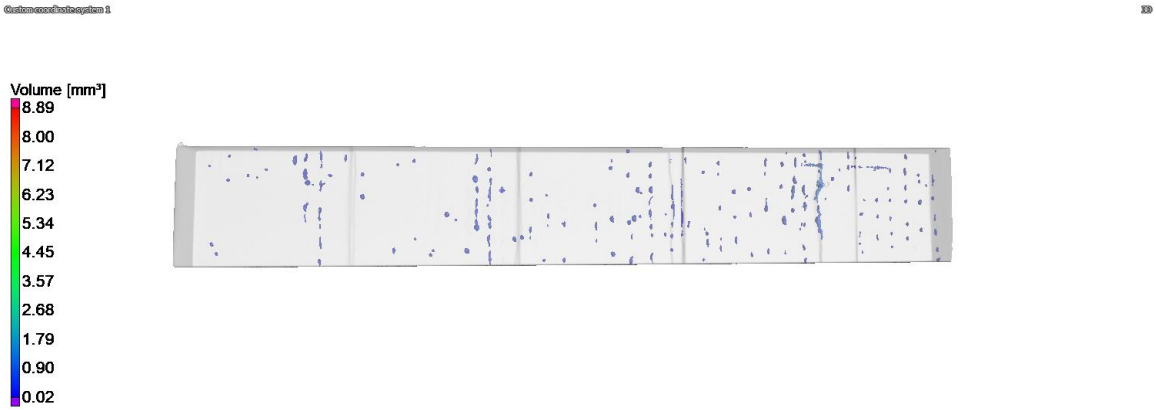

Figure 118: Hexagon 5 X-Ray Computed Tomography

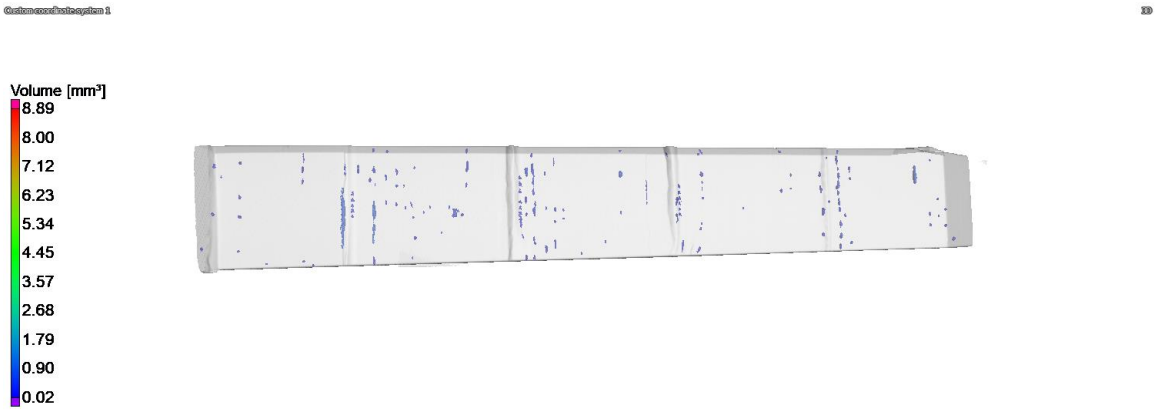

Figure 119: Hexagon 6 X-Ray Computed Tomography

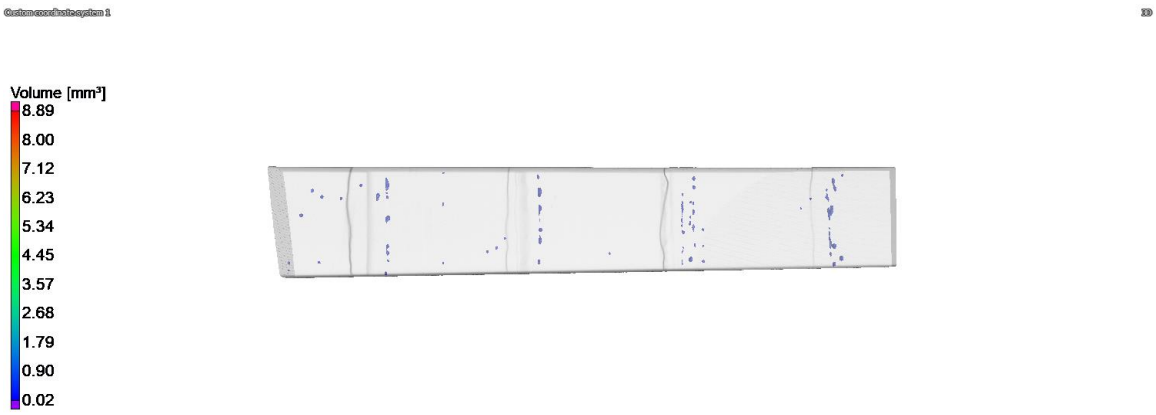

Figure 120: Hexagon 7 X-Ray Computed Tomography

Figure 121: Hexagon 8 X-Ray Computed Tomography

APPENDIX C. HYBRID STRUCTURE DATA

This appendix contains the mechanical and material data used in the discussion in Chapter 5. Resulting structure images, stress-strain curves, and X-ray computed tomography data is provided in the ensuing section for each hybrid structure. Discussion and conclusions drawn from the results are provided in Chapter 5.

C.1 Hybrid Structure Figures

Figure 122: Flat Stainless Structure

Figure 123: Angled Stainless Structure

Figure 124: Scalloped Stainless Structure

Figure 125: Tongue and Groove Stainless Structure

Figure 126: Dovetail Stainless Structure

Figure 127: Flat Cast Iron Structure

Figure 128: Angled Cast Iron Structure

Figure 129: Scalloped Cast Iron Structure Front View

Figure 130: Scalloped Cast Iron Structure Side View

Figure 131: Tongue and Groove Cast Iron Structure Front View

Figure 132: Tongue and Groove Cast Iron Structure Side View

C.2 Hybrid Structure Tensile Data

Table 27: Hybrid Structure Yield Strength

Hybrid Structure	Yield Strength [MPa] - Stainless Steel	Standard Deviation [MPa]	Yield Strength [MPa] - Cast Iron	Standard Deviation [MPa]
Flat	298.8	3.9	174.1	8.9
Angled	302.1	2.3	155.7	0.6
Scalloped	295.7	1.2	57.3	61.3
Tongue & Groove	272.8	6.2	298.8	3.9

Table 28: Hybrid Structure Ultimate Tensile Strength

Hybrid Structure	Ultimate Tensile Strength [MPa] - Stainless Steel	Standard Deviation [MPa]	Ultimate Tensile Strength [MPa] - Cast Iron	Standard Deviation [MPa]
Flat	561.0	1.4	210.0	4.6
Angled	529.7	25.8	179.9	7.8
Scalloped	541.8	4.4	161.4	4.7
Tongue & Groove	464.7	17.9	137.6	73.3

Table 29: Hybrid Structure Elongation at Failure

Hybrid Structure	Elongation at Failure [%] - Stainless Steel	Standard Deviation [%]	Elongation at Failure [%] - Cast Iron	Standard Deviation [%]
Flat	42.15	2.60	0.20	0.04
Angled	28.62	7.41	0.15	0.03
Scalloped	29.67	7.69	0.19	0.05
Tongue & Groove	18.09	6.26	0.19	0.13

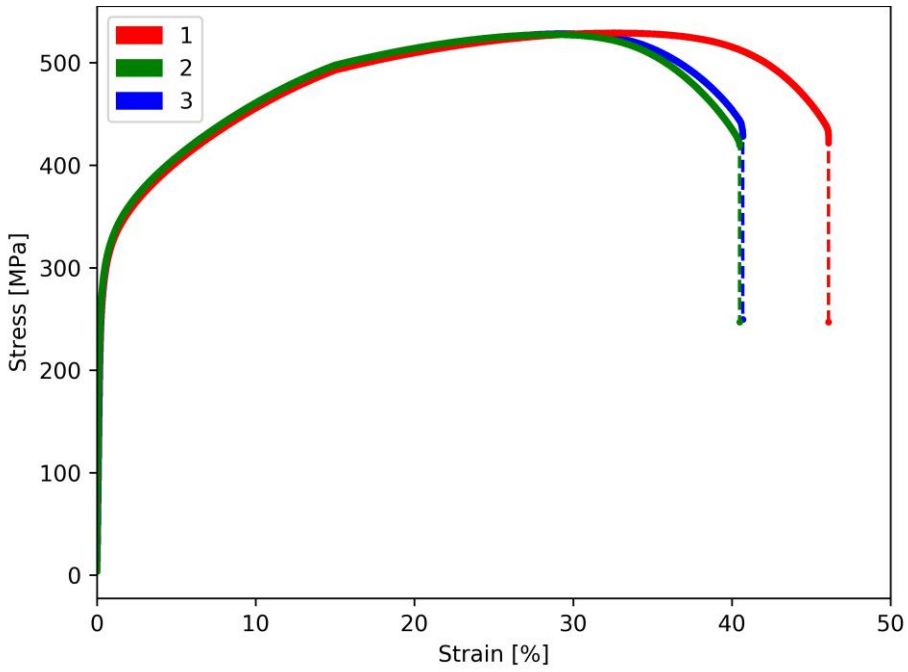

Figure 133: Flat Stainless Steel Structure

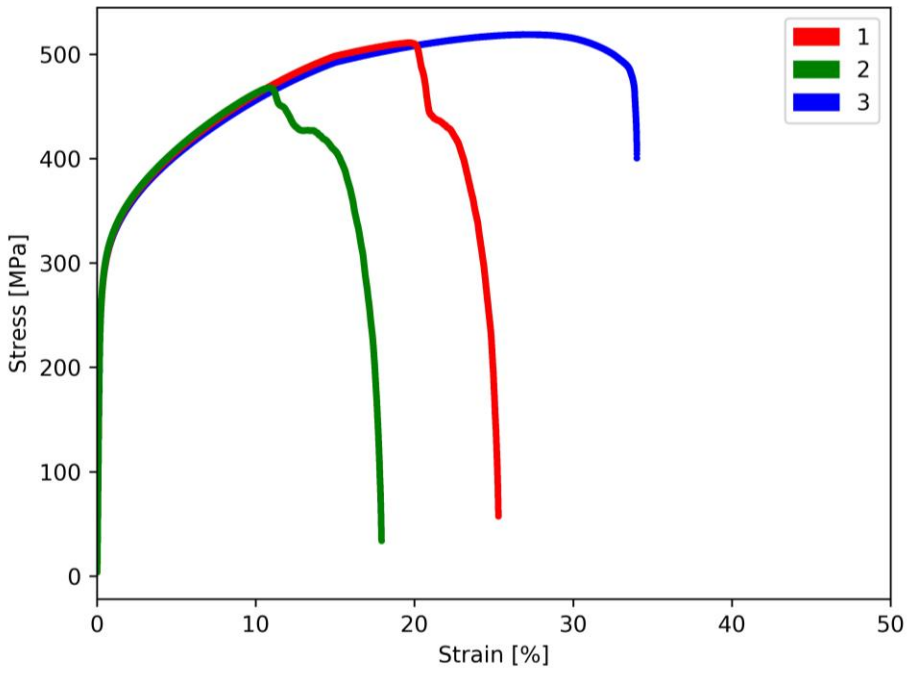

Figure 134: Angled Stainless Steel Structure

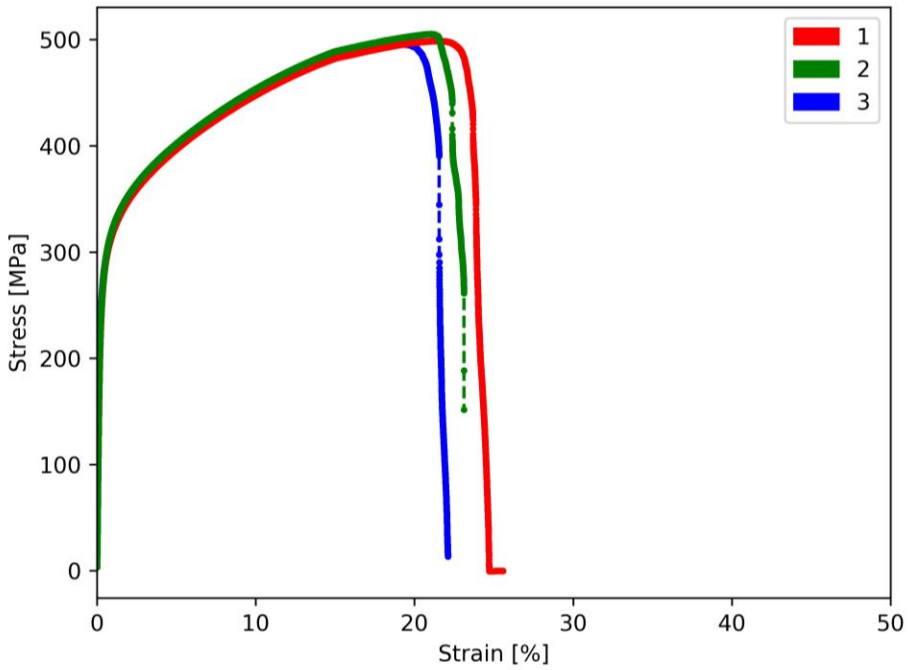

Figure 135: Scalloped Stainless Steel Structure

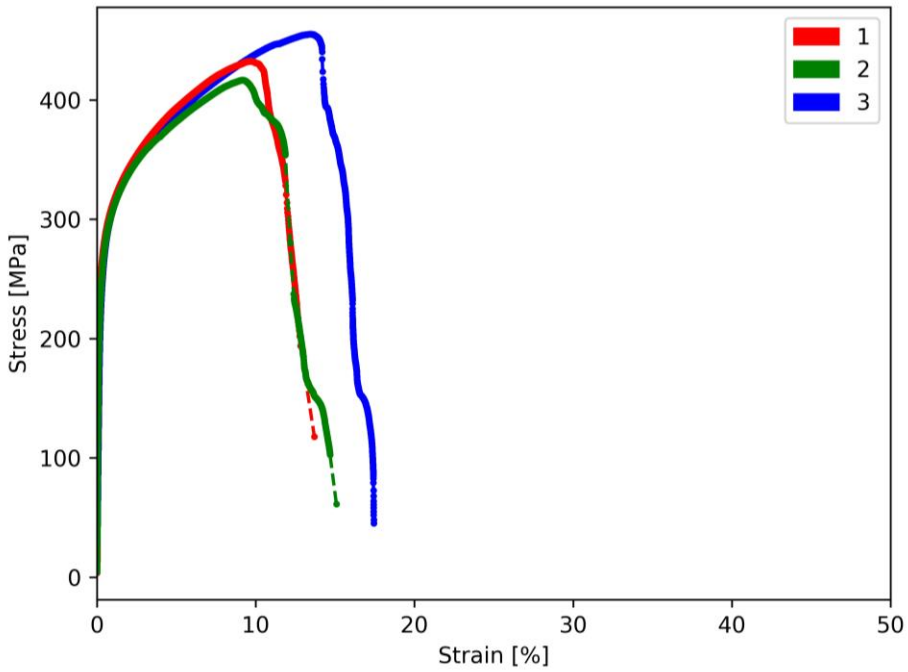

Figure 136: Tongue and Groove Stainless Steel Structure

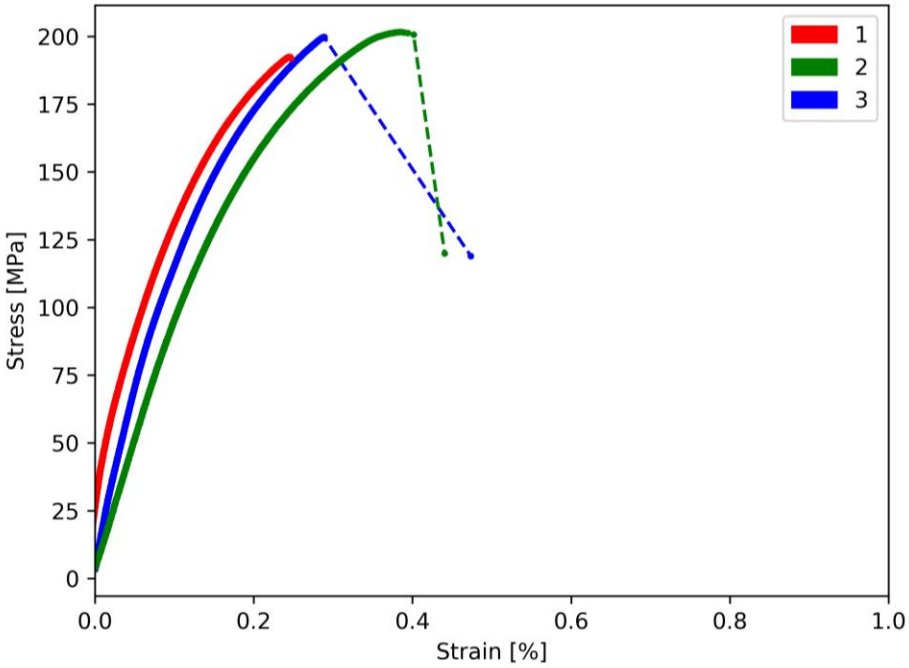

Figure 137: Flat Cast Iron Structure

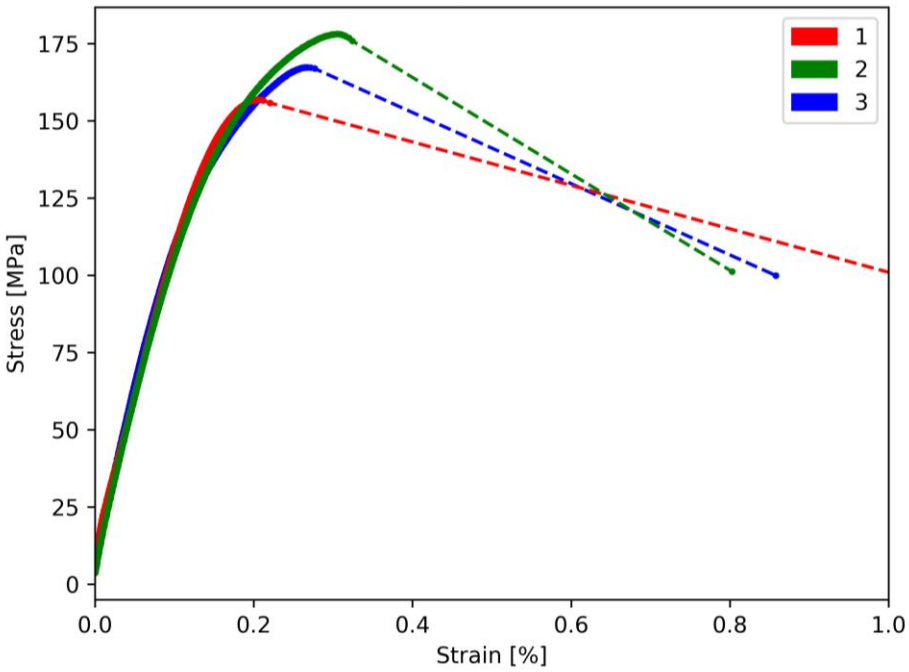

Figure 138: Angled Cast Iron Structure

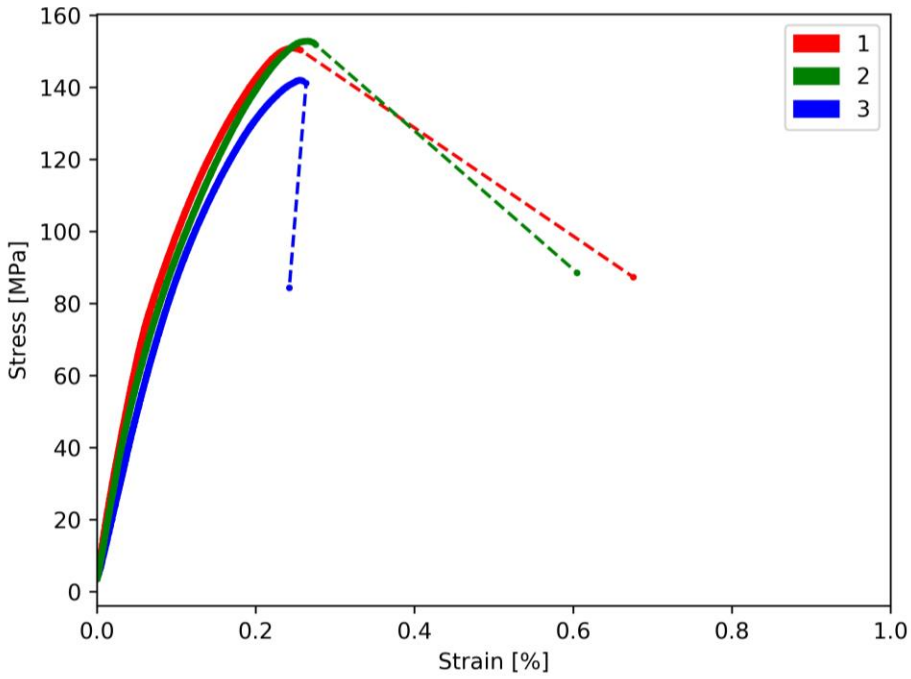

Figure 139: Scalloped Cast Iron Structure

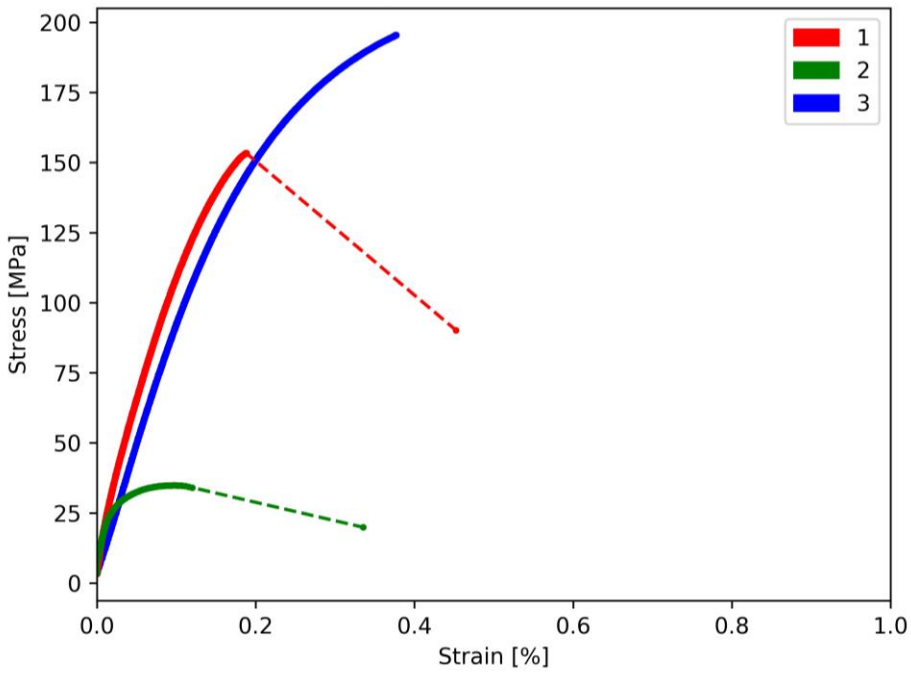

Figure 140: Tongue and Groove Cast Iron Structure

C.3 Hybrid Structure X-ray Computed Tomography Data

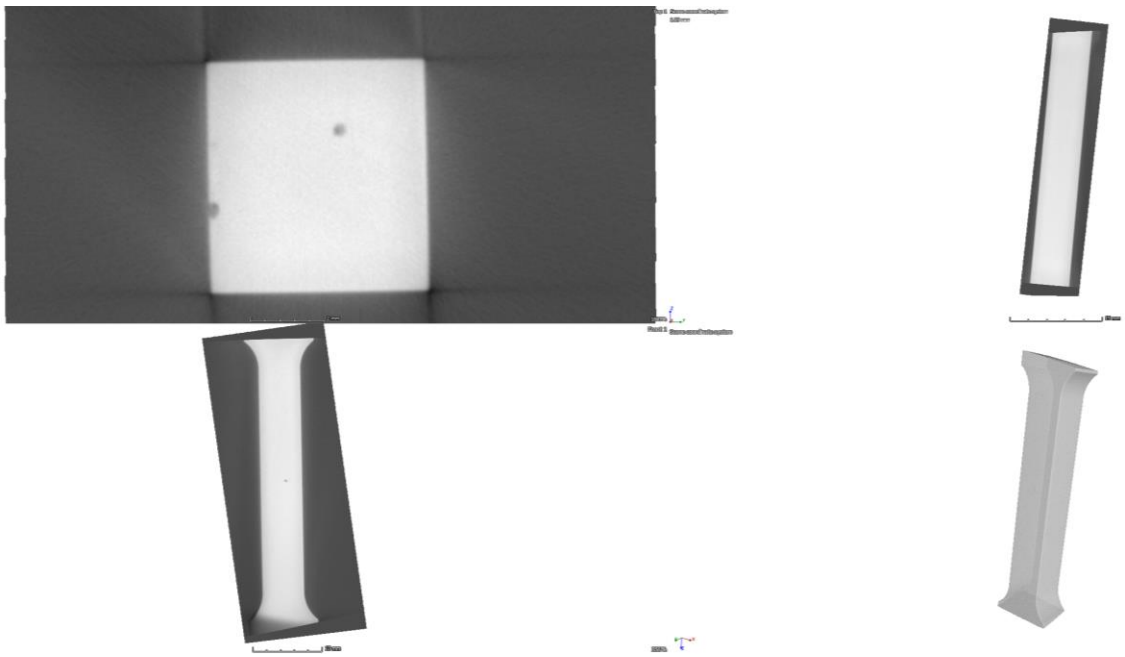

Figure 141: Stainless Steel Flat Structure CT

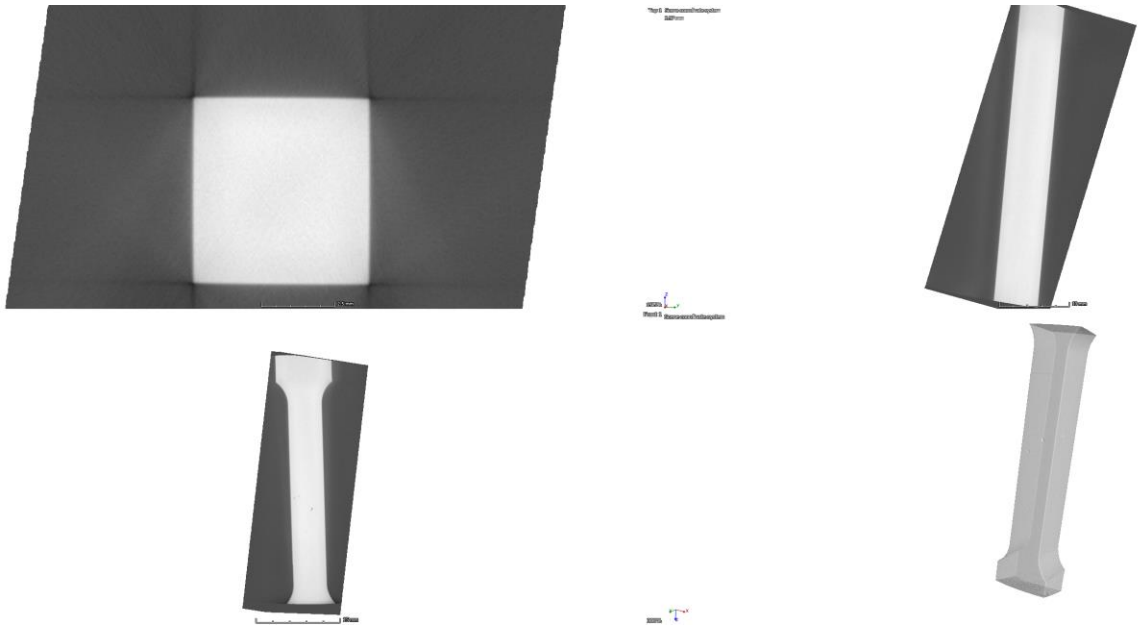

Figure 142: Stainless Steel Angled Structure CT

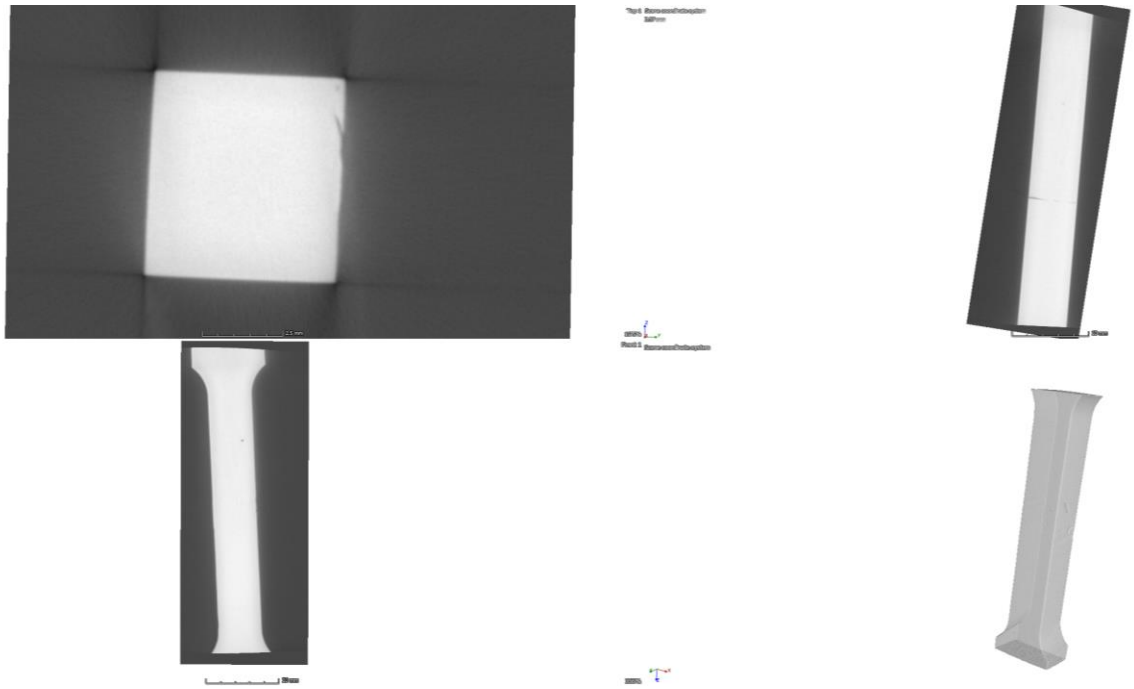

Figure 143: Stainless Steel Scalloped Structure CT

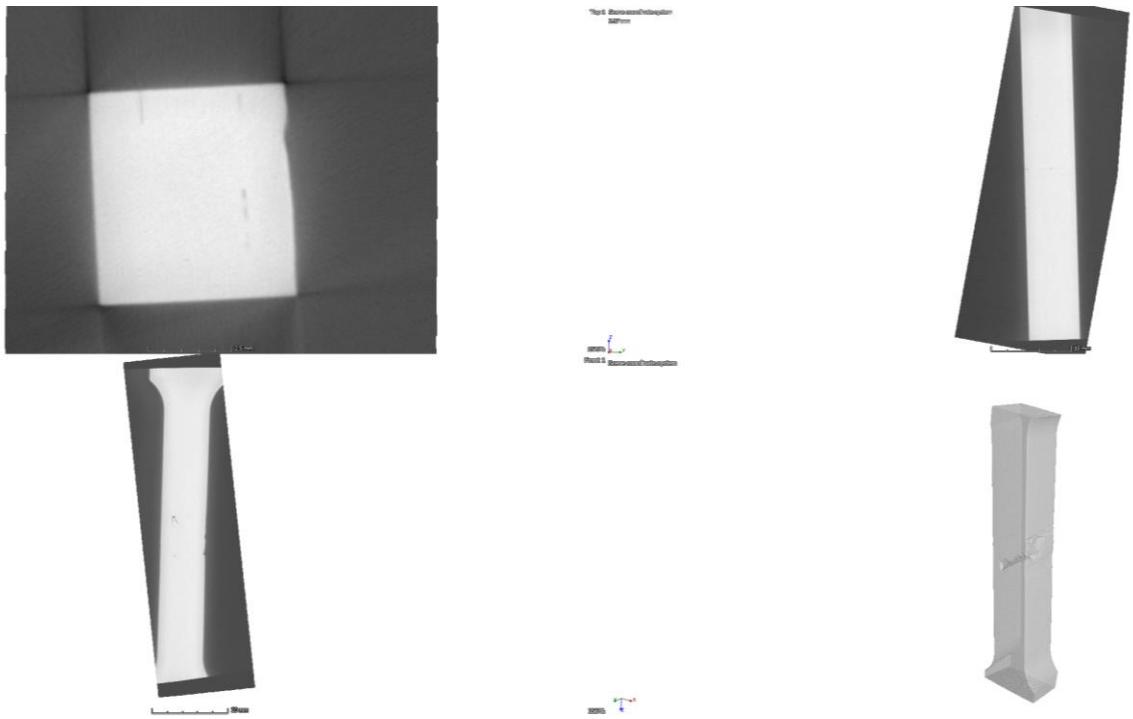

Figure 144: Stainless Steel Tongue and Groove Structure CT

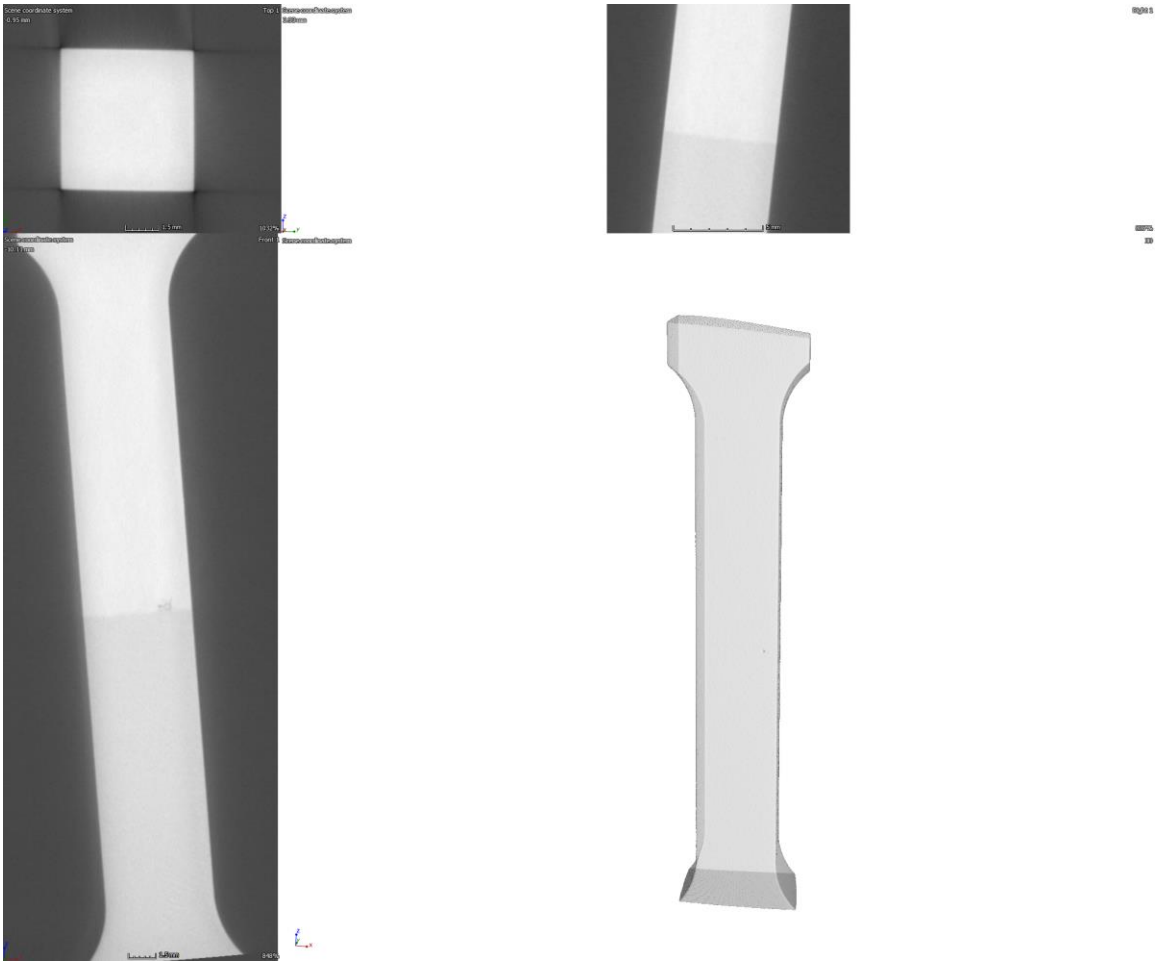

Figure 145: Cast Iron Flat Structure CT

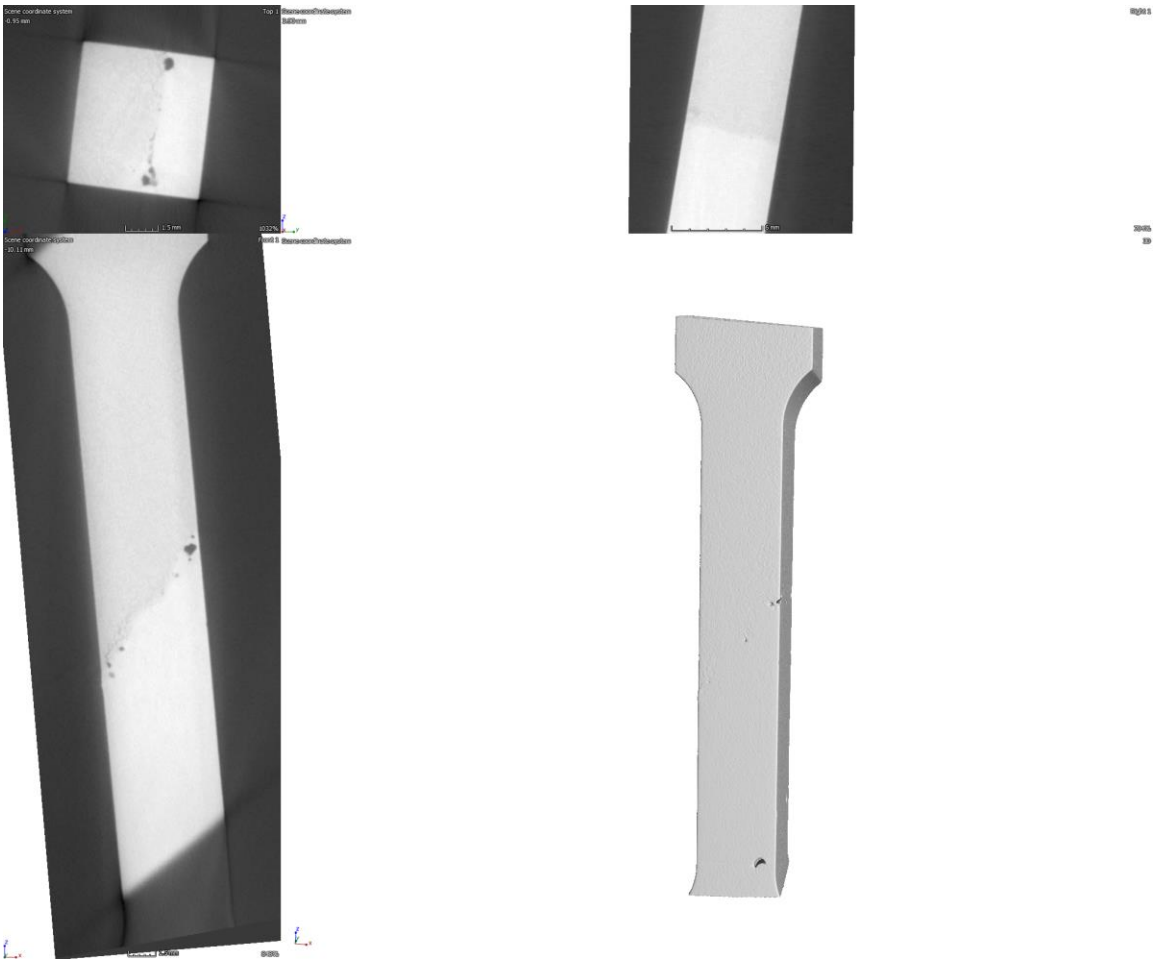

Figure 146: Cast Iron Angled Structure CT

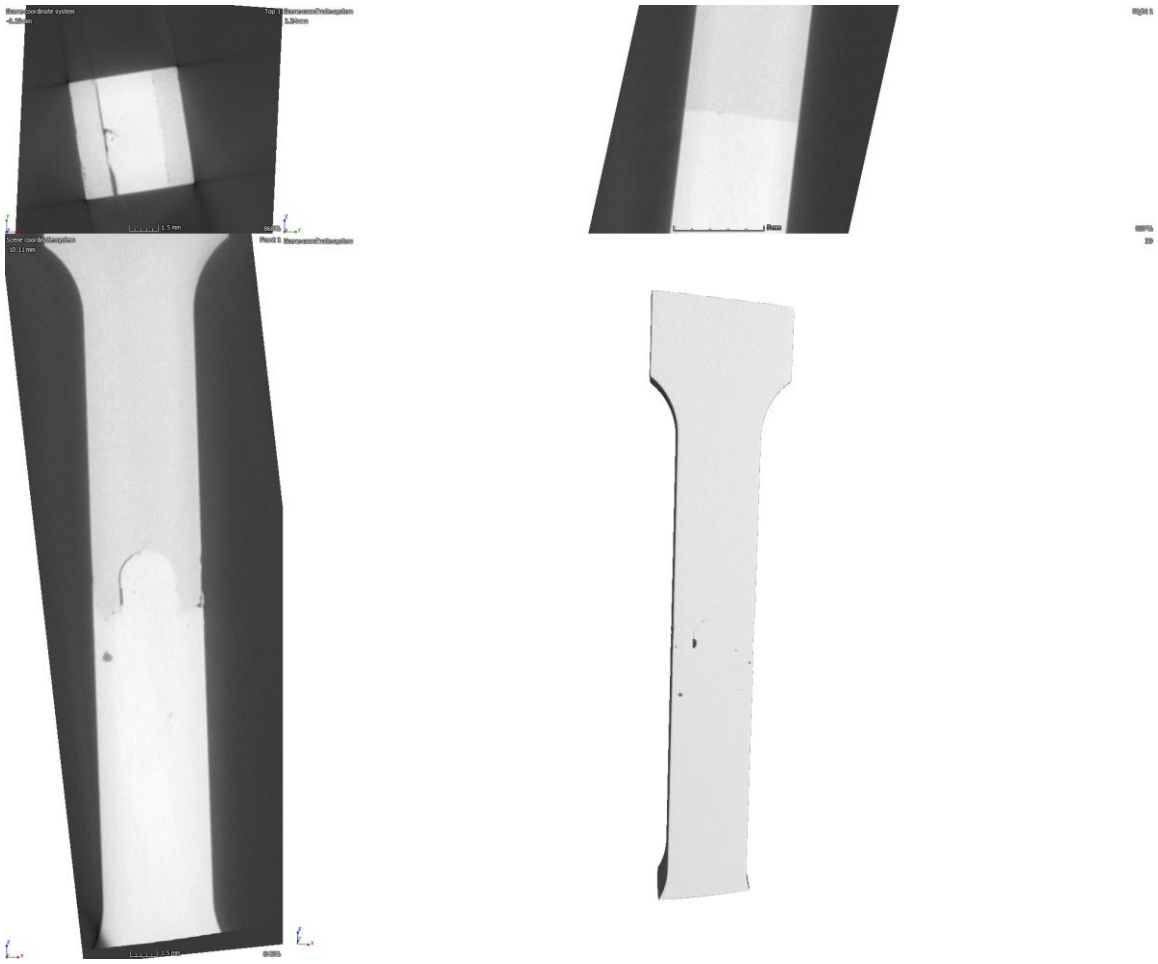

Figure 147: Cast Iron Scalloped Structure CT

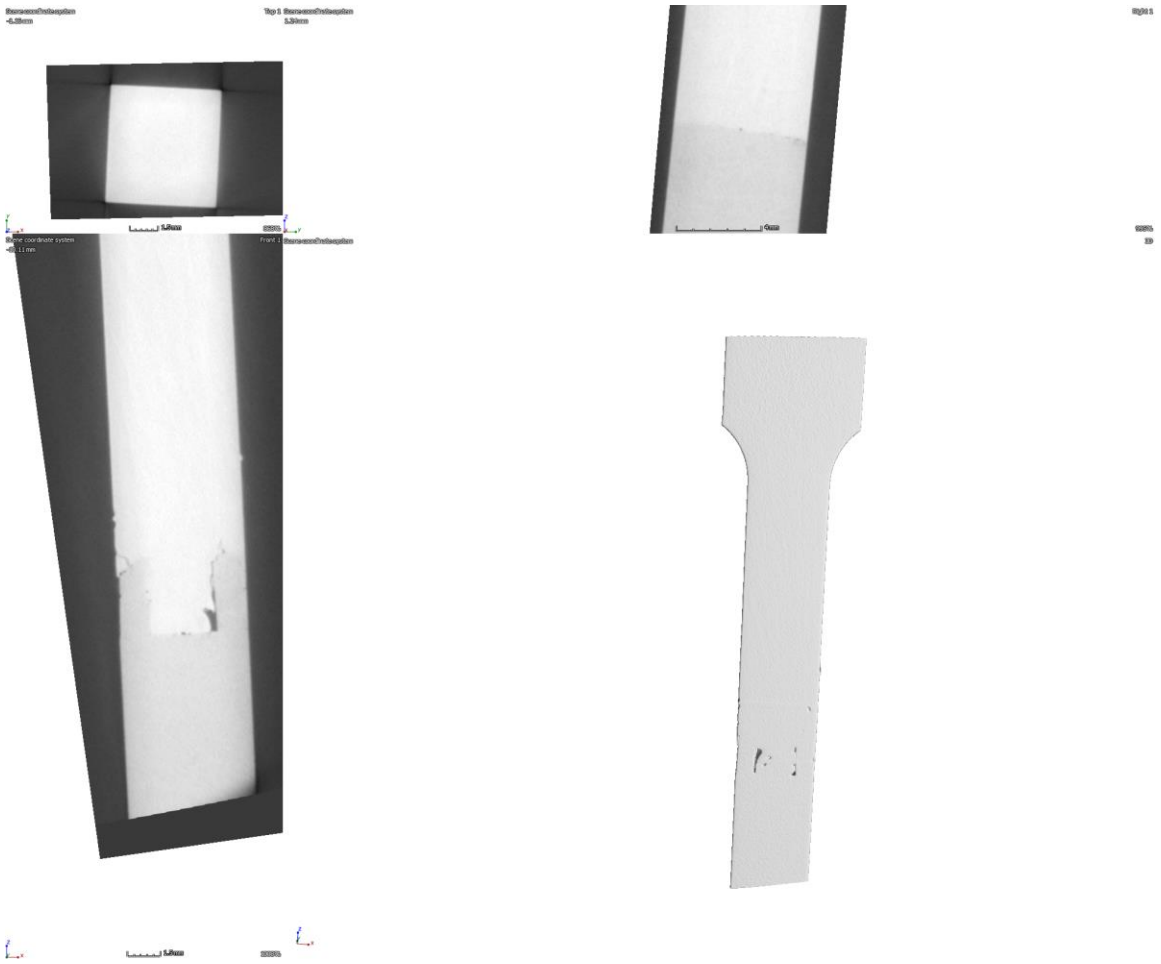

Figure 148: Cast Iron Tongue and Groove Structure CT

REFERENCES

[1] C. A. Brice, S. D. Needler, and B. T. Rosenberger, "Direct Manufacturing at Lockheed Martin Aeronautics Co.," presented at the AeroMat Conference, Seattle Washington, 2010.

[2] W. E. Frazier, "Metal additive manufacturing: a review," *Journal of Materials Engineering and Performance,* vol. 23, no. 6, pp. 1917-1928, 2014.

[3] J. M. Flynn, A. Shokrani, S. T. Newman, and V. Dhokia, "Hybrid additive and subtractive machine tools–Research and industrial developments," *International Journal of Machine Tools and Manufacture,* vol. 101, pp. 79-101, 2016.

[4] *Standard Terminology for Additive Manufacturing - General Principles - Terminology*. [Online]. Available: http://dx.doi.org/10.1520/f3177-15

[5] J. K. Nagel and F. W. Liou, "Hybrid Manufacturing System Design and Development," in *Manufacturing System*: IntechOpen, 2012.

[6] K. Lorenz, J. Jones, D. Wimpenny, and M. Jackson, "A review of hybrid manufacturing," in *Solid Freeform Fabrication Conference Proceedings*, 2015, vol. 53, pp. 96-108.

[7] M. Soshi, K. Odum, and G. Li, "Investigation of novel trochoidal toolpath strategies for productive and efficient directed energy deposition processes," *CIRP Annals,* 2019.

[8] U. De Oliveira, V. Ocelik, and J. T. M. De Hosson, "Analysis of coaxial laser cladding processing conditions," *Surface and Coatings Technology,* vol. 197, no. 2-3, pp. 127-136, 2005.

[9] Mazak, "Operating Manual VC500 5X AM," ed, 2018.

[10] M. Corporation. "VC-500A/5X AM HWD." https://www.mazakusa.com/machines/vc-500a-5x-am-hwd/ (accessed June 29, 2019.

[11] F. Liou, K. Slattery, M. Kinsella, J. Newkirk, H.-N. Chou, and R. Landers, "Applications of a hybrid manufacturing process for fabrication of metallic structures," *Rapid Prototyping Journal,* vol. 13, no. 4, pp. 236-244, 2007.

[12] J. B. Jones, "The synergies of hybridizing CNC and additive manufacturing," *Hybrid Manufacturing Technologies Ltd,* 2014.

[13] D. A. Miller and T. G. Langdon, "Creep fracture maps for 316 stainless steel," *Metallurgical Transactions A,* vol. 10, no. 11, pp. 1635-1641, 1979.

[14] D. Radaj, *Heat effects of welding: temperature field, residual stress, distortion*. Springer Science & Business Media, 2012.

[15] B. Nau, A. Roderburg, and F. Klocke, "Ramp-up of hybrid manufacturing technologies," *CIRP Journal of Manufacturing Science and Technology,* vol. 4, no. 3, pp. 313-316, 2011.

[16] P. Åkerfeldt, M.-L. Antti, and R. Pederson, "Influence of microstructure on mechanical properties of laser metal wire-deposited Ti-6Al-4V," *Materials Science and Engineering: A,* vol. 674, pp. 428-437, 2016.

[17] T. Mukherjee and T. DebRoy, "Printability of 316 stainless steel," *Science and Technology of Welding and Joining,* vol. 24, no. 5, pp. 412-419, 2019.

[18] S. Liu, W. Liu, and R. Kovacevic, "Experimental investigation of laser hot-wire cladding," *Proceedings of the Institution of Mechanical Engineers, Part B: Journal of Engineering Manufacture,* vol. 231, no. 6, pp. 1007-1020, 2017.

[19] A. Hansel *et al.*, "Study on consistently optimum deposition conditions of typical metal material using additive/subtractive hybrid machine tool," *Procedia CIRP,* vol. 46, pp. 579-582, 2016.

[20] Z. Y. Chua, I. H. Ahn, and S. K. Moon, "Process monitoring and inspection systems in metal additive manufacturing: Status and applications," *International Journal of Precision Engineering and Manufacturing-Green Technology,* vol. 4, no. 2, pp. 235-245, 2017.

[21] S. Liu, W. Liu, M. Harooni, J. Ma, and R. Kovacevic, "Real-time monitoring of laser hot-wire cladding of Inconel 625," *Optics & Laser Technology,* vol. 62, pp. 124-134, 2014.

[22] "Additive Process Parameter Ranges," ed. VC-500A/5x AM HWD Human-Machine Interface: Mazak Corporation, 2019.

[23] A. Standard, "E8/E8M-16a," *Standard test methods for tension testing of metallic materials. ASTM International, West Conshohocken, PA,* 2016.

[24] F. Klocke, H. Wirtz, and W. Meiners, "Direct manufacturing of metal prototypes and prototype tools," in *1996 International Solid Freeform Fabrication Symposium*, 1996.

[25] T. Amine, J. W. Newkirk, and F. Liou, "An investigation of the effect of direct metal deposition parameters on the characteristics of the deposited layers," *Case Studies in Thermal Engineering,* vol. 3, pp. 21-34, 2014.

[26] K. Eiamsa-ard, J. Zhang, and F. W. Liou, "Skeleton-based Geometric Reasoning for Adaptive Slicing in a Five-axis Laser Aided manufacturing Process System," in *Solid Freeform Fabrication Conference, University of Texas-Austin*, 2001.

[27] K. Eiamsa-ard, F. W. Liou, R. G. Landers, and H. Choset, "Toward automatic process planning of a multi-axis hybrid laser aided manufacturing system: skeleton-based offset edge generation," in *ASME 2003 International Design Engineering Technical Conferences and Computers and Information in Engineering Conference*, 2003: American Society of Mechanical Engineers, pp. 227-235.

[28] T. Yamazaki, "Development of a hybrid multi-tasking machine tool: integration of additive manufacturing technology with CNC machining," *Procedia Cirp,* vol. 42, pp. 81-86, 2016.

[29] K. Karunakaran, S. Suryakumar, V. Pushpa, and S. Akula, "Low cost integration of additive and subtractive processes for hybrid layered manufacturing," *Robotics and Computer-Integrated Manufacturing,* vol. 26, no. 5, pp. 490-499, 2010.

[30] J.-Y. Jeng and M.-C. Lin, "Mold fabrication and modification using hybrid processes of selective laser cladding and milling," *Journal of Materials Processing Technology,* vol. 110, no. 1, pp. 98-103, 2001.

[31] M. Kerschbaumer and G. Ernst, "Hybrid manufacturing process for rapid high performance tooling combining high speed milling and laser cladding," in *International Congress on Applications of Lasers & Electro-Optics*, 2004, vol. 2004, no. 1: LIA, p. 1710.

[32] R. Kovacevic and M. E. Valant, "System and method for fabricating or repairing a part," ed: Google Patents, 2006.

[33] J. B. Jones, P. McNutt, R. Tosi, C. Perry, and D. I. Wimpenny, "Remanufacture of turbine blades by laser cladding, machining and in-process scanning in a single machine," 2012.

[34] J. B. Jones. "World's first commercially available hybrid CNC." http://www.hybridmanutech.com/news.html (accessed 2019).

[35] J. Woodcock. "Euromold roundup - Bigger, bolder, busier." https://www.tctmagazine.com/blogs/jwblog/euromold-roundup-2013/ (accessed June 10, 2019.

[36] M. Molitch-Hou. "Mazak Adds Hybrid Metal 3D Printer to Machine Tool Lineup." https://3dprintingindustry.com/news/mazak-hybrid-metal-3d-printer-35803/ (accessed 2019).

[37] D. Sher. "10 top hybrid manufacturing companies." https://www.3dprintingmedia.network/the-top-ten-hybrid-manufacturing-companies/ (accessed 2019).

[38] J. Ruan, K. Eiamsa-ard, and F. W. Liou, "Automatic process planning and toolpath generation of a multiaxis hybrid manufacturing system," *Journal of manufacturing processes,* vol. 7, no. 1, pp. 57-68, 2005.

[39] H. Paris and G. Mandil, "Process planning for combined additive and subtractive manufacturing technologies in a remanufacturing context," *Journal of Manufacturing Systems,* vol. 44, pp. 243-254, 2017.

[40] M. Ma, Z. Wang, D. Wang, and X. Zeng, "Control of shape and performance for direct laser fabrication of precision large-scale metal parts with 316L Stainless Steel," *Optics & Laser Technology,* vol. 45, pp. 209-216, 2013.

[41] T. Hua, C. Jing, L. Xin, Z. Fengying, and H. Weidong, "Research on molten pool temperature in the process of laser rapid forming," *journal of materials processing technology,* vol. 198, no. 1-3, pp. 454-462, 2008.

[42] M. Griffith *et al.*, "Understanding thermal behavior in the LENS process," *Materials & design,* vol. 20, no. 2-3, pp. 107-113, 1999.

[43] K. Mills, B. Keene, R. Brooks, and A. Shirali, "Marangoni effects in welding," *Philosophical Transactions of the Royal Society of London. Series A: Mathematical, Physical and Engineering Sciences,* vol. 356, no. 1739, pp. 911-925, 1998.

[44] M. Gharbi *et al.*, "Influence of various process conditions on surface finishes induced by the direct metal deposition laser technique on a Ti–6Al–4V alloy," *Journal of materials processing technology,* vol. 213, no. 5, pp. 791-800, 2013.

[45] J. Liu and L. Li, "In-time motion adjustment in laser cladding manufacturing process for improving dimensional accuracy and surface finish of the formed part," *Optics & Laser Technology,* vol. 36, no. 6, pp. 477-483, 2004.

[46] C. Doumanidis and Y.-M. Kwak, "Geometry modeling and control by infrared and laser sensing in thermal manufacturing with material deposition," *J. Manuf. Sci. Eng.,* vol. 123, no. 1, pp. 45-52, 2001.

[47] A. Tadamalle, Y. Reddy, and E. Ramjee, "Influence of laser welding process parameters on weld pool geometry and duty cycle," *Advances in Production Engineering & Management,* vol. 8, no. 1, 2013.

[48] F. Cus, U. Zuperl, and T. Irgolic, "Effects of laser cladding parameters on microstructure properties and surface roughness of graded material," *Proceedings in Manufacturing Systems,* vol. 10, no. 2, p. 77, 2015.

[49] L. Wang and S. Felicelli, "Analysis of thermal phenomena in LENS™ deposition," *Materials Science and Engineering: A,* vol. 435, pp. 625-631, 2006.

[50] R. Unocic and J. DuPont, "Process efficiency measurements in the laser engineered net shaping process," *Metallurgical and materials transactions B,* vol. 35, no. 1, pp. 143-152, 2004.

[51] L. Costa, R. Vilar, T. Reti, and A. Deus, "Rapid tooling by laser powder deposition: Process simulation using finite element analysis," *Acta Materialia,* vol. 53, no. 14, pp. 3987-3999, 2005.

[52] P. Aggarangsi and J. L. Beuth, "Localized preheating approaches for reducing residual stress in additive manufacturing," in *Proc. SFF Symp., Austin*, 2006, pp. 709-720.

[53] A. Vasinonta, J. L. Beuth, and M. Griffith, "Process maps for predicting residual stress and melt pool size in the laser-based fabrication of thin-walled structures," 2007.

[54] B. Dillingh, G. Hayes, M. Hoppenbrouwers, V. Westerwoudt, and G. van Baars, "Control of microstructural evolution in powder bed fusion additive manufacturing in relation to functional properties of metals," in *ASPE 2014 Spring Topical Meeting: Dimensional Accuracy and Surface Finish in Additive Manufacturing*, 2014: American Society of Precision Engineering (ASPE), pp. 205-208.

[55] O. Oyelola, P. Crawforth, R. M'Saoubi, and A. T. Clare, "Machining of additively manufactured parts: implications for surface integrity," in *Procedia Cirp*, 2016, vol. 45: Elsevier, pp. 119-122.

[56] B. M. Lane, S. P. Moylan, and E. P. Whitenton, "Post-process machining of additive manufactured stainless steel," in *Proceedings of the 2015 ASPE Spring Topical Meeting: Achieving Precision Tolerances in Additive Manufacturing*, 2015, pp. 27-29.

[57] F. Montevecchi, N. Grossi, H. Takagi, A. Scippa, H. Sasahara, and G. Campatelli, "Cutting forces analysis in additive manufactured AISI H13 alloy," *Procedia Cirp,* vol. 46, pp. 476-479, 2016.

[58] Y. Zhao, J. Sun, and J. Li, "Study on chip morphology and milling characteristics of laser cladding layer," *The International Journal of Advanced Manufacturing Technology,* vol. 77, no. 5-8, pp. 783-796, 2015.

[59] P. Guo, B. Zou, C. Huang, and H. Gao, "Study on microstructure, mechanical properties and machinability of efficiently additive manufactured AISI 316L stainless steel by high-power direct laser deposition," *Journal of Materials Processing Technology,* vol. 240, pp. 12-22, 2017.

[60] M. Akbari, Y. Ding, and R. Kovacevic, "Process development for a robotized laser wire additive manufacturing," in *ASME 2017 12th International Manufacturing Science and Engineering Conference collocated with the JSME/ASME 2017 6th*

International Conference on Materials and Processing, 2017: American Society of Mechanical Engineers, pp. V002T01A015-V002T01A015.

[61] Y.-a. Jin, Y. He, J.-z. Fu, W.-f. Gan, and Z.-w. Lin, "Optimization of tool-path generation for material extrusion-based additive manufacturing technology," *Additive manufacturing,* vol. 1, pp. 32-47, 2014.

[62] T. A. Rodrigues, V. Duarte, J. A. Avila, T. G. Santos, R. Miranda, and J. Oliveira, "Wire and arc additive manufacturing of HSLA steel: Effect of thermal cycles on microstructure and mechanical properties," *Additive Manufacturing,* vol. 27, pp. 440-450, 2019.

[63] Y. Ding, J. Warton, and R. Kovacevic, "Development of sensing and control system for robotized laser-based direct metal addition system," *Additive Manufacturing,* vol. 10, pp. 24-35, 2016.

[64] G. Kasperovich and J. Hausmann, "Improvement of fatigue resistance and ductility of TiAl6V4 processed by selective laser melting," *Journal of Materials Processing Technology,* vol. 220, pp. 202-214, 2015.

[65] W. Du, Q. Bai, and B. Zhang, "A novel method for additive/subtractive hybrid manufacturing of metallic parts," *Procedia Manufacturing,* vol. 5, pp. 1018-1030, 2016.

[66] A. B. Spierings, T. L. Starr, and K. Wegener, "Fatigue performance of additive manufactured metallic parts," *Rapid prototyping journal,* 2013.

[67] I. Tabernero, A. Lamikiz, S. Martínez, E. Ukar, and J. Figueras, "Evaluation of the mechanical properties of Inconel 718 components built by laser cladding," *International Journal of Machine Tools and Manufacture,* vol. 51, no. 6, pp. 465-470, 2011.

[68] T. R. Smith, J. D. Sugar, C. San Marchi, and J. M. Schoenung, "Orientation effects on fatigue behavior of additively manufactured stainless steel," in *ASME 2017 Pressure Vessels and Piping Conference*, 2017: American Society of Mechanical Engineers Digital Collection.

[69] R. Shrestha, J. Simsiriwong, and N. Shamsaei, "Fatigue behavior of additive manufactured 316L stainless steel parts: Effects of layer orientation and surface roughness," *Additive Manufacturing,* vol. 28, pp. 23-38, 2019.

[70] E. O. Olakanmi, R. Cochrane, and K. Dalgarno, "A review on selective laser sintering/melting (SLS/SLM) of aluminium alloy powders: Processing, microstructure, and properties," *Progress in Materials Science,* vol. 74, pp. 401-477, 2015.

[71] H. H. Alsalla, C. Smith, and L. Hao, "Effect of build orientation on the surface quality, microstructure and mechanical properties of selective laser melting 316L stainless steel," *Rapid Prototyping Journal,* 2018.

[72] N. Yang *et al.*, "Process-structure-property relationships for 316L stainless steel fabricated by additive manufacturing and its implication for component engineering," *Journal of Thermal Spray Technology,* vol. 26, no. 4, pp. 610-626, 2017.

[73] K. Zhang, S. Wang, W. Liu, and X. Shang, "Characterization of stainless steel parts by laser metal deposition shaping," *Materials & Design,* vol. 55, pp. 104-119, 2014.

[74] I. Gibson, D. Rosen, and B. Stucker, "Directed energy deposition processes," in *Additive Manufacturing Technologies*: Springer, 2015, pp. 245-268.

[75] D. Rosenthal, "Mathematical theory of heat distribution during welding and cutting," *Welding journal,* vol. 20, pp. 220-234, 1941.

[76] A. Bandyopadhyay and B. Heer, "Additive manufacturing of multi-material structures," *Materials Science and Engineering: R: Reports,* vol. 129, pp. 1-16, 2018.

[77] X.-L. Wang, C. Hoffmann, C. Hsueh, G. Sarma, C. Hubbard, and J. Keiser, "Influence of residual stress on thermal expansion behavior," *Applied physics letters,* vol. 75, no. 21, pp. 3294-3296, 1999.

[78] M. B. Bauza *et al.*, "Study of accuracy of parts produced using additive manufacturing," Lawrence Livermore National Lab.(LLNL), Livermore, CA (United States), 2014.

[79] R. Paul, S. Anand, and F. Gerner, "Effect of thermal deformation on part errors in metal powder based additive manufacturing processes," *Journal of Manufacturing Science and Engineering,* vol. 136, no. 3, p. 031009, 2014.

[80] K. Salonitis, L. D'Alvise, B. Schoinochoritis, and D. Chantzis, "Additive manufacturing and post-processing simulation: laser cladding followed by high speed machining," *The International Journal of Advanced Manufacturing Technology,* vol. 85, no. 9-12, pp. 2401-2411, 2016.

[81] J. G. Hicks, *Welded joint design*. Industrial Press Inc., 1999.

[82] Z. Feng, *Processes and mechanisms of welding residual stress and distortion*. Elsevier, 2005.

[83] Y. Ueda, K. Fukuda, and M. Tanigawa, "New measuring method of three dimensional residual stresses based on theory of inherent strain (welding mechanics, strength & design)," *Transactions of JWRI,* vol. 8, no. 2, pp. 249-256, 1979.

[84] Y. Ueda, H. Murakawa, and N. Ma, *Welding deformation and residual stress prevention*. Elsevier, 2012.

[85] T. Kasuya and N. Yurioka, "Prediction of welding thermal history by a comprehensive solution," *WELDING JOURNAL-NEW YORK-,* vol. 72, pp. 107-s, 1993.

[86] J. Goldak, A. Chakravarti, and M. Bibby, "A new finite element model for welding heat sources," *Metallurgical Transactions B,* vol. 15, no. 2, pp. 299-305, 1984/06/01 1984, doi: 10.1007/BF02667333.

[87] L.-E. Lindgren, A. Lundbäck, M. Fisk, R. Pederson, and J. Andersson, "Simulation of additive manufacturing using coupled constitutive and microstructure models," *Additive Manufacturing,* vol. 12, pp. 144-158, 2016.

[88] G. Fu, J. Gu, M. I. Lourenco, M. Duan, and S. F. Estefen, "Parameter determination of double-ellipsoidal heat source model and its application in the multi-pass welding process," *Ships and Offshore Structures,* vol. 10, no. 2, pp. 204-217, 2015.

[89] M. Abid and M. J. Qarni, "3D Thermal finite element analysis of single pass girth welded low carbon steel pipe-flange joints," *Turkish J. Eng. Env. Sci,* vol. 33, pp. 281-293, 01/01 2009, doi: 10.3906/muh-0912-6.

[90] "Netfabb Local Simulation Keyword User Manual." Autodesk. https://knowledge.autodesk.com/support/netfabb/learn-explore/caas/CloudHelp/cloudhelp/2020/ENU/NETF-Utility-Local-Simulation/files/GUID-C83C2153-30C1-4E17-8E81-3AF5F51D02CC-htm.html (accessed 2020).

[91] A. F. Padilha, R. L. Plaut, and P. R. Rios, "Annealing of cold-worked austenitic stainless steels," *ISIJ international,* vol. 43, no. 2, pp. 135-143, 2003.

[92] F. Cverna, *ASM ready reference: thermal properties of metals*. ASM International, 2002.

[93] D. Susan, T. Crenshaw, and J. Gearhart, "The effects of casting porosity on the tensile behavior of investment cast 17-4PH stainless steel," *Journal of Materials Engineering and Performance,* vol. 24, no. 8, pp. 2917-2924, 2015.

[94] L. Chen, K. Xu, and K. Tang, "Optimized sequence planning for multi-axis hybrid machining of complex geometries," *Computers & Graphics,* vol. 70, pp. 176-187, 2018.

[95] M. C. Frank, F. Peters, X. Luo, F. Meng, and J. E. Petrzelka, "A hybrid rapid pattern manufacturing system for sand castings," 2009.

[96] B. K. Choi, D. H. Kim, and R. B. Jerard, "C-space approach to tool-path generation for die and mould machining," *Computer-Aided Design,* vol. 29, no. 9, pp. 657-669, 1997.

[97] H.-T. Young, "Cutting temperature responses to flank wear," *Wear,* vol. 201, no. 1-2, pp. 117-120, 1996.

[98] F. W. Taylor, "On the art of metal cutting," *Trans. ASME,* vol. 28, pp. 31-35, 1907.

[99] J. Tlusty, *Manufacturing processes and equipment*. 2000.

[100] S. J. Lee and D. G. Lee, "Optimal design of the adhesively-bonded tubular single lap joint," *The Journal of Adhesion,* vol. 50, no. 2-3, pp. 165-180, 1995.

[101] T.-L. Teng, C.-P. Fung, P.-H. Chang, and W.-C. Yang, "Analysis of residual stresses and distortions in T-joint fillet welds," *International Journal of Pressure Vessels and Piping,* vol. 78, no. 8, pp. 523-538, 2001.

[102] Y. Wang, H. Tang, Y. Fang, and H. Wang, "Microstructure and mechanical properties of hybrid fabricated 1Cr12Ni2WMoVNb steel by laser melting deposition," *Chinese Journal of Aeronautics,* vol. 26, no. 2, pp. 481-486, 2013.

[103] M. Corporation. "New Mazak VC-500 AM Combines 5-Axis and Additive Technology to Revolutionize Product Design." https://www.mazakusa.com/news-events/news-releases/new-mazak-vc-500-am-combines-5-axis-and-additive-technology/ (accessed 2020).

[104] H. Kim, Z. Liu, W. Cong, and H.-C. Zhang, "Tensile fracture behavior and failure mechanism of additively-manufactured AISI 4140 low alloy steel by laser engineered net shaping," *Materials,* vol. 10, no. 11, p. 1283, 2017.

[105] K. Zhang, W. Liu, and X. Shang, "Research on the processing experiments of laser metal deposition shaping," *Optics & Laser Technology,* vol. 39, no. 3, pp. 549-557, 2007.

[106] S. Rao, M. Gong, Y. Chui, and M. Mohammad, "Effect of geometric parameters of finger joint profile on ultimate tensile strength of single finger-joined boards," *Wood and Fiber Science,* vol. 44, no. 3, pp. 263-270, 2012.

[107] F. P. Laboratory, *Wood handbook: Wood as an engineering material*. The Laboratory, 1987.

[108] Z. Sun and J. Ion, "Laser welding of dissimilar metal combinations," *Journal of Materials Science,* vol. 30, no. 17, pp. 4205-4214, 1995.

[109] E. El-Banna, "Effect of preheat on welding of ductile cast iron," *Materials Letters,* vol. 41, no. 1, pp. 20-26, 1999.

[110] U. Dilthey and X. Shu, "Studies into laser beam welding of the material combination cast iron with spheroidal graphite/steel using nickel filler wire," *SCHWEISSEN UND SCHNEIDEN,* pp. E 103-E 103, 1993.

[111] S. Kim, S. Lee, K. Han, S. Hong, and C. Lee, "Cracking behavior in a dissimilar weld between high silicon nodular cast iron and ferritic stainless steel," *Metals and Materials International,* vol. 16, no. 3, pp. 483-488, 2010.